Multiphase flow for power processes

PSO 6364

Final report

Department of ENERGY TECHNOLOGY
Aalborg University

AALBORG UNIVERSITY

Contents

Summary

This project has focussed on the interaction between large, non-spherical particles and fluid turbulence in the near-burner field. Due to the anticipated and announced increase in the fraction of biomass being fired into Danish thermal power plants, understanding the conditions governing the local mixing and reaction processes in the near-burner field is essential in order to maintain high efficiencies and low emissions. As biomass particles prepared for suspension firing are typically at least an order of magnitude larger than conventional coal particles and demonstrate significantly greater non-sphericity, conventional methods and knowledge need to be supplemented. Furthermore, as the volume fraction of biomass necessary to replace an equivalent amount of coal by energy is significantly larger than the amount of coal, it is to be expected that the local conditions for burners firing biomass will differ significantly from those of burners firing coal.

A complete description of the motion of non-spherical particles is still lacking. However, evidence suggest that the equation of motion for a sphere only represent an asymptotical value for a more general, but yet unformulated, description of the motion of non-spherical particles. In order to address this topic, experimental investigations have been combined with theoretical studies and numerical modelling. A test rig has been constructed to investigate a range of particles and their interaction with well-defined jet turbulence using optical methods. A novel approach to multiphase investigations using Laser Doppler Velocimetry (LDV) has been proposed, and shown to be comparable in error to the more commonly used Phase Doppler Anemometry (PDA) technique. An extensive parametric study concerning the measurement of turbulence intensity in a particle-laden jet compared to that of a clear jet has been undertaken. The effect of three different sizes of spherical particles as well as two distinct non-spherical shapes is measured at different concentrations. Emphasis has been put towards developing a method to evaluate the additional influence of shape. Results suggest that non-spherical particles follow the same tendency as that observed for spheres, only with seemingly greater effect for comparable parameters. This is believed to be due to the increase in drag coefficient for increasing aspects ratios.

Based on the results, a detailed model for particle-turbulence interaction to be used in CFD simulations has been developed and proposed. The model has been theoretically derived from the governing conservative equations for fluid flow, the Navier-Stokes equations, considering the additional influence resulting from the interaction with particles. Validation, using existing measurements as well as those obtained for the particle-laden jet, demonstrate that the new model is able to predict the experimentally observed tendencies and thus represent an improvement compared to existing models. The additional effect of shape is modelled through the modification of the drag coefficient.

Furthermore, a semi-empirical 1D model has been developed and proposed, which can be used by burner manufacturers and operators to obtain an a priori indication of the influence on mixing characteristics by introducing a biomass fuel with certain physical size and shape characteristics in different ratios.

Finally, the acquired knowledge is synthesized into the development of techniques to predict the combustion of large non-spherical straw particles in suspension fired power plants which are to replace coal in tomorrow's society. Although the straw particles are significantly larger than coal particles, the larger drag coefficient associated with straw particles ultimately leads to an attenuation of the carrier phase turbulence. Compared to other modelling choices the inclusion of a model for turbulence modulation is found to be important for the correct prediction of combustion efficiency.

During the project, the initial partners (Vattenfall Utveckling ab and the Department of Energy Technology, AAU) were joined by BW Energy in 2007. Furthermore, the project was extended for a full year due to unused funds during the original period. The project has produced 1 PhD candidate, where the thesis serves as a major part of the documentation of the project. Furthermore, two (2) peer reviewed conference contributions, one (1) poster, four (4) peer reviewed journal contributions and one (2) journal manuscript in the review process have been produced as results of the project. The PhD candidate spent three months at McMaster University, Toronto, Canada, as well as a month-long internship with Vattenfall Utveckling ab, Älvkarleby, Sweden.

In conclusion, the work carried out in this project has provided a substantial contribution to knowledge in the field of multiphase flow for power processes. Through the close collaboration with an energy utility company and, for part of the project, a burner manufacturer, this knowledge has been made directly available to relevant industrial partners, and through these, been put to practical use. However, the results of the project also clearly indicate that there is still a significant challenge in fully understanding the mechanisms involved in this complex type of flow, the importance of the different parameters and using this knowledge in modelling, operation and design of advanced biomass burners.

It was an ambition of the project to build on the knowledge gained and seek continued funding for activities within this field. Unfortunately, activities were initiated in another context without all partners of the current project, and activities at the Department of Energy Technology, AAU, have only been continued through master projects and other educational activities.

Organisation and investigators

Department of Energy Technology, Aalborg University

- Professor Lasse Rosendahl, project manager
- PhD student Matthias Mandøe (100% funded by project)
- Assoc. professor Chungen Yin (partially funded)
- Assoc. professor Henrik Sørensen (partially funded)

Vattenfall Utveckling ab, Sweden

- Jan Eriksson, senior researcher
- Karin Eriksson, researcher
- Mogens Berg, engineer

BW Energy, Denmark

- Peter Hougaard, department head
- Lisbeth Myllerup, CFD engineer
- Sune Hansen, CFD engineer

Objectives

The main goal of the work outlined in this proposal is to improve the understanding of the governing multiphase aspects of biomass combustion and thus further the achievements made to date in designing and operating combustion equipment suitable for biomass. Over the last decades, R&D activities have been on-going to bring renewables in the form of biomass and waste into play as serious alternatives or supplements to fossil fuels in primary power conversion processes. Two main approaches have been adopted in Denmark as well as world-wide: to fire biomass alone or with a fossil fuel in a suspension burner, or to burn the biomass on a grate in a dedicated plant. Most of the national research initiatives have naturally focused on these two technologies, and they have provided us with a comprehensive view of the feasibility, problems and difficulties, and possible solutions in terms of the technological challenges. But there remains a comprehensive effort in order to achieve a better and more fundamental understanding of the flow, coupling and heterogeneous reactions in biomass combustion; an understanding, which is required in order to lift the conversion technologies to a higher level in terms of efficiency, sustainability and flexibility. For this, the particle-gas two-phase flow plays a vital role.

Production of heat and power from biomass utilization has a promising future due to the renewable and environmentally sustainable nature of the fuel source. Among the thermo-chemical conversion technologies (i.e., combustion, gasification and pyrolysis), combustion of biomass is the only proven technology for heat and power production and accounts for approximately 97% of the worlds production of bio-energy (Demirbas, 2005; Nussbaumer, 2003). In fact, biomass co-firing has been tested and demonstrated on various types of combustion technologies, such as cyclone boilers, pulverized coal boilers, fluidized bed boilers and stoker fired boilers and so on (e.g., Hein and Bemtgen, 1998; Sami et al., 2001; Tillman, 2000). However, biomass-firing technology has some technological problems (Demirbas, 2005), e.g., combustor fouling and corrosion caused by the alkaline nature of the biomass ash due to high content of sodium and potassium, which lower the melting point of ash; increase of NOx levels; the maximum particle size of a given biomass that can be fed to and burned in a given boiler; maintaining burner stability and so forth. All the problems are more or less related to the gas-particle two-phase flows in boilers. A wide range of research activities have focussed on multiphase flow in power systems, including fundamental physics and chemistry (e.g., particle-fluid interaction), model development, simulation and computational methods, as well as experimental methods [ESR21, 2003], but still a lot of uncertainties remain.

Thus, the purpose of this project is to conduct research into aspects of multiphase flow such that the following will be brought into focus:

- understanding of mixing in the near burner field of a solid fuel burner

- understanding of coupling between main particle shape parameters and turbulence characteristics
- understanding the effect of high volumetric loads on turbulent properties
- application of this knowledge to burner design
- application of this knowledge to burner operation issues, specifically using this knowledge to enhance stability and low emissions at low burner loads using primary measures

On particle dispersion in turbulent flows

The accurate description of turbulent dispersed phase motion still remains an unfinished task, partly due to unavailability of accurate first-principle Lagrangian equations governing the particle's motion, temperature, and its other properties of interest in the presence of other particles in turbulent flows (Mashayek and Pandya, 2003). In recent years, works on particle dispersion in turbulent flows have generally been based on the equation proposed by Maxey and Riley (1983), which is known as the MR equation. The MR equation of motion for a small rigid sphere in a nonuniform flow balances particle inertia with drag, gravity, fluid acceleration force, added mass force and the Basset history force. The expressions for drag, added mass and Basset history forces are modified due to the flow curvature effect. A slightly modified MR equation, in which the drag term is replaced by a more general expression valid for higher values of Re_p is commonly used, and a Saffman lift force can be added for highly sheared flows, and a Magnus force for rotating particles. In terms of accounting for dispersion due to fluid turbulence, it is common to include two main effects, one due to particle inertia and one due to the dissipative nature of turbulence (crossing trajectory effect), which accounts for the effect of particles crossing from one eddy to another. For the vast majority of these models, it is assumed that the particles are very small, smaller than the smallest turbulent scales (the Kolmogorov scales), and that for the duration of interaction with a single eddy, all fluid properties remain constant. Although quite detailed, even this is not an accurate equation of motion for particles in turbulent flows. For applications in biomass conversion, it is quite likely that other forces are important and should be included in the equation of motion, depending not only on local fluid and flow properties, but also on particle properties such as size, shape, particle charge, acceleration, and rotation.

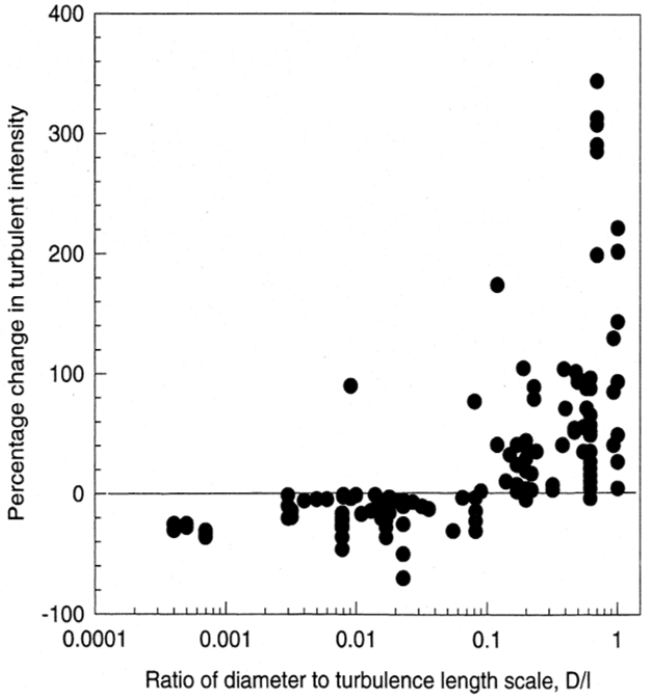

Figure 1 Effect of particle size on turbulent intensity (Gore & Crowe 1989)

On turbulence modulation due to the presence of particles

Comparing to particle dispersion, turbulence modulation is far from being well understood. In the modelling of multiphase flows, source terms involved in order to simulate the momentum and heat exchange between the phases are well known, and various effects, for example associated with the drag force and the lift force on one hand, or the heat transfer by convection/radiation on the other hand, are properly taken into account. This has been correctly included in commercial CFD codes, e.g Fluent (Fluent, 2005). However in the frame of *turbulent* flows, the formulation of the source terms associated with the various existing closure schemes is sometimes far from fully satisfactory, for instance, the effect of particles on fluid turbulence has not yet been included in transport equations for k and ε in $k-\varepsilon$ models in academic or commercial CFD codes.

Interaction between the particles and the gas phase lead to the changes in the level of the gas-phase turbulence intensity. A number of factors known to affect the gas-phase turbulence modulation in gas–particle flow systems have been studied extensively. These factors include particle size, particle density, and particle loading (defined as the ratio of the particle mass flow rate to the gas mass flow rate). Gore and Crowe (1989) found by experiments that small particles decrease the turbulent intensity of fluid by increasing the apparent viscosity of the fluid, and larger particles increase the intensity of the turbulence due to vortex shedding. Therefore a criterion was proposed to be the ratio $d_p / l_e = 0.1$, where d_p is the particle diameter and l_e is the characteristic length of the most energetic eddy. Both mechanisms are strongly affected by the volume and mass fraction of particles (the latter is indicated in ***Figure 2*** – corresponding data for volume fraction, which is more appropriate regarding biomass, is very scarce). However, Hadinoto et al. (2005) found that the criterion proposed by Gore and Crowe (1989) is not sufficient to explain the gas turbulence enhancement in the presence of smaller particles reported in literature, leaving this an open issue even for spherical particles.

Crowe (2000) derived in a more rigorous way a source term formulation featuring the particle–turbulence interaction. His analysis is that the usual formulation suffers from the fact that the conventional modelling for the forces acting on the particles provides an averaged value that is then treated like a local one. He therefore re-derived the complete formulation starting with an initial mechanical energy, where the forces acting on the particle are not modelled as equivalent point forces. On the contrary, an exact description of the exchanges taking into account the real interfacial area is performed. Two contributions may be identified in the source term: a generation of k by the particle drag and a transfer of kinetic energy of the particle motion to kinetic

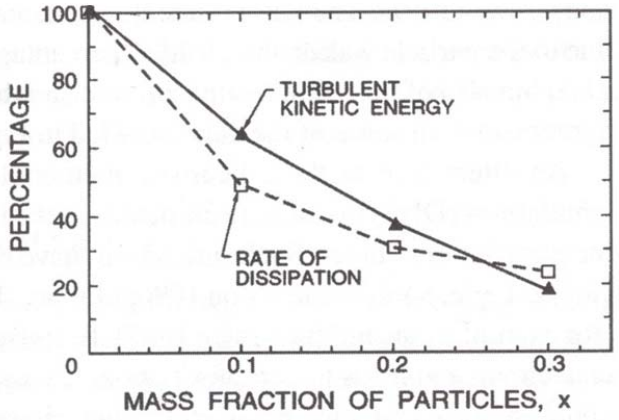

Figure 2 Effect of particle mass fraction on turbulent kinetic energy and dissipation in a channel flow with air and 150 μm glass beads (Paris & Eaton 2001)

energy of the fluid. Boulet and Moissette (2002) found by simulations that the formulation of the source term for the fluid turbulent kinetic energy based on Crowe (2000) yields very interesting results, but that a fully satisfactory solution on both theoretical and numerical points of view still has to be sought.

On the fluid-particle interaction associated with non-spherical particles

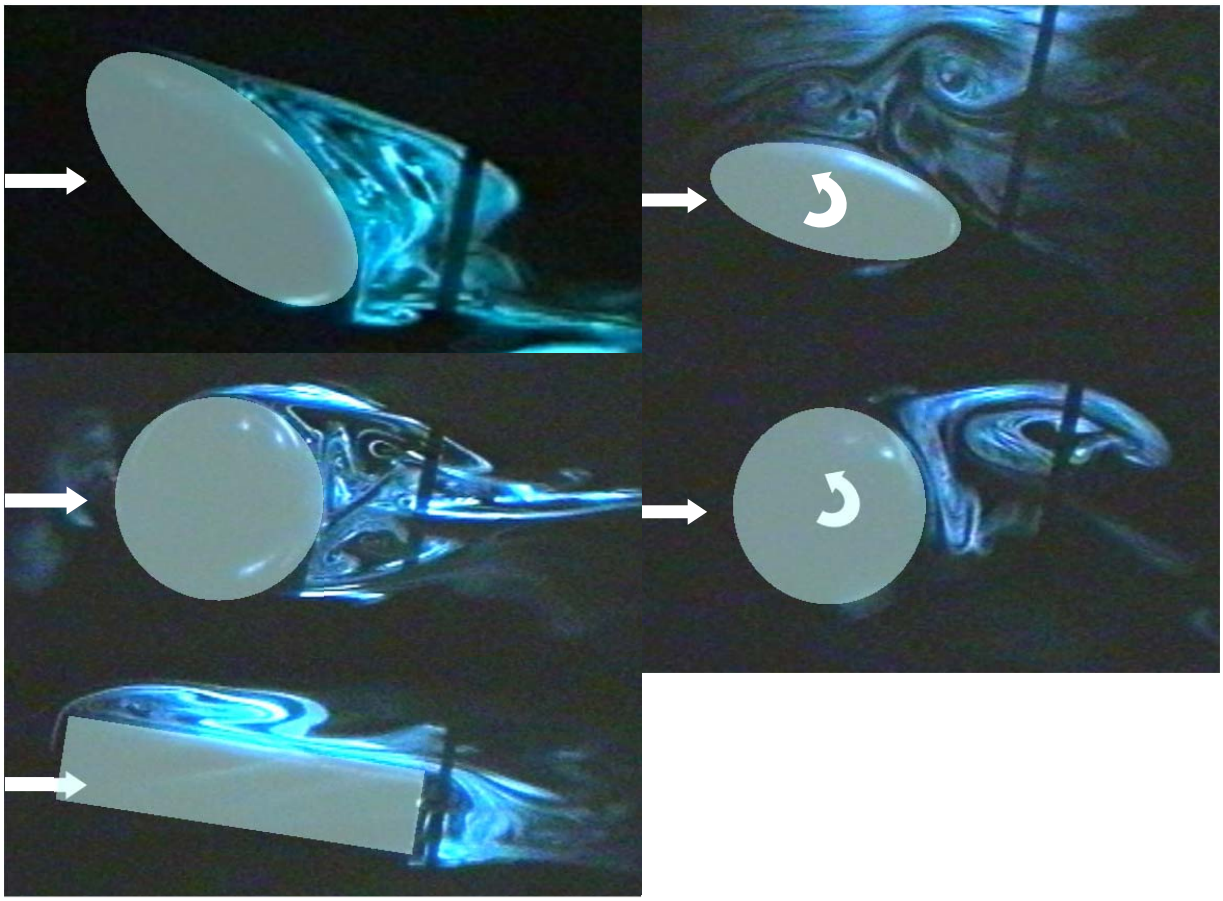

Figure 3 LSV images of wakes generated by stationary (left) and rotating (right) particles at Reynolds numbers of approximately 5000. (Rosendahl 1998)

All the above backgrounds are for the fluid-particle systems in dilute regimes, in which the particles are small rigid spheres. Nonspherical particles further complicate the issue in terms of availability of well-accepted knowledge or uncertainty. The motions of non-spherical particles in flows are very complicated because the orientation and the rotation are strongly coupled with the translation. This can be seen in ***Figure 3***, where differently shaped particles (though in all cases, $d_p >> l_e$) are placed in a flow. It is quite clear, that there is a distinct connection between shape and motion and the resulting vertical flow structures. Another example of this is Klett (1995), who presented a theoretical investigation on the orientation of free-falling nonspherical particles in the atmosphere. He noted that very small particles tend to be oriented randomly, however larger particles in a turbulent flow field will adopt a preferred orientation with some type of wobbling motion caused by turbulence. Further, experiments have been performed to assess the influence of particle shape on the particle dynamics (Black and McQuay, 2001). Their results from phase-Doppler particle

analyzer (PDPA) show significant differences between spherical and nonspherical particles observed for both co-axial jet and swirling flows in regions where velocity gradients are high. Sun *et al.* (2004) derived a set of new fluid fluctuating velocity equations with a source term which reflects the action of non-spherical particles. The results show that the difference between the particle fluctuating velocity and fluid fluctuating velocity reduces the turbulence of the fluid, and the turbulent intensity and the Reynolds stress are decreased almost inversely proportional to the fluctuating velocity ratio of particle to fluid. The dynamic shape factor in the range given in this paper plays a role in suppressing turbulence, and non-spherical particles have a greater effect on the turbulence than spherical particles.

Modelling of biomass particles in the near burner zone

Wall-bounded particle-laden turbulent flows are important in a variety of engineering applications. Of particular interest is the determination of the dispersion of the particles in the flows, which influences reaction and concentration patterns, and ultimately also effects such as wall deposits. The physics of such flows is extremely complex, and, in the ultimate sense, to correctly resolve these and include coupling aspects requires the use turbulence models which do not rely on Reynolds averaging of the Navier Stokes equations, such as Large Eddy Simulation (LES).

LES of swirling particle-laden flows in a coaxial-jet combustor was studied by Apte et al. (2003). In LES, the incompressible, spatially filtered NS equations are solved to compute the turbulent gas-phase. In order to obtain a dynamic representation of the dispersed phase, approximately a million particles are tracked within the flowfield in a Lagrangian framework. The particles are treated as point sources and influence the gas phase ("two-way" coupling) only through momentum-exchange terms. The authors compared their simulations with the measurements done by Sommerfeld *et al.* (1992) and concluded that the LES results are significantly more accurate than the RANS predictions of the same problem.

Project tasks and documentation

The project has been divided into the following tasks, with detailed documentation indicated below each task. The detailed documentation is included in the appendix of this report.

Task 0. Litterature review
- a. On the motion of non-spherical particles at high Reynolds number.
- b. On the modelling of motion of non-spherical particles in two-phase flow
- c. Aerodynamics of large non-spherical particles
- d. PhD thesis Turbulence Modulation by Non-Spherical Particles

Task 1. Experimental investigation of coupling parameters
- a. Measurement of Turbulence Modulation by Non-Spherical Particles
- b. PhD thesis Turbulence Modulation by Non-Spherical Particles

Task 2. Model development and validation
- a. PhD thesis Turbulence Modulation by Non-Spherical Particles
- b. Numerical Investigation of Large Particles in Upward Pipe Flow with Sinusoidal Wall Boundary Condition.

c. On the motion of non-spherical particles at high Reynolds number.

Task 3. Application of models to burner flow

a. PhD thesis Turbulence Modulation by Non-Spherical Particles
b. Pulverized straw combustion in a low-NOx multifuel burner : Modeling the transition from coal to straw.
c. On the modelling of motion of non-spherical particles in two-phase flow

In the framework of multi-phase flows the influence of particles on the carrier phase turbulence is commonly known as turbulence modulation. The interaction between solid particle and gas phase turbulent flows is important for many engineering devices as well as natural accruing processes. Examples of these are the pneumatic transport of fine powders, the combustion of pulverized solid fuels, dust storms and the pollutant dispersion in the atmosphere. In each of these cases a fundamental understanding concerning the underlying phenomena, which is responsible for the complex interaction between the particulate phase and the turbulent carrier flow, is required to advance the design of engineering devices in which these flows occur. Most research up to date concerning particle-gas interaction has been focused on spherical particles although the vast majority of particulate flows involves non-spherical particles which flight can be significant different than that of a sphere. This study is part of a larger research initiative concerning the combustion of biomass in suspension fired power plants. Particular attention is drawn to the influence of non-spherical particles on the carrier phase turbulence. This is achieved by performing measurements on a particle-laden jet with the intention to gain a better understanding of the mechanisms involved in turbulence modulation, by development of appropriate source terms for the turbulence equations in the framework of Computational Fluids Dynamics to account for the presence of particles and by demonstrating the practical implementation of this model extension on multifuel pulverized fuel burner.

Currently, there is little or no consensus towards the influence of particles on the carrier phase turbulence and no model has so far been able to reproduce the entire spectrum of experimental measurements. Although several mechanisms for turbulence modulation have been suggested in the past, the only general consensus in the scientific community appears to be that small particles tend to attenuate the carrier phase turbulence while large particles tend to augment the turbulence. To gain insight into the general mechanisms concerning particle turbulence interaction a test rig was constructed and the turbulence modulation resulting from different particle sizes, concentration and shapes were measured using laser-optical methods. Using this parametric study is was possible to evaluate some of the suggested criteria for turbulence modulation based on proposed mechanisms. The results showed a strong correlation with particle concentration as expected and the measureable lower boundary for two-way coupling was found to be around 10^{-5} which matches that of previous investigations. An often mentioned mechanism for turbulence production is the unsteady wake of large particles and from the study of large spheres it is known that this is best described by the particle Reynolds number, Re_p. The present study reveals that this mechanism alone is not sufficient to explain the observed trends. However, there does seem to be a tendency towards an enhancement of turbulence for large values of Re_p and a decrease for low values. Another suggested mechanism is the correlated motion between particles and the fluid motion. As a small particle enters an eddy it will be accelerated by fluid motion and momentum exchange via the drag force act to decrease the velocity of the eddy and thereby reduce the turbulence intensity. This phenomenon is best described by

the Stokes number. The present investigation involves particle Stokes numbers which are much greater unity, implying that particles are only little affected by the eddies and thus that only augmentation of the carrier phase turbulence is to be expected. However, the present results show that the presence of particles is able to dampen the turbulence intensity at some locations downstream of the jet. Clearly, at those locations the largest, most energetic eddies are still larger than the particles and thus there should still be a basis for this mechanism to proceed. These observations is an indicator for that the mechanisms involved in the modulation of turbulence is the result of two or more distinct mechanisms and that a single non-dimensional number is not sufficient to explain/predict the observed trends. This is factored into the derivation of the theoretical model where the forcing term, resulting from the presence of particle, to the momentum equation is split in two. Subsequently, the two different approaches to derive the source term to the turbulence equations are applied on each part of the momentum forcing term resulting in the new model. This novel model consists of three contributions to the turbulent kinetic energy:

$$S_{kp} = \frac{\alpha \rho_p}{\tau_p}\left(\underbrace{\left|\overline{u}_i - \overline{u}_{pi}\right|^2}_{I} + \underbrace{\overline{u'_{pi}u'_{pi}}}_{II} \underbrace{-2k}_{III} \right) \tag{1}$$

Contribution I, the slip velocity squared, is interpreted as the production of turbulence resulting from the velocity gradients which again is due to the no slip condition imposed on the particle surface. Contribution II and III, respectively the particle and the fluids turbulent kinetic energy times two, is interpreted as the average effect of particle – eddy interaction. The mechanisms as explained from equation (89) are illustrated in Figure 4. It can be imagined that contribution I is the steady forcing term which can be related to the local flow field around an individual particle whereas term II and III is related to the average flow field energy balance or more vividly to the interaction between particles and eddies in an average formulation.

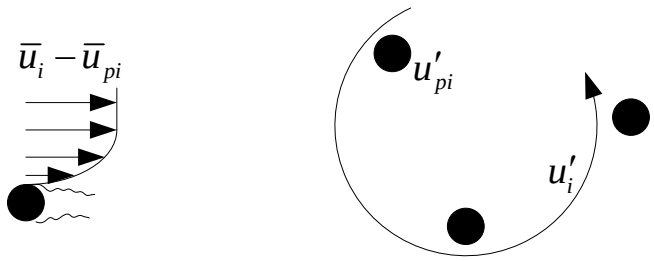

Figure 4: Illustration of mechanisms involved in particle – turbulence interaction.

The eddies/turbulence, represented by term III, are dampened by the presence of particles while simultaneously the fluctuating kinetic energy of the particles, represented by term III, act to transfer their energy to the turbulent eddies. For most practical cases contribution III are larger than contribution II which fit with the notion that the particles are accelerated by motion of the eddies. Figure 5 shows the evaluation of the different terms for pipe flow. It can be seen that contribution II decreases proportional to the distance of the wall indicating the particle wall collision influence on the fluctuating particle kinetic energy.

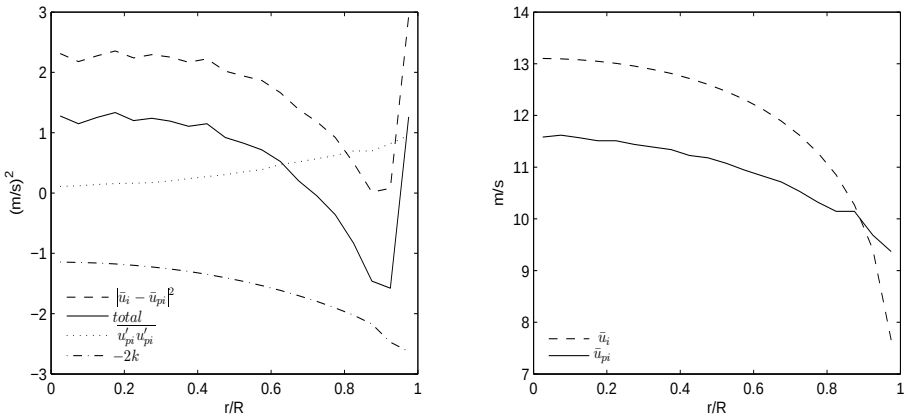

Figure 5: Evaluation of the different terms in the new model and mean flow velocity profiles for case 2.

Contribution I can be significantly greater than both contributions II and III for larger particles accelerated by gravity and totally negligible for very small particles or other cases where the drag force is much greater than the body forces. The experiments revealed that the magnitude of intensity change scaled with the particle volume fraction, the particle Reynolds number and the d_p/l_e ratio, but that none of these non-dimensional numbers alone could explain the observed trends. Each of these numbers can be interpreted as characterizing the mechanisms reveled by the rigorous theoretical derivation of the source term to the turbulent kinetic energy balance resulting from the presence of particles. As such the particle Reynolds number scales with the slip velocity which is found in contribution I and similarly the d_p/l_e ratio is inherently connected to the particle – eddy interaction which is reflected in contribution II and III.

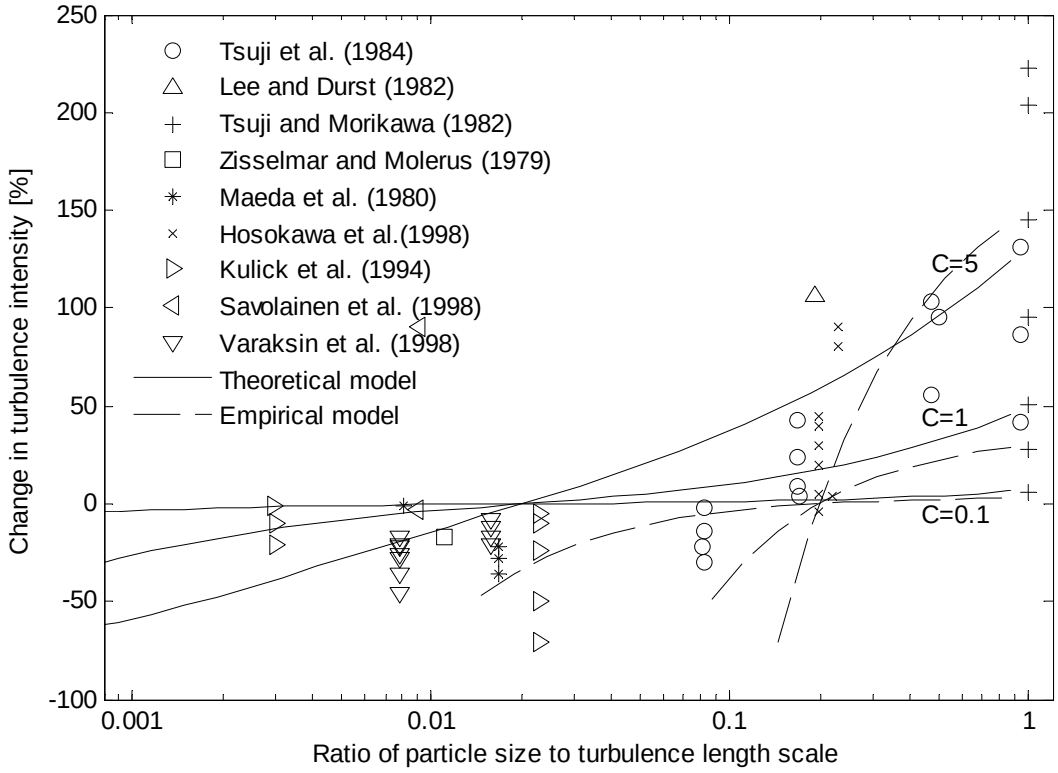

Figure 6: Comparison of model prediction and data for the turbulence modulation at the centerline of a vertical pipe.

The large amount of data generated from the parametric study also allowed the formulation of a pure empirical model which was able to predict the turbulence modulation for spherical particles in the range of experimental parameters:

$$\frac{\sigma-\sigma_0}{\sigma_0}\cdot 100\% = \frac{\dot{m}_p}{\mu d_p}\left(0.34\frac{d_p}{l_e}-0.05\right) \tag{2}$$

This is used to compare the turbulence modulation resulting from spherical particle with that experienced by non-spherical particles to determine the additional effect of shape. Note that this expression is only valid in the given range of values on which the expression is based. This can be emphasized by applying the expression to predict the intensity change at the centerline of a pipe. In Figure 6 it can be seen that the empirical expression predicts unrealistic values for low values of the d_p/l_e ratio suggesting that a higher order correlation is required.

However, as can be seen in Figure 7 top right it was found that this correlation was sufficient to predict the result for spheres for using different loading and size in the performed range of parameters. Performing additional experiments, using non-spherical particles with similar size and for similar loading, it is possible to show the additional effect of shape. For this two well-defined shapes were selected, disk and prolate spheroids. Firstly, it can be seen that the result for the non-spherical particles follows the seam trend as that

observed for spherical particles when the characteristic dimension used is the diameter of a volume equivalent sphere. Secondly, when compared with the expected values from the empirical model it is clear that there is some additional effect due to shape and that this effect is different for the two shapes considered.

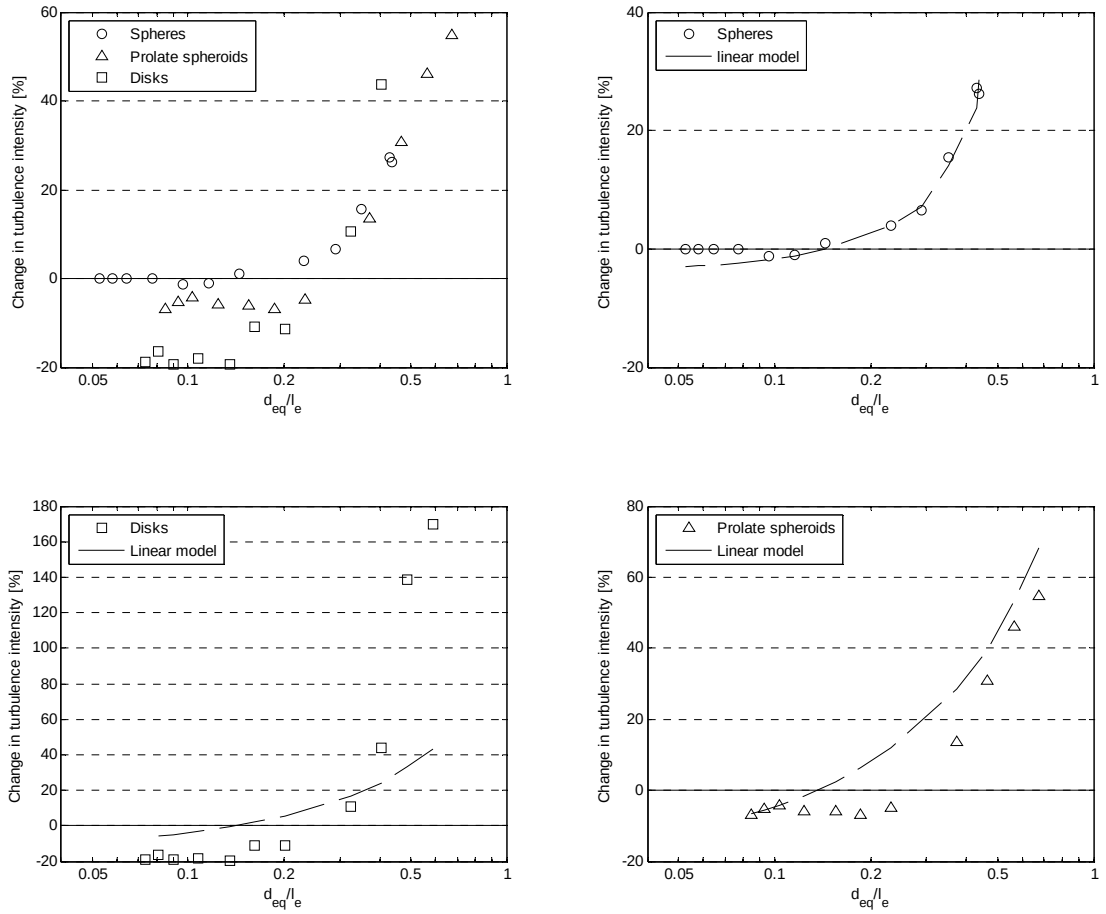

Figure 7: The percentage change in turbulence intensity versus the ratio of the volume equivalent particle diameter to the integral length scale of the clear flow for different particle types. Experimental results have been compared with an empirical model to predict the turbulence modulation inflicted by spherical particles. Notice that the y-axes are not the same for the figures.

The disks seem to have both a greater augmenting effect at high d_p/l_e ratios and greater attenuating effect at low ratios compared to spheres whereas prolate spheroids tended to attenuate the turbulence at all d_p/l_e ratios compared to spheres. The actual mechanisms involved for non-spherical particles is difficult state from this experiment and any statement made must be considered as speculation. However, it can be argued that the additional turbulence modification is a result of partly the mean motion and partly the interaction of the non-spherical particles with the turbulent eddies.

The theoretical model has been implemented into the framework of Computational Fluid Dynamics and coupled to the commercial code Fluent using User Defined Functions. The derived model is applied as a source term for the standard k-ε model. The choice of a

commercial code and the standard k-ε model is made such that the model can be applied for a wide range of engineering flows since additional sub-models can be added by selection using the Fluent GUI. When this model is applied on the combusting flow emerging from a commercial multifuel burner firing straw and coal respectively it is shown that straw combustion is associated with a significant longer flame and smaller recirculation zones compared to coal combustion.

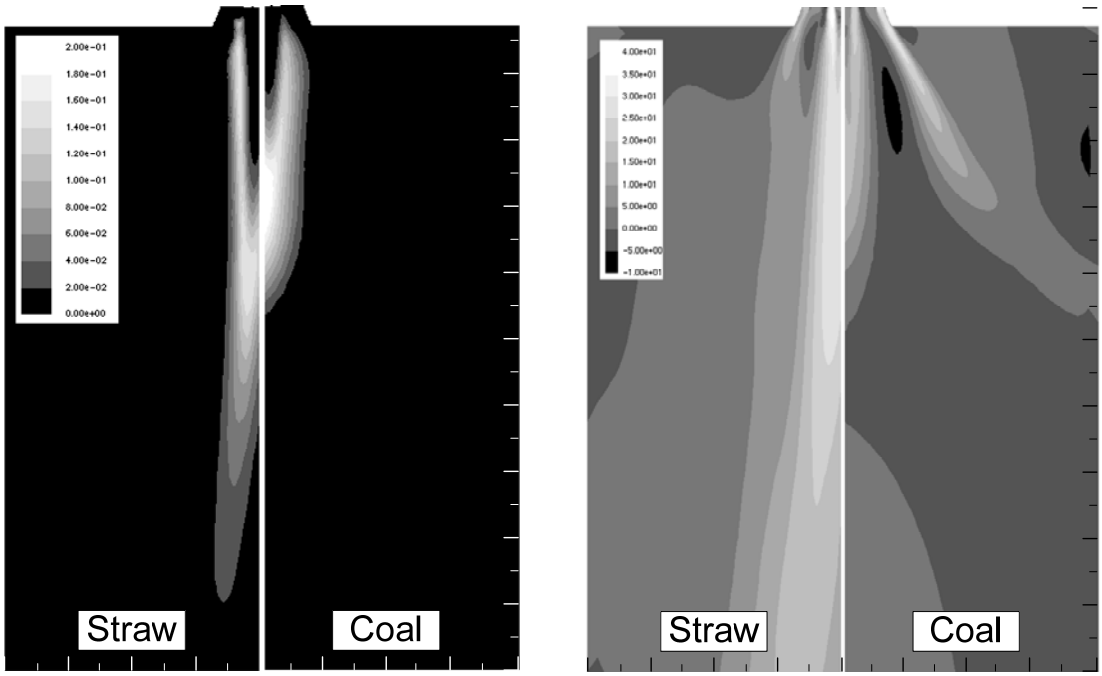

Figure 8: Left: Contours of CH_xO_y volume fraction on horizontal half plane. Right: Contours of axial velocity [m/s] on horizontal half plane. Grid: 4x10m

List of publications

Aerodynamics of large non-spherical particles (2010). Mandø, Matthias, Rosendahl, Lasse. ERCOFTAC Bulletin, Vol. 82, 2010, p. 55-60.

Measurement of Turbulence Modulation by Non-Spherical Particles (2010). Mandø, Matthias, Rosendahl, Lasse. Proceedings of the International Conference on Multiphase Flow, ICMF 2010. University of Florida, 2010.

Numerical Investigation of Large Particles in Upward Pipe Flow with Sinusoidal Wall Boundary Condition (2010). Mandø, Matthias, Rosendahl, Lasse. Poster presented at International Conference on Multiphase Flow, ICMF 2010, Tampa, Florida, United States.

On the motion of non-spherical particles at high Reynolds number (2010). Mandø, Matthias, Rosendahl, Lasse. Powder Technology, Vol. 202, No. 1-3, 10.2010, p. 1-13.

Pulverized straw combustion in a low-NOx multifuel burner: Modeling the transition from coal to straw (2010). Mandø, Matthias, Rosendahl, Lasse, Yin, Chungen, Sørensen, Henrik. Fuel , Vol. 89, No. 10, 10.2010, p. 3051-3062

Turbulence Modulation by Non-Spherical Particles. Mandø, Matthias. PhD Dissertation, Department of Energy Technology, Aalborg University, 2009.

Turbulence modulation in dilute particle-laden flow (2009). Mandø, Matthias, Lightstone, M. F., Rosendahl, Lasse, Yin, Chungen, Sørensen, Henrik. International Journal of Heat and Fluid Flow, Vol. 30, No. 2, 19.01.2009, p. 331-338.

On the modelling of motion of non-spherical particles in two-phase flow (2007). Mandø, Matthias, Yin, Chungen, Sørensen, Henrik, Rosendahl, Lasse. Proceedings of The 6th International Conference on Multiphase Flow, ICMF 2007: CD-Rom. 2007.

In review:
Mando, M. and Rosendahl, L. "Particle statistics of gas-solid pipe flow with smooth and rough wall boundary conditions", submitted to International Journal of Multiphase Flow

Mandø, M., Sørensen, H., Yin, C., Rosendahl, L., and Eriksson, J. "Experiences in measurement of turbulence modulation by large particles using LDA", Journal paper, submitted to Experiments in Fluids

Conferences & meetings attended

6th International Conference on Multiphase Flow, ICMF 2007, Leipzig, Germany, 9-13 July 2007
ITI International Conference on Turbulence, 2008, Bertino, Italy
3rd Nordic Conference on Fluid Dynamics in the Power Industry, 2009, Copenhagen
SIAMUF Multiphase Flows Meeting, 2009, Gothenburg, Sweden
7th International Conference on Multiphase Flow, ICMF 2010, Tampa, Florida, USA, 30 May – 4 June 2010
12th ERCOFTAC Workshop on Multiphase Flows, 22-25 March 2010, Halle, Germany
DANSIS research seminar, 2010, Copenhagen

References

Apte, S.V., Mahesh, K., Moin, P., Oefelein, J.C. 2003. *Large-eddy simulation of swirling particle-laden flows in a coaxial-jet combustor*. International Journal of Multiphase Flow, 29, 1311–1331.

Bharadwaj, A., Baxter, L.L., Robinson, A.L. 2004. *Effects of Intraparticle Heat and Mass Transfer on Biomass Devolatilization: Experimental Results and Model Predictions*. Energy & Fuels, 18, 1021-1031

Black, D.L., and McQuay, M.Q. 2001. *Laser-based particle measurements of spherical and nonspherical particles.* International Journal of Multiphase Flow, 27, 1333-1362.

Boulet, P., Moissette, S. 2002. *Influence of the particle–turbulence modulation modeling in the simulation of a non-isothermal gas–solid flow.* International Journal of Heat and Mass Transfer, 45, 4201–4216.

Bryden, K.M. & Hagge M.J. 2003. *Modeling the combined impact of moisture and char shrinkage on the pyrolysis of a biomass particle*. Fuel, 82, 1633-1644.

Crowe, C.T. 2000. *On models for turbulence modulation in fluid-particle flows*. International Journal of Multiphase Flow, 26, 719-727.

Demirbas, A. 2005*. Potential applications of renewable energy sources, biomass combustion problems in boiler power systems and combustion related environmental issues*. Progress in Energy and Combustion Science, 31, 171–192.

Di Blasi, C. 1996. *Heat, momentum and mass transport through a shrinking biomass particle exposed to thermal radiation*. Chemical Engineering Science, 51, 1121-1132.

ESR21. 2003. ESR21 Network research strategy 'Particulates in Electricity Generation Plant'. 05/2003, from Electricity Supply Research network website, http://www.nottingham.ac.uk/esrnetwork

Fluent6.2.16. 2005. User's Guide. Chapter 9 and Chapter 23. Fluent Inc.

Gera, D., Mathur, M.P., Freeman, M.C., Robinson, A., 2002. *Effect of large aspect ratio of biomass particles on carbon burnout in a utility boiler*. Energy & Fuels, 16, 1523-1532.

Gore, R.A., Crowe, C.L. 1989. *Effect of particle size on modulating turbulent intensity*. International Journal of Multiphase Flow, 15, 279-291.

Grow, D.T., 1990. *Mass and heat transfer to an ellipsoidal particle*. Combustion and Flame, 80, 209-213.

Hadinoto, K., Jones, E.N., Yurteri, C., Curtis, J.S. 2005. *Reynolds number dependence of gas-phase turbulence in gas-particle flows*. International Journal of Multiphase Flow, 31, 416–434

Hein, K.R.G., Bemtgen, J.M., 1998. *EU clean coal technology— co-combustion of coal and biomass*. Fuel Processing Technology, 54, 159-169.

Jianren Fan, Kun Luo, Man Yeong Ha and Kefa Cen. *Direct numerical simulation of a near field particle-laden plane turbulent jet. Physical Review E.*, 2004,70,026303.

[Jianren Fan, Kun Luo, Youqu Zheng, Hanhui Jin and Kefa Cen. *Modulation on coherent vortex structures by dispersed solid particles in a three-dimensional mixing layer*. *Physical Review E.*, 2003, 68(3), 036309.

Klett, J.D., 1995*. Orientation model for particles in turbulence*. J. Atmos. Sci. 52, 2276-2285.

Kun Luo, Jianren Fan and Kefa Cen. *DNS of the modulation on turbulent characteristics by dispersed particles in gas-solid two-phase jets*. *Proceedings of the Royal Society of London A*, 2005 (Accepted).

Kussin, J., Sommerfeld, M. 2002. *Experimental studies on particle behaviour and turbulence modification in horizontal channel flow with different wall roughness*. Experiments in Fluids, 33, 143–159.

Mashayek, F., and Pandya, R.V.R. 2003. *Analytical description of particle/droplet-laden turbulent flows*. Progress in Energy and Combustion Science, 29, 329–378.

Maxey, M.R., Riley, J.J., 1983. *Equation of motion for a small rigid sphere in a nonuniform flow.* Physics of Fluids, 26, 883-889.

Nussbaumer, T., 2003. *Combustion and co-combustion of biomass: fundamentals, technologies, and primary measures for emission reduction*. Energy & Fuels, 17, 1510-1521.

Sami, M., Annamalai, K., Wooldridge, M., 2001. *Co-firing of coal and biomass fuel blends*. Progress in Energy and Combustion Science, 27, 171-214.

Paris, A.D. and Eaton, J.K. (2001). Turbulence attenuation in a particle laden channel flow. Mech. Eng. Dept., Stanford University Report.

Rosendahl, L. (1998). Extending the modelling framework for gas-particle systems. Applications of multiparameter shape descriptions to non-conventional solid fuels in reacting and non-reacting environments. PhD Thesis, Aalborg University 1998. ISBN 87-89179-25-0

Rosendahl, L. (January, 2000). *Using a Multi-parameter Particle Shape Description to Predict the Motion of Non-spherical Particle Shapes in Swirling Flow.* Applied Mathematical Modelling, January 2000, Vol. 24, pp 11-25

Shin, D. & Choi, S. 2000. *The combustion of simulated waste particles in a fixed bed*. Combustion and Flame, 121, 167-180.

Appendix

Aerodynamics of large non-spherical particles (2010). Mandø, Matthias, Rosendahl, Lasse. ERCOFTAC Bulletin, Vol. 82, 2010, p. 55-60.

Measurement of Turbulence Modulation by Non-Spherical Particles (2010). Mandø, Matthias, Rosendahl, Lasse. Proceedings of the International Conference on Multiphase Flow, ICMF 2010. University of Florida, 2010.

Numerical Investigation of Large Particles in Upward Pipe Flow with Sinusoidal Wall Boundary Condition (2010). Mandø, Matthias, Rosendahl, Lasse. Poster presented at International Conference on Multiphase Flow, ICMF 2010, Tampa, Florida, United States.

On the motion of non-spherical particles at high Reynolds number (2010). Mandø, Matthias, Rosendahl, Lasse. Powder Technology, Vol. 202, No. 1-3, 10.2010, p. 1-13.

Pulverized straw combustion in a low-NOx multifuel burner: Modeling the transition from coal to straw (2010). Mandø, Matthias, Rosendahl, Lasse, Yin, Chungen, Sørensen, Henrik. Fuel , Vol. 89, No. 10, 10.2010, p. 3051-3062

Turbulence modulation in dilute particle-laden flow (2009). Mandø, Matthias, Lightstone, M. F., Rosendahl, Lasse, Yin, Chungen, Sørensen, Henrik. International Journal of Heat and Fluid Flow, Vol. 30, No. 2, 19.01.2009, p. 331-338.

On the modelling of motion of non-spherical particles in two-phase flow (2007). Mandø, Matthias, Yin, Chungen, Sørensen, Henrik, Rosendahl, Lasse. Proceedings of The 6th International Conference on Multiphase Flow, ICMF 2007: CD-Rom. 2007.

Turbulence Modulation by Non-Spherical Particles. Mandø, Matthias. PhD Dissertation, Department of Energy Technology, Aalborg University, 2009 (separate file).

Aerodynamics of Large Non-Spherical Particles

M. Mandø & L. Rosendahl

Aalborg University, Department of Energy Technology, Denmark.
mma@iet.aau.dk, lar@iet.aau.dk

1 Introduction

Non-spherical particles are found in most industrial particulate flows. However, the vast majority of scientific investigations of particulate flows assume particles to be perfect spheres. For irregular, near spherical particles modification to the drag coefficient using shape factors can be applied, but these becomes increasingly inaccurate at increasing aspect ratios. Non-spherical particles at Re>100 are associated with significant secondary motion which also can affect the primary motion of the particle. This entitles an altogether different methodology, where also the orientation of the particle should be considered. This paper attempts to give an account of the present state of modeling the motion of large non-spherical particles. The relevance of this paper also becomes evident considering the increasing efforts towards the replacement of pulverized coal with biomass in existing and new power plants. Whereas pulverized coal particles are small and the spherical ideal is considered a good approximation, pulverized biomass particles can be characterized as being large and with high aspect ratios due to their fibrous nature. This investigation is limited to the Eulerian-Lagrangian methodology and to solid non-deforming particles in Newtonian fluids.

2 Equations of motion

Whether spherical or non-spherical, regular or irregular, the motion of particles is derived by considering the conservation of linear and angular momentum. In differential form the equations can be stated as:

$$\frac{d\vec{x}}{dt} = \vec{u}_p, \qquad m_p \frac{d\vec{u}_p}{dt} = \sum_i \vec{F}_i \tag{1}$$

$$\frac{d\vec{\theta}}{dt} = \vec{\omega}_p, \qquad \vec{I}_p \frac{d\vec{\omega}_p}{dt} = \sum_i \vec{T}_i \tag{2}$$

where x is the position vector, u_p is the particle linear velocity, m_p is the particle mass, F is the force acting on the particle, θ is the angle between the principle axis of the particle and the inertial coordinate system, ω_p is the angular velocity, I_p is the moment of inertia and T is the torque acting on the particle. Where eq. (1) deals with the location and linear velocity of the particle, eq. (2) is responsible for the orientation and the angular velocity. Eq. (1) and (2) nicely demonstrate the similarity between translational and rotational motion. However, these equations are only strictly correct for a particle which is symmetric around the center of mass (a sphere). For a generic non-spherical particle it is necessary to include additional terms which address the difference of the moment of inertia in the different directions:

$$\begin{aligned} I_{x'} \tfrac{d\omega_{x'}}{dt} &= \textstyle\sum T_{x',i} + \omega_{y'}\omega_{z'}\left(I_{y'} - I_{z'}\right) \\ I_{y'} \tfrac{d\omega_{y'}}{dt} &= \textstyle\sum T_{y',i} + \omega_{z'}\omega_{x'}\left(I_{z'} - I_{x'}\right) \\ I_{z'} \tfrac{d\omega_{z'}}{dt} &= \textstyle\sum T_{z',i} + \omega_{x'}\omega_{y'}\left(I_{x'} - I_{y'}\right) \end{aligned} \tag{3}$$

Generally, the particle translation is evaluated in the inertial coordinate system whereas the particle rotation is evaluated in the co-rotational coordinate system as seen in Figure 1.

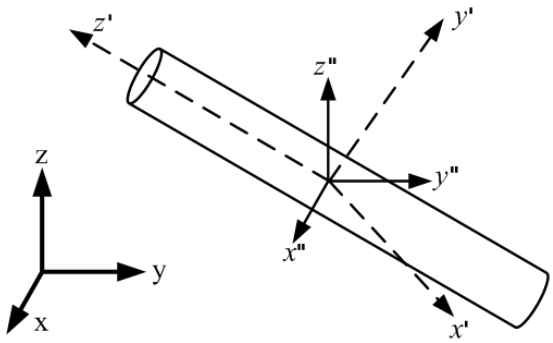

Figure 1: *The inertial* (x, y, z)*, the co-rotational* (x', y', z') *and the co-moving* $(x", y", z")$ *coordinate systems.*

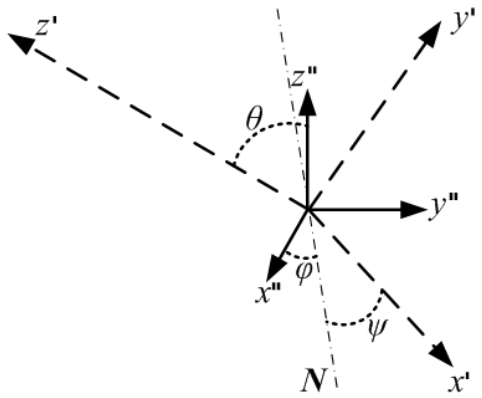

Figure 2: *Euler angles:* N*=plane*$(x', y') \cap$ *plane*(x'', y'').

The transformation between the co-moving and the co-rotational coordinates is accomplished by means of a transformation matrix, **A** [1]:

$$\vec{x}' = \mathbf{A}\vec{x}'' \tag{4}$$

where the elements in A represent the directional cosines of the angles $[\theta, \phi, \psi]$ between the principle axis of the co-rotational and the co-moving coordinate system as seen in Figure 2. These angles are also known as the Euler angles. However, these angles are not suitable for particles which undergo full rotation due to a singularity which occurs when they are used in relation to the angular velocities of the particle. Instead Euler's four parameters $[\varepsilon_1, \varepsilon_2, \varepsilon_3, \eta]$, which are also known as quaternions, are used. The four Euler parameters represent an expansion of the three Euler angles to eliminate the singularity. The transformation matrix, **A**, using the Euler parameters is given as [2]:

$$\begin{bmatrix} 1-2\left(\varepsilon_2^2+\varepsilon_3^2\right) & 2\left(\varepsilon_2\varepsilon_1+\varepsilon_3\eta\right) & 2\left(\varepsilon_1\varepsilon_3-\varepsilon_2\eta\right) \\ 2\left(\varepsilon_2\varepsilon_1-\varepsilon_3\eta\right) & 1-2\left(\varepsilon_3^2+\varepsilon_1^2\right) & 2\left(\varepsilon_3\varepsilon_2+\varepsilon_1\eta\right) \\ 2\left(\varepsilon_1\varepsilon_3+\varepsilon_2\eta\right) & 2\left(\varepsilon_3\varepsilon_2-\varepsilon_1\eta\right) & 1-2\left(\varepsilon_1^2+\varepsilon_2^2\right) \end{bmatrix} \tag{5}$$

Where the Euler parameters are related to the Euler angles by the following relations:

$$\begin{array}{ll} \varepsilon_1 = \cos\frac{\phi-\psi}{2}\sin\frac{\theta}{2}, & \varepsilon_2 = \sin\frac{\phi-\psi}{2}\sin\frac{\theta}{2}, \\ \varepsilon_3 = \sin\frac{\phi-\psi}{2}\cos\frac{\theta}{2}, & \eta = \cos\frac{\phi-\psi}{2}\cos\frac{\theta}{2} \end{array} \tag{6}$$

and the time rate of change of the Euler parameters is calculated by:

$$\begin{bmatrix} \frac{d\varepsilon_1}{dt} \\ \frac{d\varepsilon_2}{dt} \\ \frac{d\varepsilon_3}{dt} \\ \frac{d\eta}{dt} \end{bmatrix} = \frac{1}{2}\begin{bmatrix} \eta\omega_{x'} - \varepsilon_1\omega_{y'} + \varepsilon_2\omega_{z'} \\ \varepsilon_3\omega_{x'} + \eta\omega_{y'} - \varepsilon_1\omega_{z'} \\ -\varepsilon_2\omega_{x'} + \varepsilon_1\omega_{y'} + \eta\omega_{z'} \\ -\varepsilon_1\omega_{x'} - \varepsilon_2\omega_{y'} - \varepsilon_3\omega_{z'} \end{bmatrix} \tag{7}$$

Similar to that most studies involving particles assume a spherical shape, most studies involving non-spherical particles assumes Stokes flow. For a non-spherical particle in Stokes flow it is possible to derive the steady states resistance force and torque which act on the particle on a theoretical basis [3]. However, unsteady forces, such as virtual mass and Basset history force remain to be formulated for non-spherical particles. The main difficulty seems to be the coupling of the unsteady terms with the orientation of the particle. One study tried to derive the full equated motion for creeping flow by simplifying the problem. As such, Lawrence and Weinbaum [4],[5] conducted a study on a slightly eccentric ellipsoid of revolution with major semi-axis $b = a(1+\varepsilon)$, in oscillatory cross flow, where only translational motion was considered. In addition to relevant expansions of the steady state, virtual mass and Basset force a new time dependent term emerged related to the eccentricity. This shows the magnitude of the awaiting challenge and suggests that BBO-equation perhaps only is an asymptotic solution for a more general formulation as the shape goes towards complete symmetry around the center of geometry. When considering non-spherical particles in Stokes flow especially the work by Fan and Ahmadi [6],[7] should be accentuated. There a complete formulation of the resistance forces as well as shear induced lift can be found along with a discussion of the importance of the individual terms.

For non-spherical particles at higher Reynolds numbers, appropriate expansions could be obtained by including empirical coefficients in front of the force and torques. However, it is also necessary to account for the offset of the center of pressure in relation to the center of geometry, x_{cp}, as seen in Figure 3.

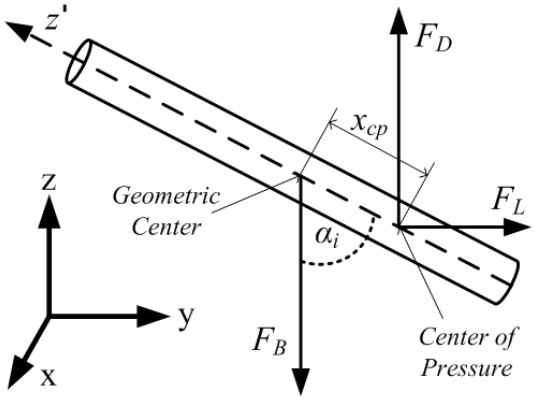

Figure 3: *The location of the center of pressure, the inclination angle α and the resulting forces acting on a falling non-spherical particle.*

The pressure distribution on the surface of a particle inclined to the flow direction does no longer follow the symmetry of that particle. This gives rise to an additional lift force as well as an addition torque due to the displacement of the center of pressure. Besides this, the main complication when considering non-spherical particles is the endless variations of the shape of the particle. To combat this, most investigations include some sort of parameter variation in the formulation of forces and torques. The most popular being the ellipsoid of revolution which can be used to resemble a large array of different shapes including flake-like particles and rod-like particles. A distinctive advantage of the ellipsoid of revolution is that it has no sharp edges which in a mathematical analysis would be seen as discontinuities.

3 Orientation dependent drag

With regards to the drag force the main advantage for an orientation dependent calculation method is that the drag is calculated on basis of the projected area, evaluated at the present orientation of the particle:

$$\vec{F}_{Drag} = \frac{1}{2}C_D\rho A_p\left|\vec{u}-\vec{u}_p\right|\left(\vec{u}-\vec{u}_p\right) \tag{8}$$

The challenge, with regards to the drag force, is the proper formulation of the drag coefficient which is applicable for a large range of Reynolds numbers, shapes and orientations. It has become common practice to procure empirical fits at a range of Reynolds number for a specific shape. Some fits also includes a parametric variation of the shape e.g. the aspect ratio of a cylinder or a spheroid. However, these expressions are usually based on either a fixed orientation or a freely falling particle. Thus, correlations of the drag coefficient, which consider the inclination angle, are not widely available. Two approaches have been proposed to address this predicament: The work of Rosendahl [8] suggests using a 'blending' function between the drag coefficient for flow normal and parallel to the major axis of the particle:

$$C_D\left(\alpha\right) = C_{D,\alpha=0} + \left(C_{D,\alpha=90} - C_{D,\alpha=0}\right)\sin^3\alpha \tag{9}$$

where α is the angle between the major axis of the particle and the flow direction. Here the projected area at the evaluated orientation is used in the calculation of the drag force. Secondly, the work by Yin et al. [9] suggests using available drag correlations expressed by the

sphericity and thus solely accounting for the dependence of orientation by using the projected area in the calculation of the drag force. Recently, a third option has been presented. Based on a plethora of empirical data for fixed and freely falling particles Hölzer and Sommerfeld [10] came up with an expression which uses a cross-wise, $\psi_\perp$, and lengthwise sphericity, $\psi_{||}$, to account for the drag coefficient of different shapes at different orientations:

$$C_D = \frac{8}{\mathrm{Re}}\frac{1}{\sqrt{\psi_\parallel}} + \frac{16}{\mathrm{Re}}\frac{1}{\sqrt{\psi}} + \frac{3}{\mathrm{Re}}\frac{1}{\sqrt{\psi^{3/4}}} + 0.4210^{0.4(-\log\psi)^{0.2}}\frac{1}{\psi_\perp} \quad (10)$$

Here the cross-wise sphericity is the ratio between the cross-sectional area of the volume equivalent sphere and the projected area of the actual particle. The lengthwise sphericity is the ratio between the cross-sectional area of the volume equivalent sphere and the difference between half of the surface area and the mean projected area. The cross-wise sphericity should thus aid in the correlation of the form drag while the lengthwise sphericity is expressive of the friction drag. Note that here the Reynolds number and the drag coefficient are based on the volume equivalent sphere.

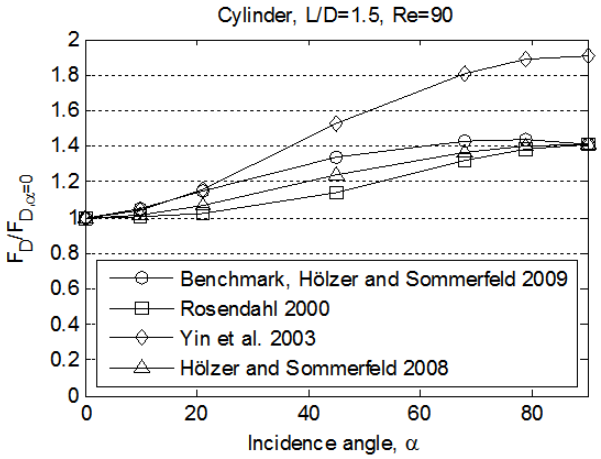

Figure 4: *Evaluation of the different approaches to correlate the drag coefficient with the incidence angle.*

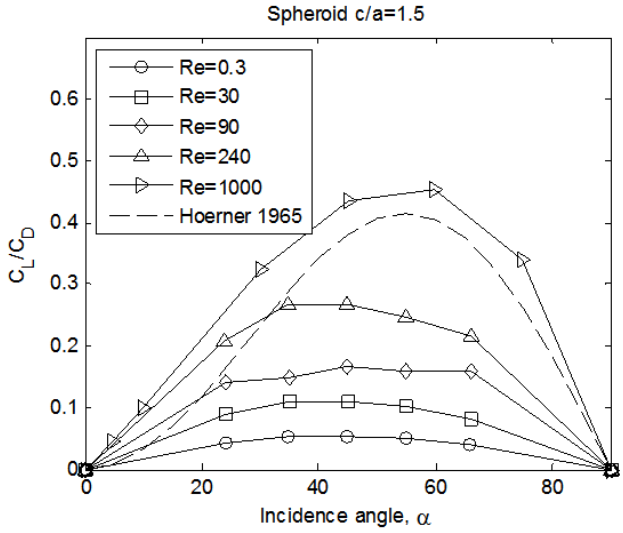

Figure 5: *Lift/drag ratio at different Reynolds numbers [11], [15].*

Figure 4 shows the drag force for a cylinder at different orientations, normalized with the drag force at zero incidence angle, calculated using the three suggested methods and compared to the benchmark (lattice-Boltzmann simulations) by Hölzer and Sommerfeld [11]. Overall, it may be noted that the drag force increases with increasing incidence angles due to the increase in projected area. However, this alone is not sufficient to properly account for the observed results.

The method by Rosendahl [8] provides a pragmatic way to calculate the drag force at different incidence angles but also relies upon the availability of experimental data. For regular shapes these can typically be found for particles at 90 degree incidence angle whereas empirical fits for particles at zero incidence angle are not widely available. In this regard it might be useful to refer to the studies by Militzer et al. [12] which provide a parametric fit for spheroids as a function of the Reynolds number and the aspect ratio as well as Isaacs and Thodos [13] which provide the same for disks and cylinders at 90 degrees incidence angle. For the present benchmark data it may be noted that a 'blending' function using $\sin(\alpha)$ instead of $\sin^3(\alpha)$ provides a superior fit. Hölzer and Sommerfeld [10] constitute a good fit of the present benchmark data and attractively addresses all possible shapes at all Reynolds numbers in a single expression. However, this also indicates that for some specific shapes such a correlation, similar to the one by Yin et al. [9], might be associated with relatively large errors compared to correlations developed for that specific shape.

4 Orientation dependent lift

The lift force accounts for the sideward motion and is present whenever the particles principle axis is inclined to the main flow direction. With a concept taken from aerodynamics this can be explained as 'profile' lift. The theoretical and empirical basis of predicting the profile lift relies at much more scant information compared to that available for drag. For symmetric particles the lift is zero at both α=0° and α=90° and it assumes a maximum somewhere in between, depending on the shape and Reynolds number. The usual assumption has been to assume that the lift is proportional to the drag and that the dependence with the orientation is given by the so-called 'cross-flow principle' [14]:

$$\frac{C_L}{C_D} = \sin^2\alpha \cdot \cos\alpha \quad (11)$$

This relationship was developed for infinite cylinders at Reynolds numbers in the Newtons law regime. Figure 5 shows data for a spheroid with small aspect ratio together with the cross-flow principle from eq. (11).

It can be seen that the cross-flow principle provides a fair fit to the present data at Reynolds numbers in the Newtons law regime whereas the maximum lift/drag ratio diminishes as the Reynolds number decreases. This is related to the relative importance of the friction and pressure drag at these intermediate Reynolds numbers. Here we provide the following fit to the present data set ($30<Re<1500$) to correlate the influence of the Reynolds for the cross-flow principle:

$$\frac{C_L}{C_D} = \frac{\sin^2\alpha \cdot \cos\alpha}{0.65 + 40Re^{0.72}} \quad (12)$$

This expression gives correct asymptotic values for large and small Reynolds numbers but is based on a narrow dataset with resulting low accuracy. It should also

be noted that data shown in Figure 5 is for a spheroid with relatively low aspect ratio. It seems like the better the shape approximates an infinite long cylinder the clearer the resemblance with the cross-flow principle becomes. Once the lift coefficient is specified the lift force can be found using an expression equivalent to eq. (8).

5 Offset of the center of pressure

In order to correctly predict the incidence angle for estimating the forces and torques, it is of prime importance to locate the center of pressure. As previously stated a non-spherical particle tends to fall with its largest cross-sectional area normal to the flow direction i.e. α=90°. Here the center of pressure is coincidental with the geometric center and lift force and torque are zero. Hence this can be described as the state of stable equilibrium of the particle. A non-spherical particle inclined to the flow direction with α=0° will also experience no lift or torque but this can instinctively be perceived as an unstable equilibrium. At this extreme, the center of pressure must therefore be no-coincidental with the geometric center to match observed behavior. Using concepts from airfoil theory the center of pressure at this extreme inclination is placed at the 'quarter chord point' which is equivalent to half the distance from the geometric center to the end of the particle being oriented towards the flow [8],[9]. Please refer to Figure 3 for visual illustration. Marchildon et al. [16] provides a linear approximation to the derivation by Rayleigh [17] for the pressure distribution on an infinite flat plate to predict the center of pressure of a cylinder. This is reported by Marchildon et al. [16] to be valid for inclinations above α=15° due to the uniformity of the pressure distribution above this angle. Both Rosendahl [8] and Yin et al. [9] present expressions which close the gap with regards to the location of the center of pressure between the two extremes.

Rayleigh [17]	$x_{cp}/L = (3/4)\,(\sin\alpha_i)/(4+\pi\cos\alpha_i)$
Marchildon et al.[16]	$x_{cp}/L = (90-\alpha_i)/480$
Rosendahl [8]	$x_{cp}/L = 0.25\left(1-\sin^3\alpha_i\right)$
Yin [9]	$x_{cp}/L = 0.25\cos^3\alpha_i$

Table 1: *Expressions to find the center of pressure.*

Figure 6 shows an illustration of the different expressions and it can be seen there is some discrepancy in the prediction of the center of pressure. More unfortunately, there seems not to be any guidelines towards which expression is the most appropriate to use. A freely falling non-spherical particle will spend most of the time close to α=90° and effort should thus be directed towards finding the best fit close to this point.

Assuming that Rayleigh's derivation is valid for general non-spherical particles at intermediate Reynolds numbers it seems attractive to use the simple linear fit by Marchildon et al. [16]. Once the lift and drag forces are found as well as the location of their point of attack, i.e. the center of pressure, it is a small matter of calculating the resulting torque which is due to the offset from the geometric center, T_{offset}.

$$\vec{T}_{offset} = x_{cp}\left(\vec{F}_{Lift} + \vec{F}_{Drag} + \vec{F}_{Other}\right) \qquad (13)$$

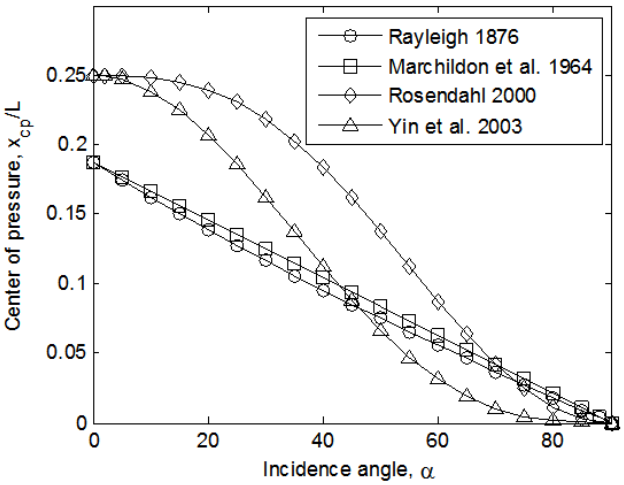

Figure 6: *Location of the center of pressure for a cylinder with length L, using the different expressions.*

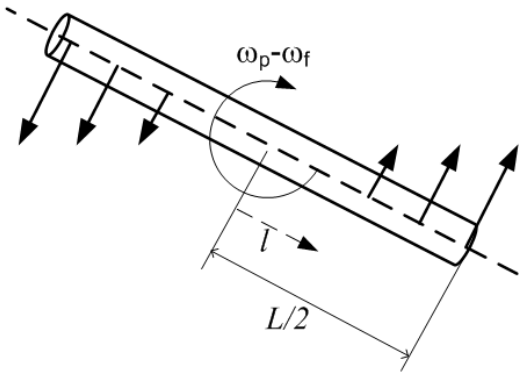

Figure 7: *Resistance towards rotation.*

6 Rotational resistance

The torque due to resistance can be directly derived by integration of the friction, caused by rotation, over the length of the particle. For spheroids subject to the Stokes conditions, solutions have been known since Jeffery [3] and have since been expanded to other shapes [18]. Relevant expansions for higher Reynolds number can be found by incorporating appropriate fits for the drag coefficient in the definition of the drag force before the integration is performed.

$$\begin{aligned}\vec{T}_{resist} &= 2\int_0^{L/2}\vec{F}_{resist}dl \\ &= \int_0^{L/2} C_{D,cyl}\rho\,(\omega_f-\omega_p)^2 l^2 A_p dl\end{aligned} \qquad (14)$$

This integral can be evaluated with increasing degree of sophistication. Note that if the particles aspect ratio is sufficiently large the angular velocity will tend to be low and an assumption of creeping flow may suffice.

7 Other forces and torques

The unraveling of orientation dependent models up to now constitutes a description of the minimum number of forces and torques which are required for the modeling of non-spherical particles. For specific problems it may be necessary to address additional forces and torques. For general fluid flow, these other forces are primary those

caused by pressure and velocity gradients as well as unsteady forces such as virtual mass and Basset history force. Some of these forces may be evaluated by simple expansions of the equivalent expressions derived for a sphere whereas others, such as the Basset force, are utterly hopeless to be evaluated for non-spherical particles even in creeping flow. As a general guideline these forces may be accounted for by using the projected area or an equivalent diameter as is suggested in the approach by Rosendahl [15]. Clearly, order-of-magnitude estimates may be performed for the unsteady forces acting on non-spherical particles similar to those which are custom to be performed for spheres and thus for most gas-solid flows it is justified to neglect the unsteady forces. For a freely falling cylinder in water it is not possible to neglect the unsteady forces. By the nature of this process these non-spherical particles are oscillating. As such Sorensen et al. [19] found that the terminal velocity of a steady falling cylinder slightly oscillated in tune with the larger oscillations of the angular velocity. For that investigation an intricate expansion of the drag force, depending on the angular acceleration was developed to account for the unsteady forces. However, the general application of this expression in the calculation procedure presented here is not possible. For small non-spherical particles it might be necessary to model non-continuum effects. This is addressed in the study by Fan and Ahmadi [6] which introduces both an additional Brownian force and a Brownian torque in the equations of motion to supplement the fluid dynamic forces. At the same time the fluid dynamic forces are modified by introducing approximations of the translational and rotational slip factors. There, in an Eulerian-Lagrangian framework, the nature of Brownian motion is modeled as a Gaussian random process. Considering the similarities between Brownian and turbulent motion such an approach also indicates possible approaches for non-spherical particles in turbulent flow. Also note that the effect of velocity gradients has already been incorporated into the expression for rotational resistance, eq.(14), though the vorticity of the flow field.

8 Conclusion

This outline on the motion of large non-spherical particles is made to give an overview of the present status of this topic. The additional consideration of orientation and angular velocity gives a number of decisive advantages. Firstly, by modeling the orientation dependent forces and torques it is possible to predict the secondary motion caused by the non-spherical shape. Secondly, the modeling of non-spherical particles in the Lagrangian reference frame, without the severe restriction of creeping flow allows for the possibility to use this methodology on a variety of engineering flows which contain large non-spherical particles. Thirdly, it should be noted that the solution procedure is only around twice as computational intensive compared to the present implementation in commercial codes.

References

[1] Goldstein, H. 1980, *Classical Mechanics*, Addison-Wesley Press.

[2] Hughes, P.C. 1986, *Spacecraft Attitude Dynamics*, Wiley.

[3] Jeffery, G.B. 1922, *The Motion of Ellipsoidal Particles Immersed in a Viscous Fluid*, Proceedings of the Royal Society of London.Series A, vol. 102, no. 715, pp. 161-179.

[4] Lawrence, C.J., Weinbaum, S. 1988, *The Unsteady Force on a Body at Low Reynolds-Number - the Axisymmetric Motion of a Spheroid*, Journal of Fluid Mechanics, vol. 189, pp. 463-489.

[5] Lawrence, C.J., Weinbaum, S. 1986, *The Force on an Axisymmetrical Body in Linearized, Time-Dependent Motion - a New Memory Term*, Journal of Fluid Mechanics, vol. 171, pp. 209-218.

[6] Fan, F.G., Ahmadi, G. 2000, *Wall deposition of small ellipsoids from turbulent air flows - A Brownian dynamics simulation*, Journal of Aerosol Science, vol. 31, no. 10, pp. 1205-1229.

[7] Fan, F.G., Ahmadi, G. 1995, *Dispersion of Ellipsoidal Particles in an Isotropic Pseudo-Turbulent Flow-Field*, Journal of Fluids Engineering-Transactions of the ASME, vol. 117, no. 1, pp. 154-161.

[8] Rosendahl, L. 2000, *Using a multi-parameter particle shape description to predict the motion of non-spherical particle shapes in swirling flow*, Applied Mathematical Modelling, vol. 24, no. 1, pp. 11-25.

[9] Yin, C.G., Rosendahl, L., Kaer, S.K., Sorensen, H. 2003, *Modelling the motion of cylindrical particles in a nonuniform flow*, Chemical Engineering Science, vol. 58, no. 15, pp. 3489-3498.

[10] Hölzer, A., Sommerfeld, M. 2008, *New simple correlation formula for the drag coefficient of non-spherical particles*, Powder Technology, vol. 184, no. 3, pp. 361-365.

[11] Hölzer, A., Sommerfeld, M. 2009, *Lattice Boltzmann simulations to determine drag, lift and torque acting on non-spherical particles*, Computers & Fluids, vol. 38, no. 3, pp. 572-589.

[12] Militzer, J., Kan, J.M., Hamdullahpur, F., Amyotte, P.R., Al Taweel, A.M. 1989, *Drag coefficient for axisymmetric flow around individual spheroidal particles*, Powder Technology, vol. 57, no. 3, pp. 193-195.

[13] Isaacs, J.L., Thodos, G. 1967, *Free-Settling of Solid Cylindrical Particles in Turbulent Regime*, Canadian Journal of Chemical Engineering, vol. 45, no. 3, pp. 150.

[14] Hoerner, J.F. 1965, *Fluid-dynamics drag*, Hoerner Fluid Dynamics (Published by the author).

[15] Rosendahl, L.A. 1998, *Extending the modelling framework for gas-particle systems*, PhD thesis, Aalborg University.

[16] Marchildon, E.K., Clamen, A., Gauvin, W.H. 1964, *Drag + Oscillatory Motion of Freely Falling Cylindrical Particles*, Canadian Journal of Chemical Engineering, vol. 42, no. 4, pp. 178.

[17] Rayleigh, Lord. 1876, *On the resistance of fluids*, Philosophical Magazine Series 5, vol. 2, no. 13, pp. 430-441.

[18] Cox, R.G. 1971, *Motion of Long Slender Bodies in a Viscous Fluid. Part 2. Shear Flow*, Journal of Fluid Mechanics, vol. 45, pp. 625-657.

[19] Sorensen, H., Rosendahl, L., Yin, C., Mandoe, M. 2007, *Settling of a cylindrical particle in a stagnant fluid*, Proceedings of The 6th International Conference on Multiphase Flow, ICMF 2007.

Measurement of Turbulence Modulation by Non-Spherical Particles

Matthias Mandoe and Lasse Rosendahl

Aalborg University, Department of Energy Technology
Pontoppidanstraede 101, 9220 Aalborg, Denmark
mma@iet.aau.dk

Keywords: Turbulence-particle interaction, particle-laden jet, Laser optical methods

Abstract

The change in the turbulence intensity of an air jet resulting from the addition of particles to the flow is measured using Laser Doppler Anemometry. Three distinct shapes are considered: the prolate spheroid, the disk and the sphere. Measurements of the carrier phase and particle phase velocities at the centerline of the jet are carried out for mass loadings of 0.5, 1, 1.6 and particle sizes 880µm, 1350µm, 1820µm for spherical particles. For each non-spherical shape only a single size and loading are considered. The turbulence modulation of the carrier phase is found to highly dependent on the turbulence length scale, the mass loading, and the particle size and less dependent on the particle Reynolds number and the Stokes number for the investigated range. The results are compared with existing criteria and an expression is suggested to predict the turbulence modulation given the particle size, the particle mass flow and the integral length scale of the flow. The expression developed on basis of spherical particles only is applied on the data for the non-spherical particles. The results suggest that non-spherical particles attenuate the carrier phase turbulence significantly more than spherical particles of similar size and concentration. The shape effect is more pronounced for disks than for prolate spheroids.

Introduction

The interaction between solid particles and gas phase turbulent flows is important for many engineering devices as well as natural accruing processes. Examples of these are the pneumatic transport of fine powders, the combustion of pulverized solid fuels, dust storms and the pollutant dispersion in the atmosphere. In each of these cases a fundamental understanding of the underlying phenomena which are responsible for the complex interaction between the particulate phase and the turbulent carrier flow is required to improve the design of engineering devices in which these flows occur. In the context of modeling dispersed multiphase flows, source terms to account for the momentum and heat exchange between the phases are well known and have been implemented correctly into commercial CFD codes (Crowe et al. 1977). However, in the framework of turbulent flows, the formulation of the source terms associated with the various closure schemes is sometimes far from satisfactory and the effect of particles on the carrier phase turbulence has yet to be convincingly implemented in many academic or commercial CFD codes.

General observations seem to suggest that small particles attenuate the carrier phase turbulence while larger particles tend to augment it. A number of effects are believed to be influencing the turbulence modulation observed. The most successful models, in the context of CFD, address this by having mechanisms for both the attenuation and the augmentation of turbulence. Additional turbulence is thus often seen as a result of the unstable wake behind large particles and the reduction of turbulence is seen as being dependent of the particles ability to follow the turbulent eddies (Yuan and Michaelides 1992). A small particle caught in a turbulent eddy will thus be accelerated by the fluid motion and momentum exchange through the drag force will act to dampen the turbulent kinetic energy. This indicates that the Reynolds number and the Stokes number should be important parameters in the description of turbulence modulation (Hetsroni 1989; Elghobashi 1994). Furthermore, the magnitude of either effect is proportional to the presence of particles typically expressed either by the concentration or the loading (Kenning 1996).

Gore and Crowe (1989) sought to summarize the effects of particles on the fluid turbulence by compiling the experimental data available in literature from pipe and jet flow. The critical parameter was proposed to be the ratio of the length scale of the particles to the length scale of the turbulence, dp/le. This study suggested that for length scale ratios $d_p/l_e > 0.1$ particles will only augment the turbulence while for $d_p/l_e < 0.1$ particles will attenuate the turbulence.

Most measurements have been performed for a pipe with fully developed turbulent flow or for an axisymmetric jet in the self-similar region. For the case of pipes it is usual practice that the inlet length required for the fully developed condition is at least 75 pipe diameters. Considering the typical size of laboratories and the extent of the measuring volume of the LDA system this leads to pipe diameters around 30-40mm. The integral length scale in the center of the pipe for a single phase fully developed turbulent pipe flow have been shown to be approximately proportional to the pipe diameter, l_e/D=0.1, for different Reynolds numbers (Hutchinson et al. 1971). The variation in the length scale

ratio is thus achieved solely by varying the particle size. For the case of an axisymmetric jet measurements are most often reported for the self similar region which is located far downstream of the jet nozzle, $x/D \approx 30$. In this region the integral length scale for a single phase free jet is proportional to the distance from the nozzle, $l_e/x=0.039$, independently of the jet Reynolds number or nozzle diameter (Wygnanski and Fiedler 1969; Tennekes and Lumley 1972). For practical applications this combination yields small length scale ratio d_p/l_e as well as small dispersed phase concentrations, approaching the one-way coupling regime where turbulence modulation effects are negligible.

Table 1: Properties of test particles.

	Sphere	Sphere	Sphere
Nominal diameter (μm)	880	1350	1815
Standard deviation (μm)	87	165	191
Density (kg/m^3)	2500	2500	2500
	Disk	Prolate Spheroid	
Aspect ratio, *L/D*	250:6480	6460:1860	
Nominal diameter* (μm)	2444	2815	
Standard deviation* (μm)	81	505	
Density (kg/m^3)	1100	750	

*based on the volume equivalent diameter.

Considering previous experimental investigations and the parameters which have been suggested to be important for the observed turbulent modulation an experiment where the integral length scale is varied for a fixed particle diameter is the focus of the present investigation. Considering the range of integral length scales present in the flow, the particles have been chosen to cover a range above and below the $d_p/l_e=0.1$ criterion. As can be seen from table 1 this means that the selected particles are rather large compared to previous studies. Furthermore, with particle diameters in this range, the Stokes number is much larger than unity and the particles can be considered as being unable to follow the motion of the turbulent eddies. The properties of the axisymmetric jet is used to provided the systematic variation of the length scale while unique inlet conditions are used to ensure a smooth transition between the length scale present at the nozzle inlet and further downstream. A commercial LDA system is used to measure the mean and RMS axial velocity along the centerline of the jet. The use of LDA for multiphase flow together with the measurement in the developing region of the jet raises a number of concerns which is discussed in the following section.

Nomenclature

d_p	particle diameter (m)
D	pipe diameter (m)
f	Schiller and Naumann (1933) correction
l_e	turbulence length scale (m)
$\dot{m}_p$	particle mass flow rate (kg/s)
u	axial air velocity (m/s)
x	axial distance (m)
z	mass loading (-)

Greek letters

α	volume fraction (-)
μ	viscosity (kg/s·m)
ρ	density (kg/m^3)
σ	turbulence intensity (-)
τ	time scale (s)

Subsripts

0	clear flow
c	carrier phase
e	eddy
eq	volume equivalent
p	particle

Experimental Methods

The experimental setup is show schematically in figure 1. A 70W ventilation fan re-circulates the airflow and maintains a constant nozzle velocity of 7m/s. The air flow rate is measured using an orifice meter placed on the return section of the pipe. Ventilation by-pass valves are used to quickly reduce the density of the tracer particles by taking fresh air in and rejecting the seeded air. Additionally, tracer particles are also added to the flow at the ventilation by-pass valves. Test particles are added to the flow via a gravimetric particle dispenser, which produced a repeatable steady flow of particles. Particle mass flow was measured by weighing particles after collection for a timed period. The test particles are allowed to mix with the air flow over a short distance, where the pipe is made of Plexiglas to allow for visual inspection. A wire-mesh combined with a flow contraction is placed at the entrance to a rectangular enclosure, with dimensions of 2000x500x500mm, to condition the flow further. Particles are separated from the airflow and collected for reused at the settling chamber in bottom of the test rig. Mean and fluctuating gas velocities were measured using a commercial LDA system mounted on a 2-axis traversing system. The tracer particles where generated by means of a commercial liquid seeding generator, generating oil droplets in the range ~ 1μm. The jet nozzle has an inside diameter of 40 mm, and the ambient temperature and pressure was respectively 296K and 97kPa. Particle size distributions were measured using a microscope with a sample of more than 100 particles for each size group. Detail of the test conditions are summarized in table 2.

Table 2: Summary of test conditions.

	Particle type	Loading
Case 0	Clear flow	0
Case 1	Sphere, 1815 μm	0.60
Case 2	Sphere, 1815 μm	0.95
Case 3	Sphere, 1815 μm	1.70
Case 4	Sphere, 1350 μm	0.40
Case 5	Sphere, 1350 μm	0.95
Case 6	Sphere, 1350 μm	1.60
Case 7	Sphere, 880 μm	1.05
Case 8	Sphere, 880 μm	1.45
Case 9	Disk	1.34
Case 10	Prolate spheroid	2.00

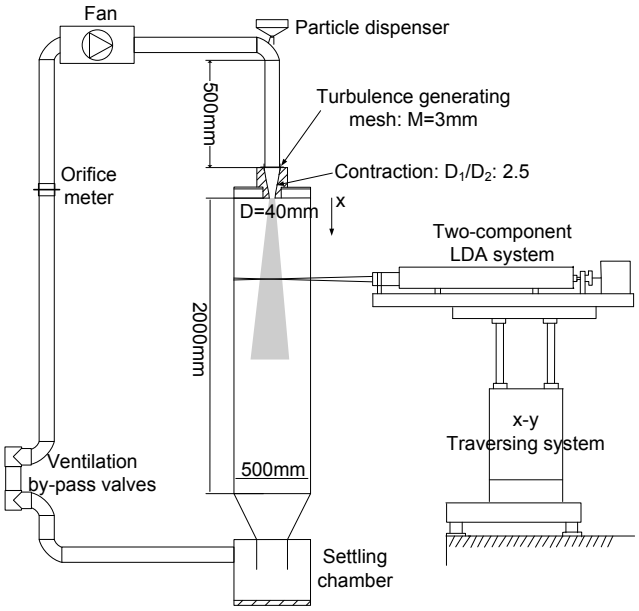

Figure 1: Sketch of the experimental setup

A quick survey of previously published results concerning turbulence modulation reveals a large spread in data which lead to the conflicting conclusions mentioned in the previous section. A few remaining issues concerning the present and previously used test rigs and the experimental techniques for particle laden-flows are therefore relevant for further elaboration. The key to understanding this experiment is that the particles used are substantially larger than previous studies, which both create new problems and diminish issues often associated with the use of smaller particles.

To allow comparison with numerical models it is important to ensure that particles are spherical with a narrow size distribution. Furthermore, the particles should be solid, non-evaporating, non-agglomerating, non-static etc. To meet these criteria it is common to use either glass or polymer beads. However, in literature, it is also possible to find experimentalists using sand particles (Shuen et al. 1985) or even cylindrical particles (Tsuji et al. 1984) to approximate the spherical ideal. Furthermore, particle size sorting techniques does not discriminate between ideally spherical particles and particles with imperfections and some techniques produced size distributions with a large spread. When particles are pneumatically transported, electrostatic charging of the particles, especially for small particles, increases the change of clustering or adhesion to walls (Tsuji et al. 1984). Also any residual humidity might cause particle to cluster together and thus introduce the need for drying. All of these factors can lead to an increase in the drag coefficient compared to that of an ideal sphere, which cause a modification to the coupling with the carrier phase and thus makes it difficult to evaluate the turbulence modification. All of these issues are diminished using larger particles whose size also allow for a continuous visual monitoring of any possible deterioration of particle conditions.

For the present experiment glass beads have been used. The particles have been studied using microscopy and subsequent picture analysis. Due to problems with the glare point and other reflections from the transparent glass particles meant it was not possible to use any automated algorithm to check for circularity. Instead circles were manually fitted to each particle, thus providing both an accurately determination of the diameter and a means of visually checking for consistency. An image of the spherical particles is shown in figure 2. For all tested particles the majority appeared to be spherical, although the largest particles in each group had a tended to be slightly ellipsoidal in nature which is consistent with the sieve separation technique. Test particles was collected and recycled at the bottom of the settling chamber and recycled by manually replenishing the particle dispenser. This procedure unavoidably caused some degradation of the particles which was dependent on the particle material. For the spheres, which were made of glass no degradation could be detected after the experiments where concluded, although a few were audibly pulverized during adjustment of the mass flow rate in the particle dispenser. For the disks, which were made of polystyrene, both deformation and fragmentation was noticeable. However, this was visually evaluated as only a smaller fraction being affected. For the prolate spheroids only fragmentation was detected which similarly only affected a smaller portion.

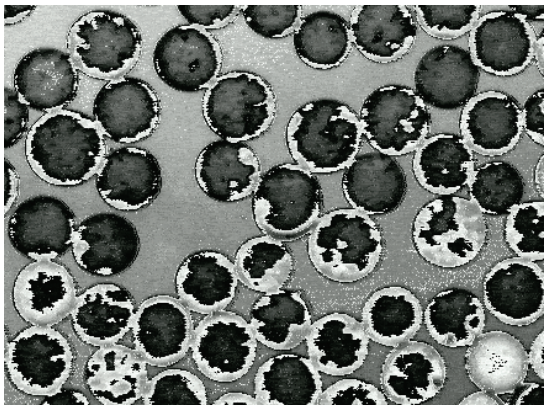

Figure 2: Glass particles, d_p=1.820μm.

The inlet condition of a jet should be easily reproducible and allow for an inlet boundary profile to be applied for Computational Fluid Dynamics. For a single phase jet these conditions are met either by using a nozzle, which produces an approximate top-hat profile, or by a fully developed pipe flow velocity profile. For particle laden flow fully developed turbulent two-phase flow is most often used as the inlet condition. The usual practice is to choose the development length of the pipe between 75*D* and 135*D* which is three to four times more that what would is required for the similar single phase flow case. However, a criterion only based on the length of the pipe is not sufficient to unambiguously state whether the particle-laden flow is fully developed. For a single particle released from rest in a uniform flow field it is possible to determine the time it takes the particle to reach its steady state velocity. Similarly, it is possible to determine the residence time of the accelerating particle given the length of the pipe. Thus it is possible to determine if the particle reaches its steady state velocity, a criteria for fully developed flow, before the start of the measurement section. A survey of previous experiments is shown in figure 3 were the particle response time is based on the particle having reached 95% of their steady state value. The solid line indicates when the particle residence time equals their response time.

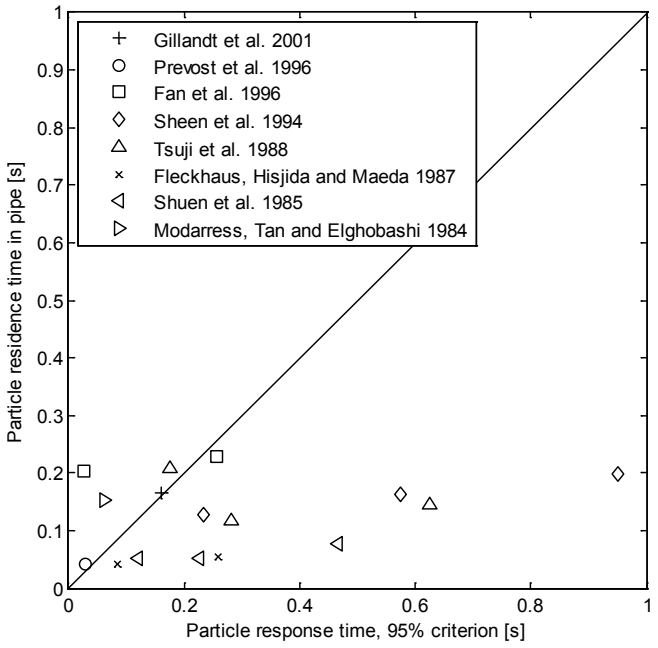

Figure 3: Evaluation of previous experiments ability to be fully developed.

It is evident that only a few investigations can claim to have a fully developed two-phase flow base on this criterion. Furthermore, this criterion only considers the development of the mean translation velocity of the particles and not the fluctuating velocity of the particles which is often influential for the two-way coupling between the phases (Elghobashi 1994). For pipe flows the development of the fluctuating component of the particle velocity is very dependent of the initial conditions together with the roughness of the internal surface. The experiments by Govan et al. (1990) which focused on measuring the Lagrangian statistics of 500μm particles in a 20m vertical pipe, 620*D* section indicated that the fully-developed behavior was not achieved after 19m. Thus to achieve a truly fully developed two-phase flow it is necessary to use a pipe length which is difficult to implement in typical laboratory settings.

For the measurement of turbulence modulation often a systematic variation of a single parameter, which is hypothesized to influence the properties of the flow, is desired while other parameters are held constant. This has previously been achieved by varying the mass loading or the size of the particles. However, for the fully developed condition this variation also gives rises to differences in the concentration profile in the radial direction of the pipe (Vreman 2007). Thus for a variation of the particle diameter, with constant loading, a fully developed condition inflicts the local particle concentration.

To counter the above issues a design using a combination of a wire-mesh grid and a nozzle to create a flow to approximate a uniform profile for both carrier phase velocity and particle concentration is suggested. This design is similar to that used by Barlow and Morrison (1990) for dense jets. The interaction between the particles, the wire-mesh and the walls of the nozzle creates an inlet condition for the particle velocity which is best described as a spray with an angle of 27 degrees. The acceleration of the air as it passes through the contraction entails that the mean air velocity is greater than the mean axial particle velocity at the nozzle exit. Since the mean particle velocity increases and surpasses that of the mean velocity downstream of the nozzle this special inlet condition allows for measurements at the same particle Reynolds number but at different values of the d_p/l_e ratio. Furthermore, it will also give an indication whether the acceleration of the particles close to the nozzle acts to decrease or increase the carrier phase turbulence. Figure 4 shows the evolution of the mean velocity of both phases together with the investigated range of Reynolds numbers.

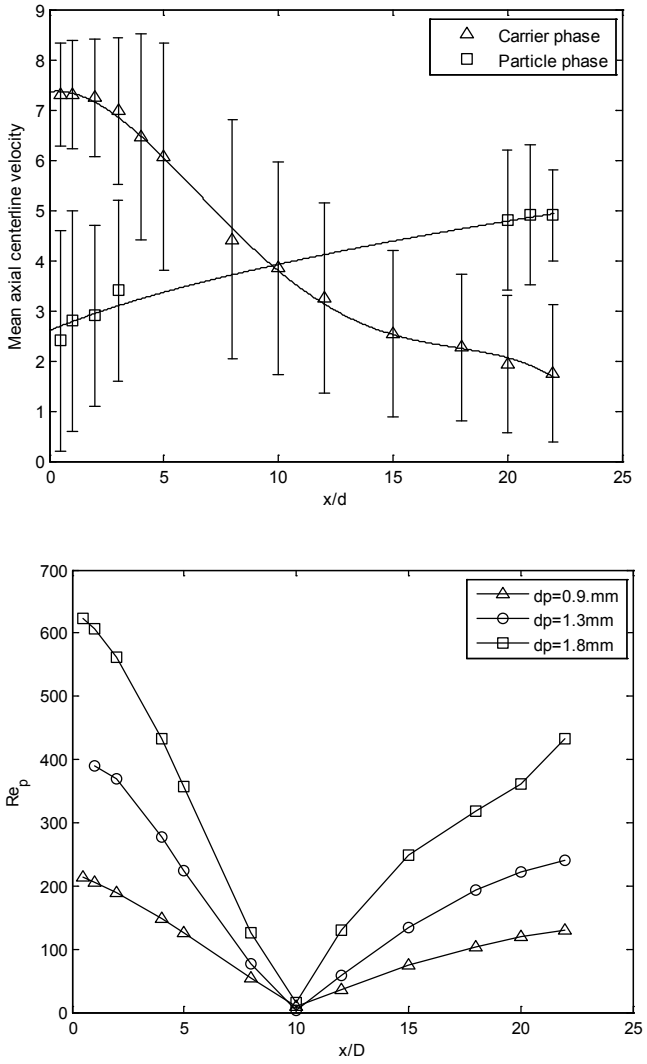

Figure 4: Top: Mean velocity and spread of the carrier phase and the particle phase for 1815 μm particles. The standard deviation times 2 is shown as error bars. Bottom: Investigated range of particle Reynolds number.

Most previous investigations of two phase flow have been made by seeding the continuous phase with small seeding particles and use amplitude discrimination to distinguish between LDA signals originating from the large test particle and signals from the much smaller seeding particles. Amplitude discrimination techniques have been associated with bias resulting from the non-uniform light intensity distribution in the measurement volume (Modarress, Tan and Elghobashi 1984). Furthermore, low amplitude signals resulting from large particles intersecting the edge can be interpreted as coming from seeding particles. For dilute flow the data rate for the seeding particles far exceed that of

the test particles and the resulting error can be assumed to be statistically insignificant (Modarress 1982). Recent investigations have also relied on the PDA technique to distinguish between the two phases, however, for the present experiment the size difference between the seeding and test particles exceeds the range for simultaneous measurement of both phases. Moreover, the PDA technique assumes all particles to be ideal spheres and cannot be applied on the generic non-spherical particles used in the present investigation. For the present investigation a velocity filtering approach based on the axial velocity probability density function has been applied to distinguish between the two phases. This technique requires that there is a velocity difference (slip velocity) between the two phases so the resulting velocity pdf for the combined signals for both phases, is bimodal. In particular, the velocity statistics can be determined with great accuracy if the mean slip velocity between the phases is greater than the sum of the standard deviations of the two fluctuating velocities for the two phases. Figure 5 shows a sample normalized pdf which has been fitted assuming a normal distribution for both phases. This technique has previously been applied by Lee and Durst (1982) for vertical particle-laden pipe flow and by Barlow and Morrison (1990) for a dense two-phase jet flow.

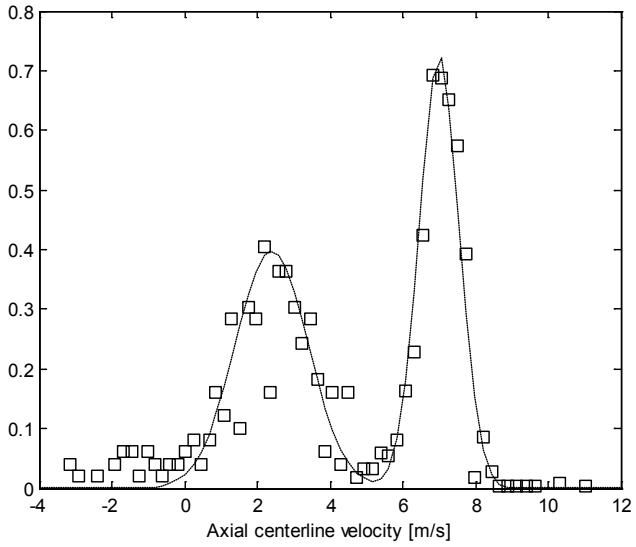

Figure 5: Sample normalized velocity distribution at x/D=1 for 700 μm particles with mean nozzle speed of 7 m/s.

In order to contain and re-circulate the seeding a closed loop design has been opted for. Using this design the concentration bias which otherwise would exist when measuring in the outskirts of the jet is also avoided. However, this design generally also impedes the development of the jet due to the friction of the walls. In order for comparability with other investigations, measurement has only been conducted in the range where the jet can be considered as a free jet i.e. where the influence of the walls and exit is minimal. This has been verified by comparing the measurements of the single phase jet to available literature. Thus only the top half of the test section, x/D=0-25, was used for measurements to avoid the influence from the outlet as well as the walls. It is desired to categorize any measured turbulence modifications according to the length scale correlation, d_p/l_e, suggested by Gore and Crowe (1989). For this, a correlation of the integral length scale at the centerline of a clear jet, l_e=0.039x, originally submitted by Wygnanski and Fiedler (1969) has been used. This is the same correlation as used by Gore and Crowe (1989). They also suggested to obtain an estimate of the integral length scale immediately after the nozzle exit by using the criteria of l_e=0.1D (Hutchinson, Hewitt and Dukler 1971). The length scale in the overlap region is very dependent on the particular case. For this case a linear dependence is assumed between the near nozzle region and the point where the correlations for the clear jet can be used. For this particular case this assumption works well since the predicted length scales are of similar magnitude and because the jet flow itself is turbulent. Thus a peak or drop in the integral length scale is not to be expected. For the self preserving free jet both the spreading rate and the turbulence length scale depend on the distance from the inlet (Tennekes and Lumley 1972). These can be considered to be proportional to each other. Figure 6 shows a graphical representation of the used expressions for the integral length scale along with measurements of the jet width. It can be seen that the measured jet width is consistent with that of Wygnanski and Fiedler (1969).

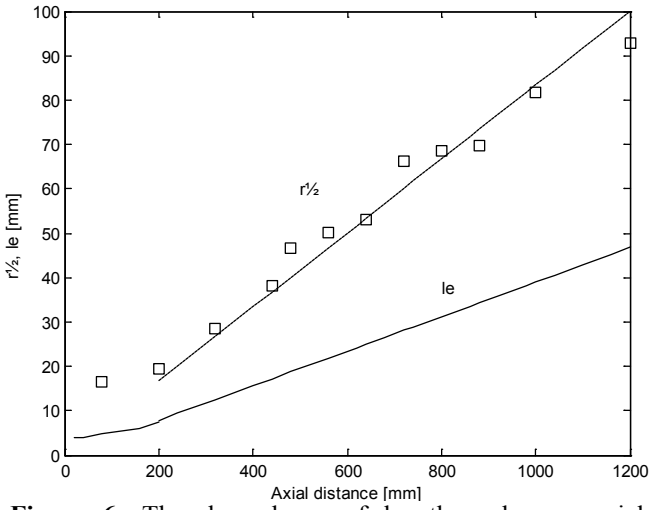

Figure 6: The dependence of length scales on axial distance downstream of the nozzle. --, r½ from (Wygnanski and Fiedler 1969); □, r½ from present clear flow measurements.

To quantify the modification of turbulence due to the addition of particles the percentage change in the turbulence intensity is used:

$$\frac{\sigma - \sigma_0}{\sigma_0} \cdot 100\% \qquad (1)$$

Here σ denotes the turbulence intensity of the particle laden flow and σ_0 the turbulence intensity of the clear flow. All values are local values and only the axial velocity is considered. This can be categorized as a parameter which is easy to measure, since it only involves one velocity component, but also a parameter with limited accuracy. The division between two values, each associated with a limited accuracy, results in a value with even poorer accuracy. As it can be deduced from equation (1) two such divisions are performed for the evaluation. Other parameters to evaluate turbulence modulation can be based on the turbulent kinetic

energy or even on the Reynolds stresses. However, these expressions are more difficult to measure and evaluate since they require measurement of three velocity component and/or cross-correlation of fluctuating velocity components. Furthermore, the inclusion of several measurements does not necessarily make the final evaluation more precise. The fluctuating velocity in the axial direction is the most prominent of the fluctuating velocity components and it thus makes sense to base the evaluation of turbulence modulation on this parameter solely. Often it is also chosen to normalize parameters using quantities which exist at a base point such as a jet inlet or at the centerline of a fully developed pipe flow. However, this again makes the direct comparison with other studies more difficult. Finally it should be stated that no matter which parameter which is chosen for the evaluation of the turbulence modulation the accuracy will always be less than that which is associated with the measurement of the mean and fluctuation velocities. This turbulence modulation parameter has frequently been used in existing literature and is used in the present investigation to allow for easy comparison with previously published results. It should be mentioned that the radial velocity component often is more affected by the presence of particle than the axial velocity.

The precision of the x-y system for position adjustment was 12.5μm for all axes. The uncertainty of the mass loading was estimated to 3%. For the Laser Doppler Anemometry measurements a minimum of 1500 samples were collected for each data point. This yields a maximum error of 4% for the velocity measurements while for the intensity measurements this figure doubles to 8% which again doubles to 15% for the intensity change since this involves the multiplication of values and their associated errors.

Results and Discussion

From the study of large fixed spheres it is known that flow instabilities in the free surface layer causes the wake of the sphere to oscillate and detach discrete pockets of vorticity. The onset of wake instability is reported to occur at particle Reynolds numbers, $Re_p \approx 130$, while $Re_p \approx 270$ is the lower critical Reynolds number for which vortex shedding occurs (Clift, Grace and Weber 2005). Considering vortex shedding to be responsible for the observed turbulence augmentation Hetsroni (1989) suggested that the lower critical Reynolds number could be used as a declamation criterion for enhancement or suppression of the carrier phase turbulence. Figure 7 shows the turbulence modulation for all measurements versus their particle Reynolds number. Close to the inlet the slip velocity is large with the carrier phase velocity being larger than the particle velocity. This results in equally large particle Reynolds numbers close to the inlet, which decreases as the velocity of the two phases approaches each other as they evolve downstream of the jet. The region close to the inlet is associated with augmentation of the carrier phase turbulence for all the investigated particles while the region far downstream is always associated with attenuation. Thus, there does not seem to be a strong correlation between the turbulence modulation and the particle Reynolds number regardless of the shape of particle. For large particle Reynolds number both attenuation and augmentation is encountered. For spheres there seems to be some indication that attenuation is more prominent at low particle Reynolds numbers and that augmentation is only occurring at values above Re_p=110 and is exclusive at Reynolds numbers higher then Re_p=400. However, it is clear that the shift between attenuation and augmentation is dependent on the particle size in addition to the particle Reynolds number. Since vortex shedding only occurs at values above Re_p=270 the phenomenon of vortex shedding cannot solely explain the significant increase in the intensity change observed for the smallest particles. Interesting to note is that augmentation is prominent close to the jet inlet where the mean particle velocity is lower than the mean carrier phase velocity so this increase in the turbulence intensity cannot be explained by energy transfer resulting from interfacial forces. For the disks and prolate spheroids there seem to be no correlation with the Reynolds number as attenuation is encountered at high Reynolds numbers. If the particle Reynolds number was evaluated on basis of the largest dimensions of the non-spherical particles it would generally result in larger particle Reynolds numbers making the Reynolds number correlation further unlikely.

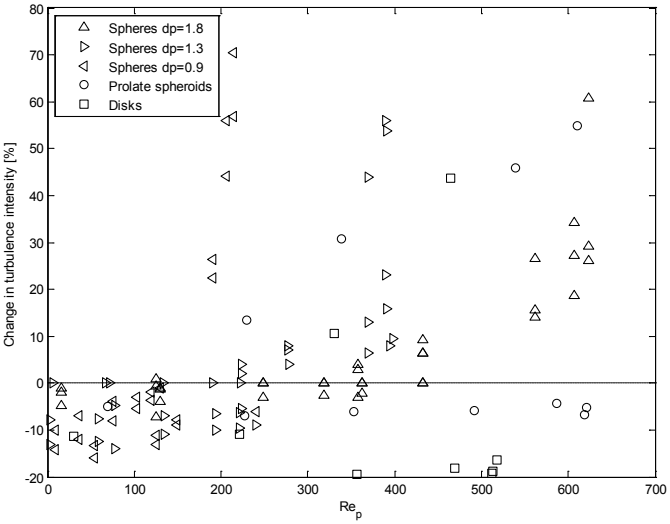

Figure 7: Percentage change in the turbulence intensity versus the particle Reynolds number. For disks and prolate spheroids the particle Reynolds number is evaluated on basis of the volume equivalent diameter.

From studies of power-spectral measurements of the fluctuating velocity it has been observed that the addition of particles results in a decrease of the turbulence energy in the high wave number region (Jou, Sheen and Lee 1993). This is interpreted as a result of the turbulence energy transfer from eddies to particles following the eddies (Tu and Fletcher 1994). The ability for particles to follow the flow is best described by the Stokes number, the ratio of the particle response time, τ_p, to the eddy turnover time, τ_e. The criterion for turbulence augmentation based on timescales is a Stokes number above unity (Elghobashi 1994). The Stokes number is formed by the ratio of the response time of the particles, τ_p, to the timescale of the large eddies, τ_e:

$$St = \frac{\tau_p}{\tau_e} = \frac{\tau_V / f}{l_e / u'} \qquad (2)$$

where τ_V is the Stokes response time, $\rho_p d_p^2/18\mu$, and f is the

Schiller and Naumann (1933) correction for spheres at higher Reynolds numbers. Figure 8 shows the intensity change for all measurement points against the Stokes number, *St*. For all particles the Stokes number is greater than unity which indicates that the motion of the particles is only little affected by the motion of the large eddies; a perception which is also confirmed by visual observation of the particle phase. It is clear that turbulence modulation effects do not correlate well with the Stokes number. Large particles which do not follow the characteristic eddies are still able to attenuate the carrier phase turbulence and measurements at large Stokes numbers do not necessarily augment the turbulence intensity. This result thus also indicates that another mechanism is necessary to predict the attenuation which is caused at larger Stokes numbers.

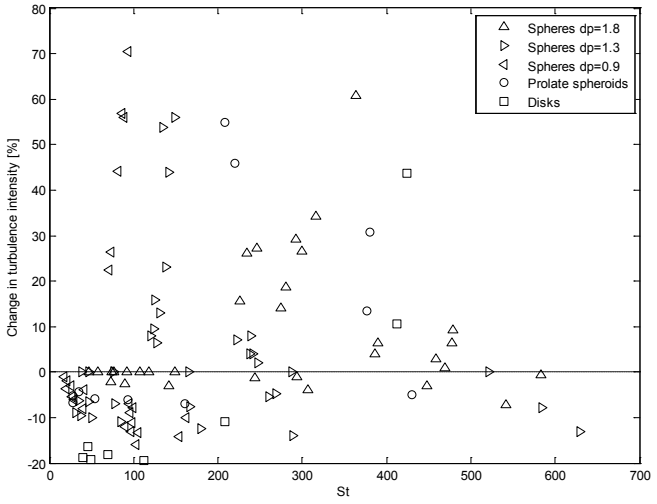

Figure 8: Percentage change in the turbulence intensity versus the Stokes number. For disks and prolate spheroids the particles response time is evaluated on basis of the volume equivalent diameter.

Gore and Crowe (1989) sought to summarize the effects of particles on the fluid turbulence by compiling the data available in literature. The critical parameter was proposed to be the ratio of the length scale of the particles to the length scale of the turbulence, d_p/l_e. This was in line with the observation that particles which were sufficiently smaller than the turbulence length scale would follow the motion of the most energetic eddies while larger particles would create their own turbulence in their wake. From experimental data available in literature at that time a threshold value of d_p/l_e=0.1 between attenuation and augmentation was suggested. Figure 9 shows data for the modulation of the carrier phase turbulence at the centerline of the jet. The suggested criteria for turbulence modulation, d_p/l_e =0.1, by Gore and Crowe (1989) is indicated with a slashed line. It can be seen that attenuation is possible at length scale ratios above the suggested criterion. This is possible due to a combination of very large particles combined with high mass loading and the development of the relative velocity. However, there is a clear trend that for large ratio there is only enhancement of the carrier phase and for low ratios there is only attenuation. For low length scale ratios the measured modulation seems to approach the clear flow instead of attenuating the flow even more. This is due to the decrease in the particle concentration as the jet is developing and the particles are both increasing in speed and are further apart.

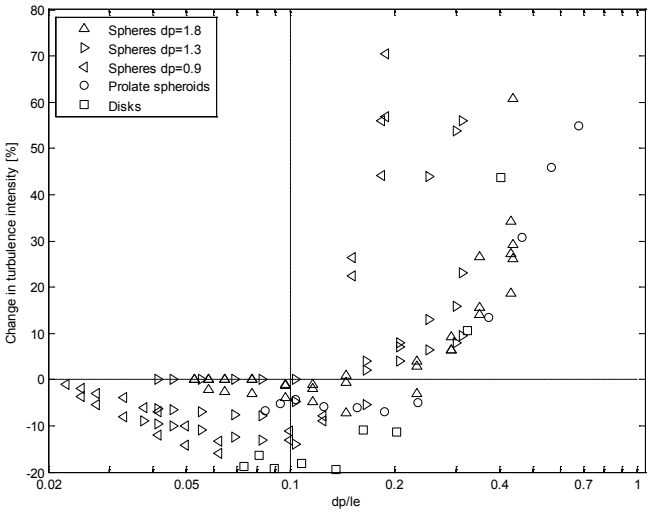

Figure 9: Percentage change in the turbulence intensity versus the length scale ratio d_p/l_e. For disks and prolate spheroids the particles size is evaluated on basis of the volume equivalent diameter. The criteria by Gore and Crowe (1989), d_p/l_e = 0.1, is shown as a vertical line.

Another often used measure associated with the magnitude of the coupling is the mass loading, the ratio of particle mass flux to the carrier phase mass flux. Generally when using the mass loading as a measure of the coupling between the phases it is also necessary to consider the density ratio and the particle size as this determines the number of particles available for interaction. These parameters can inherently be combined to yield the number density as a third measure of the magnitude of interaction. Geiss et al. (2004) reports that turbulence modulation is only observed above a threshold value of number density of 30-40 particles/cc, corresponding to a volume fraction of around α=3·10^{-5}. Fan, Zhao and Jin (1996) reports that turbulence modulation effects were strongly correlated with both the mass loading and the particle diameter. Other related parameters are the mass fraction, used by Geiss et al. (2004), and the volume loading, the ratio of volume fluxes. By studying dense jets Barlow and Morrison (1990) found that high volume loading reduces the mean slip velocity between the phases whereas in the dilute regime the mean slip velocity was equal to the terminal velocity of the particles. By arguing that particles represent surfaces which are able to support stresses Kenning and Crowe (1997) suggested that the characteristic length scale associated with dissipation no longer is the Kolmogorov scales but that also the inter-particle spacing and the particle diameter needs to be considered. For the use of computational fluid dynamics the appropriate parameter to express the presence of particles in the Eulerian reference frame is the concentration of particles represented in units of kg per cubic meters. The volume fraction are closely related to both the inter particle spacing, lint, and the particle mass concentration, *C*. For dilute two-phase flow applies that:

$$\pi d_p^3 \big/ 6 l_{int}^3 = \alpha = C\, \rho_c / \rho_p \qquad (3)$$

which suggest that these parameters can be used as substitutes for one another. Turbulence modulation effects are present for all particulate flows. However, for very dilute flow this effect is not measureable while for dense flows inter-particle collisions have a dominating effect on the flow. The ratio between the particle response time and the time between collisions is the best measure for evaluating if the flow is dense or dilute, but the time between collisions is difficult to quantify since it depends on the relative velocity between particles. Most often the volume fraction of particles is used a rough criterion to distinguish between the different regimes. For volume fractions less than $\alpha=10^{-6}$ (one-way coupling) particles have negligible effect on turbulence while for volume fractions larger then $\alpha=10^{-3}$ (four-way-coupling) particle collisions significantly influence the interaction between the particle and carrier phase which is present between $10^{-6}<\alpha<10^{-3}$ (two-way coupling) (Elghobashi, 1994). It is evident that the coupling between the phases is stronger as more particles are added to the flow. The particle concentration can be found by counting particles and registering their velocity as they pass a control volume during a time period. For the current setup this was not possible. Alternatively, the volume fraction of the particles, α, can be approximated by considering the particle velocity, v_p, and the particle mass flux, $\dot{m}_p$, at the centerline. The following expression is used to calculate the volume fraction at the centerline:

$$\alpha = \frac{\dot{m}_p}{\rho_p v_p A_s} \tag{4}$$

where A_s is the cross-sectional area of the particle stream. This expression assumes that the particle concentration is evenly distributed across the cross-sectional area of the particle stream which contradicts previous experimental findings which suggest that the particle concentration is greatest in the center of the jet. However, this estimate should provide the correct order of magnitude of the volume fraction. For the present investigation the greatest particle concentrations are found near the inlet where α is in the order of 10^{-3}. The volume fraction decreases downstream due to the spreading of the jet and the increase in mean velocity of the particles. As a consequence, the volume fraction is correlated with the length scale of the large eddies and the influence of these two parameters cannot be separated using the current setup. For locations far downstream of the jet the volume fraction is in the order of 10^{-6} and the flow can be considered as one-way coupled and the particle phase are not able to affect the turbulence of the carrier phase.

Figure 10 shows the intensity change for the investigated range of particle volume fraction, α. For a large range of volume fractions it is possible to have both attenuation and augmentation. However, it is clear that at low volume fractions only attenuation is encountered whereas at high volume fractions only augmentation is encountered. However, the volume fraction for the present experiment is very closely correlated with the turbulence length scale and it is not possible to separate the effects of these two parameters. As the volume fraction approaches the one-way coupling regime the turbulence modulation effect diminishes. The lowest value for which a change in the turbulence intensity has been measured is $\alpha=4\cdot10^{-6}$. In fact it seems that the modulation effects are being impeded by the lower volume fraction at values below $\alpha=10^{-5}$. Furthermore, the volume fraction of the tracer particles is estimated to be in the order of $\alpha=10^{-10}$ which is significant below the limit for two-way coupling and it is assumed that they have only negligible effect on the carrier phase.

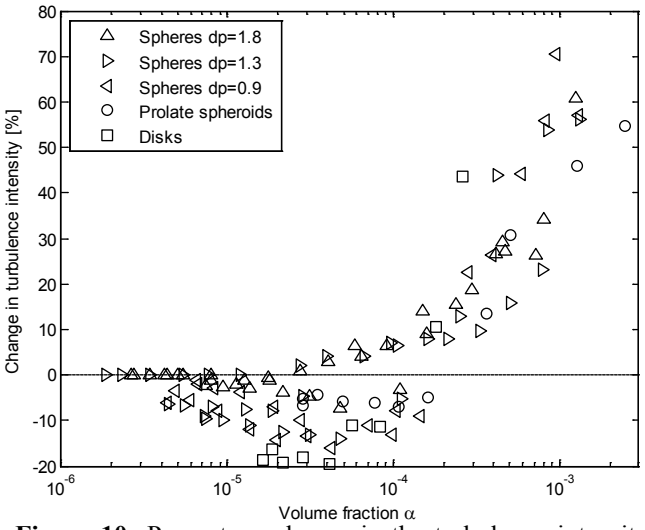

Figure 10: Percentage change in the turbulence intensity versus the volume fraction α.

It can be acknowledged that there does not exist any single universal parameter able to predict the turbulence modulation which has been observed at the spectrum of experimental investigations of particle-laden flows. In view of the failure of existing criteria and models it is thus desired to develop an expression which can correlated the existing data using the databank of the present investigation where information of many different quantities is stored. The methods which have been used to derive the aforementioned criteria have been based either on a mechanistic approach like the particle Reynolds number and the Stokes number. If these had turned out to correlate well with the observed turbulence modulation it would have resulted in a new insight into particle-fluid interaction which explains the efforts. However, in lieu of these methods it is possible to develop criteria and correlations which are based purely on experimental observations. A prime example of this is the length scale criteria by Gore and Crowe (1989) which is based on observations with only little theoretical support. It should be noted that such a model may be of little value for the development of numerical models, but has the potential to serve as a base model for which to evaluate the performance of non-spherical particles. Especially in the view, that it has not been able to acquire non-spherical and spherical particles with exactly the same diameter and density. To develop such an expression it is prudent to examine the dependence of each parameter individually. It has already been stated that the particle volume fraction is important and there seem also to be some justification that the length scale ratio plays a significant role. Other key parameters are the mass loading, which does not necessarily scale with the concentration, the slip velocity and the particle size itself.

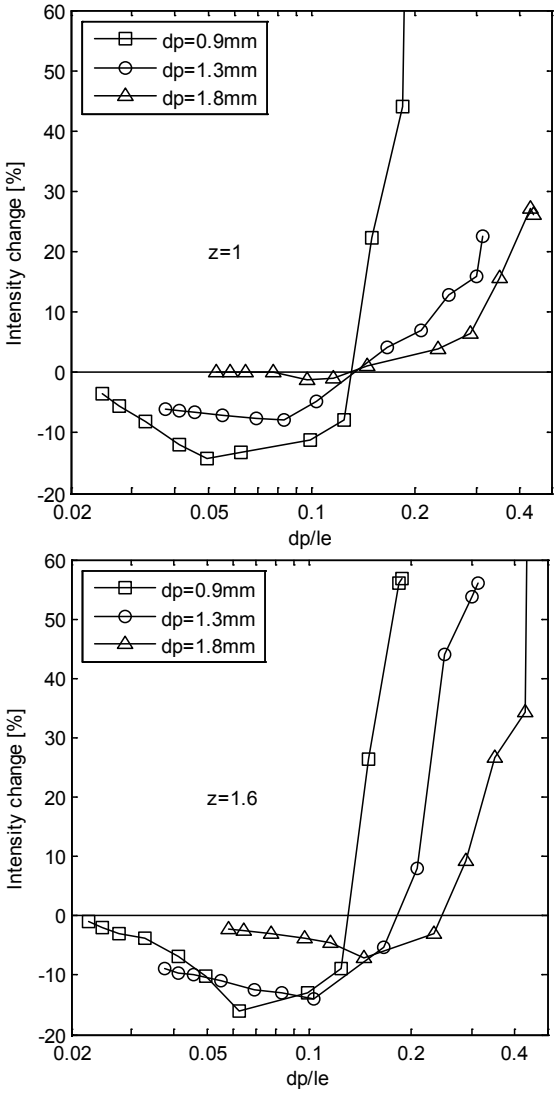

Figure 11: Dependency on particle size. The percentage change in turbulence intensity as function of the length scale ratio for different particle sizes and constant global mass loading.

Figure 11 shows the dependence of the percentage change in turbulence intensity for constant mass loading as series of the length scale ratio, d_p/l_e, for each particle size used in the present investigation. It appears that the influence of the particle phase on the carrier phase turbulence increases with decreasing particle size. However, for constant mass loading the volume fraction increases as the particle size decreases and it is clear that the volume fraction also has an effect of the coupling between the phases. More notably it can be seen that for the same particle size and mass loading this can both have an attenuating or augmenting effect depending on the length scale of the turbulence. In the lower range of length scale ratios the volume fraction approaches the one-way coupling regime and the results approach the single phase values. Especially the results for z=1.0 seem to exhibit a pivot point for which the results for all three series collapse into one point. This is a little less clear for z=1.6 and the eligible pivot point do not coincide with the zero intensity change line but is located slightly below. Interesting to note is that both pivot points are located roughly at the same values on the d_p/l_e axis.
Figure 12 shows in a similar way the dependence of the intensity change on the loading for constant particle size. The results show that an increase in the mass loading also corresponds to an increase in the magnitude of turbulence modulation experienced by the carrier phase velocity. Similar to the effect of the particle size the mass loading both promotes the attenuation or augmentation depending on the value of dp/le. Similar to the case of particle size an increase in mass loading also increases the volume fraction. Considering both Figure 11 and Figure 12 it is evident that for some configurations there is very large increment in the intensity change as the particle phase begins to augment the carrier phase.

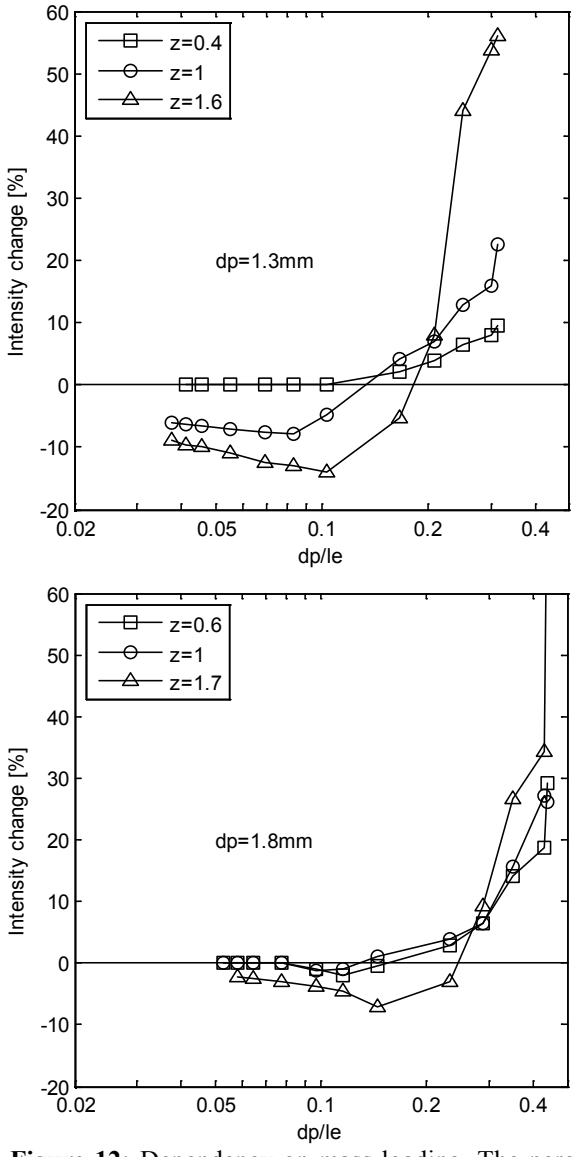

Figure 12: Dependency on mass loading. The percentage change in turbulence intensity as function of the length scale ratio for different global mass loadings and constant particle size.

Combining the observed effects of the mass loading and the particle diameter by and realizing that the mass flow rate of the carrier phase is constant for the present investigation it is possible to define a non-dimensional number as:

$$N_M = \frac{\dot{m}_p}{\mu d_p} \tag{5}$$

where the viscosity of the carrier phase is the only additional parameter. It is clear that this factor cannot stand alone when predicting turbulence modulation and it is necessary to incorporate a functional dependency of both the length scale ratio and the concentration of particles. Figure 13 emerges as the fractional change in turbulence intensity is divided by the non-dimension number from equation (5). All measurements with a volume fraction lower then $\alpha=2\cdot10^{-5}$ has been disregarded since these fall in the transition zone between the one- and two-way coupling regime and the modulation effects are consequently weakened. Similarly, measurements with a volume fraction higher then $\alpha=10^{-3}$ are not shown since these borders to the dense regime. Given the accuracy of the experiment a rough correlation can be identified. The following empirical expression is suggested to predict the turbulence modulation experience by the carrier phase in the presence of particles:

$$\frac{\sigma-\sigma_0}{\sigma_0}\cdot 100\% = \frac{\dot{m}_p}{\mu d_p}\left(0.34\frac{d_p}{l_e}-0.05\right) \tag{6}$$

The scatter of the results justifies the use of a simple linear fit considering the error associated with the experiment. The validity of the proposed expression is restricted by the extent of the data for which it is based on. Thus it can only claim to be valid for volume fractions between $\alpha=2\cdot10^{-5}$ and $\alpha=10^{-3}$, mass loadings between 0.5 to 1.7, particle diameters between 0.9 to 1.8 mm and d_p/l_e ratios between 0.1 and 0.5. However it should be noted that this expression produces the expected trends in the limits of both high and low values of the length scale ratio. It should be noted that the suggested correlation does not identify any fundamental mechanisms for production or dissipation of turbulence due to the presence of particles. This correlation merely addresses the observed trends in the measurements.

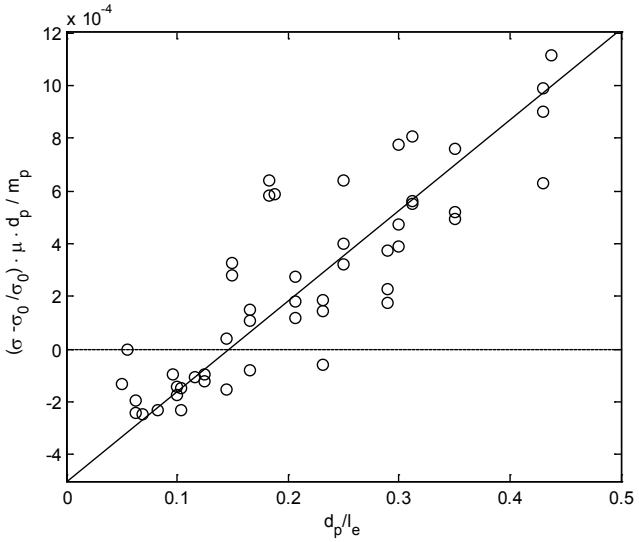

Figure 13: Fractional change in turbulence intensity versus d_p/l_e. Only measurement points with a volume fraction between $\alpha=2\cdot10^{-5}$ and $\alpha=10^{-3}$ are shown.

Figure 14 shows the results for the length scale ratio suggested by Gore and Crowe (1989). In the upper left figure it can be seen that the change in the turbulence intensity is similar for the investigated particles for a short range of the d_{eq}/l_e ratio while they diverges for lower and higher ranges. For low ranges of d_{eq}/l_e the disk shape cause significantly more attenuation than other shapes and the prolate spheroid attenuates the turbulence slightly more than the spherical particles. Using the empirical model presented above for the prediction of the turbulence modulation by spherical particles it is possible to examine the derivation of the results obtained for non-spherical shapes compared to the expected results. First, for good order, it can be seen that there is excellent agreement between the empirical model and the result for spheres. Here the case of d_p=1.8 mm, z=1 have been chosen to be representative for the experiments conducted for sphere and this particular case most closely matches that of the non-spherical cases. For the results in the lower range of d_{eq}/l_e the measurements are made for settings with a low volume fraction where the flow can be considered as one-way coupled, where the model is not valid.

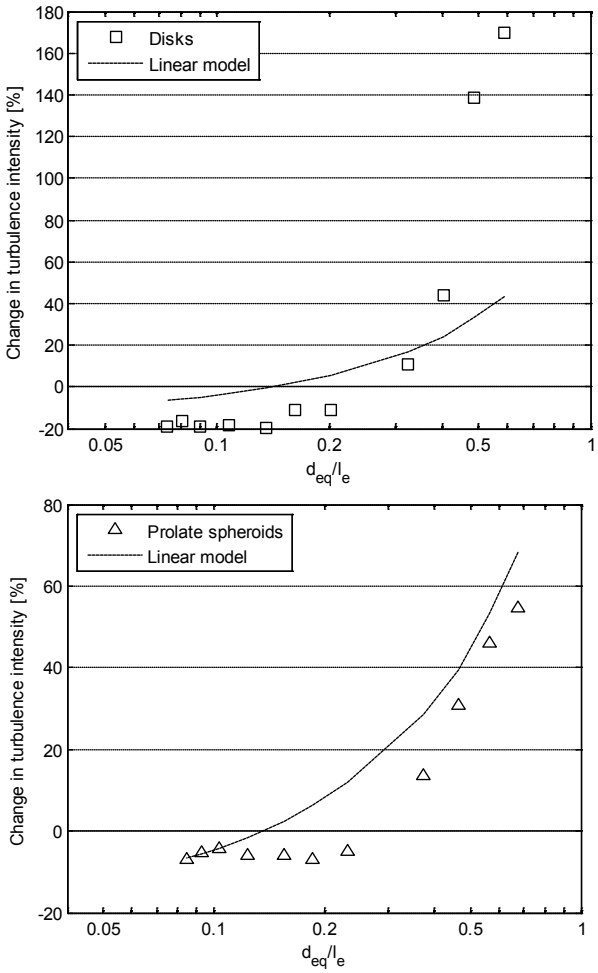

Figure 14: The percentage change in turbulence intensity versus the ratio of the volume equivalent particle diameter to the integral length scale of the clear flow for different particle types. Experimental results have been compared with an empirical model to predict the turbulence modulation inflicted by spherical particles. Notice that the y-axes are not the same for the figures.

For the disks and the prolate spheroids the correlation between the measurements and the empirical model is poor. Since the empirical model is developed for spheres the discrepancy can be considered as the additional effect attributed to the shape of the particles. For both the disks and the prolate spheroids most measurements are lower than that predicted by the empirical model, indicating that both shapes cause additional attenuation. For the disks the turbulence modulation in the high d_{eq}/l_e range are significant above that predicted by the model. Considering the high volume fraction at these settings and that the longest dimension of the disks is almost three times longer than the volume equivalent diameter this additional effect may be due to particle collisions or other phenomenon's related to dense flows. It is clear that the disk shaped particles have the greatest effect on the turbulence for the range of shapes encountered, both with regards to attenuation and augmentation. This result can be explained to a part by the difference in drag coefficients. There are significant differences in results for large values of the particle Reynolds number when there is significant difference in the drag coefficient while the results seems to collapse for results with low values of the particle Reynolds number. The effect of the secondary motion is difficult to estimate considering the present measurements and requires more detailed information of the turbulence as well as the flight of the non-spherical particles.

Conclusions

The influence of different parameters for turbulence modulation on a particle laden jet was studied by Laser Doppler Anemometry. The following conclusions can be made:

In the investigated range of the Stokes number St=101 – 103 both augmentation and attenuation of the carrier phase turbulence is detected. The turbulence modulation does not correlate well with the Stokes number and the perception that it is the particles following the turbulent eddies which are solely responsible for the attenuation of the carrier phase turbulence cannot be verified.

For spheres turbulence attenuation is only measured for values below Re_p=400 while significant augmentation is observed at Re_p =200. Since vortex shedding in the wake of particles is restricted to particle Reynolds numbers above Re_p=400 the perception that vortex shedding is solely responsible for the augmentation of the carrier phase cannot be confirmed.

For volume fractions above $\alpha=2\cdot10^{-4}$ only augmentation is observed while for values below $\alpha=2\cdot10^{-5}$ only attenuation is detected. This indicates that turbulence modulation and the volume fraction are correlated. However, the effect of the volume fraction cannot be separated from the influence of the length scale ratios for the present experiment since these are both proportional to the distance from the jet nozzle. No turbulence modulation have been detected below $\alpha=4\cdot10^{-6}$ which indicate that the suggested criteria of $\alpha=10^{-6}$ is sufficient for the distinction between the one- and two-way coupling regimes.

For low values of the length scale ratio of the particle size to the turbulence eddy size, d_p/l_e, particles tend to attenuate the turbulence while for high values they tend to augment the turbulence. For the combination of large particles with high mass loading attenuation of the carrier phase turbulence have observed beyond the criterion, d_p/l_e =0.1.

An empirical expression to predict the turbulence modulation has been proposed. This correlates the fractional change in turbulence intensity with the mass loading, particle diameter and the integral length scale. This is able to predict the turbulence modulation for spherical particles within the range of the present investigation.

The turbulence modulation expression developed for spherical particles perform exceedingly poorer when applied on non-spherical particles with increasing extremity in shape. For the range of shapes investigated the empirical model for turbulence modulation under-predicted the attenuation effect of the non-spherical particles. This indicate that the departure from the spherical ideal act to decrease the turbulence intensity.

Acknowledgements

This work was supported by Energinet.dk, under grant PSO 2006 1 6364.

References

Barlow, R.S. & Morrison, C.Q. "2-Phase Velocity-Measurements in Dense Particle-Laden Jets", Experiments in Fluids, Vol. 9, no. 1-2, pp. 93-104 (1990)

Clift, R., Grace, R. & Weber, M.E. Bubbles, drops, and particles, Dover Publications, Inc., Mineola, New York, (2005)

Crowe, C.T., Sharma, M.P. & Stock, D.E. "Particle-Source in Cell (PSI-Cell) Model for Gas-Droplet Flows", Journal of Fluids Engineering-Transactions of the Asme, Vol. 99, no. 2, pp. 325-332 (1977)

Elghobashi, S. "On Predicting Particle-Laden Turbulent Flows", Applied Scientific Research, Vol. 52, no. 4, pp. 309-329 (1994)

Fan, J.R., Zhao, H. & Jin, J. "Two-phase velocity measurements in particle-laden coaxial jets", Chemical Engineering Journal, Vol. 63, no. 1, pp. 11-17 (1996)

Fleckhaus, D., Hishida, K. & Maeda, M. "Effect of Laden Solid Particles on the Turbulent-Flow Structure of a Round Free Jet", Experiments in Fluids, Vol. 5, no. 5, pp. 323-333 (1987)

Geiss, S., Dreizler, A., Stojanovic, Z., Chrigui, M., Sadiki, A. & Janicka, J. "Investigation of turbulence modification in a non-reactive two-phase flow", Experiments in Fluids, Vol. 36, no. 2, pp. 344-354 (2004)

Gillandt, I., Fritsching, U. & Bauckhage, K. "Measurement

of phase interaction in dispersed gas", International Journal of Multiphase Flow, Vol. 27, no. 8, pp. 1313-1332 (2001)

Gore, R.A. & Crowe, C.T. "Effect of Particle-Size on Modulating Turbulent Intensity", International Journal of Multiphase Flow, Vol. 15, no. 2, pp. 279-285 (1989)

Govan, A.H., Hewitt, G.F. & Terry, J.W. "Axial-View Measurements of Particle Motion in a Turbulent Pipe-Flow", Particle & Particle Systems Characterization, Vol. 7, no. 2, pp. 60-69 (1990)

Hetsroni, G. "Particles Turbulence Interaction", International Journal of Multiphase Flow, Vol. 15, no. 5, pp. 735-746 (1989)

Hutchinson, P., Hewitt, G.F. & Dukler, A.E. "Deposition of Liquid Or Solid Dispersions from Turbulent Gas Stream - Stochastic Model", Chemical Engineering Science, Vol. 26, no. 3, pp. 419-& (1971)

Jou, B.H., Sheen, H.J. & Lee, Y.T. "Particle Mass Loading Effect on a 2-Phase Turbulent Downward Jet Flow", Particle & Particle Systems Characterization, Vol. 10, no. 4, pp. 173-181 (1993)

Kenning, V.M. Self-induced turbulence in soild-liquid flow, Ph.D. thesis, Washington State University (1996)

Kenning, V.M. & Crowe, C.T. "On the effect of particles on carrier phase turbulence in gas-particle flows", International Journal of Multiphase Flow, Vol. 23, no. 2, pp. 403-408 (1997)

Lee, S.L. & Durst, F. "On the Motion of Particles in Turbulent Duct Flows", International Journal of Multiphase Flow, Vol. 8, no. 2, pp. 125-146 (1982)

Modarress, D., Tan, H. & Elghobashi, S. "2-Component LDA Measurement in a 2-Phase Turbulent Jet", AIAA Journal, Vol. 22, no. 5, pp. 624-630 (1984)

Modarress, D., Wuerer, J. & Elghobashi, S. "An experimental study of a round two-phase jet", AIAA Paper 82-0964 (1982)

Prevost, F., Boree, J., Nuglisch, H.J. & Charnay, G. "Measurements of fluid/particle correlated motion in the far field of an axisymmetric jet", International Journal of Multiphase Flow, Vol. 22, no. 4, pp. 685-701 (1996)

Schiller, L. and Naumann, A. Fundamental calculations in gravitational processing, Zeitschrift Des Vereines Deutscher Ingenieure, Vol. 77, pp. 318-320 (1933)

Shuen, J.S., Solomon, A.S.P., Zhang, Q.F. & Faeth, G.M. "Structure of Particle-Laden Jets - Measurements and Predictions", AIAA Journal, Vol. 23, no. 3, pp. 396-404 (1985)

Tennekes, H. & Lumley, J.L. A First Course in Turbulence, The MIT Press, Cambridge, Massachusetts. (1972)

Tsuji, Y., Morikawa, Y. & Shiomi, H. "LDV Measurements of an Air Solid 2-Phase Flow in a Vertical Pipe", Journal of Fluid Mechanics, Vol. 139, no. FEB, pp. 417-434 (1984)

Tsuji, Y., Morikawa, Y., Tanaka, T., Karimine, K. & Nishida, S. "Measurement of an Axisymmetric Jet Laden with Coarse Particles", International Journal of Multiphase Flow, Vol. 14, no. 5, pp. 565-574 (1988)

Tu, J.Y. & Fletcher, C.A.J. "An Improved Model for Particulate Turbulence Modulation in Confined 2-Phase Flows", International Communications in Heat and Mass Transfer, Vol. 21, no. 6, pp. 775-783 (1994)

Vreman, A.W. "Turbulence characteristics of particle-laden pipe flow", Journal of Fluid Mechanics, Vol. 584, pp. 235-279 (2007)

Wygnanski, I. & Fiedler, H. "Some Measurements in Self-Preserving Jet", Journal of Fluid Mechanics, Vol. 38, pp. 577-612 (1969)

Yuan, Z. & Michaelides, E.E. "Turbulence Modulation in Particulate Flows - a Theoretical Approach", International Journal of Multiphase Flow, Vol. 18, no. 5, pp. 779-785 (1992)

Department of
ENERGY TECHNOLOGY

E.T.

AALBORG UNIVERSITY

Numerical Investigation of Large Particles in Upward Pipe Flow with Sinusoidal Wall Boundary Condition

Matthias Mandø and Lasse Rosendahl

Aalborg University, Department of Energy Technology, Site: http://iet.aau.dk
Pontoppidanstraede 101, DK-9220 Aalborg, Phone: +45 9940 9248, Email: mma@iet.aau.dk

Abstract

Numerical simulation of upward turbulent particle-laden pipe flow is performed with the intension to reveal the influence of surface roughness on the velocity statistics of the particle phase. A rough wall collision model, which models the surface as being sinusoidal, is proposed to account for the wall boundary condition ranging for smooth surfaces to very rough surfaces. Simulations are performed using the Eulerian-Lagrangian methodology for the dilute one-way coupling regime. Results are reported for 3 sizes of glass spheres: 50μm, 200μm and 550μm.

Conclusions

Particle statistics are greatly affected by the wall BC. As such, the mean axial velocity at the centerline was up to *7% higher* for smooth wall BC compared to rough wall BC while the particle TKE was similarly found to be *two orders of magnitude greater*. The particle RMS velocities require somewhat longer time/distance compared to the mean velocity before the flow can be considered to be fully developed. The entry length was not found to depend on the surface roughness.

Model

A rough wall boundary condition has been implemented into a CFD context by assuming a sinusoidal surface. The shadow effect and the geometric constraints are included by limiting the range of the inclination angle. For each collision the range of possible collision within the 2π period of the sinus function is calculated according to the "shadow" zone which occurs for small impact angles α. Thereafter the inclined plane which the particle collides with is determined using a uniform random function.

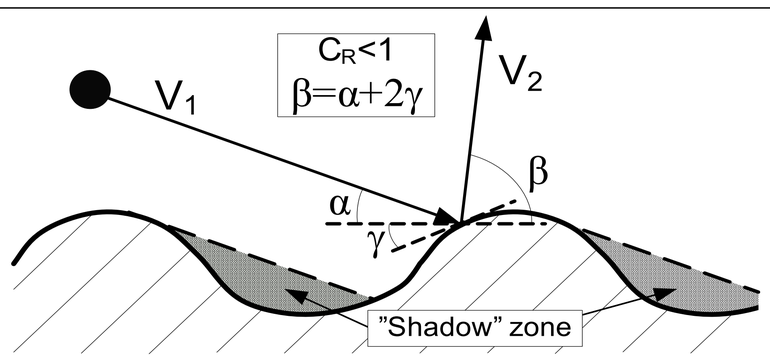

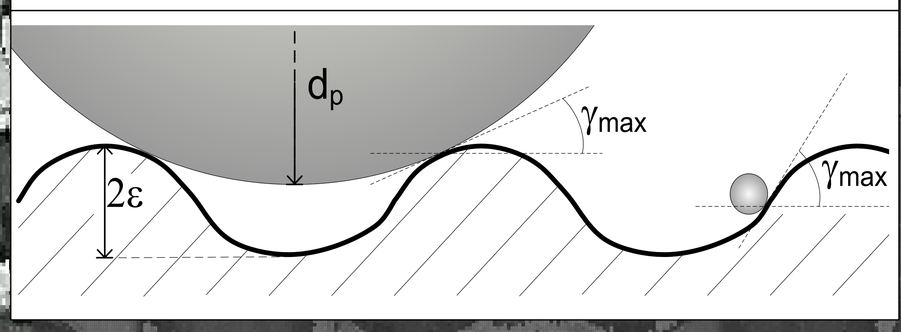

Performance Map

Due to the shadow effect small impact angles result in a greatly enhanced normal coefficient and the particles tend to 'jump' out normally to the wall. For larger impact angles the shadow effect abates and the rebound angles becomes fully random.a large ratio between the particle diameter and the surface roughness will only yield small maximum inclination angles whereas the opposite, a small particle diameter relative to the surface roughness, will result in larger maximum inclination angles.

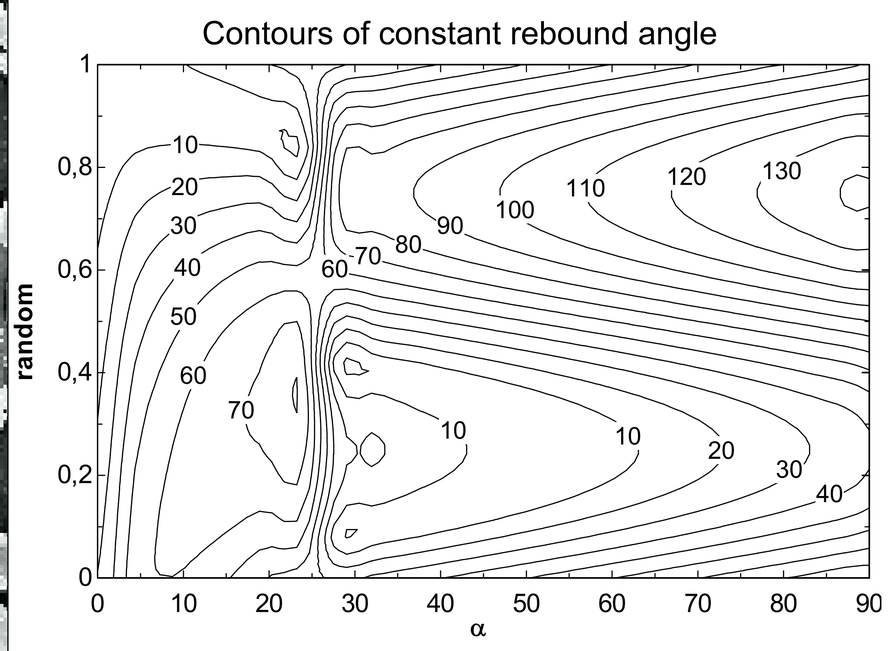

Effect on Entry Length

For all cases the particles RMS velocity takes a considerable longer distance to become fully developed compared to the mean velocity. There is a clear correlation between the entry length and the particle size and the largest particles require up to 200 pipe diameters before fully developed conditions are achieved. There does not seem to be a strong correlation between development length and the surface roughness. For the ideal collision with a perfectly smooth wall the entry length increases significant whereas simulation considering an almost smooth wall produce better results.

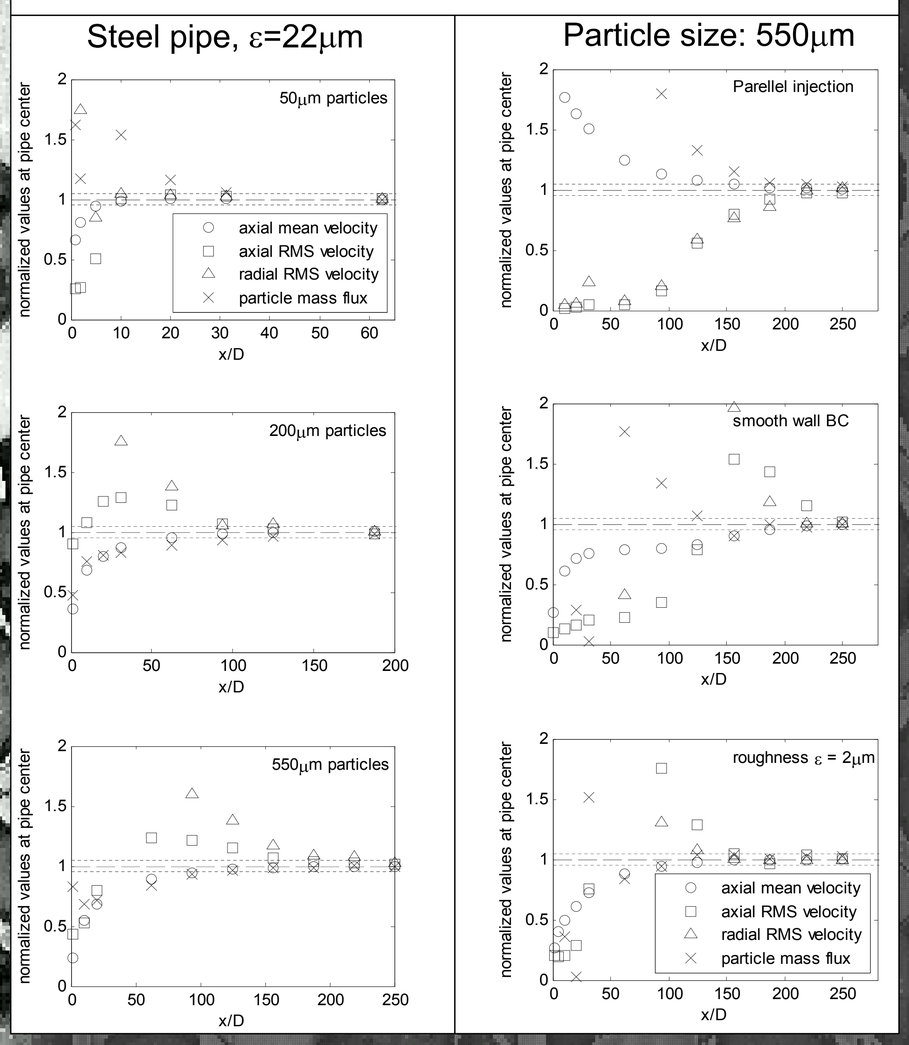

Influence of Roughness, d_p=550μm

It is necessary to take the surface roughness into account to correctly predict the particle RMS velocity. The surface roughness tends to reduce the mean velocity of the particles and increase the concentration at the centerline of the pipe. The present results are overall found to agree with that of Mathiesen et al. (2008) and this shows the importance of using correct wall boundary conditions to predict the particle RMS velocity. The particle RMS velocity is stongly coupled to the surface roughness of the wall and results show that the particle velocity reaches a maximum level where an additional increase in surface roughness yields no increase in the RMS and mean slip velocity.

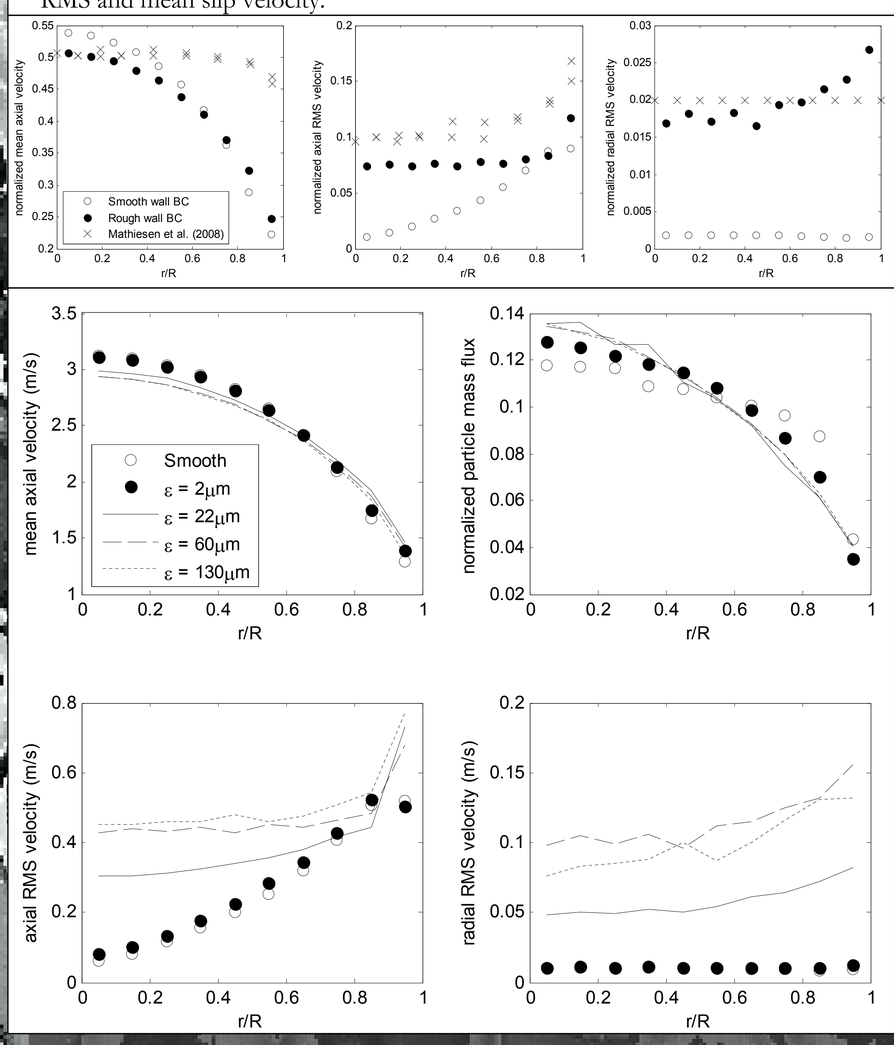

Powder Technology 202 (2010) 1–13

Contents lists available at ScienceDirect

Powder Technology

journal homepage: www.elsevier.com/locate/powtec

Review

On the motion of non-spherical particles at high Reynolds number

Matthias Mandø *, Lasse Rosendahl

Aalborg University, Institute of Energy Technology, Pontoppidanstraede 101, 9220, Aalborg East, Denmark

ARTICLE INFO

Article history:
Received 13 August 2009
Received in revised form 29 March 2010
Accepted 3 May 2010
Available online 7 May 2010

Keywords:
Non-spherical particles
Particle equation of motion
Gas–solid interaction
Dispersed multiphase flow

ABSTRACT

This paper contains a critical review of available methodology for dealing with the motion of non-spherical particles at higher Reynolds numbers in the Eulerian–Lagrangian methodology for dispersed flow. First, an account of the various attempts to classify the various shapes and the efforts towards finding a universal shape parameter is given and the details regarding the significant secondary motion associated with non-spherical particles are outlined. Most investigations concerning large non-spherical particles to date have been focused on finding appropriate correlations of the drag coefficient for specific shapes either by parameter variation or by using shape parameters. Particular emphasis is here placed on showing the incapability of one-dimensional shape parameters to predict the multifaceted secondary motion associated with non-spherical particles. To properly predict secondary motion it is necessary to account for the non-coincidence between the center of pressure and center of gravity which is a direct consequence of the inertial pressure forces associated with particles at high Reynolds number flow. Extensions for non-spherical particles at higher Reynolds numbers are far in between and usually based on semi-heuristic approaches utilizing concepts from airfoil theory such as profile lift. Even for regular particles there seems to be a long way before a complete theory can be formulated. For irregular particles with small aspect ratio, where the secondary motion is insignificant compared to the effect of turbulence, the drag correlations based on one-dimensional shape parameters come to their right. The interactions between non-spherical particles and turbulence are not well understood and modeling attempts are limited to extending methods developed for spheres.

Contents

1. Introduction

Irregular non-spherical particles are found in most industrial particulate flows and similarly most engineering flows are turbulent. However, the vast majority of scientific investigations of particulate flows assume particles to be perfectly spherical particles. The exact governing equations for turbulent flow have been known for over a century but the utilization of these is significantly impeded by the need to resolve the smallest flow structures and time scales. Consequently, for most practical uses, turbulence is modeled using Reynolds or Favre averaging and the interaction with particles is handled by random walk models. Large non-spherical particles present their own set of particular problems in the context of Computational Fluids Dynamics (CFD): How to define and quantify the shape? How to deal with secondary motion? How well will the methodology developed for spheres work for highly non-spherical shapes? How to handle turbulence? This paper attempts to give an account of the present state of modeling the motion of large non-spherical particles. The relevance of this paper also becomes evident

* Corresponding author.
E-mail addresses: mma@iet.aau.dk (M. Mandø), lar@iet.aau.dk (L. Rosendahl).

0032-5910/$ – see front matter © 2010 Elsevier B.V. All rights reserved.
doi:10.1016/j.powtec.2010.05.001

considering the increasing efforts towards the replacement of pulverized coal with biomass in existing and new power plants. Whereas pulverized coal particles are small and the spherical ideal is a fair approximation, pulverized biomass particles are characterized as large and with high aspect ratios due to their fibrous nature. This investigation has been limited to the Eulerian–Lagrangian methodology and to solid non-deforming particles in Newtonian fluids. Please refer to Sommerfeld et al. [68] for an updated outline on existing knowledge concerning multiphase flow and Chhabra [13] for particle motion in non-Newtonian fluids.

2. Classification of shape

Particles come in all sort of shapes and sizes, in fact, due to the arbitrary nature of naturally occurring particles there are an indefinite number of possible shapes. This necessitates the need for a set of parameters to aid in the description of different particle shapes for the implementation in the numerical models and the relay of relevant information to other scientists. This information is available in many books on the subject, e.g. Rhodes [61] or Clift et al. [18] contain much useful information, and here we limit ourselves to focus on the most pertinent issues involved in the classification of shapes. One such issue seems to be the terminology used. The word non-spherical most often, and somehow also in the title of this paper, refers to all shapes which are not perfect spheres. However, the true meaning of the word spherical is: "shape which is sphere-like" which thus implies a subjective distinction. In the context of CFD it is useful to use this to objectively distinguish between shapes which with reasonable accuracy can be approximated as spheres and shapes which require a more intricate handling. Another often used terminology to characterize shapes which are not spheres[1] is the word "irregular" whose true definition is counter to that of regular shapes. Table 1 outlines the categorization using the above discussed terminology.

Table 1 serves as a reference for the following discussion of different simulation strategies in this work. Spherical particles have no or only little secondary motion associated with their trajectories, assume no preferred orientation but rather tumbles and thus it would be justified to base the simulation methodology on that used for spherical particles i.e. not considering orientation or shape induced lift. Possible extensions to the simulation methodology thus revolve around modifications to the drag coefficient considering the shape or by specifying an equivalent diameter and using drag correlations based on spheres. Non-spherical particles on the other hand are associated with shape induced lift, orientation dependent lift and drag forces, significant secondary motion and may assume a preferred orientation depending on the regime of motion. Thus, it is necessary to revise the usual strategy to properly capture these phenomena. This involves keeping track of the orientation and rotation of the particle as well as the formulation of appropriate orientation dependent lift and drag force on a per shape basis. For irregular non-spherical particles common strategies involve the approximation of the shape to a regular counterpart e.g. cylinder for a wood splinter, disk for a flake. The distinction between spherical and non-spherical particles is principally subjective and thus open for interpretation. Here, it is suggested that the distinction is made on the basis of the aspect ratio, β. This simple criterion can be easily measured via microscopy techniques and is a good representative for when secondary effects become important. According to Christiansen and Barker [15] and Clift et al. [18] a suitable value for this criterion is $\beta = 1.7$ which also roughly corresponds to the aspect ratio for a cube (based on the diagonal to the side length). Thus, particles below this ratio are considered spherical and can be treated with reasonable accuracy using a single drag correlation of choice. Particles above this ratio should be classified according to which generic shape they resemble the most e.g. cylinder, disk, spheroid, super-ellipsoid of revolution and treated accordingly.

Table 1
One possible categorization of shapes.

	Spherical	Non-spherical
Regular	Polygons, spheroids with low aspect ratio	Cubes, cylinders, disks, tetrahedron, spheroids with high aspect ratio
Irregular	Pulverized coal, sand, many powders, particulate matter	Pulverized biomass, flakes, splinters, agglomerates

For spherical particles it is only necessary to specify an equivalent diameter and optionally a shape factor to account for the departure in shape from a sphere. Table 2 gives an outline of commonly used diameter definitions after Allen [1]. Note that projected area, Ferets and Martins diameters are determined directly from image analysis while area and volume equivalent diameters often are based on image analysis by assuming a thickness. The other diameters listed correspond to a particular analysis method e.g. Stokes diameter which is found from sedimentation techniques.

The main difficulties are thus reduced to a matter of measurement and it seems appropriate to offer a few comments about available measurement methods. The basis for all methods is that they provide the same result when applied to a perfect sphere while marked differences occur as the shape becomes non-spherical due to the differences in the diameter definitions. In some scientific or industrial fields specific methods are prevailing due to the individual strengths of particular methods e.g. sieve analysis is often preferred whenever a wide size distribution is encountered while it may be unsuitable for very fine powders. Aerodynamic separation and sedimentation techniques are used for fine powders and particulate matter which tends to be spherical in nature and due to the diameter definitions the size distributions can be used directly in Lagrangian trajectory calculations using the drag coefficient of a sphere. Due to practical and theoretical considerations these methods are not used for particles larger than 50 μm and thus any discussion concerning large non-spherical particles becomes somewhat irrelevant. Image analysis is regarded as a benchmark compared to other techniques as this involves direct determination of the diameter. However, as image analysis is based on a two-dimensional measurement this method becomes increasingly biased as the particles deviate from the spherical ideal. For example the volume equivalent diameter of flake-like particles will be systematically overestimated if their thickness is assumed to be proportional to their 2D extent while

Table 2
Commonly used diameter definitions.

Aerodynamic/drag diameter	Diameter of a sphere of unity density with the same terminal velocity as the particle
Stokes diameter	Diameter of a sphere of same density and the same terminal velocity as the particle
Projected area diameter	Diameter of a circle having the same area as the projection of the particle
Ferets diameter	The mean value of the distance between pairs of parallel tangents to the projected outline of the particle
Martins diameter	The mean chord length of the projected outline of the particle
Area equivalent diameter	Diameter of a sphere having the same surface area as the particle
Volume equivalent diameter	Diameter of a sphere having the same volume as the particle
Sieve/mesh diameter	The width of the minimum square aperture through which the particle will pass
Laser diffraction diameter	Diameter is calculated according to the Mie or Fraunhofer diffraction theory

[1] The appropriate term non-sphere is surprisingly hardly ever used.

laying flat on a plate [59]. This bias can somewhat be rectified by analyzing images of particles in free fall but the failure to resolve the third dimension ultimately means that this method is associated with significant measurement uncertainty. Full 3D analysis which would involve the use of two or more cameras set at an angle to each other has the potential to provide accurate measurement of the shape and volume. However, the complicity of such a method has so far hindered the implementation into commercially available equipment. Popular methods to determine the size distribution of particles are by sieves and laser diffraction. Although these methods are very different they are associated with similar types of uncertainty. Sieve analysis allows slender particles to pass through a fine mesh compared to the particle volume equivalent diameter while flake-like particles will be stopped by a coarse mesh relative to the particle volume equivalent diameter. Similarly, the laser diffraction technique relates the diameter to the orientation of the particle crossing the measurement volume [3]. As the particle is allowed to rotate freely, this means that a slender particle can be assessed on the basis of its smallest dimension while the flake-like particle might be assessed on the basis of its largest dimension. As such both methods are associated with similar, wider size distributions [55]. Furthermore, the cross-sectional area averaged over all orientations for a non-spherical particle is larger than for an equal volume sphere [23]. Depending on predominant shape in a given sample sieve analysis might predict a larger or a smaller mean value compared to the true mean while laser diffraction tends to overestimate the true size distribution [55,58]. As a final remark on the use of single dimension definitions for non-spherical particles, it may be said that they are often reported indiscriminately and used without any regard to the requirement of the drag correlation [6]. Significant biases are associated with the measurement of particle sizes for non-spherical particles for all measurement methods and the problem severely deteriorates for increasing aspect ratios. By using equivalent diameters all data about the shape of the particle is essentially lost and to be able to retain this information additional shape factors have been suggested to quantify the geometry/irregularity of non-spherical particles. These can be seen as a parallel to the roughness factors which are commonly used for pipe flow. Note that only image analysis is capable of supplying the additional information regarding the shape of the particle and that this information is often based on the assumption that 2D images of particles can be directly related to the 3D shape of the particle. Table 3 gives an outline of the most commonly used shape factors.

These shape factors can be used for both regular and irregular particles, but especially suited for the latter since the shape of irregular particles cannot be expressed in any other way [44]. Many alternative shape factors [18,21,48,72] have also been suggested, but none has won greater acceptance or use despite clamed superiority. Fractal dimensions and harmonics have also been used to characterize the shape/morphology of irregular particles [16,67,76]. However, these have not been used in conjunction with CFD simulations and are not addressed further. Automated algorithms in image processing software allow for quick determination of shape factors as well as dimensions but the accuracy is limited by the previously mentioned assumptions for 2D images of 3D particles. Presently, the most commonly used shape factor is the sphericity, ψ. This does not seem to be due to superior performance when used in correlations of the drag coefficient or because it is easier to measure than other shape factors. A closer look at the formulation of sphericity shows that it represents the inverse of a surface enhancement factor for a sphere with equivalent volume and can thus be used in combusting flows to additionally account for the surface area available for reactions. However, the true reason for the greater popularity of the sphericity is most likely that it simply seems to be the most elegant way to quantify the shape of an arbitrary particle. In lack of significantly better shape factors, evaluated on their ability to correlate the drag coefficient, the more elegant formulation has won predominance.

Table 3
Commonly used shape factors [34,75].

Corey shape factor	Ratio of the smallest principal length axis of the particle to the square root of the intermediate and longest principle length axis
Volumetric shape factor	Ratio of the volume of the particle to the diameter of a sphere with the same projected area as the particle cubed
Roundness	Ratio of the average radius of curvature of the corners to the radius of the largest inscribed circle
Sphericity	Ratio of the surface of a sphere with the same volume as the particle and the surface area of the actual particle

3. Drag correlations for translational motion

Shape factors form the basis for most attempts to describe the motion of spherical and non-spherical particles at higher Reynolds numbers. Most of these correlations employ the volume equivalent sphere diameter, d_{Veq}, as the characteristic size and the sphericity, ψ, to quantify the shape and is thus expressed as:

$$C_D = f(\mathrm{Re}, \psi) \tag{1}$$

where the characteristic size is usually taken as the diameter of a sphere with the same volume as the particle. Five different correlations of the drag coefficient for non-spherical particles have been compared against a large database of independent experimental data in the study of Chhabra et al. [14]. The average error reported varies between 16% and 43% whereas the maximum reported error for all correlations is above 100%. The largest errors are encountered for hollow cylinders and agglomerates of spherical particles. These shapes represent extremes in terms of the sphericity and they have little resemblance with a sphere. The general rule which can be drawn is that the further away from the spherical ideal the shape of the particles is, the poorer the correlations perform. Depending on the flow regime and the shape, particles which have the same value of sphericity might take on very different motion patterns or preferred directions and are thus associated with very different drag coefficients when the projected area used, is that of a sphere with the same volume as the particle. The classical example to illustrate this is by considering particles shaped as cylinders of different length to diameter ratio. The sphericity of a cylindrical particle can be expressed as:

$$\psi = \frac{2\left(\frac{3}{2}\beta\right)^{2/3}}{1+2\beta},\ \beta = \frac{L}{D} \tag{2}$$

where β is the aspect ratio expressed for a cylinder as the length, L, to the diameter, D, of the cylinder. From this expression it can be realized that both a cylinder with an aspect ratio less than one, commonly referred to as a disk, and a cylinder with an aspect ratio above unity can have the same value of sphericity.

From the experimental data from McKay et al. [53] for the drag coefficient of falling cylinders, it can be realized that the drag coefficient for disks is distinctively different from that of cylinders, even when only small aspect ratios are considered. In Fig. 1 the difference between the measured drag coefficient and that calculated on basis of the correlation by Ganser [28], the most accurate of the correlations investigated by Chhabra et al. [14], is indicated as percentage error. To provide a relevant reference, the error obtained from using a correlation developed strictly for spheres [17] and a correlation for freely falling cylinders with finite length in liquids [39] is also indicated. It can be seen that the correlation by Ganser [28] provides an acceptable fit for aspect ratios below unity whereas for aspect ratios above unity the correlation becomes exceedingly poorer. Using correlations developed for specific shapes gives the most

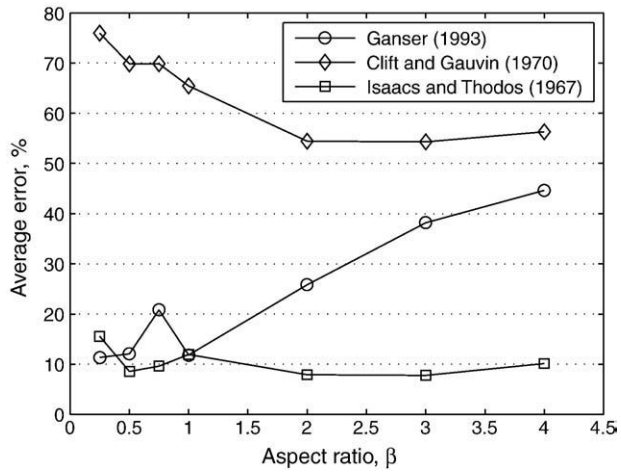

Fig. 1. The error using the correlations by Clift and Gauvin [17], by Isaacs and Thodos [39] and by Ganser [28] evaluated by the experimental data for disk and cylinders obtained by McKay et al. [53] with $1000<Re<30{,}000$.

satisfying result whereas the practice of using the diameter of a volume equivalent sphere in correlations of the standard drag curve for a sphere gives poor results. An overview of references on the drag for regular non-spherical shapes is provided in [18] and this topic is therefore not dealt with further. For irregular shapes, it is recommended to only use correlations based on the sphericity for particle shapes with a sphericity approaching unity. This corresponds to shapes with small aspect ratios and which thus only deviates slightly from the spherical ideal. However, if an investigation centers on a specific shape, the best result is obtained by making an empirical fit of the drag coefficient as a function of the Reynolds number for that specific shape. For distinctive non-spherical irregular particles, where the ratio of the maximum length to the minimum length is above 1.7, the shape should be classified either as rod-like, which can be approximated by a cylinder, or flake-like, which can be approximated by a disk [15]. Again it should be pointed out that although it is possible to specify a drag coefficient for a free falling non-spherical particle, which correlates with the primary translational motion, non-spherical particles are associated with significant secondary motion which again may alter their main trajectory. Note also that, although correlations exist for many regular non-spherical shapes, these are often based on scant data sets, which are associated with considerable scatter, due to the secondary motion.

4. Classification of regimes of secondary motion

For spheres expansions of the equation of motion to higher Reynolds numbers are usually achieved by empirical fits of the drag coefficient. For spherical particles this approach works well because the motion pattern is not associated with noticeable secondary motion nor does it assume a preferred direction. The drag coefficient can be expressed by properly accounting for the increase in particle surface area either by using an aerodynamic equivalent diameter or by using shape factors. However, the drag on a non-spherical particle is dependent on its orientation. Primarily, the projected area, on which the drag is based, may differ by several orders of magnitude from one orientation to another but also the drag coefficient varies significantly depending on the orientation. Also, rotational effects are important when considering orientable particles and the equations for conservation of rotational momentum must be taken into consideration as translational motion depends directly on them. Non-spherical particles are associated with characteristic secondary motion depending on the Reynolds number regime and their shape. Moreover, in some Reynolds number regimes particles will take on a preferred direction. Most investigations of the motion of non-spherical particles deal with the generic shapes of ellipsoids, cylinders and disks since these can be made, by parameter variation, to resemble a great number of different shapes. Particles with an oblong shape, such as a prolate ellipsoid or a cylinder, are often used to resemble fibers, while particles with a flat shape, such as an oblate ellipsoid or a disk, can be used to represent flakes.

For very low Reynolds number flow, $Re_p<0.1$ (Stokes flow), both oblong and flat particles in a shear flow will move in slow orbits, known as Jeffery's orbits, after G.B. Jeffery [40] who was the first to describe the motion. One restriction in this analysis is that the particles have to obey certain symmetry conditions which strictly speaking would exclude all irregular particles. Characteristic for non-spherical particles in Stokes flow is that, although they move in orbits the majority of the time, they will be aligned or be at a small angle to the flow [4]. In practical terms it is thus more useful to state that the particles tend to align themselves with the flow. This effect has also been observed for fibers used in the manufacturing of paper and thus it seems sensible to also assume that irregular particles would exhibit this behavior providing that they have a large aspect ratio. The motion of particles in Stokes flow represents the only purely theoretical approach to the motion of non-spherical particles and consequently most investigations on the motion of non-spherical particles dwell on this topic. The motion of particles in creeping flow has been extensively reviewed by Leal [49] and more recently in the work by Carlsson [12] and this topic is therefore not dealt with further.

At moderate Reynolds number flow, $0.1<Re_p<100$, inertial effects become important, and a steady recirculation zone starts to build up in the wake of the particles. The pressure distribution on the particle, due to the recirculation zone, forces the particles to align themselves with their maximum cross-section normal to the flow. Generally this effect is more pronounced at higher Reynolds numbers and for particles with a more pronounced non-spherical shape. Since the particles are steadily aligned perpendicular to the flow, empirical data for the generic shapes, such as an infinite long cylinder in cross-flow, may be used to model the motion. For disks expressions for fixed disks in cross-flow can be used directly while for cylinders appropriate corrections for end effects should be applied for cylinders with finite length.

High Reynolds number flow, $Re_p>100$, is characterized by significant secondary motion which is superimposed on the particles' steady fall or rise. The secondary motion is initiated by the onset of wake instability and also signals the beginning of vortex shedding from the wake of the particles. The secondary motion may be in the form of large periodic swings around a mean vertical path or chaotic tumbling which can take place at an angle to the vertical fall or rise direction. The oscillatory motion is coupled with the wake instability and photographic evidence using dye injected in the wake of a falling disk show that the end of each swing is followed by the shedding of a vortex [78]. Besides the Reynolds number the motion patterns have been shown to correlate well with the non-dimensional moment of inertia; here shown for a disk:

$$I^* = \frac{I_{disk}}{\rho D^5} = \frac{\pi\rho_p}{64\rho}\beta. \tag{3}$$

For a disk this is obtained by dividing the moment of inertia with the fluid density and disk diameter times five. Note that the dimensionless moment of inertia for a disk is thus transformed into an expression involving the density ratio and the aspect ratio. These two parameters are often used in the description of the motion of non-spherical particles. As such these two parameters were previously used to correlate the drag coefficient of a freely falling cylinder [39]. The dimensionless moment of inertia can similarly be defined for other regular shapes using the associated moment of inertia and the appropriate characteristic length for that shape. However, it is only for

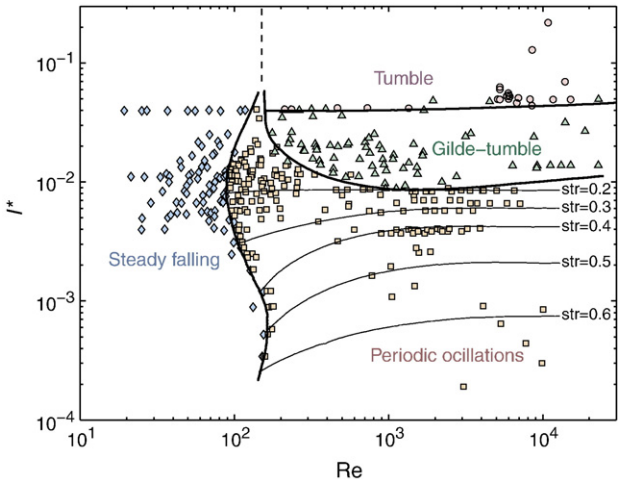

Fig. 2. Flowmap showing the behavior of disks ($L/D<0.1$) as function of the Reynolds number and the dimensionless moment of inertia. Data from Stringham et al. [70], Willmarth et al. [78] and Field et al. [26]. Contours of constant Strouhal number are shown for periodic oscillations.

disks that the dimensionless moment of inertia has been used to construct intricate flow maps as seen in Fig. 2.

The dimensionless moment of inertia is also known as a stability number [70] and basically indicates the inertial resistance of non-spherical particle to rotate. Thus thin disks, with very low I^*, will not perform a full rotation and tends to fall in great arcs of periodic sideward motion for high Re whereas more bulky disks, with high I^*, provide little rotational stability and undergo full rotation, tumbling motion, for Re>150. An intermediate regime where disks switch between periodic oscillations and tumbling motion is referred to as the glide–tumble regime. The different motion patterns for a disk are shown in Fig. 3.

The steady fall, periodic oscillation and tumbling regimes can be categorized as *stable* regimes where the frequency of rotation, in regime IV, approaches the oscillation frequency of regime II. Furthermore, the Strouhal number for disks has been shown to a linear function of the dimensionless moment of inertia for constant Reynolds numbers [78]. The glide–tumble motion is unstable and it can be interpreted as a transition regime for periodic oscillations with intermittent bursts of tumbling [26].

For freely falling cylinders only two distinct motion patterns can be identified. Depending on the Reynolds number cylinders assume either steady falling or periodic oscillations with their maximum cross-section normal to the direction of the flow. For periodic oscillating cylinders in free fall Marchildon et al. [52] provide the following empirical fit of the Strouhal number:

$$Str = c\sqrt{\frac{\rho\beta}{\rho_p}} \tag{4}$$

where $c=0.095$ and the Strouhal number have been based on the length of the cylinder as the characteristic dimension. This fit has since been verified by Sørensen et al. [69] for a wider range of Reynolds numbers although with a constant of proportionality approximately half of that given by Marchildon et al. [52]. Notice that for cylinders the aspect ratio and the density ratio are still important parameters but the relationship with the Strouhal number is not linear as it was for disks. Following Marchildon et al. [52] analysis it can realized that a Strouhal number based on a characteristic length which is a combination of the length and the diameter can reduce Eq. (4) to a relation only depending on the density ratio. However, the physical significance of such an approach is uncertain. It is also reported that the steady oscillatory motion around the horizontal plane is accompanied with rotation around the axis parallel to the fall direction or even a mean sideward motion [69,70]. There does not seem to be any clear pattern of this and the best explanation is possible that it relates to either initial condition, the release mechanism, or has to do with the vicinity of the walls of the experimental setup.

The analysis up to now has only looked at particles with uniform mass distribution. However, large naturally occurring particles are also often characterized by having a non-uniform mass distribution which can be related to cavities in the shape. A prime example is the case of shredded straw which can be described as being mainly hollow, but where the presence of solid nodes seriously disrupts the uniformity of the mass distribution. Generally, for an otherwise symmetric particle, the movement of the center of mass away from the center of geometry acts to turn the particle to fall with its heaviest side downward. Clearly, this significantly alters the motion characteristics and can considerably increase the terminal velocity of that particle [64]. A particle with a non-uniform mass distribution but with a coincident location of the center of mass with the center of geometry, i.e. a straw particle with a node in the middle, will have the same resistance characteristics as the uniformly distributed case [5]. However, since the moment of inertia can be different this has the potential to affect the secondary motion pattern of that particle.

Regular and irregular particles with aspect ratio close to unity falls with no preferred orientation and with a motion pattern which best can be described as tumbling. Indeed, if a dimensionless moment of inertia was calculated based on Eq. (3) for these particles it would

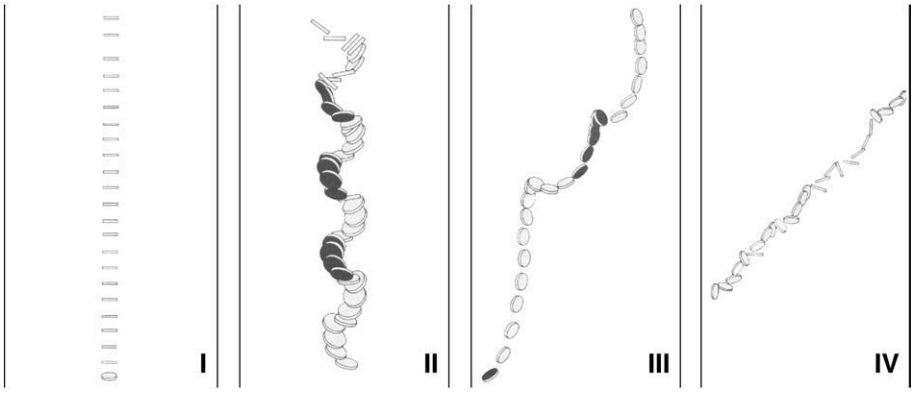

Fig. 3. Regimes of motion for a disk. (I.) Steady fall. (II.) Periodic oscillations. (III.) Glide–tumble. (IV.) Tumbling. Modified from Stringham et al. [70].

indicate the instability of their motion. To sum up, it can be stated that the stability of a path, or resistance towards tumbling, increases with increasing aspect ratio. The density ratio is known to be correlated with the steady fall or rise velocity. Moreover, as the relative velocity of the particle increases so do the inertial effects acting to destabilize the particle. As the Reynolds number increases the recirculation zone in the wake of the particle becomes unstable and the particle initiates its secondary motion characteristic for that shape. In the absence of turbulence, the wake instability is the only source acting to promote the secondary motion.

5. Orientation dependent models

Whether spherical or non-spherical, regular or irregular the motion of particles is derived by considering the conservation of linear and angular momentum. In differential form the equations can be stated as:

$$\frac{d\vec{x}}{dt} = \vec{u}_p, \quad m_p \frac{d\vec{u}_p}{dt} = \sum_i \vec{F}_i \tag{5}$$

$$\frac{d\vec{\theta}}{dt} = \vec{\omega}_p, \quad \vec{I}_p \frac{d\vec{\omega}_p}{dt} = \sum_i \vec{T}_i \tag{6}$$

where x is the position vector, u_p is the particle linear velocity, m_p is the particle mass, F is the force acting on the particle, θ is the angle between the principle axis of the particle and the inertial coordinate system, ω_p is the angular velocity, I_p is the moment of inertia and T is the torque acting on the particle. Where Eq. (5) deals with the location and linear velocity of the particle Eq. (6) is responsible for the orientation and the angular velocity of the particle. Eqs. (5) and (6) nicely demonstrate the similarity between translational and rotational motion. However, these equations are only strictly correct for a particle which is symmetric around the center of mass (a sphere). For a generic non-spherical particle it is necessary to include an additional cross-linked term which addresses the difference in the moment of inertia in the different directions, see Appendix A. Generally, the particle translation is evaluated in the inertial coordinate system whereas the particle rotation is evaluated in a coordinate system parallel to the principle axis of the particle. Fig. 4 shows the relationship between the different coordinate systems.

Since surface forces acting in the inertial system are based on the orientation of the particle this necessitates the use of transformation between coordinates. Moreover, besides solving for the particle position as well as the particle linear and angular velocity, it is required to solve for the particle orientation represented by the angles between the co-rotational and the co-moving coordinate systems; the so-called Euler angles. The entire procedure relating to the translation and rotation of a non-spherical particle has been outlined in Appendix A. There it can be seen that it is also necessary to use an additional ordinary differential equation for particles which undergo full rotation to avoid the singularity which would otherwise occur when the Euler angles are used in relation to the co-rotational coordinate system. Despite this, it may be stated that the additional evaluation of particle rotation and orientation only require approximately twice the processing power and memory. Thus, there is no strong argument not to consider particle rotation due to computational requirements! With regard to the mathematical procedure previously published studies usually translate the particle for a sufficiently short time interval with fixed orientation after which the particle is rotated for an equal time interval [27,79]. Physically, this implies that the translational and rotational motion is decoupled. Furthermore, such a procedure also assumes that the change in linear velocity is smaller than the change in the angular velocity. Remaining issues with regard to optimization of the numerical procedure relate to the possible use of different time steps for Eqs. (5) and (6), preferably as multiples of each other, and the use of accuracy control for each time step. The use of different time steps would ensure against redundant evaluations if the change in one velocity is much smaller than the other. It should also be noted that it is possible to use a weak coupling between the Lagrangian and Eulerian phase meaning that trajectories and the continuous phase can be updated independently during the iterations. Previous investigations have not focused on optimization of the numerical procedure but rather on the formulation of the forces and torques which act on the particle.

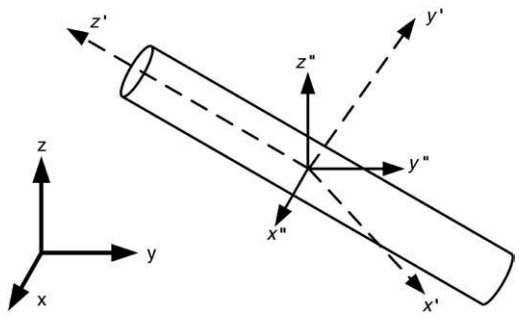

Fig. 4. Relationship between the inertial (x,y,z), the co-rotational (x',y',z') and the co-moving (x'',y'',z'') coordinate systems.

Similar to the assumption of a spherical shape in most studies involving particles, most studies involving non-spherical particles assume Stokes flow. For non-spherical particles in Stokes flow it is possible to derive the forces and torques which act on the particle on a theoretical basis similar to the procedure used for spheres to derive the BBO-equation. The usual procedure for spheres, which involves the formulation of appropriate empirical coefficients to account for the difference from Stokes flow, is also applied for non-spherical particles. However, it is also necessary to account for the offset of the center of pressure in relation to the center of geometry, see Fig. 5.

The pressure distribution on the surface of a particle inclined to the flow direction no longer follows the symmetry of that particle. This gives rise to an additional lift force as well as an additional torque due to the displacement of the center of pressure. Besides this, the main complication when considering non-spherical particles is the endless variations of the shape of the particle. To combat this, most investigations include some sort of parameter variation in the formulation of forces and torques. The most popular being the ellipsoid of revolution which can be used to resemble a large array of different shapes including flake-like particles and rod-like particles. A distinctive advantage of the ellipsoid of revolution is that it has no sharp edges which in a mathematical analysis would be seen as discontinuities. The groundbreaking work on the motion of ellipsoids was made by Jeffery [40] for suspension in uniform shear flow under Stokes conditions where the formulation for the resistance force and torque is derived. This analysis has later been expanded by Brenner[2] in the 1960s to arbitrary flow fields although still only under Stokes flow conditions. Following the formal notation by Gavze [29] the equation of motion for a non-spherical particle can be formulated compactly as:

$$\mathbb{F} = -\mathbb{R}\boldsymbol{u} - \mathbb{P}\cdot\dot{\boldsymbol{u}} - \int_0^t \mathbb{T}(t-\tau)\cdot\dot{\boldsymbol{u}}(\tau)d\tau, \quad \mathbb{F} = \begin{bmatrix}\mathbf{F}\\ \mathbf{M}\end{bmatrix}, \ \boldsymbol{u} = \begin{bmatrix}\mathbf{U}\\ \boldsymbol{\omega}\end{bmatrix} \tag{7}$$

where $\mathbb{R}$, $\mathbb{P}$ and $\mathbb{T}$ are respectively the steady, potential and Basset tensors. However it should be noted that the coupling of the unsteady terms with the orientation of the particle is still a remaining challenge.

[2] The work of Jeffery was extended in the 1960s by Professor Howard Brenner in a series of publications: [7–10,32] and [11].

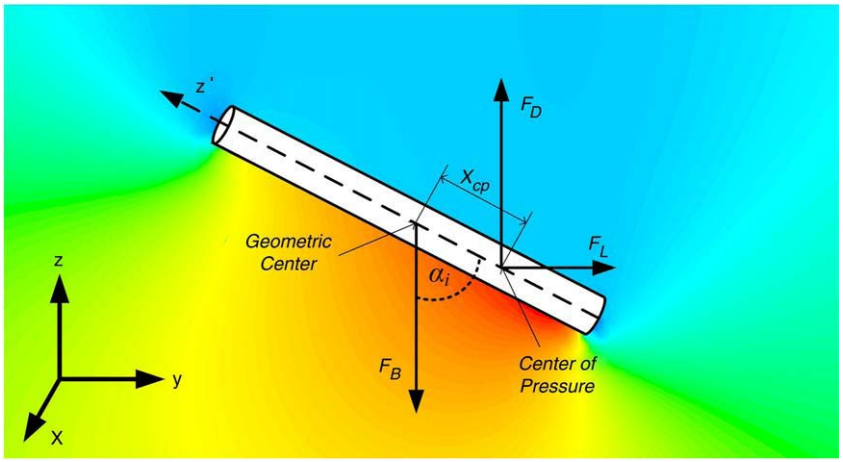

Fig. 5. The pressure distribution around an inclined cylinder, the location of the center of pressure, the inclination angle α and the resulting forces acting on the particle. Pressure distribution generated by steady 2D CFD simulation. Red indicates high pressure whereas blue indicates low pressure.

One study tried to derive the full equated of motion for creeping flow by simplifying the problem. As such, Lawrence and Weinbaum [46,47] conducted a study on a slightly eccentric ellipsoid of revolution with major semi-axis $b = a(1+\varepsilon)$, in oscillatory cross-flow, where only translational motion was considered. In addition to relevant expansions of the steady state, virtual mass and Basset a new time dependent term emerged related to the eccentricity. This shows the magnitude of the awaiting challenge and suggests that BBO-equation perhaps only is an asymptotic solution for a more general formulation as the shape goes towards complete symmetry around the center of geometry. When considering non-spherical particles in Stokes flow especially the work by Fan and Ahmadi [24,25] should be accentuated. There a complete formulation of the resistance forces as well as shear induced lift can be found along with a discussion of the importance of the individual terms.

Omitting the advection part of the Navier–Stokes equations, allows for the analytical formulation of the time dependent equation of motion for spheres and the steady state solution for axis-symmetric shapes. This formulation, utilizing the Stokes flow assumption, is especially useful in the paper and pulp industry to predict the flow of fibers or in the description of blood flow. However, for many practical engineering applications it is necessary to also consider the effects of higher Reynolds number flow. For example Jeffery's [40] solution is only strictly valid for zero Reynolds number and even at $Re \sim O(10^{-3})$ it has been proved that the inertial effect is sufficient to force non-spherical particle in a different orbit than that predicted by Jeffery [42,43]. For higher Reynolds numbers, $Re > 0.1$, the effect of flow separation will tend to slow down and stop any rotation caused by a velocity gradient [20]. Empirical expansions of especially the steady state term have long been the backbone in investigations at higher Reynolds number flow for both spheres and non-spherical shapes alike. For non-spherical particle this is usually done by inclusion of equivalence factors, such as the sphericity. However, as previously discussed such an approach does not address the secondary motion associated with high aspect ratio shapes.

In order to model the primary and secondary motions of a steady falling non-spherical particle the following forces and torques can be proposed as the *minimum* required to explain the observations:

$$m_p \frac{d\vec{u}_p}{dt} = \vec{F}_{Drag} + \vec{F}_{Lift} + \vec{F}_{Buoyancy} + \vec{F}_{Other} \tag{8}$$

$$\vec{I}_p \frac{d\vec{\omega}_p}{dt} = \vec{T}_{resist} + \vec{T}_{offset} + cross\ terms + \vec{T}_{Other}. \tag{9}$$

For a particle falling at its terminal velocity the steady state drag force is equal in magnitude to the buoyancy force. The lift force accounts for the sideward motion and is present when the particles principle axis is inclined to the main flow direction. With a concept taken from aerodynamics this can be explained as 'profile' lift. The resistance torques is the angular parallel to the steady state drag. Note that these always act to dampen the rotational motion. The torques resulting from the offset of the center of pressure from the geometric center accounts for the periodic oscillations of the particle around an axis parallel to the flow direction. Other forces acting on the particle are in this case related to the unsteady behavior of the particle. These forces will act as additional resistance towards acceleration and can generally not be assumed to be negligible. The reported secondary motion of non-spherical particles in a uniform flow field at higher Reynolds number flow, as outlined previously, was suggested to be caused by the wake of the particles. The pressure distribution is not symmetric and the particle is forced away from its initial horizontal alignment. Consider a particle failing at its terminal velocity in a uniform flow field as illustrated in Fig. 6. The pressure distribution, indicated with + and −, causes the resulting forces to work at the center of pressure rather than at the center of geometry. This non-coincidence of the center of pressure and center of gravity causes the sustained oscillations. Additionally, the pressure distribution also results in a lift force, known as profile lift, which moves the particle away from its otherwise vertical path.

With regard to the drag force the main advantage for an orientation dependent calculation method that this is calculated on basis of the projected area instead of that of a sphere with the same volume as the particle:

$$\vec{F}_{Drag} = \frac{1}{2} C_D \rho A_p \left|\vec{u} - \vec{u}_p\right| \left(\vec{u} - \vec{u}_p\right). \tag{10}$$

The challenge with regard to the drag force is the proper formulation of the drag coefficient which is applicable for a large range of Reynolds numbers, shapes and orientations. It has become a common practice to procure empirical fits at a range of Reynolds number for a specific shape. Some fits also include a parametric variation of the shape e.g. the aspect ratio of a cylinder or of an ellipsoid of revolution. However, these expressions are usually based on either a fixed orientation or a freely falling particle. Thus correlations of the drag coefficient, which consider the inclination angle, are not widely available. Two approaches have been proposed to address this predicament: The work of Rosendahl [63] suggests

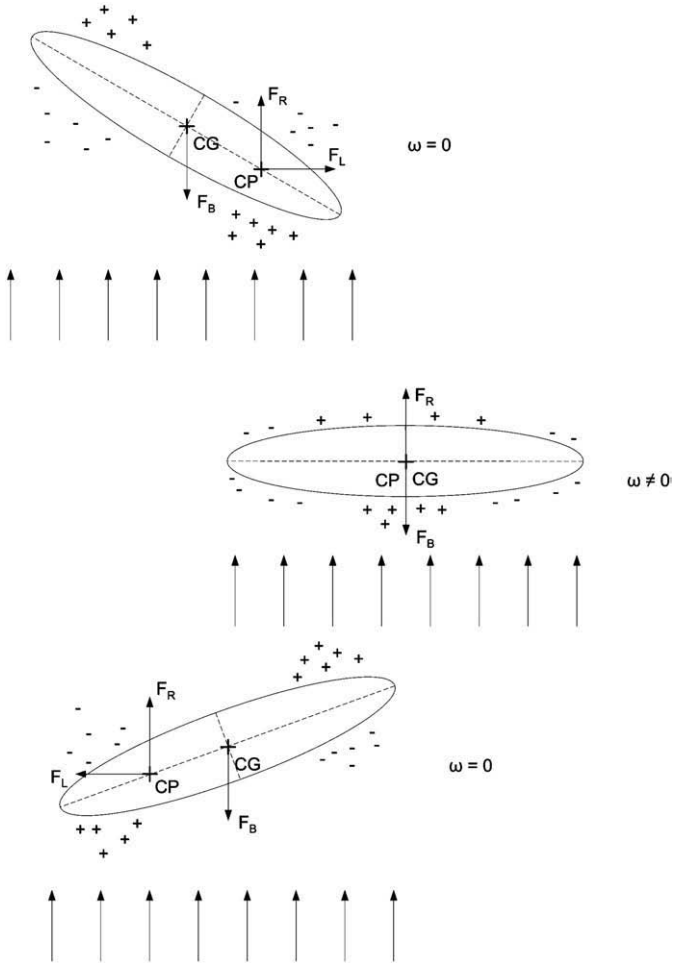

Fig. 6. Illustration of resultant forces and the pressure distribution of a particle at higher Reynolds numbers (Re>100) in uniform flow. CP is the Center of Pressure and CG is the Center of Gravity/Geometry. F_B is the buoyancy force, F_L is the lift force and F_D is the drag force.

using a 'blending' function between the drag coefficient for flow normal and parallel to the major axis of the particle:

$$C_D(\alpha) = C_{D,\alpha=0} + \left(C_{D,\alpha=90} - C_{D,\alpha=0}\right)\sin^3\alpha \tag{11}$$

where α is the angle between the major axis of the particle and the flow direction. Here the projected area at the evaluated orientation is used in the calculation of the drag force. Secondly, the work by Yin et al. [79] suggests using available drag correlations expressed by the sphericity and thus solely accounting for the dependence of orientation by using the projected area in the calculation of the drag force. Recently, a third option has presented itself. Based on a plethora of empirical data for fixed and freely falling particles Hölzer and Sommerfeld [37] came up with an expression which uses a cross-wise, $\psi_\perp$, and lengthwise sphericity, $\psi_\parallel$, to account for the drag coefficient of different shapes at different orientations:

$$C_D = \frac{8}{\mathrm{Re}}\frac{1}{\sqrt{\psi_\parallel}} + \frac{16}{\mathrm{Re}}\frac{1}{\sqrt{\psi}} + \frac{3}{\mathrm{Re}}\frac{1}{\sqrt{\psi^{3/4}}} + 0.4210^{0.4(-\log\psi)^{0.2}}\frac{1}{\psi_\perp} \tag{12}$$

Here the cross-wise sphericity is the ratio between the cross-sectional area of the volume equivalent sphere and the projected area of the actual particle. The lengthwise sphericity is the ratio between the cross-sectional area of the volume equivalent sphere and the difference between half of the surface area and the mean projected area. The cross-wise sphericity should thus aid in the correlation of the form drag while the lengthwise sphericity is expressive of the friction drag. Note that here the Reynolds number and the drag coefficient are based on the volume equivalent sphere.

Fig. 7 shows the drag force for a cylinder at different orientations, normalized with the drag force at zero incidence angle, calculated using the three suggested methods and compared to the benchmark (lattice-Boltzmann simulations) by Hölzer and Sommerfeld [36]. Overall, it may be noted that the drag force increases with increasing incidence angles due to the increase in projected area. However, this alone is not sufficient to properly account for the observed results. The method by Rosendahl [63] provides a pragmatic way to calculate the drag force at different incidence angles but also relies upon the availability of experimental data. For regular shapes these can typically be found for particles at 90° incidence angle whereas empirical fits for particle at zero incidence angle are not widely available. In this regard it might be useful to refer to the studies by Militzer et al. [54] which provide a parametric fit for spheroids as a function of the Reynolds number and the aspect ratio as well as Isaacs and Thodos [39] which provides the same for disks and cylinders at 90° incidence angle. For the present benchmark data it may be noted that a 'blending' function using $\sin(\alpha)$ instead of $\sin^3(\alpha)$ provides a superior fit. Hölzer and Sommerfeld [37] constitute a good fit of the present benchmark data and attractively address all possible shapes at all Reynolds numbers in a single expression. However, this also indicates that for some specific shapes such a correlation, similar to the one by Yin et al. [79], might be associated with a relatively large error compared to correlations developed for that specific shape.

The theoretical and empirical basis of predicting the profile lift relies on much more scant information compared to that available for drag. For symmetric particles the lift is zero at both $\alpha=0°$ and $\alpha=90°$ and it assumes a maximum somewhere in between dependent on the shape and Reynolds number. The usual assumption has been to assume that the lift is proportional to the drag and that the dependence with the orientation is given by the so-called 'cross-flow principle' with reference to Hoerner [35]:

$$\frac{C_L}{C_D} = \sin^2\alpha\cdot\cos\alpha. \tag{13}$$

This relationship was developed for infinite cylinders at Reynolds number in the Newton law regime. Fig. 8 shows data for a spheroid with small aspect ratio together with the cross-flow principle from Eq. (13).

It can be seen that the cross-flow principle provides a fair fit to the present data at Reynolds numbers in the Newton law regime whereas the maximum lift/drag ratio diminishes as the Reynolds number

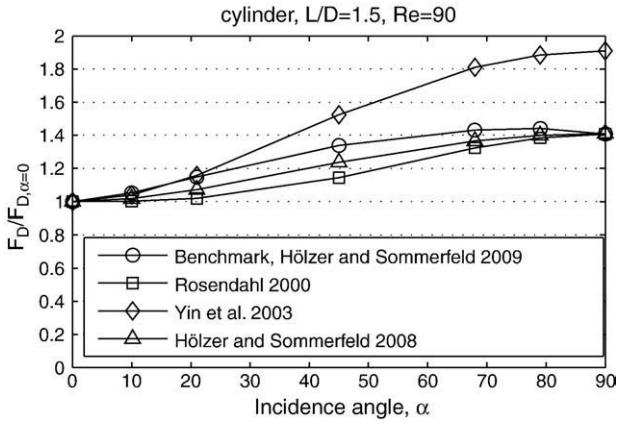

Fig. 7. Evaluation of the different approaches to correlate the drag coefficient with the incidence angle.

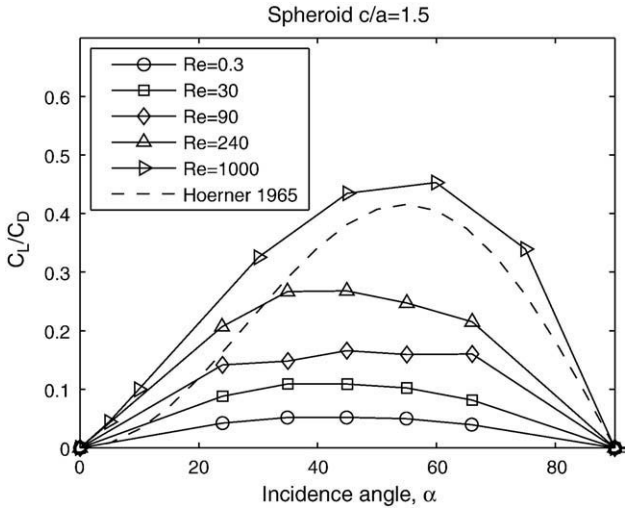

Fig. 8. Lift/drag ratio at different Reynolds numbers. Data by Hölzer and Sommerfeld [36] and Rosendahl [62].

decreases. This is related to the relative importance of the friction and pressure drag at these intermediate Reynolds numbers. Here we provide the following fit to the present data set ($30<\mathrm{Re}<1500$) to correlate the influence of the Reynolds number for the cross-flow principle:

$$\frac{C_L}{C_D} = \frac{\sin^2\alpha\cdot\cos\alpha}{0.65 + 40\mathrm{Re}^{0.72}} \tag{14}$$

This expression gives the correct asymptotic values for large and small Reynolds numbers but is based on a narrow data set with following low accuracy. It should also be noted that data shown in Fig. 8 is for a spheroid with relatively low aspect ratio. It seems as if the better the shape approximates an infinitely long cylinder, the clearer the resemblance with the cross-flow principle becomes. Once the lift coefficient is specified the lift force can be found using an expression equivalent to Eq. (10).

In order to correctly predict the incidence angle, to estimate the forces and torques, it is of prime importance to locate the center of pressure. As previously stated, a non-spherical particle tends to fall with its largest cross-sectional area normal to the flow direction i.e. $\alpha=90°$. Here the center of pressure is coincidental with the geometric center and the lift force and torque is zero. Hence this can be described as the state of *stable equilibrium* of the particle. A non-spherical particle inclined to the flow direction with $\alpha=0°$ will also experience no lift or torque but this can instinctively be perceived as an *unstable equilibrium*. At this extreme the center of pressure must therefore be non-coincidental with the geometric center to match observed behavior. Using concepts from airfoil theory the center of pressure at this extreme inclination is placed at the "quarter chord point" which in this case is equivalent to half the distance from the geometric center to the end of the particle which is oriented towards the flow [63,79]. Please refer to Fig. 5 for visual illustration. Marchildon et al. [52] provide a linear approximation to the derivation[3] by Rayleigh [60] for the pressure distribution on an infinite flat plate to predict the center of pressure of a cylinder. This is reported by Marchildon et al. [52] to be valid for inclinations above $\alpha=15°$ due to the uniformity of the pressure distribution above this angle. Both Rosendahl [63] and Yin et al. [79] present expressions which close the gap with regard to the location of the center of pressure between the two extremes (Table 4).

Table 4
The different expressions used to correlate the location of the center of pressure.

Rayleigh [60]	$x_{cp}/L = (3/4)(\sin\alpha_i)/(4+\pi\cos\alpha_i)$
Marchildon et al. [52]	$x_{cp}/L = (90-\alpha_i)/480$
Rosendahl [63]	$x_{cp}/L = 0.25\left(1-\sin^3\alpha_i\right)$
Yin et al. [79]	$x_{cp}/L = 0.25\cos^3\alpha_i$

Fig. 9 shows an illustration of the different expressions and it can be seen that there is some discrepancy in the prediction of the center of pressure. More unfortunately, there seem not to be any guidelines towards which expression is most appropriate to use. A freely falling non-spherical particle will spend most of the time close to $\alpha=90°$ and effort should thus be directed towards finding the best fit close to this point. Assuming that Rayleigh's derivation is valid for general non-spherical particles at intermediate Reynolds numbers it seems attractive to use the simple linear fit by Marchildon et al. [52]. Once the lift and drag forces are found as well as the location of their point of attack, i.e. the center of pressure, it is a small matter of calculating the resulting torque which is due to the offset from the geometric center, T_{offset}.

$$\vec{T}_{offset} = x_{cp}\left(\vec{F}_{Lift} + \vec{F}_{Drag} + \vec{F}_{Other}\right). \tag{15}$$

The torque due to resistance can be directly derived by integration of the friction, caused by rotation, over the length of the particle. For spheroids subject to the Stokes conditions solutions have been known since Jeffery [40] and have since been expanded to other shapes [19]. Relevant expansions for higher Reynolds number can be found by incorporating appropriate fits for the drag coefficient in the definition of the drag force before the integration is performed.

$$\vec{T}_{resist} = 2\int_0^{L/2}\vec{F}_{resist}dl = \int_0^{L/2}C_{D,cyl}\rho\left(\omega_f-\omega_p\right)^2 l^2 A_p dl. \tag{16}$$

This integral can be evaluated with increasing degrees of sophistication. Note that if the particle aspect ratio is sufficiently large the angular velocity will tend to be low and an assumption of creeping flow may suffice. For the completeness of this investigation

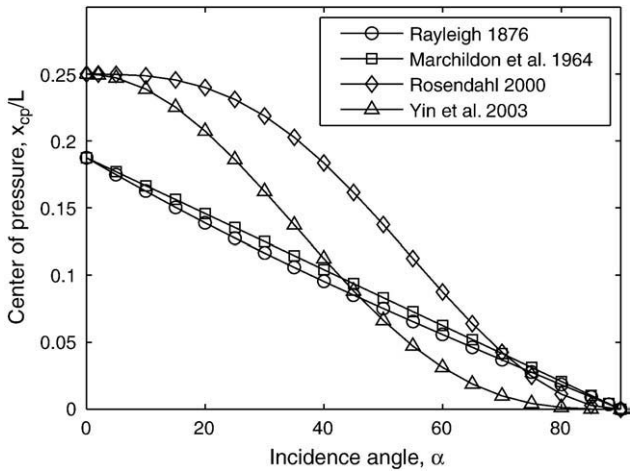

Fig. 9. Location of the center of pressure for a cylinder with length *L*.

[3] Derived by the application of discontinuous potential flow theory.

an evaluation of Eq. (16) for a cylinder rotating around its minor axis, see Fig. 10, may be performed as:

$$\vec{T}_{resist} = \rho D\left(\omega_f - \omega_p\right)^2 L^4 \left(\frac{1}{64} + \frac{1}{3.36\left(\frac{\rho D\left(\omega_f-\omega_p\right)L}{\mu}\right)^{2/3}} \right) \quad for \quad (17)$$

$$C_{D,cyl} = 1 + \frac{10}{\mathrm{Re}^{2/3}}.$$

Here the drag coefficient, suggested by White [77], is valid for the entire subcritical region for a cylinder in cross-flow. The rotation around the major axis is not considered here since it does not influence the oscillating motion which is the prime feature desired to be modeled.

The unraveling of orientation dependent models up to now constitutes a description of the *minimum* number of forces and torques which are required for the modeling of non-spherical particles. For specific problems it may be necessary to address additional forces and torques. For general fluid flow, these would be the forces caused by pressure and velocity gradients as well as unsteady forces such as virtual mass and Basset history force. Some of these forces may be evaluated by simple expansions of the equivalent expressions derived for a sphere whereas others, such as the Basset force, are utterly hopeless to evaluate for non-spherical particles even in creeping flow. As a general guideline these forces may be accounted for by using the projected area or an equivalent diameter as is suggested in the approach by Rosendahl [62]. Clearly, order-of-magnitude estimates may be performed for the forces acting on non-spherical particle similar to those which it is custom to perform for spheres and thus for most gas–solid flows it is justified to neglect the unsteady forces. For a freely falling cylinder in water it is not possible to neglect the unsteady forces since these particles are oscillating. As such Sørensen et al. (2007) found that the terminal velocity of a steady falling cylinder varied slightly in tune with the larger oscillations of the angular velocity. For that investigation an intricate expansion of the drag force, depending on the angular acceleration was developed to account for the unsteady forces. However, the general application of this expression in the calculation procedure presented here is not possible. For small non-spherical particles it might be necessary to model non-continuum effects. This is addressed in the study by Fan and Ahmadi [24] who introduce both an additional Brownian force and a Brownian torque in the equations of motion to supplement the fluid dynamic forces. At the same time the fluid dynamic forces are modified by introducing approximations of the translational and rotational slip factors. There, in an Eulerian–Lagrangian framework the nature of Brownian motion is modeled as a Gaussian random process. Considering the similarities between Brownian and turbulent motion such an approach also indicates possible approaches for non-spherical particles in turbulent flow. Also note that the effect of velocity gradients has already been incorporated into the expression for rotational resistance, Eq. (16), through the vorticity of the flow field. The present methods do not account for the disturbance which initiates the periodic oscillatory motion for an initial horizontal aligned particle. However, if placed in a turbulent environment the turbulence would provide this initial disturbance.

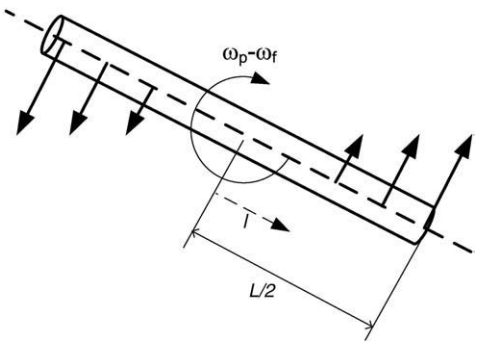

Fig. 10. Resistance towards rotation.

6. Interaction with turbulence

The presence of turbulence significantly affects the motion pattern of a particle. Large uncertainty exists concerning the interaction between non-spherical particles and turbulence. Suffice to say that the presence turbulence may severely alter the motion pattern of non-spherical particles and similarly, the motion of non-spherical particles may alter the properties of the turbulence. Consequently, the treatment of this subject will here rely more on a discussion of the underlying mechanics and suggestions for implementation strategies in the Eulerian–Lagrangian framework than on a critical evaluation of existing approaches which simply do not exist. Overall, we distinguish between methods which resolve the turbulent structures directly and methods which use an average description of turbulence. Similarly, it is a common procedure to distinguish between methods which only consider the effect of turbulence on the particles (one-way coupling) and methods which additionally consider the effect of the particles of on the turbulence (two-way coupling). Typically, the former approach can only be justified at sufficiently low concentrations [22]. If the turbulent structures are resolved and one-way coupling is assumed the previously described methodology can be utilized without further ado. However, the prohibitive requirements for fully resolved DNS make this option less attractive. The use of LES and LES/RANS-hybrids lessens the requirements somewhat but imposes additional uncertainties regarding influence of the sub-grid stresses on the particles. To show the flight of non-spherical particles in a turbulent flow field the most popular approach has been to imitate the turbulence by means of a predefined flow field. For isotropic turbulence Fan and Ahmadi [25] and Olson [56] used a Gaussian random field where the instantaneous velocity field is given as series of Fourier nodes with zero mean and specified standard deviation. Similarly, Fan and Ahmadi [24] modeled the turbulent boundary layer using periodic vortical flow structures at various distances from the wall while Shin and Maxey [65] used a flow field consisting of four counter rotating 2D vortices. For spheres, the application of the Eulerian–Lagrangian methodology in the context of DNS and LES has recently been demonstrated by Vreman et al. [74]. Here the interaction with turbulence formed coherent structures of particles as well as a flattening of the mean velocity profile and an increase of the streamwise turbulence intensity. Clearly, similar simulation strategy could be utilized to show the equivalent impact of/on non-spherical particles.

For practical applications it is more attractive to base the description of the turbulent flow field on the Reynolds averaged equations. Here, the conventional approach for spheres has been to model the turbulence as stochastic Markow-sequences; so-called random walk models. The most popular among these is the eddy-lifetime model which has been adjusted using empirical constants to predict the turbulent dispersion observed in a wide variety of multiphase flows [66]. For non-spherical particles this approach has only been applied in conjunction with drag correlation for translational motion using the sphericity factor [71,2]. For orientation dependent models a pragmatic approach could be to apply the eddy-life time model only on the translational motion and neglect the effect of turbulence on the rotational motion considering the lack of empirical data available. More correct would be to apply similar assumptions for rotational motion as used for the translational motion to form an expansion for the eddy-lifetime model. The main assumption of the eddy-lifetime model can be stated as: eddy

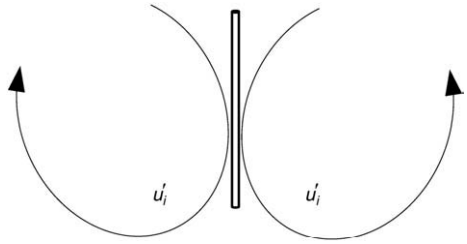

Fig. 11. Fiber alignment in the inter-vortex region.

properties is constant for the entire eddy-lifetime, particles are smaller than the smallest eddy and eddy properties are a Gaussian random function of the turbulent kinetic energy, k, and dissipation rate, ε. An appropriate expansion for rotational motion would be: constant vorticity during the lifetime of the eddy. This enters nicely into the current equation set through the fluid vorticity term in Eq. (16). The fluid vorticity is formed from the present constants in the eddy-lifetime model by considering the characteristic size, l_e, and velocity, u', of an eddy:

$$\omega_f = \frac{u'}{l_e} = \frac{\varepsilon}{Ak} \tag{18}$$

where, A is an empirical parameter which ranges between 0.135 and 0.56 [66]. However, it should be noted that such an approach is entirely untested and is merely a suggestion by the authors to include the effect on the rotational motion in the description of turbulence.

Whereas the effect of turbulence on particles is well known the effect of the particle on the turbulence is much less so. For spheres, general observations seem to suggest that small particles attenuate the carrier phase turbulence while larger particles tend to augment it [31]. From studies of power-spectral measurements of the fluctuating velocity it has been observed that the addition of particles results in a decrease of the turbulence energy in the high wave number region [41]. This is interpreted as a result of the transfer of turbulent kinetic energy from the eddies to particles which are accelerated by the eddies [73]. The production of turbulence is most often thought of as being due to the wake of the particles and as such should be a function of the velocity difference between the particles and carrier fluid [33]. In the case of turbulence modulation by non-spherical particles the type of interaction is likely to be even more complicated than that of spheres. Presently, there is no consensus concerning the modeling of turbulence modulation for spheres [50] and mechanisms for non-spherical particles must be considered as a speculation. That said, the secondary motion which is associated with all non-spherical particles while falling at higher Reynolds number, $Re_p > 100$, in an otherwise quiescent environment, suggests that they are capable of transferring mechanical energy into turbulent kinetic energy in more modes than is the case of spherical particles. On the other hand Klett [45] showed that otherwise steady falling non-spherical particles exposed to turbulence would experience a wobbling or chaotic motion depending on their size and the magnitude of the turbulence. This suggests that the secondary motion acts to attenuate the carrier phase turbulence by extracting turbulent kinetic energy into secondary motion. As such it was also revealed that non-spherical particles were able to both enhance and attenuate turbulence depending on the shape as well as the ratio between the particle diameter and the length scale of the turbulence [51]. Similarly, by considering the momentum coupling only, the additional consideration of shape leads to the conclusion that non-spherical particles have a greater effect on the turbulence, than the volume equivalent spheres, due to the larger drag coefficient [71]. Finally, using DNS to resolve the turbulent structures in the near wall region Paschkewitz et al. [57] showed how rigid slender fibers would align in inter-vortex regions as seen in Fig. 11. The large stresses generated to oppose the vortex motion thereby acted to dissipate the eddies. Drag reductions of up 26% were calculated depending on the aspect ratio and the concentration showing that the shape alone can significantly alter the turbulence characteristics. Clearly, the interaction between particles and the turbulent structures must be affected by the alignment and shape of the particle.

7. Summary/conclusions

This outline of the motion of large non-spherical particles is made not only to give an overview of the present status of this topic but also to serve as a blueprint for future implementations of orientation dependent models. The additional consideration of orientation and angular velocity gives a number of decisive advantages. Firstly, by modeling the orientation dependent forces and torques it is possible to predict the secondary motion caused by the non-spherical shape. Secondly, the modeling of non-spherical particles in the Lagrangian reference frame, without the severe restriction of creeping flow, allows for the possibility to use this methodology on a variety of engineering flows which contain large non-spherical particles. Thirdly, the solution procedure is only around twice as computational intensive compared to the present implementation in commercial codes. Finally, it is postulated that the influence of turbulence on non-spherical particles can be addressed by an appropriate expansion of the popular eddy-lifetime model.

Appendix A. Equations of motion for non-spherical particles

When the linear and angular motion of particles which are not symmetric around the center of mass is considered it is necessary to use both inertial and co-rotational coordinate systems and account

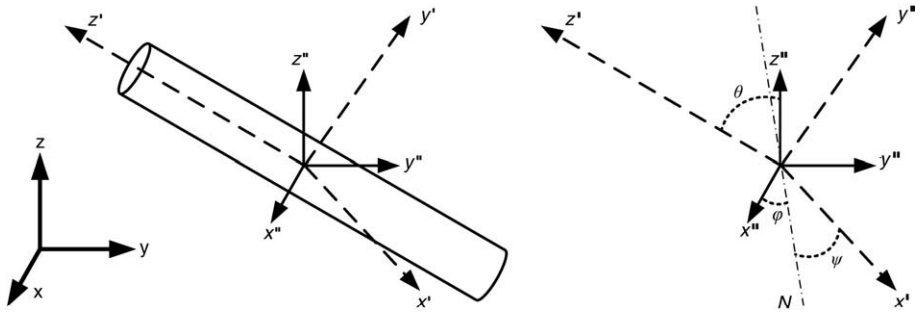

Fig. 12. Relationship between the inertial (x,y,z), the co-rotational (x',y',z') and the co-moving (x'',y'',z'') coordinate systems. $N = \text{plane}(x',y') \cap \text{plane}(x'',y'')$.

for the relation between them by transformation of coordinates. The particle position and velocity determined from the following differential equations:

$$\frac{d\vec{x}}{dt} = \vec{u_p} \tag{19}$$

$$m_p \frac{d\vec{u_p}}{dt} = \vec{F}_{Drag} + \vec{F}_{Lift} + \vec{F}_{Buoyancy} + \vec{F}_{Other} \tag{20}$$

where m_p and u_p are respectively the mass and velocity of the particle, F is a force acting on the particle, and $\vec{x}$ is the position vector expressed in the inertial frame according to Fig. 12. Notice that the evaluation of lift and drag forces is dependent on the orientation of the particle. The resulting lift and drag forces act in the center of pressure whereas the buoyancy force acts in the center of mass which for a particle with uniform mass is coincidental with the center of geometry. However, the center of pressure is generally not coincidental with the center of geometry and thus gives rise to additional torques acting on the particle. The rotational motion uses the co-rotational particle frame $\vec{x}' = [x', y', z']$ with origin at the particles mass center and its axis aligned with the primary axis of the particle while the co-moving coordinate $\vec{x}'' = [x'', y'', z'']$ has its axis aligned with that of the inertial frame.

The differential equations for calculating the angular velocity are given by:

$$\begin{aligned} I_{x'}\frac{d\omega_{x'}}{dt} &= \sum T_{x',i} + \omega_{y'}\omega_{z'}\left(I_{y'} - I_{z'}\right) \\ I_{y'}\frac{d\omega_{y'}}{dt} &= \sum T_{y',i} + \omega_{z'}\omega_{x'}(I_{z'} - I_{x'}) \\ I_{z'}\frac{d\omega_{z'}}{dt} &= \sum T_{z',i} + \omega_{x'}\omega_{y'}\left(I_{x'} - I_{y'}\right) \end{aligned} \tag{21}$$

where , $I_{x'}$, $I_{y'}$, $I_{z'}$, $T_{x'}$, $T_{y'}$, $T_{z'}$, $\omega_{x'}$, $\omega_{y'}$, and $\omega_{z'}$ are respectively the moments of inertia, the torques acting on the particle and the particle angular velocities around their principle axes. The additional terms in the angular momentum equation vanish for particles which are symmetric around the center of mass (a sphere) but needs to be retained for non-spherical particles. The main components which make up the torque are the resistance towards rotation and the offset between the center of pressure and geometric center. Notice that it is not possible to present this set of equations in vector format due to the cross-coupling of the angular velocity. The transformation between the co-moving and the co-rotational coordinates is accomplished by means of a transformation matrix, **A** [30]:

$$\vec{x}' = \mathbf{A}\vec{x}'' \tag{22}$$

where the elements in **A** represent the directional cosines of the angles $[\theta, \phi, \psi]$ between the principle axis of the co-rotational and the co-moving coordinate system. These angles are also known as the Euler angles. However, these angles are not suitable for particles which undergo full rotation due to a singularity which occurs when they are used in relation to the angular velocities of the particle. Instead Euler's four parameters $[\varepsilon_1, \varepsilon_2, \varepsilon_3, \eta]$, which are also known as quaternions, are used. The four Euler parameters represent an expansion of the three Euler angles to eliminate the singularity. The transformation matrix using the Euler parameters is given by Hughes [38]:

$$\mathbf{A} = \begin{bmatrix} 1-2\left(\varepsilon_2^2 + \varepsilon_3^2\right) & 2(\varepsilon_2\varepsilon_1 + \varepsilon_3\eta) & 2(\varepsilon_1\varepsilon_3 - \varepsilon_2\eta) \\ 2(\varepsilon_2\varepsilon_1 - \varepsilon_3\eta) & 1-2\left(\varepsilon_3^2 + \varepsilon_1^2\right) & 2(\varepsilon_3\varepsilon_2 + \varepsilon_1\eta) \\ 2(\varepsilon_1\varepsilon_3 + \varepsilon_2\eta) & 2(\varepsilon_3\varepsilon_2 - \varepsilon_1\eta) & 1-2\left(\varepsilon_1^2 + \varepsilon_2^2\right) \end{bmatrix}. \tag{23}$$

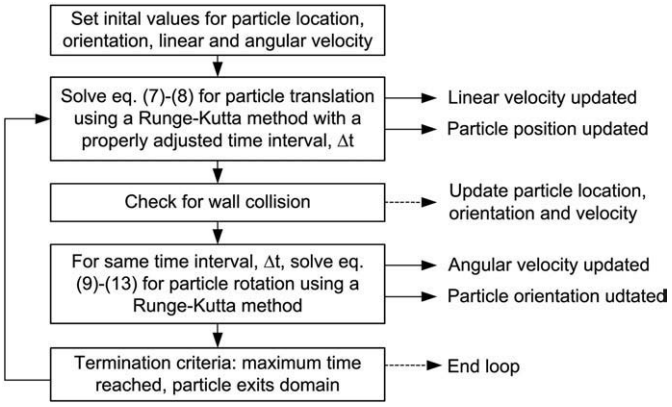

Fig. 13. Typical algorithm to solve for the translation and rotation of a non-spherical particle.

Here the Euler parameters have been related to the Euler angles by the following relations:

$$\begin{aligned} &\varepsilon_1 = \cos\frac{\phi-\psi}{2}\sin\frac{\theta}{2},\ \varepsilon_2 = \sin\frac{\phi-\psi}{2}\sin\frac{\theta}{2},\ \varepsilon_3 = \sin\frac{\phi-\psi}{2}\cos\frac{\theta}{2}, \\ &\eta = \cos\frac{\phi-\psi}{2}\cos\frac{\theta}{2}. \end{aligned} \tag{24}$$

The time rate of change of the Euler parameters, used to update the orientation of the particles, is calculated by:

$$\begin{bmatrix} \frac{d\varepsilon_1}{dt} \\ \frac{d\varepsilon_2}{dt} \\ \frac{d\varepsilon_3}{dt} \\ \frac{d\eta}{dt} \end{bmatrix} = \frac{1}{2}\begin{bmatrix} \eta\omega_{x'} - \varepsilon_1\omega_{y'} + \varepsilon_2\omega_{z'} \\ \varepsilon_3\omega_{x'} + \eta\omega_{y'} - \varepsilon_1\omega_{z'} \\ -\varepsilon_2\omega_{x'} + \varepsilon_1\omega_{y'} + \eta\omega_{z'} \\ -\varepsilon_1\omega_{x'} - \varepsilon_2\omega_{y'} - \varepsilon_3\omega_{z'} \end{bmatrix}. \tag{25}$$

A typical procedure for solving could be stated as:

Fig. 13 illustrates a conventional algorithm to solve the trajectory of a non-spherical particle where the translational and rotational motion is decoupled. Similarly, the same fixed time interval is used for both the translation and rotation of the particle.

References

[1] T. Allen, Particle size Measurement, Chapman & Hall, 1981.
[2] R.I. Backreedy, L.M. Fletcher, J.M. Jones, L. Ma, M. Pourkashanian, A. Williams, Co-firing pulverized coal and biomass: a modeling approach, Proceedings of the Combustion Institute 30 (2005) 2955–2964.
[3] F.M. Barreiros, P.J. Ferreira, M.M. Figueiredo, Calculating shape factors from particle sizing data, Particle and Particle Systems Characterization 13 (6) (1996) 368–373.
[4] O. Bernstein, M. Shapiro, Direct determination of the orientation distribution function of cylindrical particles immersed in laminar and turbulent shear flows, Journal of Aerosol Science 25 (1) (1994) 113–136.
[5] W.K. Bilanski, R. Lal, Behavior of threshed materials in a vertical wind tunnel, Transactions of the ASAE 8 (1965) 411–416.
[6] P. Bowen, J. Sheng, N. Jongen, Particle size distribution measurement of anisotropic—particles cylinders and platelets—practical examples, Powder Technology 128 (2–3) (2002) 256–261.
[7] H. Brenner, The Stokes resistance of a slightly deformed sphere, Chemical Engineering Science 19 (8) (1964) 519–539.
[8] H. Brenner, The Stokes resistance of an arbitrary particle. 2. An extension, Chemical Engineering Science 19 (9) (1964) 599–629.
[9] H. Brenner, The Stokes resistance of an arbitrary particle. 3. Shear fields, Chemical Engineering Science 19 (9) (1964) 631–651.
[10] H. Brenner, The Stokes resistance of an arbitrary particle. 4. Arbitrary fields of flow, Chemical Engineering Science 19 (10) (1964) 703–727.
[11] H. Brenner, D.W. Condiff, Transport mechanics in systems of orientable particles. 3. Arbitrary particles, Journal of Colloid and Interface Science 41 (2) (1972) 228-&.
[12] A. Carlsson, Orientation of fibres in suspensions flowing over a solid surface, licentiate thesis, Royal Institute of Technology, Stockholm (2007).

[13] R.P. Chhabra, Bubbles, Drops, and Particles in Non-Newtonian FluidsSecond edition, CNR Press, 2006.
[14] R.P. Chhabra, L. Agarwal, N.K. Sinha, Drag on non-spherical particles: an evaluation of available methods, Powder Technology 101 (3) (1999) 288–295.
[15] E.B. Christiansen, D.H. Barker, Effect of shape and density on free settling of particles at high Reynolds number, AICHE Journal 11 (1) (1965) 145.
[16] N.N. Clark, A new scheme for particle shape characterization based on fractal harmonics and fractal dimensions, Powder Technology 51 (3) (1987) 243–249.
[17] R. Clift, W.H. Gauvin, The motion of particles in turbulent gas streams, Proc. Chemeca '70 1 (1970) 14–28.
[18] R. Clift, R. Grace, M.E. Weber, Bubbles, Drops, and Particles, Academic Press, New York, 1978.
[19] R.G. Cox, Motion of long slender bodies in a viscous fluid. Part 2. Shear flow, Journal of Fluid Mechanics 45 (1971) 625–657.
[20] E.J. Ding, C.K. Aidun, The dynamics and scaling law for particles suspended in shear flow with inertia, Journal of Fluid Mechanics 423 (2000) 317–344.
[21] A. Elfasakhany, Modeling of Pulverized Wood Flames, Ph.D. thesis, Lund University 2005.
[22] S. Elghobashi, On predicting particle-laden turbulent flows, Applied Scientific Research 52 (4) (1994) 309–329.
[23] G. Eshel, G.J. Levy, U. Mingelgrin, M.J. Singer, Critical evaluation of the use of laser diffraction for particle-size distribution analysis, Soil Science Society of America Journal 68 (3) (2004) 736–743.
[24] F.G. Fan, G. Ahmadi, Wall deposition of small ellipsoids from turbulent air flows—a Brownian dynamics simulation, Journal of Aerosol Science 31 (10) (2000) 1205–1229.
[25] F.G. Fan, G. Ahmadi, Dispersion of ellipsoidal particles in an isotropic pseudo-turbulent flow-field, Journal of Fluids Engineering—Transactions of the ASME 117 (1) (1995) 154–161.
[26] S.B. Field, M. Klaus, M.G. Moore, F. Nori, Chaotic dynamics of falling disks, Nature 388 (6639) (1997) 252–254.
[27] I. Gallily, A. Cohen, On the orderly nature of the motion of nonspherical aerosol particles. II. Inertial collision between a spherical large droplet and an axially symmetrical elongated particle, Journal of Colloid and Interface Science 68 (2) (1979) 338–356.
[28] G.H. Ganser, A rational approach to drag prediction of spherical and nonspherical particles, Powder Technology 77 (2) (1993) 143–152.
[29] E. Gavze, The accelerated motion of rigid bodies in non-steady stokes flow, International Journal of Multiphase Flow 16 (1) (1990) 153–166.
[30] H. Goldstein, Classical Mechanics, Addison-Wesley Press, 1980.
[31] R.A. Gore, C.T. Crowe, Effect of particle-size on modulating turbulent intensity, International Journal of Multiphase Flow 15 (2) (1989) 279–285.
[32] J. Happel, H. Brenner, Low Reynold's Number Hydrodynamics, Prentice-Hall, Englewood Cliffs, 1965.
[33] G. Hetsroni, Particles turbulence interaction, International Journal of Multiphase Flow 15 (5) (1989) 735–746.
[34] H. Heywood, Uniform and nonuniform motion of particles in fluids, Proceedings of the Symposium on the Interaction between Fluids and Particles, 1962, pp. 1–8.
[35] J.F. Hoerner, *Fluid-dynamics drag,* Hoerner Fluid Dynamics, 1965 (Published by the author).
[36] A. Hölzer, M. Sommerfeld, Lattice Boltzmann simulations to determine drag, lift and torque acting on non-spherical particles, Computers & Fluids 38 (3) (2009) 572–589.
[37] A. Hölzer, M. Sommerfeld, New simple correlation formula for the drag coefficient of non-spherical particles, Powder Technology 184 (3) (2008) 361–365.
[38] P.C. Hughes, Spacecraft Attitude Dynamics, Wiley, 1986.
[39] J.L. Isaacs, G. Thodos, Free-settling of solid cylindrical particles in turbulent regime, Canadian Journal of Chemical Engineering 45 (3) (1967) 150-&.
[40] G.B. Jeffery, The motion of ellipsoidal particles immersed in a viscous fluid, Proceedings of the Royal Society of London.Series A, Containing Papers of a Mathematical and Physical Character 102 (715) (1922) 161–179.
[41] B.H. Jou, H.J. Sheen, Y.T. Lee, Particle mass loading effect on a 2-phase turbulent downward jet flow, Particle & Particle Systems Characterization 10 (4) (1993) 173–181.
[42] A. Karnis, H.I. Goldsmit, S.G. Mason, Flow of suspensions through tubes. V. Inertial effects, Canadian Journal of Chemical Engineering 44 (4) (1966) 181-&.
[43] A. Karnis, S.G. Mason, H.L. Goldsmith, Axial migration of particles in Poiseuille flow, Nature 200 (490) (1963) 159-&.
[44] G. Kaspers, Dynamics and measurement of smokes. I Size characterization of nonspherical particles, Aerosol Science and Technology 1 (2) (1982) 187–199.
[45] J.D. Klett, Orientation model for particles in turbulence, Journal of the Atmospheric Sciences 52 (12) (1995) 2276–2285.
[46] C.J. Lawrence, S. Weinbaum, The unsteady force on a body at low Reynolds-number—the axisymmetric motion of a spheroid, Journal of Fluid Mechanics 189 (1988) 463–489.
[47] C.J. Lawrence, S. Weinbaum, The force on an axisymmetrical body in linearized, time-dependent motion—a new memory term, Journal of Fluid Mechanics 171 (1986) 209–218.
[48] J.P. Le Roux, Settling velocity of ellipsoidal grains as related to shape entropy, Sedimentary Geology 101 (1–2) (1996) 15–20.
[49] L.G. Leal, Particle motions in a viscous fluid, Annual Review of Fluid Mechanics 12 (1) (1980) 435–476.
[50] M. Mando, M.F. Lightstone, L. Rosendahl, C. Yin, H. Sørensen, Turbulence modulation in dilute particle-laden flow, International Journal of Heat and Fluid Flow 30 (2009) 331–338.
[51] M. Mandoe, L. Rosendahl, Measurement of turbulence modulation by non-spherical particles, Proceedings of the 7th International Conference on Multiphase Flow, ICMF, 2010.
[52] E.K. Marchildon, A. Clamen, W.H. Gauvin, Drag + oscillatory motion of freely falling cylindrical particles, Canadian Journal of Chemical Engineering 42 (4) (1964) 178-&.
[53] G. Mckay, W.R. Murphy, M. Hillis, Settling characteristics of disks and cylinders, Chemical Engineering Research & Design 66 (1) (1988) 107–112.
[54] J. Militzer, J.M. Kan, F. Hamdullahpur, P.R. Amyotte, A.M. Al Taweel, Drag coefficient for axisymmetric flow around individual spheroidal particles, Powder Technology 57 (3) (1989) 193–195.
[55] V. Olaisen, N. Nesse, H. Volden, Use of laser diffraction for particle size distribution measurements in duodenal digesta, Journal of Animal Science 79 (2001) 761–765.
[56] J.A. Olson, The motion of fibres in turbulent flow, stochastic simulation of isotropic homogeneous turbulence, International Journal of Multiphase Flow 27 (12) (2001) 2083–2103.
[57] J.S. Paschkewitz, Y. Dubief, C.D. Dimitropoulos, E.S.G. Shaqfeh, P. Moin, Numerical simulation of turbulent drag reduction using rigid fibres, Journal of Fluid Mechanics 518 (2004) 281–317.
[58] S. Paulrud, J.E. Mattsson, C. Nilsson, Particle and handling characteristics of wood fuel powder: effects of different mills, Fuel Processing Technology 76 (1) (2002) 23–39.
[59] M.N. Pons, H. Vivier, K. Belaroui, B. Bernard-Michel, F. Cordier, D. Oulhana, J.A. Dodds, Particle morphology: from visualisation to measurement, Powder Technology 103 (1) (1999) 44–57.
[60] L. Rayleigh, On the resistance of fluids, Philosophical Magazine Series 5 2 (13) (1876) 430–441.
[61] M. Rhodes, Introduction to Particle TechnologySecond edn, Wiley, 2008.
[62] Rosendahl, L.A. 1998, Extending the modelling framework for gas-particle systems, PhD thesis, Aalborg University.
[63] L. Rosendahl, Using a multi-parameter particle shape description to predict the motion of non-spherical particle shapes in swirling flow, Applied Mathematical Modelling 24 (1) (2000) 11–25.
[64] J.E. Shellard, R.H. Macmillan, Aerodynamic properties of threshed wheat materials, Journal of Agricultural Engineering Research 23 (3) (1978) 273–281.
[65] H. Shin, M.R. Maxey, Chaotic motion of nonspherical particles settling in a cellular flow field, Physical Review E 56 (5) (1997) 5431–5444.
[66] J.S. Shirolkar, C.F.M. Coimbra, M. Queiroz McQuay, Fundamental aspects of modeling turbulent particle dispersion in dilute flows, Progress in Energy and Combustion Science 22 (4) (1996) 363–399.
[67] S.J.R. Simons, Modelling of agglomerating systems: from spheres to fractals, Powder Technology 87 (1) (1996) 29–41.
[68] M. Sommerfeld, B. van Wachem, R. Oliemans, Best practice guidelines—on computational multiphase dynamics for turbulent dispersed multiphase flows, Version 16-Oct-07 edn, ERCOFTAC Special Interest Group on "Dispersed Turbulent Multi-Phase Flow", 2007.
[69] H. Sørensen, L. Rosendahl, C. Yin, M. Mandoe, Settling of a cylindrical particle in a stagnant fluid, Proceedings of the 6th International Conference on Multiphase Flow, ICMF, 2007.
[70] G.E. Stringham, D.B. Simons, H.P. Guy, The behaviour of large particles falling in quiescent liquids, United States Geological Survey professional paper 562-C (1969) C1–C36.
[71] L. Sun, J. Lin, F. WU, Y. Chen, Effect of non-spherical particles on the fluid turbulence in a particulate pipe flow, Journal of Hydrodynamics, Ser B 16 (6) (2004) 721–729.
[72] T.L. Thompson, N.N. Clark, A holistic approach to particle drag prediction, Powder Technology 67 (1) (1991) 57–66.
[73] J.Y. Tu, C.A.J. Fletcher, An improved model for particulate turbulence modulation in confined 2-phase flows, International Communications in Heat and Mass Transfer 21 (6) (1994) 775–783.
[74] B. Vreman, B. Geurts, N. Deen, J. Kuipers, J. Kuerten, Two- and four-way coupled Euler–Lagrangian large-eddy simulation of turbulent particle-laden channel flow, Flow Turbulence and Combustion 82 (1) (2009) 47–71.
[75] H. Wadell, The coefficient of resistance as a function of Reynolds number for solids of various shapes, Journal of the Franklin Institute 217 (4) (1934) 459–490.
[76] B.W. Whalley, J.D. Orford, The use of fractals and pseudofractals in the analysis of two-dimensional outlines: review and further exploration, Computers & Geosciences 15 (2) (1989) 185–197.
[77] F.M. White, Viscous Fluid FlowSecond edition, McGraw-Hill, 1991.
[78] W.W. Willmarth, N.E. Hawk, R.L. Harvey, Steady and unsteady motions and wakes of freely falling disks, Physics of Fluids 7 (2) (1964) 197–208.
[79] C.G. Yin, L. Rosendahl, S.K. Kaer, H. Sørensen, Modelling the motion of cylindrical particles in a nonuniform flow, Chemical Engineering Science 58 (15) (2003) 3489–3498.

Fuel 89 (2010) 3051–3062

Contents lists available at ScienceDirect

Fuel

journal homepage: www.elsevier.com/locate/fuel

Pulverized straw combustion in a low-NO_x multifuel burner: Modeling the transition from coal to straw

M. Mandø *, L. Rosendahl, C. Yin, H. Sørensen

Institute of Energy Technology, Aalborg University, Pontoppidanstræde 101, 9220 Aalborg, Denmark

ARTICLE INFO

Article history:
Received 13 May 2009
Received in revised form 10 May 2010
Accepted 11 May 2010
Available online 25 May 2010

Keywords:
Pulverized straw combustion
Gas-particle flow
Low-NO_x burner
CFD
Biomass

ABSTRACT

A CFD simulation of pulverized coal and straw combustion using a commercial multifuel burner have been undertaken to examine the difference in combustion characteristics. Focus has also been directed to development of the modeling technique to deal with larger non-spherical straw particles and to determine the relative importance of different modeling choices for straw combustion. Investigated modeling choices encompass the particle size and shape distribution, the modification of particle motion and heating due to the departure from the spherical ideal, the devolatilization rate of straw, the influence of inlet boundary conditions and the effect of particles on the carrier phase turbulence. It is concluded that straw combustion is associated with a significantly longer flame and smaller recirculation zones compared to coal combustion for the present air flow specifications. The particle size and shape distribution is the most influential parameter for the correct prediction of straw combustion. The inlet boundary conditions and the application of a turbulence modulation model can significantly affect the predicted combustion efficiency whereas the choice of devolatilization parameters was found to be of minor importance.

1. Introduction

Globally, there is an increasing interest in the co-firing of biomass with coal in order to reduce net CO_2 emissions and the dependence of foreign fossil fuel resources.

In Denmark the suspension fired CHP plant Amager unit 1, scheduled for re-commissioning in 2009, has been refitted for co-firing of estimated 50% on mass basis with pulverized straw and wood. This estimate has later been modified to as much biomass as possible promising even greater use of biomass. Raw biomass are to arrive to the power plant in the form of pellets, which are subsequently ground separately in traditional coal mills and pneumatically transported to the burners. Several steps have been taken in order to adapt the boiler for the introduction of biomass. These are mainly material and fuel additive choices to combat the enhanced slagging and corrosion but also encompass the use of low mill air temperature for biomass, due to the risk of ignition. The main solid biomass fuel in Denmark is straw, where an estimated annual 2 mio. ton of surplus straw is available for energy generation [24]. Of this, about 1/3 is currently used for power generation in Denmark [16].

The present work investigates the influence of different model choices on the combustion characteristics of an industrial multifuel low-NO_x burner as is to be installed in Amager unit 1. A base case simulation for both coal and straw is shown using the design airflow conditions provided by the boiler manufacturer Burmeister and Wain Energy, BWE.

Lignocellulosic biomass has a fibrous structure and is difficult to fracture by applying compression forces unlike coal which is a brittle material. This results in an increase in the energy used for the milling process together with biomass particles which are inherently non-spherical in shape. The shape distribution of resulting biomass particles consists of a large part of near-spherical particles, similar to coal, but in addition biomass dust contains particles which can be described as flake-like or rod-like, both with aspect ratios exceeding 10. It is also clear that the energy consumed in the milling process also decreases proportionally to the size of the final biomass particles. Using a size limit where 95% by weight of the dry matter has to pass through a 1000 μm mesh and at least 12% has to pass through a 125 μm mesh the electric power requirements is estimated to 150 kW/t for dry pine chips or 3% of the heating value of the fuel [17]. Thus an increased effort to reduce the size of the biomass particles will result in a decrease of the total efficiency of the plant and cannot justify the use of dust firing compared to other combustion technologies.

Table 1 highlights some of the critical differences between straw and coal. Straw has significantly higher volatile matter content than coal and the fixed carbon-to-volatile matter ratio is much below unity. Additionally, straw also begins to release volatiles at a lower temperature and more rapidly than coal, thus reducing the ignition temperature compared to coal. This also indicates that

* Corresponding author. Tel.: +45 9940 9248; fax: +45 9815 1411.
E-mail address: mma@iet.aau.dk (M. Mandø).

0016-2361/$ - see front matter © 2010 Elsevier Ltd. All rights reserved.
doi:10.1016/j.fuel.2010.05.016

Nomenclature

A	pre-exponential factor (1/s)
A_p	particle surface area (m^2)
C_D	drag coefficient (–)
C_p	specific heat capacity (J/kg K)
d_p	particle diameter (m)
E	activation energy (J)
F	force (N)
g	gravity (m/s^2)
h	convective heat transfer coefficient (W/m^2 K)
k	turbulent kinetic energy (m^2/s^2), rate of reaction (1/s)
m	mass (kg)
R	universal gas constant (J/K kmol)
Re	Reynolds number (–)
S_{kp}	turbulent kinetic energy source term (m^2/s^2)
t	time (s)
T	temperature (K)
u	velocity (m/s)
y^+	dimensionless distance from wall

Greek symbols

α	volume fraction (–)
ε	dissipation rate (m^2/s^3), particle emissivity (–)
ρ	density (kg/m^3)
Θ	combustion enhancement factor (–)
ψ	sphericity factor (–)
μ	viscosity (kg/m s)
θ_R	radiation temperature
σ	Stefan–Boltzmann constant
τ	time scale/constant (s)

Superscripts

–	time average
$'$	fluctuating quantity

Subscripts

i,j	index
∞	local fluid property at particle position
p	particle
u	momentum
k	turbulent kinetic energy
ε	dissipation rate
ave	average

Abbreviations

CHP	combined heat and power
CFD	computational fluid dynamics
LHV	lower heating value
A/F	air–fuel ratio
PA	primary air
SA	secondary air
TA	tertiary air
GUI	graphical user interface

special care should be given to the design of the air supply to provide sufficient oxygen for the faster release of volatile matter in order not to delay combustion [48]. However, this is somewhat offset by the lower requirement of oxygen for straw combustion.

Furthermore, the heating value of straw is significantly lower compared to coal requiring a larger fuel throughput for the same power output as that of coal firing.

Biomass is known to produce higher concentrations of NH_3 and a lower HCN content as a Nitrogen-laden product gas compared to coal [5]. In addition, biofuels often have less fuel bound nitrogen which act to reduce NO_x emissions, as demonstrated on co-firing tests at Seward station [4].

Previously, some experimental studies of pulverized biomass firing in laboratory test furnaces have been undertaken.

Ballester et al. [3] compared the flames of bituminous coal, lignite and wood, for similar operating conditions and found that wood flames display two distinct combustion zone: an intense combustion of volatiles released from small particles close to the burner and a second further downstream which is attributed to devolatilization of larger particles and char burnout. Furthermore, the wood flame is significant longer and is associated with more unburnt hydrocarbons due to the lower temperatures downstream in the furnace.

Table 1
Coal and straw simulation parameters as specified by Burmeister and Wain Energy.

	Coal	Straw
Volatiles	40.0 wt%	72.0 wt%
Ash	13.1 wt%	4.5 wt%
Moisture	9.0 wt%	10.0 wt%
Char	37. 9 wt%	13.5 wt%
LHV	24.7 MJ/kg	15 MJ/kg
A/*F* – PA	1.9	2.2
A/*F* – total	9.47	5.24
Excess air ratio	1.14	1.10
(SA + TA)/PA	5.0	1.3

Lokare et al. [32] measured the ash deposition rates from different solid biomass fuels and showed that this varies greatly depending on the type.

The NO_x precursor formation investigation for straw and coal co-firing by Wu et al. [46] suggest that biomass predominately forms NH_3 whereas coal predominately forms HCN as gas-phase compounds.

The study by Damstedt et al. [11] dealt with 50 wt% straw and coal co-firing and shoved that large particles penetrate the internal recirculation zones and elongates the flame structure by forming a secondary combustion zone downstream of the burner.

Bharadwaj et al. [6] and Lu et al. [33] looked at the devolatilization of large non-spherical biomass particles and demonstrated the insufficiency of modeling such particles as spheres.

Similarly, a number of numerical investigations have also been published.

Abbas et al. [1] undertook a parametric study of the co-firing of sawdust and coal and found an optimum of 30% wood co-firing for minimum NO_x emissions and maximum particle burnout. Apparently, the faster devolatilization of wood creates an intense near burner combustion zone which enhanced the coal combustion in the internal recirculation zones. Unfortunately, it seems that a poor choice of model constants for the devolatilization of wood might have corrupted the results.

Gera et al. [21] compared spherical particles with no internal conduction with that of cylindrical particles with internal gradients of same equivalent diameter and found that there is a significant difference in the burnout statistics for particles larger than 1 mm.

Similarly Yin et al. [48] developed a 6 degree-of-freedom model for cylindrical particle motion and found that the trajectories differ significantly from those of perfect spheres of the same equivalent diameter.

Backreedy et al. [2] and Ma et al. [34] used a modified expression for the drag coefficient as a function of the sphericity but did not to incorporate the modified surface area into the combustion model.

Elfasakhany and Bai [14] looked at the influence of several sub-models for wood combustion. It is found that the flame temperature and major species are less sensitive towards the devolatilization mechanisms while the predictions of unburned hydrocarbons and CO are very dependent of the devolatilization sub-model.

Elfasakhany et al. [15] developed an expression for the force acting on combusting particles due to the anisotropic release of volatiles.

Many additional biomass combustion and co-firing issues are thoroughly covered in the review articles by Williams et al. [45], Nussbaumer [37], Demirbas [12] and Cui and Grace [10].

Current models used to predict the motion of pulverized coal particles rely on a spherical assumption, which may deviate significantly from reality for the case of bio-dust. Qualitative observations suggest that pulverized straw particles are highly non-spherical (flake-like, rod-like), greatly enhancing the surface area, compared to a sphere, which represents the minimum in terms of surface-to-volume ratio. Clearly this affects the motion, heating and surface reactions of a biomass particle and appropriate modeling choices have to be taken to improve the design for co-firing of biomass in utility boilers.

For the present work straw particles, traveling at terminal velocity, have a Reynolds number around unity based on the equivalent diameter. The flow around particles in this range is influenced by inertial forces which stabilize the motion of the non-spherical particles making them orientate themselves with maximum cross-section normal to the flow [8,18]. Thus, there is no secondary particle motion induced by the flow field and only for wall bounded flows is it justified to resolve the rotational motion of the particles. The influence of turbulence tends to cause particles to "wobble" [27]. However, it seems prudent to assume that a traditional random walk model for turbulent dispersion is sufficient to model any additional effect of secondary motion due to the non-sphericity of straw particles. Similarly, for the present work, straw particles have a Biot number around 0.1 which justifies the assumption of lumped particles. The combined heat transfer of radiation and convection only act to enforce the assumption of a lumped system analysis especially when the increased surface area is taken into consideration. Indeed, the enhanced surface area of a non-spherical particle compared to a sphere seems to be a key factor to model the additional heat transfer. A revisit to Newton's law of cooling and the Stefan–Boltzmann's law reveals that the surface area is the only parameter it is necessary to modify. The convective heat transfer coefficient can be calculated with sufficient accuracy using correlations of the Nusselt number developed for equivalent volume spheres if based on the characteristic dimension of the non-spherical particle [8]. However, since the exact dimensions of an individual arbitrary shaped particle are unknown it is clear that the rate of heat transfer can only be predicted with a low accuracy.

The philosophy behind the model selection of this paper is that they are relevant for the prediction of the flow in industrial boilers. Key factors are to limit the computational intensity, focus on stability of model and tweak existing standard models rather than implement advanced sub-models. Similarly, it can be argued that the total accuracy of a given simulation is not greater than the accuracy of the least accurate sub-model or assumption. Thus implemented model choices should be of the same general accuracy.

2. Fuel characterization

A number of issues arise in the transition from firing with coal to firing with straw. Traditional low-NO_x burner's are designed and optimized for coal combustion, thus the introduction of straw is foreseen to require addition design considerations for optimal firing. As a first iteration in this process the introduction of the multifuel burner, where the shift from coal to straw is handled solely by changing burner settings for the internal air distribution and the level of swirl [22]. As can be seen in Table 1 the difference in chemical composition, as well as other considerations, results in a significant difference in air flow settings.

Modeling challenges dealt with in the present work, in the context of CFD, can be summarized as follows:

- Particle size and shape distribution.
- Devolatilization kinetics.
- Inlet boundary conditions.
- Particle-turbulence interaction.

2.1. Particle size and shape distribution

Undoubtedly the specified particle size and shape have a significant influence upon the combustion process. However, existing data is scarce and generally unreliable. Qualitative observations of pulverized wood and straw suggest that particles are highly non-spherical, mainly flake-like and rod-like. The size and shape distribution observed is similarly highly dependent on the combined comminution process of mill and pre-pelleting processes as well as dependent of the type of biomass. As such it is observed that wood particles tend to be more rod-like whereas straw particles tend to be flattened.

However, sieve analyses, on which most reported size distributions are based, tend to either over or under predict the size of the particles based on their equivalent volume diameter depending on their shape. Moreover, sieve analysis does not foretell anything of the enhancement of the surface area of a non-spherical particle compared to a sphere of equivalent volume.

No quantitative data regarding the shape of pulverized straw particles exists, whereas several authors have published data regarding the size distribution of biomass particles. This data have been summarized in Fig. 1 and appropriate Rosin–Rammler is specified in Table 2.

It can be seen that the size distribution resulting from a laboratory cutter tends to be more narrow compared to that which results from a milling process. Similarly, the size distribution from a traditional coal mill for biomass particles is more narrow compared to that of coal (Spread $\approx$ 1.2) when evaluated on basis of

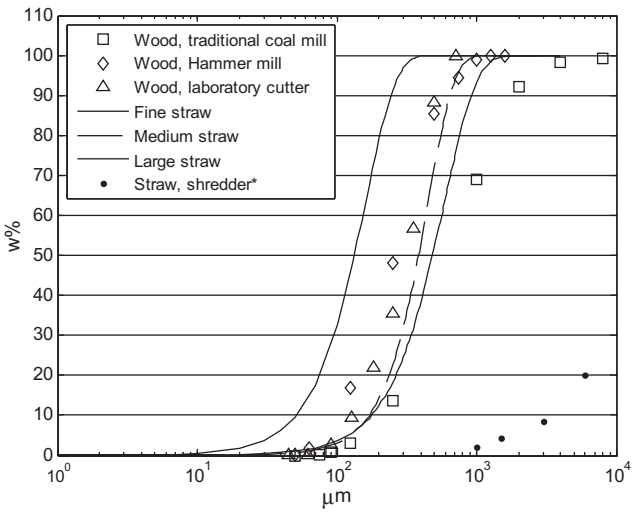

Fig. 1. Cumulative size distribution of biomass particles. *Size based on length of straws.

Table 2
Rosin–Rammler distribution parameters of biomass particles.

	Wood, hammer mill	Wood, traditional coal mill	Wood, laboratory cutter	Fine straw, laboratory cutter	Medium straw, laboratory cutter	Large straw, laboratory cutter	Straw, shredder
Source	[17]	[25]	[25]	[11]	[11]	[11]	[38]
$d_{p,ave}$	360 μm	900 μm	370 μm	160 μm	450 μm	590 μm	$l_{ave} \approx 16{,}000$ μm
Spread	1.5	1.5	2.3	2.0	2.3	1.9	1.4

the Rosin–Rammler spread parameter. No doubt that any application of mechanical and aerodynamic filters for biomass particles will act to reduce the spread of the resulting distribution.

For the present investigation we also wish to rectify the size distribution for the effect of non-sphericity. This is done by specifying a single sphericity factor to be applied for all particles in a distribution. To approximate a suitable value for the sphericity, in the absence of actual measurements, it is postulated that the Stokes number for a biomass particle should match that of an equivalent coal particle in order to pass the aerodynamic filter/trap which is endemic in the design of a traditional coal mill. Since the Stokes number for a non-spherical particle is dependent of both the Reynolds number as well as the sphericity it is possible for a large biomass particle, evaluated on basis of the equivalent diameter, to have similar aerodynamic properties as that of a much smaller coal particle provided that the sphericity is sufficiently low.

Table 3 show the calculated sphericity for three sizes of biomass particles where the air flow is assumed to be the same for the two cases and the particles are assumed to travel at terminal velocity.

Based on the sphericity factor, ψ, the burning enhancement factor compared to a sphere with the same diameter, Θ, can be calculated as [48]:

$$\Theta = \frac{0.3\psi + 0.7}{\psi} \tag{1}$$

The burning enhancement factor was developed by Gera et al. [21] who found that the increase in surface area of a cylindrical switchgrass particle was larger than the increase in the overall burning rate. Thus the burning enhancement factor can be seen as an estimate on the efficiency of the increase in surface area to promote combustion for an arbitrary shaped particle. To get a better feeling of these numbers a sphericity factor of 0.34 corresponds to a disk with an aspect ratio of 1/20, i.e. a bulky disk, whereas a sphericity factor of 0.03 corresponds to disk with an aspect ratio of 1/800, i.e. a very flat disk.

For the present investigation, three different biomass particle distributions are considered; all based on a modification of "Large straw, laboratory cutter" from Table 2. It is assumed that this distribution consists of disks with a specific aspect ratio and where the diameter of the disk is what is reflected by the sieve analysis. Depending on the aspect ratio assumed, a measure of the average volume equivalent diameter is found. The spread is similarly set to 1.5 to reflect the wider particle distribution resulting from the milling process. Table 4 gives an overview of the particle distribution parameters used in this work.

Table 3
Calculated sphericity factor and burning enhancement factor if the aerodynamic properties are to be similar to a 60 μm coal particle.

d_p (μm)	ψ	Θ
200	0.34	2.4
300	0.12	5.7
600	0.03	23

Table 4
Particle parameters.

	Assumed aspect ratio	New $d_{p,ave}$ (μm)	Sphericity
Large	1/5	500	0.64
Medium	1/25	300	0.28
Small	1/75	200	0.14
Coal	–	60	1

2.2. Devolatilization kinetics

A sensible prediction of the rate of the release of volatile matter is necessary for the success of any simulation. Whereas the size and shape of a particle for a given set of physical properties is determining for the rate of heating of the particle, the devolatilization rate determines the rate of release of volatile matter this increase in particle temperature's associated with. Determination of the devolatilization rate is typically carried out by means of thermo-gravimetric analysis. Small samples of biomass are ground so fine that that size dependence is not a factor which is to be considered and heated up with different temperature slopes. Extensive

Table 5
Single rate devolatilization constants.

	A (1/s)	E (J/kmol)
(Danish straw) [49]	1.56E+10	13.8E−07
(Corn stalks) [29]	6.30 E+06	9.15E−07
(Straw) [29]	2.43 E+04	6.46E−07
(Biomass) [47]	7.00 E+04	8.30E−07
Fluent default (Wood)	3.82 E+05	7.40E−07

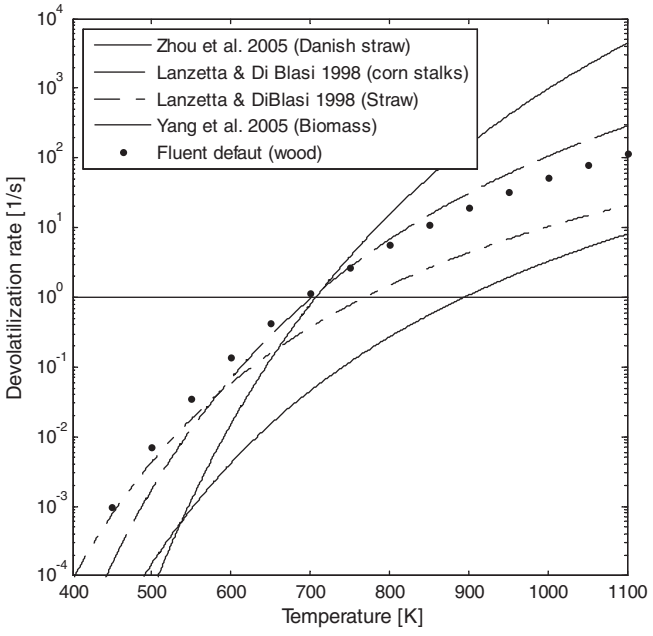

Fig. 2. Biomass devolatilization rates.

work has been done previously by several authors towards determining the devolatilization kinetics of biomass. For the present investigation we limit ourselves only to look at selected works using single-rate expressions. The kinetic rate, k, is defined by an Arrhenius type expression:

$$k = Ae^{-E/RT} \tag{2}$$

where A is the pre-exponential factor, E is the activation energy, R is the universal gas constant and T is the temperature. Model constants found in different investigations are shown in Table 5.Fig. 2 outlines the devolatilization rate dependence on temperature for the different investigation given in Table 5.

It is clear from Table 5 and Fig. 2 that there is an apparent difference in the rate expressions. This result can both represent a difference in the kinetics of the different samples but also be due to measurement accuracy and difference in methodology. Clearly, the composition and the devolatilization rate of straw and other biomass fuels are dependent on regional and seasonal differences. Thus, it is prudent to include an evaluation of devolatilization kinetics in the sensitivity analysis of a given simulation. For the present work the rate expressions for straw by Zhou et al. [49] and Lanzetta and Di Blasi [29] are evaluated.

For additional information on biomass kinetics the reader is referred to the recent review paper by Di Blasi [13].

3. Model implementation

3.1. General numerical procedure

The applied standard modeling approaches are only discussed very briefly here. For additional information of general CFD methodology and sub-models the reader is referred to dedicated literature on this subject such as Versteeg and Malalasekera [44]. The CFD simulations presented in the present paper have been accomplished using the commercial CFD code Fluent 6.3. Details about this code can be found in Fluent User Guide [19]. The grid, with highlighted details, used in this work is shown in Fig. 4. It consists of 680,000 cells; a mixture of hexagonal and polygonal cells. This represents a single burner attached to a cylindrical furnace. Additionally a funnel shaped outlet volume is attached to the furnace

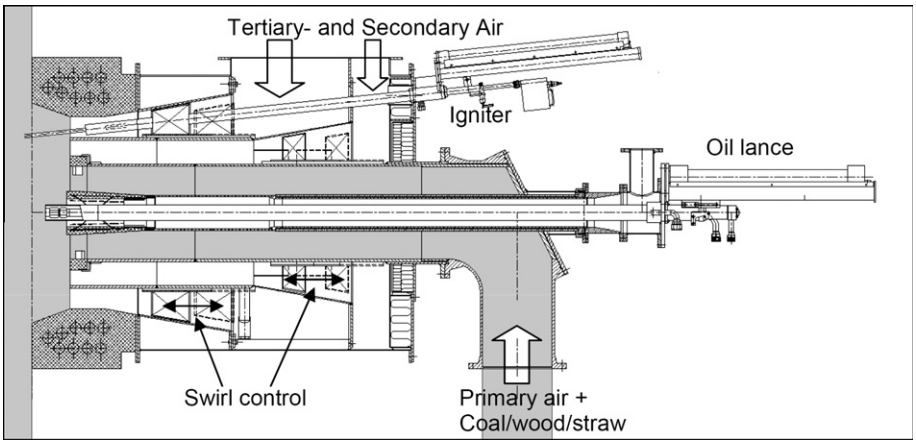

Fig. 3. Burner layout, modeled flow domains are shaded [22].

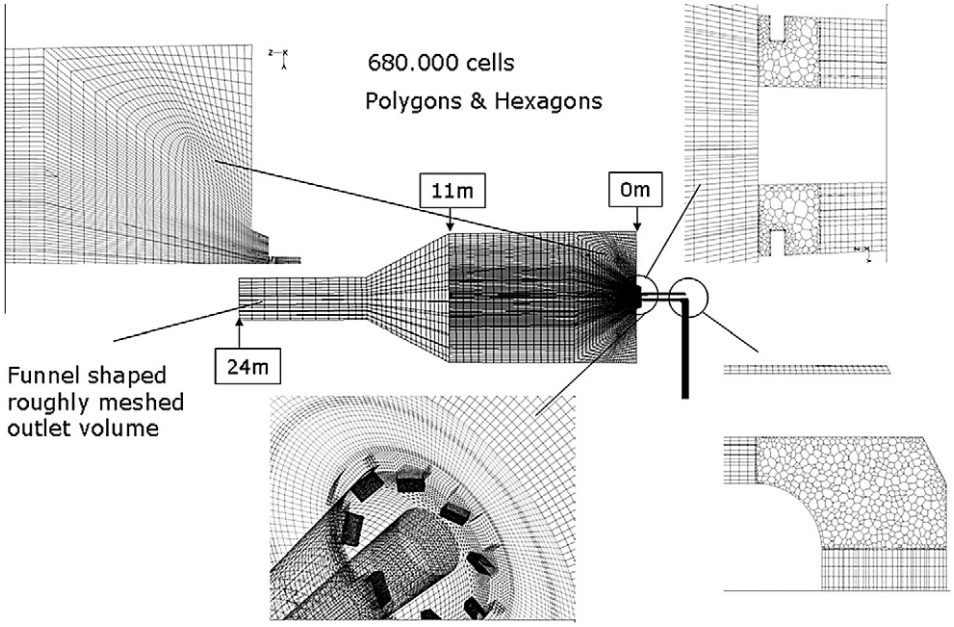

Fig. 4. Mesh for the CFD simulations.

volume to avoid backflow in the simulations and move the influence of the outlet boundary condition away from the furnace. 10 diameters of the fuel pipe leading up to the burner are simulated to get fully developed conditions at the entrance to the burner. The dimensions of the furnace are 8 m in diameter and 11 m in length. The funnel shaped outlet volume adds an additional 13 m. The depth of the burner is ~2.5 m.

3.2. Boundary conditions

The secondary and tertiary air inlets are located at the entrance to the burner and the flow in the SA and TA sections of the burner are thus not modeled. Fig. 3 shows an outline of the burner modeling methodology. The swirl blades are adjustable and the exact location of these, for straw operation, is not known beforehand. Instead swirl angle of respectively 50° and 60° for the SA and TA inlets are specified. Clearly the combustion in the near burner zone of the burner is very dependent upon the level of swirl and further measurements or simulations are necessary to determine the exact level of swirl. This would be the object of a future investigation but is out of scope of the present work. Instead, attention has been focused on determining the flow field and particle concentration at the inlet plane of the burner. Current simulation methodology most often specifies uniform velocity and concentration distribution at the inlet plane, however, the burner geometry includes a 90° bend upstream, which is known to induce a maldistributed concentration profile known as roping. Consequently, it is not possible to utilize a 2D axisymmetric geometry and it is necessary to resort to fully 3D simulation in order to capture the influence of upstream geometry. PA, SA and TA flow inlets are specified as mass flow inlets using the specification supplied by the manufactor and all outer flow constraints are specified as no slip walls. Particles are injected at the PA inlet by specifying the same velocity as the air.

3.3. Turbulence modeling

Turbulence has been simulated using the standard k–ε model with standard wall functions for a first node located at $y^+ \sim 30$–60. The standard k–ε model is generally considered inaccurate and especially for swirling flows a number of 2-equation models have been suggested for improved results. However, the standard k–ε model remain an industrial workhorse and its well documented ability, or lack of, to simulate turbulence have been preferred over more recent closures such as the SST k–ω model. A more realistic description of turbulence can only be achieved using more sophisticated closure strategies such as LES or DNS but the computational demands for the present geometry clearly excludes this possibility. The standard particle dispersion model provided by Fluent has been used to model the influence of turbulence on the particle-trajectories. This is referred to as a random walk model where the fluctuating velocity, due to turbulence, is based on the continuous phase turbulent kinetic energy and a Gaussian random function. The influence of particles on the gas-phase momentum is simulated using the PSI-Cell model [9] which has been implemented into Fluent as standard.

3.4. Turbulence modulation

The effect of particles on the carrier phase momentum equation is well known whereas the effect of particles on the turbulence equations is often neglected due to the inability of so-called turbulence modulation models to accurately predict the values observed from experimental investigations. However, it is widely accepted that large particles tend to augment turbulence whereas smaller particles tend to attenuate turbulence. Biomass particles are significantly greater than coal particles, thus it is of prime interest to determine if the modification of turbulence acts to increase or decrease the efficiency of combustion, which is coupled to the level of turbulence. Firing with coal particles, which are considered small, leads to the conclusion that they only act to decrease the carrier phase turbulence. For the present work the model described in Mandø et al. [35] are used to evaluate the effect of particles on the carrier phase turbulence. This expression is based on a theoretical derivation and is able, at least qualitatively, to predict the observed effects of turbulence modulation. Note that this modification is only implemented for a single case and not for all tested cases. The source term for the k-equation is stated as:

$$S_{kp} = \frac{\alpha\rho_p}{\tau_p}\left(\left|\bar{u}_i - \bar{u}_{pi}\right|^2 + \overline{u'_{pi}u'_{pi}} - 2k\right) \tag{3}$$

where α is the volume fraction, ρ_p is the particle density and τ_p is the particle response time. Mean velocities are indicated with a bar and fluctuating components with a prime. The combination $\alpha\rho_p$ is the particle mass concentration, which is calculated default by the solver. In order to speed up the calculation procedure and stability of the solver, the terminal particle velocity is used in place of the slip velocity and the term involving the particle fluctuating velocity is neglected. For most parts of the flow the assumption of terminal velocity is valid, however, it is well known that this assumption is not valid close to walls and in zones with large acceleration or deceleration of the fluid/ particles. The source term is incorporated into Fluent and coupled to the gas-phase equations via user-defined functions (UDF).

3.5. Particle motion

The particle equation of motion is solved for each trajectory. A total of 100,000 particle trajectories are simulated for good statistics and the particle size distribution has been resolved by specifying a total of 180 particle diameters for the Rosin–Rammler specification method. The particle equation of motion is specified as:

$$\rho_p\frac{du_p}{dt} = \frac{18\mu}{d_p^2}\frac{C_D\mathrm{Re}_p}{24}\left(u_i - u_{pi}\right) + g_i\left(\rho - \rho_p\right) + F_{\mathrm{Saffman}} \tag{4}$$

where g_i is the gravitational acceleration and F_{Saffman} is the Saffman lift force. This formulation neglects some terms compared to the BBO/MR-equation and only the steady state drag, the buoyancy and the Saffman lift force is considered. Using the usual order-of-magnitude estimates, as those that can be found in Lazaro and Lasheras [30], it is acceptable to neglect additional terms for a small and heavy particle such as a typical coal particle. Computation of order-of-magnitude estimates for a spherical straw particles show an increase of importance for the additional terms due to the lower density and larger size. However, the effect of non-sphericity has not been considered. As shown previously this acts to increase the drag coefficient compared to an equivalent volume sphere. Furthermore, it is not possible to derive the Basset history force for an arbitrary shape as this depends on the development of the boundary layer which is coupled to shape of the particle. To include the effect of non-sphericity the steady state drag coefficient is modified using the expression by Haider and Levenspiel [23]:

$$\begin{aligned} C_D &= \frac{24}{\mathrm{Re}_p}\left(1 + b_1\mathrm{Re}_p^{b_2}\right) + \frac{b_3\mathrm{Re}_p}{b_4 + \mathrm{Re}_p} \\ b_1 &= \exp\left(2.3288 - 6.4581\psi + 2.4486\psi^2\right) \\ b_2 &= 0.0964 + 0.5565\psi \\ b_3 &= \exp\left(4.905 - 13.8944\psi + 18.4222\psi^2 - 10.2599\psi^3\right) \\ b_4 &= \exp\left(1.4681 - 12.2584\psi + 20.7322\psi^2 - 15.8855\psi^3\right) \end{aligned} \tag{5}$$

where the Reynolds number Re_p is based on the diameter of a volume equivalent sphere. This is the default expression which is implemented into Fluent to correct for non-sphericity. Several other correction methods exists and the accuracy of these have been compared by Chhabra et al. [7] against a large databank of different shapes. This investigation shows that expressions developed to deal with a multitude of shapes using only a single shape parameter are associated with average errors between 20% and 30% and maximum errors up to 300%. The expression in Eq. (5) is found to perform among the best of the evaluated methods and is thus retained. In view of the large errors in the used expression for the steady state drag, the uncertainty in the actual shape of particles as well as the known issue of the methodology to model the turbulence, it seems acceptable to neglect addition terms in the equation of motion.

The Saffman lift force becomes important in presence of the strong shear fields in the combustion zones of a low-NO_x burner to model the additional translateral motion. The applicability of the known analytical expressions of the lift force is still restricted to laminar flow, concurrent motion of particle and fluid, linear shear and very small Reynolds numbers [31,36]. Furthermore, the effects of non-sphericity and rotational motion, Magnus force, may impose additional lift forces much larger than that inflicted by shear. Clearly, the use of large arbitrary shaped particles does not make the used assumptions more valid compared to the case of a small near-spherical coal particle. For the present investigation these additional effects are not modeled. It should be mentioned that an inclusion of such effects would possible require the use of a 6 degree-of-freedom model together with knowledge of the geometry and the dependence of forces for different angles of attack. Truly the challenges are stacking up for the quest of a complete description of the motion of a large arbitrary shaped particle! Additional forces resulting for the rotation and orientation of the non-spherical particle may be included by a modification/calibration of the dispersion model due to the seemingly random nature of these forces. However, this is out of the scope of the present investigation.

3.6. Wall collisions

Two different approaches towards the modeling of wall collisions have been investigated in the present work. Firstly the default approach by Fluent, assuming perfect elastic collisions, is tested. Secondly, a modified expression is used to test the influence of inelastic collisions, rough walls and eccentric collisions.

The Fluent GUI allows the possibility to modify the normal and tangential coefficient of restitution as a function of the impact angle. By default both coefficients are set to unity and the particle retains all normal and tangential momentum. The physics behind wall collisions under ideal conditions have been explored by Kharaz et al. [26]. For the collision between a smooth surface and a hard sphere the normal coefficient of restitution is constant at a value of 0.98 for all impact angles whereas the tangential coefficient of restitution reaches a minimum value 0.6 at a impact angle of 70° where an impact angle of zero imply a glancing collision. The particle kinetic energy loss (in the collision) is converted to rotational energy, to heat via frictional sliding and dissipative wave propagation.

Collisions involving rough surfaces have been thoroughly investigated by Prof. M. Sommerfeld and associates during the past couple of decades [40,41,39,43,42,28]. Observations show, that the impact on rough surfaces tend to randomize the rebound depending on the relative size of the roughness and particle involved. Especially, it is possible to gain a large increase in the normal coefficient of restitution for small impact angles. As an alternative to fully resolve the wall roughness, as demonstrated by Frank et al. [20], intricate collisions models, involving randomizing factors, have been proposed to model the impact of spheres. Similarly, to the effect of rough walls, it seems prudent to assume that the collision of an arbitrary shaped particle with a surface, smooth or rough, will exhibit random rebound and the possibility of large normal coefficients of restitution. For the present work we have focused on implementing a simple model, the applicability of which merely indicates the influence of wall collisions on combustion properties rather than using an advanced model whose applicability will be limited since there is no information available about the influence of arbitrary particle shape on the collision characteristics. The idea behind the modification is to use the adjustment possibilities given by the Fluent GUI to model a worst case scenario for the fate of each collision between an arbitrary shape particle and rough wall thus circumventing implementing a complex particle collision model. The normal and tangential restitution coefficient is modified so that the rebound angle is a constant 80° mimicking an adverse rebound for every collision. The overall coefficient of restitution is set to 0.9 to illustrate the kinetic energy loss to friction, rotation and dissipation by wave propagation. Fig. 5 shows the calculated coefficients of restitution for this scenario. It can be seen that the normal coefficient of restitution is very large at small angles according to the restrictions posed. Both coefficients of restitution approach the limit of 0.9 for an impact angle of 80°. This value has been retained for collisions with an impact angle between 80° and 90°.

3.7. Heating of non-spherical particles

The heat balance, without mass transfer, for a particle can be state as:

$$m_p C_p \frac{dT_p}{dt} = hA_p(T_\infty - T_p) + \varepsilon_p A_p \sigma\left(\theta_R^4 - T_p^4\right) \tag{6}$$

where m_p is the particle mass, C_p the particle heat capacity coefficient, T_p particle temperature, h convective heat transfer, A_p particle surface area, T_∞ local fluid temperature at particle position, ε particle emissivity, σ Stefan–Boltzmann constant and θ_R is the radiation temperature. The effect of non-sphericity has only been implemented by enhancement of the particle surface area compared to that of a volume equivalent sphere with same diameter. Thus the convective heat transfer coefficient is based on correlations developed for spheres. Similarly it may be stated that the Stefan–Boltzmann's law is only strictly valid for a sphere. Ideally efficiency factors, similar to the previously mentioned burning enhancement

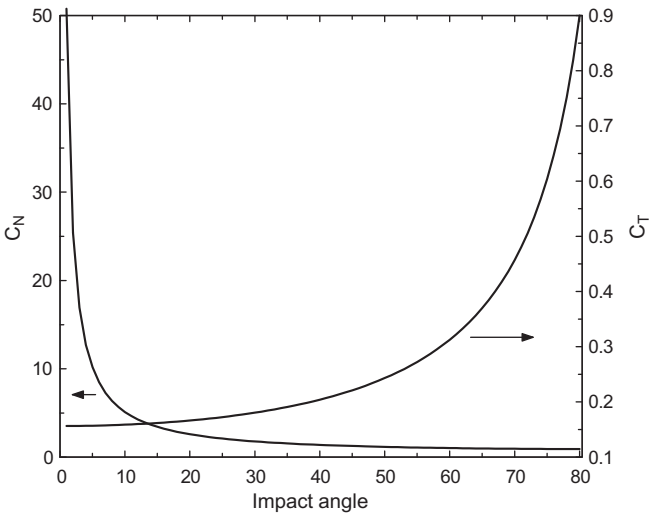

Fig. 5. Coefficients of restitution.

factor, Θ, should be developed to relate the efficiency of convective and radiative heat transfer to the sphericity factor.

For the devolatilization and char combustion the standard models in Fluent have been used. The single-rate kinetic devolatilization model is used to predict the volatile yield rate and the diffusion-limited surface reaction rate model is used to predict the char burnout of the particle. As such, additional effects of surface enhancement have not been included in these sub-models.

3.8. Gas-phase reactions

For the description of the gas composition inside the furnace the species transport approach in Fluent have been used. For this purpose 6 species have been defined: H_2O, CO, CO_2, CH_yO_y, O_2, N_2. All regions inside the furnace can be described by a mixture of these species with varying composition. These species participate in 2 homogeneous gas reactions that are assumed to describe the combustion process sufficiently:

$$\begin{aligned} &CH_yO_y + 0.54O_2 \rightarrow CO + 1.12H_2O \\ &CO + 0.5O_2 \rightarrow CO_2 \end{aligned} \tag{7}$$

where the coefficients x and y is 2.25 and 1.05 respectively. The default reactions and the associated Arrhenius parameters for the description of the reaction kinetics provided by Fluent have been used. The reaction scheme has been kept as simple as possible to enhance the numerical stability and the convergence behavior. For the description of the interaction of turbulence and chemistry the Finite rate/Eddy dissipation model has been used. For the description of the radiative heat transfer in the homogeneous gas-phase the so-called Discrete Ordinates model with 4 theta and phi divisions is used. The absorption characteristics of the different species in the gas-phase have been implemented using the Weighted Sum of Gray Gases Model (WSGGM). For more on the numerical approach, the specific schemes and models the reader is referred to the Fluent documentation [19].

4. Results and discussion

The purpose of the present work is twofold: Firstly it is intended to give a comparison between coal and straw combustion using actual firing parameters as intended for the CHP plant Amager unit 1. Secondly it is intended to give an analysis of different modeling choices influence on the simulated parameters of the straw combustion case. To do this a single simulation for straw is selected as base case to evaluate the difference between straw and coal. The different model choices for straw combustion are evaluated by changing one parameter at a time compared to the base case. The base case for straw combustion are based on the single-rate devolatilization kinetics suggested by Zhou et al. [49], the medium size and shape distribution described in Table 4, the Fluent default wall-collision model for perfect elastic collisions and no additional turbulence modulation model. The sensitivity analysis for straw simulation encompasses the following cases:

- Large particle size distribution.
- Small particles size distribution.
- Lanzetta and Di Blasi [29] devolatilization kinetics.
- Modified wall-collision model.
- Uniform particle mass flux at inlet plane.
- With turbulence modulation model.

These cases reflect in part the uncertainties associated with the biomass fuel and in part the impact of typical approximations commonly used in industrial CFD. Since the burner is not in operation it has not been possible to compare the results with experimental data.

4.1. Coal versus straw combustion

Figs. 6–9 show the result of the CFD simulation of a multifuel low-NO_x burner using respectively coal and straw as fuel. First of all it is necessary to remark that the flame is slightly misaligned compared to the center axis of the furnace. Furthermore, the effect of gravity tends to deflect the flame slightly towards the bottom of the furnace. Moreover, the inclusion of the entire inlet pipe entails that the velocity and particle distribution in the inlet plane to the furnace is not uniform which again greatly influence the characteristics of the flame. This maldistribution is mainly up-down and only to a smaller degree left–right. This maldistribution is greatly influenced by the wall-collision model which is treated later in this paper. Considering the restrictions mentioned above the results are shown on the horizontal half plane which is assumed to be representative for the entire flame. Fig. 6 shows the temperature distribution inside the furnace. It can be seen that the straw flame is significantly longer than the coal flame. Similarly, the coal flame is wider near the burner and it is attached to the flame holder whereas the straw flame seems to first ignite a bit downstream of the flame holder. Fig. 8 show a plot of the axial velocity. It can be seen that the straw flame is associated with a significantly smaller internal recirculation zone compared to the coal flame. Similarly for the straw combustion case, the jet like structure resulting from the primary air flow has a larger penetration than for the coal case. These features are direct consequences of the airflow distribution between the PA, SA and TA which again is a consequence of considerations regarding flammability, fuel entrainment, oxygen requirements etc. For the present case this gives rise to an air mass flow rate which is twice that used for the coal case for the PA. Similarly the TA air mass flow rate for the coal case is two times larger than the straw case. The larger penetration here experienced for biomass fuels is also consistent with that observed at laboratory flow reactors [3,11]. Fig. 7 shows the volume fraction of the volatile matter. It can be seen that the coal devolatilization process is complete after about 4.5 m whereas

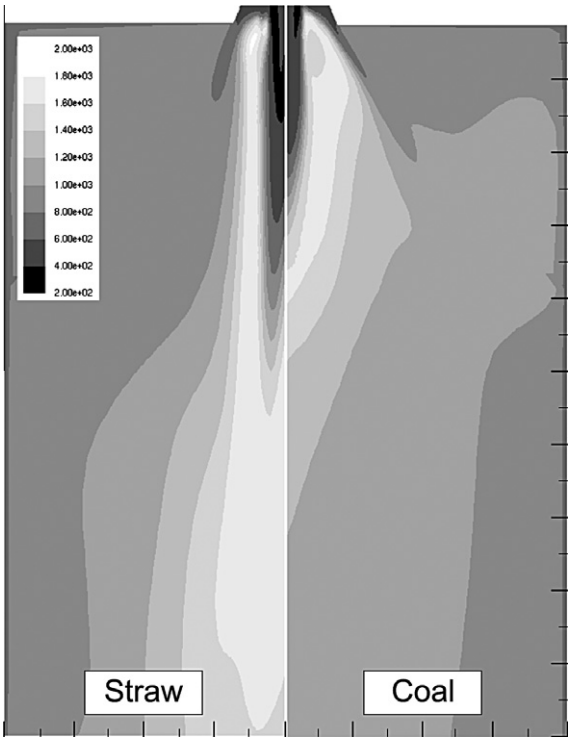

Fig. 6. Contours of temperature [K] on horizontal half plane. Grid: 4 × 10 m.

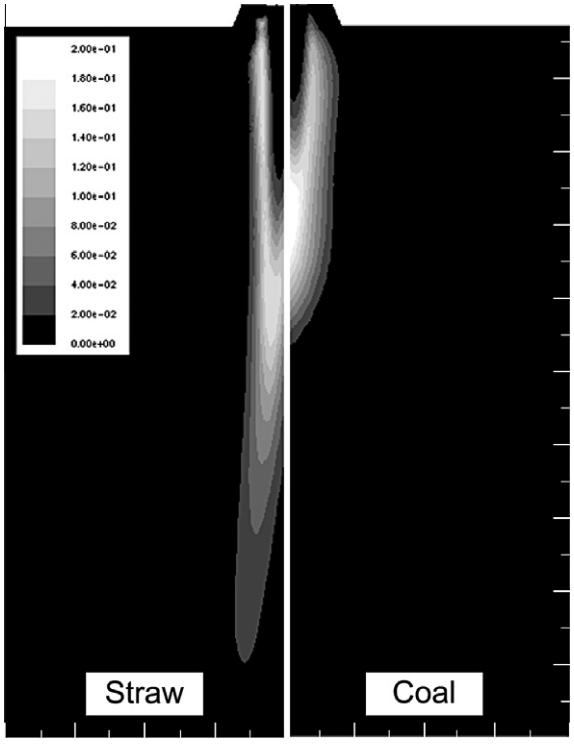

Fig. 7. Contours of CH_xO_y volume fraction on horizontal half plane. Grid: 4 × 10 m.

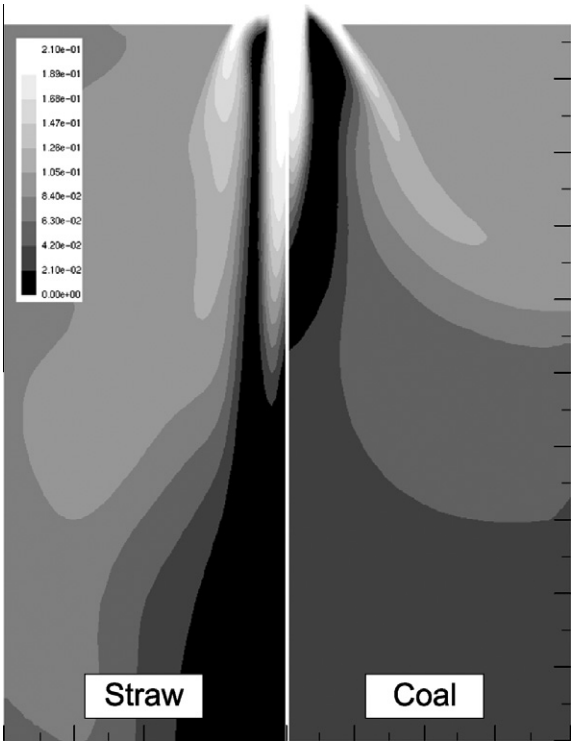

Fig. 9. Contours of O_2 volume fraction on horizontal half plane. Grid: 4 × 10 m.

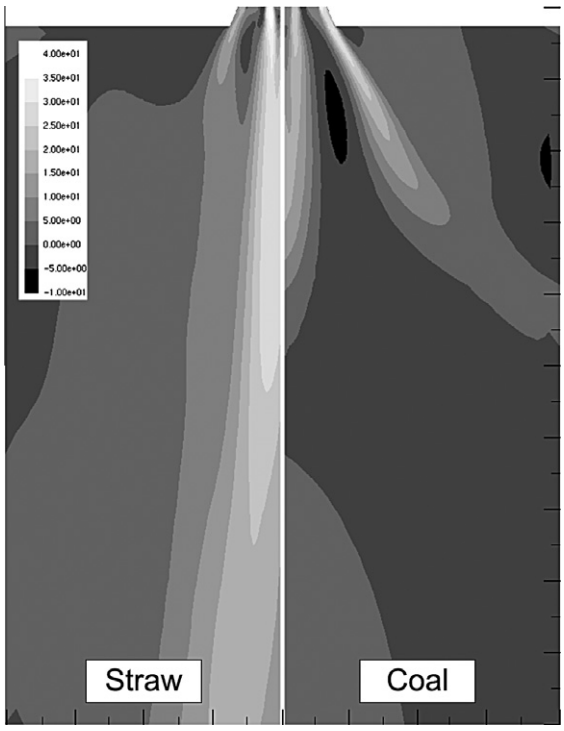

Fig. 8. Contours of axial velocity [m/s] on horizontal half plane. Grid: 4 × 10 m.

for straw combustion the devolatilization process continue up to 9 m; twice that of the coal case. Fig. 9 shows the contours of O_2 volume fraction. It can be seen that the low oxygen zone extends far downstream.

When viewing the difference between the result for coal and straw combustion it is important also to distinguish between what is inherent in the combustion of the different fuels, and what is caused by the particular design values of the burner air distribution. As such it must be stressed that the difference in air distribution is greatly determining for the final outcome. For this investigation the burner specifications for maximum load of respectively coal and straw have been used rather than showing the difference between coal and straw combustion for a fixed, and thereby unrealistic, burner air distribution.

4.2. Influence of particle size

Three different particle size and shape distributions were considered for the present investigation where the "medium" case ($d_{p,ave}$ = 300 μm, ψ = 0.28), used for the base case, was considered as the most realistic. The "medium" distribution was thus in accordance with the criteria by Esteban and Carrasco [17] for acceptable power demand in the comminution processes to obtain a specific size distribution. The "large" ($d_{p,ave}$ = 500 μm, ψ = 0.64) and "small" ($d_{p,ave}$ = 200 μm, ψ = 0.14) size distributions cases have been chosen to clearly show the impact of the particle size and shape. The simulation involving the small case shows only little or no difference compared to the medium case, whereas the large case only ignites far downstream in the boiler and the flame is "blown" off the burner. The unburnt char fraction present in the particles at the outlet decreases slightly for the small case and significantly increases for the large case. The main characteristic seems to be that the fraction of particles entrained by the recirculation zone for the large distribution is too small to allow for a sustained flame near the burner. The larger Stokes numbers associated with the large distribution entail that most particles are carried downstream in the cold central jet like structure and is only slowly heated. Considering the power demands for the comminution process and the combustion efficiency there seems to be an optimum when the particle size distribution is just small enough to allow for a sustained flame attached to the flame holder. Additional grinding to obtain smaller particle sizes will be unnecessary since the combus-

tion properties does not change significant for a smaller size distribution. This result consequently also underlines the importance to maintain a constant size and shape distribution from the mill.

4.3. Influence of wall-collision model

The often used assumption of a uniform particle and velocity distribution at the inlet to the burner is evaluated by considering the entire course of the internal burner geometry. However, this flow involves particle walls collisions whose mechanisms are highly dependent on the wall roughness and particle parameters. Two wall-collisions models have been considered and the result is compared to a simulation where particles are released 0.2 m before the inlet to the burner. This corresponds to a traditional simulation where the influence of the burner geometry is not considered i.e. the case of uniform particle distribution at the inlet plane. Figs. 10 and 11 show some sample particle trajectories inside the burner using the two different wall-collision models tested in the present investigation. Particles of different diameters have been released from a common point on the inlet plane to the simulated flow field close to the pipe wall. It can be realized that there is a significant difference between the two approaches. For the default approach in Fluent, which assumes perfect elastic collision and a smooth wall, particle-trajectories are reflected in their encounter with the wall while the modified wall-collision model imposes a strong enhancement of the particle velocity component normal to the wall.

In addition to turbulence dispersion and shear induced lift forces the modified wall-collision model act as a mechanism to redistribute particles in the vicinity of the wall. This thus alters not only the particle concentration in a cross-section of the pipe but also greatly increase the radial and the tangential velocity component and thus introduces a mechanism to transfer momentum from the main flow to the kinetic energy of the particle phase.

Fig. 12 shows the normalized particle mass flux in the burner cross-section 0.2 m upstream of the furnace inlet for standard and modified wall-collision model. It can be seen that the Fluent standard wall-collision model predicts larger particle concentration close to the wall compared to the simulation using modified wall collisions. Both approaches predict a maldistribution in the particle concentration in the up-down direction. The concentration distribution of Fig. 12 is a result of the complex flow pattern inside the burner; as the particles flow around the bend in the pipe they are moved towards the upper side of the burner annulus due to a Stokes number in the order of unity when based on the bending radius. The flow around the bend induces secondary vortices which transports particles downward. The flow around the central pipe, containing the oil-lance, seems to provoke a left right asymmetry in secondary vortices. Unsteady simulations without particles seem to suggest that this is a steady asymmetry and not vortex shedding phenomenon as is associated with a cylinder in cross-flow. The main difference between the results displayed in Fig. 12 is the additional mechanism to redistribute particles contained in the modified wall collisions. If the result for modified wall collisions are compared to a simulation where the particles are assumed uniformly distributed in the plane 0.2 m upstream of the inlet to the furnace, the main difference is the up-down maldistribution. When the unburnt char fraction of particles at the furnace outlet is evaluated for the three cases, the case of standard wall function show less unburnt char compared to both the case of modified wall functions and the case where the particle concentration is uniformly distributed at the inlet plane to the furnace. This is believed to be caused by the larger fraction of particles being entrained in the recirculation zone due to the particle concentration in the inlet plane.

We believe that this behavior of the particles for the modified wall collisions are in qualitatively agreement with the results published by Sommerfeld and Kussin [42] for 195 μm glass spheres on a rough wall. Ideally any wall-collision model should be dependent on the relative size between the roughness and the particle size. However, independently of the wall roughness it seems prudent to assume that arbitrary shaped particles will have a less than ideal rebound compared to perfect spheres on a smooth surface. Since

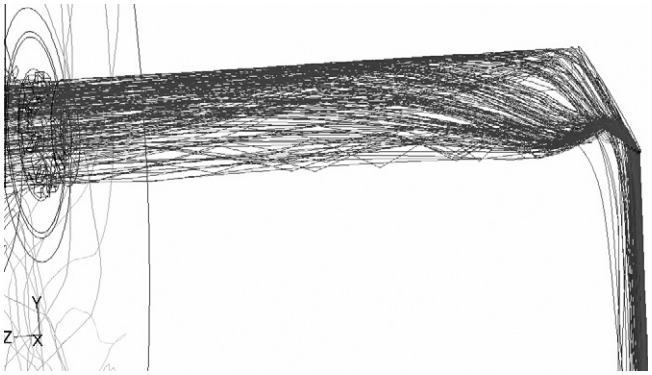

Fig. 10. Sample trajectories for standard wall collisions.

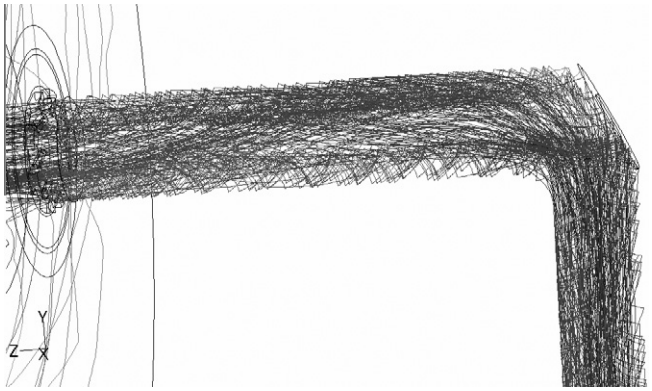

Fig. 11. Sample trajectories for modified wall collisions.

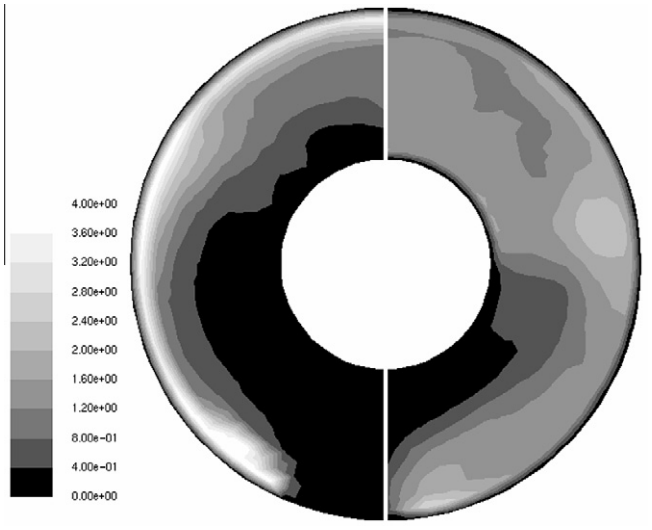

Fig. 12. Contours of normalized particle mass flux, $f_p/f_{p,ave}$ for inlet pipe cross-section 0.2 m upstream of boiler inlet. Left: Fluent default wall collisions; Right: Modified wall collisions.

the two tested models for wall collisions represent the best and worst possible scenario for each hit it is belied that the actual situation will lie somewhere between these two extremes. To assume uniform particle distribution at inlet plane is a poor choice since this scenario does not capture the maldistribution between the upper and lower part of the annular cross-section.

4.4. Influence of turbulence modulation model

It can be assumed that coal particles, which for this discussion are considered small, will act to reduce the intensity of turbulence. Biomass particles, which for this discussion often are considered large, may on the other hand act to increase the intensity of turbulence. The actual mechanisms and models to deal with turbulence modulation are still being developed and the applicability of such models must also be compared to the ability of the primary turbulence model to accurately model turbulence. When this is said, with the present work we wish to demonstrate the influence of turbulence modulation on the combustion properties.

Fig. 13 shows the turbulent kinetic energy in the horizontal half plane inside the furnace close to the burner when evaluated with and without a model for turbulence modulation. It can be seen that the presence of straw particles tends to attenuate the turbulence. Even though straw particles are considered large the shape of the particles tend to increase their drag coefficient and thereby decrease the slip/terminal velocity which is the essential to produce additional turbulent kinetic energy according to Eq. (3). Thereby, the third term in Eq. (3) becomes dominant and the turbulence is decreased accordingly. It should be noted that the second term in Eq. (3), which also acts to increase the turbulence kinetic energy, is neglected. However, according to Mandø et al. [35] this term only becomes significant close to walls where wall collisions increase the particles fluctuation velocity. For the present case this situation only occurs close to the furnace inlet. Furthermore, at this location the flow is accelerating and the assumption of particles traveling at terminal velocity is no longer strictly valid. In this area a significant level of turbulence is produced by the flame holders together with the presence of a relative large particle concentration. This tends to increase the third term but is also a notoriously difficult situation to capture using RANS based turbulence models. Thus it is expected at any inaccuracy caused by the particle source term would be of the same order-of-magnitude as that inflicted by the turbulence model itself.

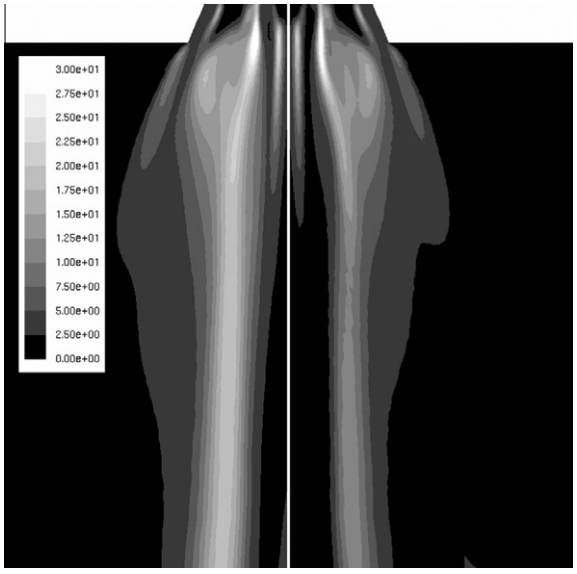

Fig. 13. Contours of turbulent kinetic energy [m^2/s^2] Left: No modification; Right: with turbulence modulation model, Grid: 2 × 4 m.

Table 6
Unburnt char fraction at outlet for different cases and change compared to the base case.

	Unburnt char (%)	Change (%)
Base case	10.2	0
Small particle size	8.6	−16
Large particle size	23.4	129
Devolatilization kinetics	9.8	−4
Modified wall collisions	16.2	59
Uniform particle mass flux	13.4	31
Turbulence modulation	15.3	50

When evaluated on basis of the unburnt char present in the particles at the outlet of the furnace the decrease in turbulence acts to increase the amount of char left in the particles. This is viewed as a consequence of the eddy dissipation model which determines the rate of combustion reactions. Thus a reduction in turbulent kinetic energy yields a reduction in reaction rate for the case using the turbulence modulation model and is indirectly coupled to the char combustion rates.

4.5. Relative importance of modeling choices

To evaluate the relative influence of each modeling choice, using a single parameter, the fraction of unburnt char present in the particles at the outlet plane is used. Clearly, it is desired to have as low as possible level of unburnt char for optimal operation of any boiler. The difference for each of the modeling choices compared to the base case gives an indication on the importance of the particular modeling choice. Table 6 outlines the amount of unburnt char at the outlet plane for each of the straw simulations.

It can be seen that using a smaller particle distribution or different devolatilization kinetics has minimal influence on this particular parameter. Whereas specifying a larger particle distribution has a great deteriorating effect due to the flame blowoff. The concentration distribution at the inlet plane, whether specified or modeled, does also have a great influence on the unburnt char fraction. When evaluated using the unburned char as parameter, the uniform particle mass flux at the inlet plane to the burner seems like good compromise despite its inability to capture the particle concentration maldistribution. The application of a turbulence modulation model ranks high on the list of relative importance for different modeling choices. However, the user should carefully consider the accuracy and interaction of applied submodels before implementing such initiatives. Here we merely wished to show the qualitative effect of turbulence modulation of larger biomass particles.

5. Conclusions

CFD simulations of pulverized coal and straw combustion using a commercial multifuel low-NO_x burner have been undertaken with specific attention of the impact of modeling choices for straw combustion. The following conclusions can be drawn:

It is possible to use the same modeling approach and sub-models used for coal combustion to model straw combustion.

For the present airflow specifications straw combustion is associated with a significantly longer flame and smaller recirculation zones compared to coal combustion.

The particle size and shape distribution is critical for the correct prediction of the combustion.

The particle mass flux at the inlet plane is not uniformly distributed. Depending on the particle–wall-collision model applied,

when the entire burner geometry is simulated, the particle mass flux specified at the inlet plane is shown to either improve or deteriorate the combustion efficiency.

Only little difference was found using two different devolatilization rates for straw for the present case.

Straw particles tend to decrease the carrier phase turbulence. However, the application of a turbulence modulation model must be carefully considered.

Acknowledgement

This work was supported by Energinet.dk, under grant PSO 2006 1 6364. Burmeister & Wain Energy A/S are acknowledged for supplying drawings and specification of the multifuel fired low NO_x burner. Vattenfall Research and Development AB, involved in the commissioning of the CHP Amager unit 1, are greatly acknowledge for their support and cooperation during this work.

References

[1] Abbas T, Costen P, Kandamby NH, Lockwood FC, Ou JJ. The influence of burner injection mode on pulverized coal and biomass cofired flames. Combust Flame 1994;99(3–4):617–25.
[2] Backreedy RI, Fletcher LM, Jones JM, Ma L, Pourkashanian M, Williams A. Co-firing pulverised coal and biomass: a modeling approach. Proc Combust Inst 2005;30:2955–64.
[3] Ballester J, Barroso J, Cerecedo LM, Ichaso R. Comparative study of semi-industrial-scale flames of pulverized coals and biomass. Combust Flame 2005;141(3):204–15.
[4] Battista JJ, Hughes EE, Tillman DA. Biomass cofiring at Seward Station. Biomass Bioenergy 2000;19(6):419–27.
[5] Baxter L. Biomass–coal co-combustion: opportunity for affordable renewable energy. Fuel 2005;84(10):1295–302.
[6] Bharadwaj A, Baxter LL, Robinson AL. Effects of intraparticle heat and mass transfer on biomass devolatilization: experimental results and model predictions. Energy Fuels 2004;18(4):1021–31.
[7] Chhabra RP, Agarwal L, Sinha NK. Drag on non-spherical particles: an evaluation of available methods. Powder Technol 1999;101(3):288–95.
[8] Clift R, Grace R, Weber ME. Bubbles, drops, and particles. Mineola, New York: Dover Publications, Inc.; 2005.
[9] Crowe CT, Sharma MP, Stock DE. Particle-source in cell (PSI-Cell) model for gas-droplet flows. J Fluids Eng – Trans ASME 1977;99(2):325–32.
[10] Cui HP, Grace JR. Fluidization of biomass particles: a review of experimental multiphase flow aspects. Chem Eng Sci 2007;62(1–2):45–55.
[11] Damstedt B, Pederson JM, Hansen D, Knighton T, Jones J, Christensen C, et al. Biomass cofiring impacts on flame structure and emissions. Proc Combust Inst 2007;31:2813–20.
[12] Demirbas A. Combustion characteristics of different biomass fuels. Progr Energy Combust Sci 2004;30(2):219–30.
[13] Di Blasi C. Modeling chemical and physical processes of wood and biomass pyrolysis. Progr Energy Combust Sci 2008;34(1):47–90.
[14] Elfasakhany A, Bai XS. Modelling of pulverised wood combustion: a comparison of different models. Progr Computat Fluid Dynam 2006;6(4–5):188.
[15] Elfasakhany A, Klason T, Bai XS. Modelling of pulverised wood combustion using a functional group model. Combust Theory Model 2008;12(5):883–904.
[16] Energistyrelsen. Energi i Danmark, Energy statistics from the Danish ministery of Climate and Energy, 2008.
[17] Esteban LS, Carrasco JE. Evaluation of different strategies for pulverization of forest biomasses. Powder Technol 2006;166(3):139–51.
[18] Field SB, Klaus M, Moore MG, Nori F. Chaotic dynamics of falling disks. Nature 1997;388(6639):252–4.
[19] Fluent Inc. Fluent 6.3 User's guide, 2006.
[20] Frank T, Schade KP, Petrak D. Numerical-simulation and experimental investigation of a gas solid 2-phase flow in a horizontal channel. Int J Multiphase Flow 1993;19(1):187–98.
[21] Gera D, Mathur MP, Freeman MC, Robinson A. Effect of large aspect ratio of biomass particles on carbon burnout in a utility boiler. Energy Fuels 2002;16(6):1523–32.
[22] Gjernes E. Fuel flexibility at Amager unit 1 using pulverized fuels. Presented at Power-Gen Europe, Cologne, Germany, 2006.
[23] Haider A, Levenspiel O. Drag coefficient and terminal velocity of spherical and nonspherical particles. Powder Technol 1989;58(1):63–70.
[24] Hilpert H, Maier J, Scheurer W, Hein KRG. Status report on firing secondary fuels in Europe. International Flame Research Foundation, 2006.
[25] Holm JK, Sørensen LH, Henriksen U, Hjuler K, Simonsen K, Berg M. Fuel preparation and characterization – part of the PSO project: biomass dust firing, 2006.
[26] Kharaz AH, Gorham DA, Salman AD. An experimental study of the elastic rebound of spheres. Powder Technol 2001;120(3):281–91.
[27] Klett JD. Orientation model for particles in turbulence. J Atmos Sci 1995;52(12):2276–85.
[28] Lain S, Sommerfeld M. Euler/Lagrange computations of pneumatic conveying in a horizontal channel with different wall roughness. Powder Technol 2008;184(1):76–88.
[29] Lanzetta M, Di Blasi C. Pyrolysis kinetics of wheat and corn straw. J Anal Appl Pyrol 1998;44(2):181–92.
[30] Lazaro BJ, Lasheras JC. Particle dispersion in a turbulent, plane, free shear-layer. Phys Fluids A – Fluid Dynam 1989;1(6):1035–44.
[31] Li A, Ahmadi G. Dispersion and deposition of spherical-particles from point sources in a turbulent channel flow. Aerosol Sci Technol 1992;16(4):209–26.
[32] Lokare SS, Dunaway JD, Moulton D, Rogers D, Tree DR, Baxter LL. Investigation of ash deposition rates for a suite of biomass fuels and fuel blends. Energy Fuels 2006;20(3):1008–14.
[33] Lu H, Robert W, Peirce G, Ripa B, Baxter LL. Comprehensive study of biomass particle combustion. Energy Fuels 2008;22(4):2826–39.
[34] Ma L, Jones JM, Pourkashanian M, Williams A. Modelling the combustion of pulverized biomass in an industrial combustion test furnace. Fuel 2007;86(12–13):1959–65.
[35] Mandø M, Lightstone MF, Rosendahl L, Yin C, Sørensen H. Turbulence modulation in dilute particle-laden flow. Int J Heat Fluid Flow 2009;30:331–8.
[36] Michaelides EE. Review – the transient equation of motion for particles, bubbles, and droplets. J Fluids Eng – Trans ASME 1997;119(2):233–47.
[37] Nussbaumer T. Combustion and co-combustion of biomass: fundamentals, technologies, and primary measures for emission reduction. Energy Fuels 2003;17(6):1510–21.
[38] Rosendahl LA, Yin C, Kær SK, Friborg K, Overgaard P. Physical characterization of biomass fuels prepared for suspension firing in utility boilers for CFD modelling. Biomass Bioenergy 2007;31(5):318–25.
[39] Sommerfeld M. Analysis of collision effects for turbulent gas-particle flow in a horizontal channel: part 1. Particle transport. Int J Multiphase Flow 2003;29(4):675–99.
[40] Sommerfeld M. Modeling of particle wall collisions in confined gas particle flows. Int J Multiphase Flow 1992;18(6):905–26.
[41] Sommerfeld M, Huber N. Experimental analysis and modelling of particle–wall collisions. Int J Multiphase Flow 1999;25(6–7):1457–89.
[42] Sommerfeld M, Kussin J. Wall roughness effects on pneumatic conveying of spherical particles in a narrow horizontal channel. Powder Technol 2004;142(2–3):180–92.
[43] Sommerfeld M, Kussin J. Analysis of collision effects for turbulent gas-particle flow in a horizontal channel. Part II. Integral properties and validation. Int J Multiphase Flow 2003;29(4):701–18.
[44] Versteeg H, Malalasekera W. An introduction to computational fluid dynamics. 2nd ed. Prentice Hall; 2007.
[45] Williams A, Pourkashanian M, Jones JM. Combustion of pulverised coal and biomass. Progr Energy Combustion Sci 2001;27(6):587–610.
[46] Wu C, Tree D, Baxter L. Reactivity of NH_3 and HCN during low-grade fuel combustion in a swirling flow burner. Proc Combust Inst 2007;31(2):2787–94.
[47] Yang YB, Ryu C, Khor A, Yates NE, Sharifi VN, Swithenbank J. Effect of fuel properties on biomass combustion. Part II. Modelling approach – identification of the controlling factors. Fuel 2005;84(16):2116–30.
[48] Yin CG, Rosendahl L, Kaer SK, Condra TJ. Use of numerical modeling in design for co-firing biomass in wall-fired burners. Chem Eng Sci 2004;59(16):3281–92.
[49] Zhou H, Jensen AD, Glarborg P, Jensen PA, Kavaliauskas A. Numerical modeling of straw combustion in a fixed bed. Fuel 2005;84(4):389–403.

International Journal of Heat and Fluid Flow 30 (2009) 331–338

Contents lists available at ScienceDirect

International Journal of Heat and Fluid Flow

journal homepage: www.elsevier.com/locate/ijhff

Turbulence modulation in dilute particle-laden flow

M. Mandø [a,*], M.F. Lightstone [b], L. Rosendahl [a], C. Yin [a], H. Sørensen [a]

[a] Institute of Energy Technology, Aalborg University, Pontoppidanstræde 101, 9220 Aalborg, Denmark
[b] Department of Mechanical Engineering, McMaster University, 1280 Main Street West, Hamilton, Ontario, Canada L8S 4L7

ARTICLE INFO

Article history:
Received 19 June 2008
Received in revised form 8 December 2008
Accepted 9 December 2008
Available online 19 January 2009

Keywords:
Turbulence modulation
Gas-particle flow
Eulerian–Lagrangian
Particle-laden pipe flow
K–ε model
Dilute flow

ABSTRACT

A new particle source term to account for the effect of particles on the turbulence equations based on the Euler/Lagrange approach is introduced and compared with existing models and experimental data. Three different sizes of particles are considered to cover the range of large particles, where augmentation of the carrier phase turbulence is expected, and small particles, for which attenuation is expected. The new model is derived directly from the balance equations of fluid flow and represents a combination of the so-called standard and consistent approaches. The performance of the new model surpasses that of the standard and consistent models and it is able to predict both the suppression and enhancement of fluid turbulence for small and large particles.

1. Introduction

Particle-laden flows have many important engineering applications such as pneumatic transport, combustion of pulverized fuels, dispersion of pollutants and spray drying. In each of these cases a fundamental understanding of the underlying phenomena which are responsible for the complex interaction between the particulate phase and the turbulent carrier flow is required to improve the design of engineering devices in which these flows occur. In the context of Computational Fluid Dynamics, Crowe et al. (1977) provided the PSI-CELL procedure for the momentum coupling between particles and the carrier phase. However, there is no consensus towards the influence of particles on the turbulence equations and no model has so far been able to reproduce the entire spectrum of experimental measurements. Experimental observation suggests that small particles tend to attenuate the carrier phase turbulence while large particles tend to augment the turbulence (Gore and Crowe, 1989). Furthermore, the magnitude of the change has been shown to scale with the particle concentration[1] (Kenning, 1996). The fundamental mechanisms which are most often associated with turbulence modulation are that the wake of particles is responsible for the additional production of turbulence while the particle-eddy interaction is responsible for the additional dissipation of turbulence (Yuan and Michaelides, 1992). For dense flows the effect of particle-particle collisions introduces another route for which turbulence modulation can proceed. Several models have been proposed to account for the influence of particles on the carrier phase turbulence. These can be divided into three distinct categories. The largest group of models derived the source term due to particles using the standard approach of Reynolds averaging used to derive the turbulence equations.

This results in a source term which always acts as sink for the turbulent kinetic energy and thus is only able to predict attenuation. This method has been labeled the "standard" approach (Lain and Sommerfeld, 2003). The turbulence equations for particle-laden flow can also be derived by considering that the instantaneous carrier phase velocity at the surface the particle must be equal to the particle velocity. This results in a term which for dilute flows is always positive and thus only acts to enhance the turbulent kinetic energy. This method is commonly referred to as the "consistent" approach (Lain and Sommerfeld, 2003). The last type of models can be referred to as semi-empirical or semi-heuristic. These are based on a mechanistic approach where additional source terms are defined as functional relationships of the wake size or other particle related parameters. In contrast to the standard and the consistent approach, models based on this approach are capable of predicting both attenuation and augmentation of turbulence. However, such an approach has been criticized for lacking rigor since the models are not derived from the balance equations of mass, momentum and energy, and thus cannot be introduced into conventional closure models without violating fundamental physical principles. The present work introduces a

* Corresponding author. Tel.: +45 9940 9248; fax: +45 9815 1411.
E-mail address: mma@iet.aau.dk (M. Mandø).

[1] In addition to the particle concentration, parameteres such as mass loading, volume loading, number concentration, mass fraction, volume fraction and interparticle spacing have been used specify the quantity of particles.

0142-727X/$ - see front matter © 2008 Elsevier Inc. All rights reserved.
doi:10.1016/j.ijheatfluidflow.2008.12.005

Nomenclature

C	constant [–]
l_e	integral length scale [m]
d_p	particle diameter [m]
g	gravity [m/s^2]
P	pressure [pa]
S	source [–]
u	velocity [m/s]
x	spatial coordinate [m]
t	time [s]
F	force [N]
V	volume [m^3]
m	mass [kg]
n	number of particles [–]
L_I	Lagrangian length scale [m]
Re	Reynolds number [–]
f	derivation from Stokes drag [–]
U	mean velocity [m/s]
k	turbulent kinetic energy [m^2/s^2]

Greek symbols

ε	dissipation rate [m^2/s^3]
ρ	density [kg/m^3]
φ	transport parameter [–]
Γ	diffusion coefficient [–]
σ	intensity, constant in k–ε model [–]
μ	viscosity [kg/m·s]
α	volume fraction [–]
τ	time scale/constant [s]

Superscripts

–	time average
$'$	fluctuating quantity

Subscripts

i,j	index
p	particle
u	momentum
k	turbulent kinetic energy
ε	dissipation rate
t	turbulent
0	clear flow
V	Stokes flow
c	clear flow

new derivation of the source term for particle-turbulence interaction consistent with the governing equations of fluid flow. The resulting source term represents a "hybrid" between the standard and consistent approaches and is capable of predicting both attenuation and augmentation. In this paper the new model has been compared to the experimental studies by Tsuji et al. (1984) and Kulick et al. (1994) as well as to a representative model for each of the aforementioned approaches.

2. Numerical approach

An Eulerian/Lagrangian approach is used to calculate the particle-laden gas flow. The continuous phase flow field is obtained from solution of the Reynolds averaged equations for fluid flow along with the k–ε turbulence model to achieve closure. The conservation equations for steady fluid flow, extended to take into account the presence of particles, is given as:

$$\frac{\partial \rho \bar{u}_j \phi}{\partial x_j} = \frac{\partial}{\partial x_j} \Gamma_\phi \frac{\partial \phi}{\partial x_j} + S_\phi + S_{\phi p} \tag{1}$$

Here ρ is the continuous phase density, $\bar{u}_j$ is the mean velocity components, φ represent the transported parameter, Γ_φ is a diffusion coefficient, S_φ is the usual fluid phase source term and $S_{\varphi p}$ is the source term due to the particles. These quantities are presented in Table 1. Here, μ is the gas phase viscosity, P is the mean pressure, g is the gravitational acceleration, k is the turbulent kinetic energy and ε is the dissipation rate.

The complete set of equations for the continuous phase is discretised using the upwind scheme and solved iteratively using the SIMPLE algorithm. In the present work the commercial solver Fluent has been used to perform the calculations. The particle trajectories are calculated using the following set of ordinary differential equations:

$$\rho_p V_p \frac{du_{pi}}{dt} = \frac{\rho_p V_p}{\tau_p}(u_i - u_{pi}) + V_p(\rho_p - \rho)g_i + F_i \qquad \frac{dx_{pi}}{dt} = u_{pi} \tag{2}$$

Here, u_{pi} are the instantaneous particle velocity components, x_{pi} are the coordinates of the particle position, ρ_p is the particle density, V_p is the particle volume, F_i represent forces other than drag and gravity and τ_p is the particle response time calculated using the following set of supporting equations:

$$\begin{aligned} &\tau_p = \tfrac{\tau_V}{f}, \quad f = 1 + 0.15\mathrm{Re}^{0.687}, \\ &\tau_V = \tfrac{\rho_p d_p^2}{18\mu}, \quad \mathrm{Re} = \tfrac{\rho|u_{pi} - u_i| d_p}{\mu} \end{aligned} \tag{3}$$

where d_p is the particle diameter. Only the Saffman lift force is considered in addition to the drag and the gravity force and all other forces such as pressure gradient, virtual mass and Basset history force are considered negligible. The instantaneous velocity is obtained by adding the mean velocity to a fluctuating velocity component which is sampled from a Gaussian probability distribution function. The interaction time for which the sampled fluctuating velocity persists, is determined from the minimum of the eddy life time and the eddy crossing time which are calculated using appropriate time and length scales associated with the k–ε model. For more on the numerical approach, the specific schemes and models the reader is referred to the Fluent documentation (Fluent, 2006).

Table 1
Summary of terms and constants in the general equation.

φ	S_φ	Γ_φ
1	0	0
$\bar{u}_i$	$\frac{\partial}{\partial x_j}\left(\Gamma_{u_i}\frac{\partial \bar{u}_j}{\partial x_i}\right) - \frac{\partial P}{\partial x_i} + \rho g_i$	$\mu + \mu_t$
k	$G_k - \rho\varepsilon$	$\mu + \mu_t/\sigma_k$
ε	$\frac{k}{\varepsilon}(C_{\varepsilon 1}G_k - C_{\varepsilon 2}\rho\varepsilon)$	$\mu + \mu_t/\sigma_\varepsilon$
$G_k = \mu_t\left(\frac{\partial \bar{u}_i}{\partial x_j} + \frac{\partial \bar{u}_j}{\partial x_i}\right)\frac{\partial \bar{u}_i}{\partial x_j}$, $\mu_t = C_\mu \rho \frac{k^2}{\varepsilon}$, $\sigma_k = 1.0$		
$C_\mu = 0.09$, $C_{\varepsilon 1} = 1.44$, $C_{\varepsilon 2} = 1.92$, $\sigma_\varepsilon = 1.3$		

3. Effect of particles on continuous phase

The momentum source due to the presence of particles is found by examining the change in momentum of a particle as it passes through each control volume. By time and ensemble averaging for each control volume it can be expressed in the following form (Gouesbet and Berlemont, 1999):

$$\overline{S_{upi}} = n\left\langle m_p\left(\frac{du_{pi}}{dt} - g_i\right)\right\rangle \tag{4}$$

where n is the mean number of particle in the per unit volume, m_p is the particle mass and $\langle \ldots \rangle$ indicate mean values over all particle trajectory realizations. This expression has been implemented into Fluent whereas the influence on the turbulence equations need to implemented using custom source terms. In the literature three different approaches exist to derive appropriate source terms for the turbulence equations.

3.1. Standard approach

The source term for the standard approach is derived by multiplying the momentum equation by u_i and applying a Reynolds averaging procedure (Chen and Wood, 1985; Gouesbet and Berlemont, 1999; Lightstone and Hodgson, 2004). After subtracting the mean kinetic energy, an expression for the turbulent kinetic energy due to the presence of particles results as:

$$S_{kp} = \overline{u_i' S_{upi}'} \tag{5}$$

If only the drag force is considered this term can be expressed as:

$$S_{kp} = \frac{\alpha\rho_p}{\tau_p}\left(\overline{u_i' u_{pi}'} - \overline{u_i' u_i'}\right), \quad \overline{u_i' u_i'} = 2k \tag{6}$$

Eq. (6) is often referred to as being dissipative considering that the particles are accelerated by the motion of the fluid and thus the particle velocity u_{pi}' is smaller than the fluid velocity u_i' (Elghobashi, 1994). Usually, models based on this approach are only capable of predicting attenuation. Several authors have presented models for the unknown first term. Here we only present the most recent development of the standard approach. Thus by considering the crossing trajectory effect, the unknown correlation can be derived analytically as (Lightstone and Hodgson, 2004):

$$\begin{aligned} &\overline{u_i' u_{pi}'} = 2k\frac{\tau^*}{\tau^* + \tau_p}, \quad \frac{1}{\tau^*} = \frac{|u_i - u_{pi}|}{L_I} + \frac{1}{\tau_{L_I}} \\ &L_I = 2\tau_{L_I}\sqrt{2k/3}, \quad \tau_{L_I} = 0.135\frac{k}{\varepsilon} \end{aligned} \tag{7}$$

where τ_{LI} and L_I is the Lagrangian time and length scale. The additional dissipation due to the particles, $S_{\varepsilon p}$, is assumed to be proportional to the similar terms in the k-equation. To get the right units each term is multiplied by ε/k:

$$S_{\varepsilon p} = C_{\varepsilon 3}\frac{\varepsilon}{k}S_{kp} \tag{8}$$

where the value of the constant $C_{\varepsilon 3}$ is suggested to be 1.1.

3.2. Consistent approach

Another approach, which provides what is commonly known as the consistent terms, starts with the mechanical energy equation for the fluid phase and subtracts the product of the mean velocity and the momentum equation to obtain an expression for the turbulent kinetic energy (Crowe, 2000). The source term due to the presence of the particles is then given as:

$$S_{kp} = \overline{u_{pi} S_{upi}} - \bar{u}_i \bar{S}_{upi} \tag{9}$$

If the drag force is again used as the momentum source term, as in Eq. (5), the following expression for the kinetic energy source term due to the presence of particles can be obtained after Reynolds averaging:

$$S_{kp} = \frac{\alpha\rho_p}{\tau_p}\left(|\bar{u}_i - \bar{u}_{pi}|^2 + \left(\overline{u_{pi}' u_{pi}'} - \overline{u_i' u_{pi}'}\right)\right) \tag{10}$$

The first term can be identified as the transfer of energy by the drag force while the last two terms is seen to represent the transfer of kinetic energy of the particle motion to the kinetic energy of the of the fluid. The first term is always positive and increases in magnitude with particle size for particles traveling at terminal velocity. According to Crowe (2000) the last two terms can be neglected for dilute flow but become important for dense flow where particle collisions tend to increase the particle kinetic energy. Thus models based on this consistent approach is only able to predict an augmentation of the carrier phase turbulence; the opposite of the standard approach. The source term to the dissipation rate is found similarly as for the standard approach, however, the value of the constant $C_{\varepsilon 3}$ should be changed to 1.8 (Lain and Sommerfeld, 2003). This value is often discussed and several observations suggest that this value is not universal (Squires and Eaton, 1992; Boulet and Moissette, 2002).

3.3. Semi-empirical or semi-heuristic approach

The third approach to formulate appropriate source terms to the turbulence equations deals with additional semi-empirical production and dissipation terms based on energy transfer mechanisms associated with the particles. The production of turbulence is most often attributed to the wake of the particle where the velocity defect and vortex shedding are well known phenomena which influence the carrier phase. Yuan and Michaelides (1992) and Yarin and Hetsroni (1994) have both presented models in which production terms rely on descriptions of the wake, while Kenning and Crowe (1997) introduces a hybrid length scale, in replacement of the traditional dissipation length scale to account for the additional dissipation. These models have succeeded in predicting some changes in the turbulence intensity but have been criticized for not providing a theoretical base consistent with the closures presented above (Boulet and Moissette, 2002).

3.4. New source term

The standard and the consistent approach are theoretical "correct" in that they both are derived considering the conservation of energy, but neither is fully capable of predicting both attenuation and augmentation of the fluid phase. Semi-empirical models use a mechanistic approach to formulate terms which with some success can account for both attenuation and augmentation, but these models are criticized for not being based on a solid theoretical basis. What is desired is thus a model which is derived on a theoretical basis but which contains both production and dissipation terms which can be related to fundamental mechanisms.

Referring to the comprehensive DNS study by Vreman (2007) for inspiration, two basic mechanisms can be identified as causes for turbulence modulation in pipe flows: One is due to the particles mean velocity profile generally being more uniform than the carrier phase mean velocity profile, and the other resulting from the particle-eddy interaction which leads to additional dissipation. The momentum source term can thus be extended to yield two simple forcing terms reflecting the basic mechanisms:

$$S_{upi} = S_{upi,1} + S_{upi,2} = \frac{\alpha\rho_p}{\tau_p}\left(u_{pi} - \bar{u}_i\right) + \frac{\alpha\rho_p}{\tau_p}\left(\bar{u}_i - u_i\right) \tag{11}$$

If the consistent approach is applied on the first term and the standard approach on the second, the source term due to particles can be expressed as:

$$S_{kp} = \frac{\alpha\rho_p}{\tau_p}\left(u_{pi} - \bar{u}_i\right)\left(u_{pi} - \bar{u}_i\right) + \frac{\alpha\rho_p}{\tau_p}u_i'\left(\bar{u}_i - u_i\right) \tag{12}$$

Performing Reynolds decomposition along with Reynolds averaging the final expression emerges as:

$$S_{kp} = \frac{\alpha\rho_p}{\tau_p}\left(|\bar{u}_i - \bar{u}_{pi}|^2 + \overline{u_{pi}' u_{pi}'} - 2k\right) \tag{13}$$

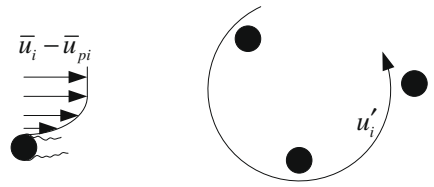

Fig. 1. Mechanisms for turbulence modulation.

This term can also be achieved by adding the source terms of the standard and consistent method and thus represent a combination of both approaches. The terms in Eq. (13) can be related to the two mechanisms for the transfer of mechanical energy of the particle phase to the turbulent kinetic energy of the fluid phase. These mechanisms are illustrated in Fig. 1.

Particles represent surfaces which are capable of supporting stresses and thus generate additional turbulence due to the flow gradient. This additional turbulence manifests itself in the wake of the particles and is often referred to as "wake induced" turbulence. This is also addressed by the consistent approach and is dependent on concentration, the relative velocity between the particle and the fluid phase which for particles traveling at terminal velocity is highly dependent on the particle size. This term reflects the conversion of mechanical work by the drag force and is thus related to the first mechanism.

The correlated motion between particles and turbulent eddies tend to attenuate the turbulence as the particles are accelerated by the fluid motion. This mechanism should be dependent on concentration, relevant turbulence quantities and the particle response time. This mechanism is also addressed by the standard approach but not the consistent approach and reflects the second mechanism.

The source term for the dissipation equation can again be found using Eq. (8) where the constant $C_{\varepsilon 3}$ is set initially to 1.0. Several different values of the proportionality constant between values of 1 and 2 have been tried, however, the effect on the final outcome is very limited and the initial value of 1.0 has been maintained. It can be realized that this derivation yields the desired effects relating to experimental observations. For small particles the first term will be small compared the third term and thus the overall effect of the source term is to attenuate turbulence. For large particles falling at terminal velocity the first term will be dominant and source term will thus be able to reproduce the large augmentation which has been observed.

3.5. Simple closures to test the new source term

The suggested equation for the turbulence kinetic energy budget for particle-laden flows now appear:

$$\rho\frac{\partial k}{\partial t}+\rho\bar{u}_j\frac{\partial k}{\partial x_i}=\frac{\partial}{\partial x_i}\left(\mu+\frac{\mu_t}{\sigma_k}\frac{\partial k}{\partial x_i}\right)-\rho\overline{u_i'u_j'}\frac{\partial \bar{u}_i}{\partial x_j}+\frac{\alpha\rho_p}{\tau_p}\left(|\bar{u}_i-\bar{u}_{pi}|^2+\overline{u_{pi}'u_{pi}'}-2k\right)-\rho\varepsilon \tag{14}$$

When this equation is applied to the thought experiment by Crowe (2000), where particles are artificially fixed in position in an otherwise steady and uniform flow,[2] Eq. (14) is reduced to the following: (See Fig. 2)

$$\frac{\alpha\rho_p}{\tau_p}\left(|\bar{u}_i|^2-2k\right)-\rho\varepsilon=0 \tag{15}$$

[2] A flow with no spatial or temporal gradients in the averaged properties. This represents an ideal case which can be used to compare models.

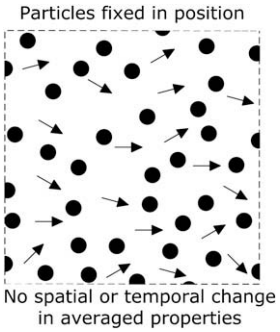

Fig. 2. Schematic of the artificial flow where particles are fixed in position developed by Crowe (2000) for test of turbulence modulation models.

which states that the turbulence produced by the particles is dissipated by the combined dissipative effect of the particles and viscosity. Thus the modeled source term is consistent in the way that it provides a plausible closure for this idealized flow.

Another simple closure for the turbulence modulation at the centerline of a pipe also presented by Crowe (2000) may also serve to evaluate this new term. When applied to the case of a fully developed dilute particle-laden flow in a vertical pipe, for which experimental data is available, Eq. (14) for the flow near the pipe centerline is reduced to:

$$-\rho\overline{u_i'u_j'}\frac{\partial \bar{u}_i}{\partial x_j}+\frac{\alpha\rho_p}{\tau_p}\left(|\bar{u}_i-\bar{u}_{pi}|^2-2k\right)-\rho\varepsilon=0 \tag{16}$$

Here it has been assumed that the particle kinetic energy is negligible at the centerline of the pipe. This assumption is addressed later in the paper. Using the closure scheme provided by Crowe (2000) where the terminal velocity $g\tau_V/f$ is used for the velocity difference, Eq. (16) reduces to:

$$\rho\frac{k_0^{3/2}}{l_e}+\frac{\alpha\rho_p f}{\tau_V}\left(\left(\frac{g\tau_V}{f}\right)^2-2k\right)-\rho\frac{k^{3/2}}{l_e}=0 \tag{17}$$

where respectively, k and k_0 are the turbulent kinetic energy of the clear flow and particle-laden flow and l_e is the integral length scale. Notice that unlike the work by Crowe (2000) it is not necessary to resort to a "hybrid" length scale. Without using the hybrid length scale in the closure scheme the model suggested by Crowe (2000) is only able to predict augmentation. However, the use of the hybrid length scale produces obviously erroneous results for low particle volume fractions. Here, the following supporting equations are used:

$$\begin{aligned} &f^{5/2}=0.058\tfrac{g\tau_V d_p\rho}{\mu}, && \tau_V=\tfrac{\rho_p d_p^2}{18\mu}\\ &\alpha=\left(\tfrac{\rho}{\rho_p}\right)C, \quad k_0=\tfrac{3}{2}(\bar{u}\sigma_0)^2, && k=\tfrac{3}{2}(\bar{u}\sigma)^2 \end{aligned} \tag{18}$$

where respectively, σ and σ_0 is the turbulence intensity of the clear and particle-laden flow. The correlation for f is an approximation which is valid for particles traveling at terminal velocity (Crowe, 2000). The fractional change of the turbulence intensity for a pipe flow with mean velocity of 10 m/s laden with glass particles in a 40 mm pipe and a particle free turbulence intensity of 0.06, have been solved using an iterative procedure. The turbulence length scale at the center of the pipe is set at $l_e = 4$ mm (Hutchinson et al., 1971). The particle size has been varied for particle mass concentrations of 0.1, 1 and 5 producing the curves seen in Fig. 3.

Similar to the model by Crowe (2000) the curves show the same trends as the experimental measurements. Furthermore, this model also predicts the correct behavior when approaching the one-way coupling regime.

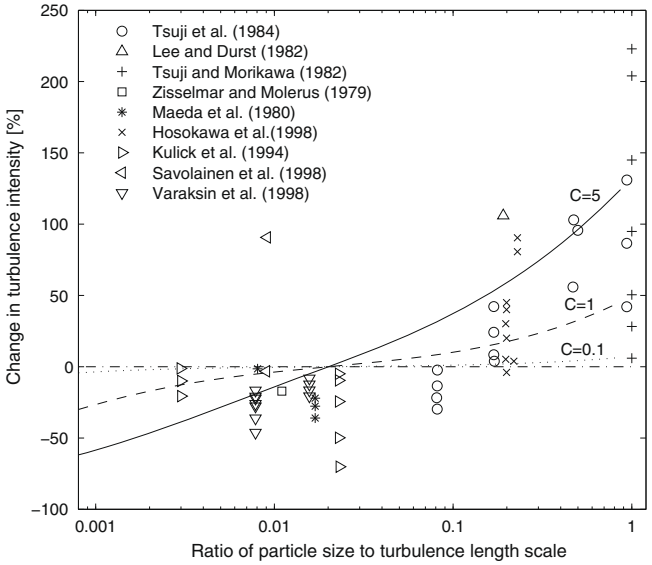

Fig. 3. Comparison of model prediction and data for the turbulence modulation at the centerline of a vertical pipe.

Making the pipe in the model smaller will generally move the curves towards the right on the x-axis while using a larger pipe will move them to the left. Using relative velocities other than the terminal velocity can similar dramatically change the prediction due to the sensitivity of the source term. In this closure scheme only the effect on the k-equation is considered whereas it is known that the effect of the momentum coupling tend to decrease the turbulence intensity further. Finally, the double correlation of the particles fluctuating velocity, which is neglected here, becomes important for dense flows in particular but also for wall bounded flows (Vreman, 2007).

The three models evaluated in this paper have been applied on the same simple closure scheme as presented above. Table 2 summarizes the source terms used in the evaluation of the different approaches. Note that some terms have been neglected for simplicity.

Table 2
Source terms evaluated in present investigation.

Standard:	$S_{kp} = \frac{\alpha\rho_p}{\tau_p}\left(2k\frac{\tau^*}{\tau^*+\tau_p} - 2k\right)$
Consistent:	$S_{kp} = \frac{\alpha\rho_p}{\tau_p}\lvert\bar{u}_i - \bar{u}_{pi}\rvert^2$
New:	$S_{kp} = \frac{\alpha\rho_p}{\tau_p}\left(\lvert\bar{u}_i - \bar{u}_{pi}\rvert^2 - 2k\right)$

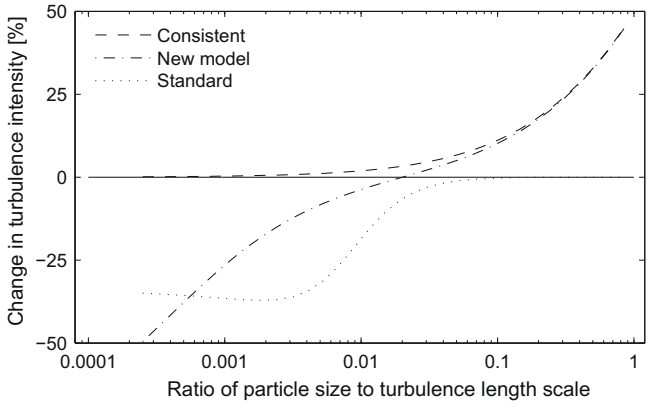

Fig. 4. Comparison of the consistent, the new model and the standard model evaluated at $C = 1$.

Fig. 4 shows the result for the same 40 mm pipe where the particle size is varied between 10 and 4000 μm with unity loading. It can be seen that the consistent model is only able to predict augmentation whereas the standard model, here represented by the model by Lightstone and Hodgson (2004) is only able to predict attenuation.

The new model, which essentially is a hybrid between the standard and consistent approach, is able to predict both augmentation and attenuation. For very large particle sizes the particle-eddy interaction mechanism diminishes and the evaluation of the consistent and the new model becomes the same while the standard model predicts zero turbulence modulation. For small particles the consistent approach predicts zero modulation whereas both the standard and new model predicts significant attenuation.

4. Results

On the basis of the preliminary evaluation of the new source term based on simple closure schemes, three cases have been chosen to evaluate the performance of the new source term in the k–ε framework. Case 1 consists of the largest particles where significant augmentation is expected while Case 3 comprises small particles where attenuation is expected. Case 2 encompass "medium" sized particles which have a d_p/l_e ratio close to the criterion defined by Gore and Crowe (1989) which marks the boundary between attenuation and augmentation and thus very little modification of the carrier phase is to be expected. Cases 1 and 2 is taken from the experimental study by Tsuji et al. (1984) while case 3 is taken from Kulick et al. (1994). Both studies deals with the air-particle flow in a vertical pipe, where Laser Doppler Velocimetry has been used to measure the carrier phase velocity in the axial direction. Experimental results are available for a range of different pipe Reynolds numbers, particle mass loadings and particle diameters. The details of the experimental settings are shown in Table 3.

Besides the differences in flow rate, pipe diameter and particle materials it should be noted that the study Tsuji et al. is an upward flow whereas the study by Kulick et al. is a downward flow. Results for all cases are given at 5 m from the inlet where the flow can be considered to be fully developed. Polystyrene (cases 1&2) and copper (case 3) particles are used which yields a density ratio of around or above 1/1000.

According to the guidelines provided in (Sommerfeld et al., 2007) the influence of added mass, Basset history force and pressure gradient is negligible for the motion of the particles. Only loadings for which the flow can be considered as dilute (Elghobashi, 1994) are used and particle collisions can thus be neglected. The pipe used in the experiments were made of glass; thus the pipe wall can be considered as being smooth and particle-wall collisions are assumed to be perfectly elastic for the no slip wall boundary. The calculations have been performed on a two dimensional axisymmetric mesh discretised with 20×800 (case 1 and 2) and 30×800 (case 3) control volumes in the radial and axial directions

Table 3
Test cases.

	Case 1	Case 2	Case 3
d_p (μm)	1420	243	70
ρ (kg/m^3)	1030	1020	8800
Loading	0.6	0.5	0.4
D_{pipe} (mm)	30.5	30.5	40.0
$u_{c,centerline}$ (m/s)	13.4	13.4	10.5
u_{mean} (m/s)	11.26	11.26	8.85
$\dot{m}_p$ (kg/s)	0.00605	0.00504	0.00545
d_p/l_e *	0.47	0.08	0.02

* Evaluated at centerline: $l_e = 0.1D$.

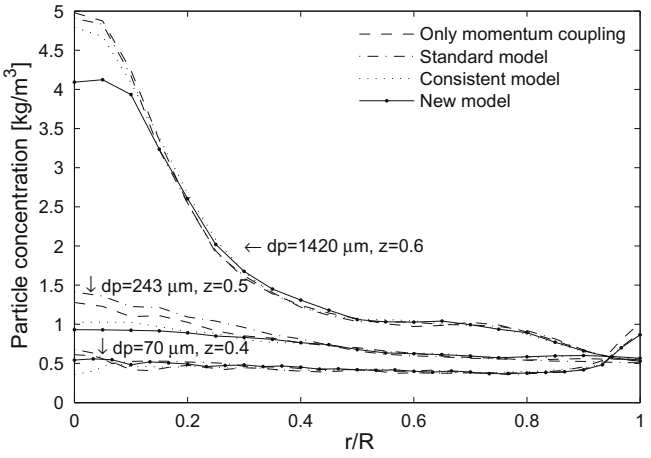

Fig. 5. Concentration profiles of the three different cases for the three models and simulations with only momentum coupling.

respectively. This mesh has been proven to produce grid independent results. At the inlet a top hat velocity profile has been specified and the initial velocities for the particles are set equal to the gas phase. A total of 25,000 particle trajectories have been simulated to provide statistically independent results. At the pipe exit zero gauge pressure has been specified across the entire boundary and the particles are allowed to escape.

Fig. 5 shows the concentration profiles for the three cases and the different models considered.

It can be seen that the largest particles are concentrated towards the center of the pipe whereas the concentration profile for the smallest particles is mostly evenly distributed except close to the wall where particles have accumulated. Since the source terms for all models considered is proportional to the particle concentration it can be concluded that for large particles the numerical values of the source terms are several magnitudes larger at the pipe center than in the near wall region. For cases 1 and 2 there is a clear coupling between the source term formulation and the particle concentration whereas for the smallest particles a flat particle concentration profile can be assumed for all source terms.

Fig. 6 comprises the results from the different models for case 1 and also shows the measurements by Tsuji et al. (1984) for this case. For the mean velocity all models tend to flatten the velocity profile slightly. This effect is most pronounced for the new model and for the model by Lightstone and Hodgson (2004). This effect is however difficult to perceive in the experimental data where the difference between the clear flow and particle-laden profiles are minimal. Furthermore it can be noticed that it is not possible to reproduce the clear flow velocity profile exactly, a problem which also can be found in other investigations dealing with the numerical simulation of this case (Lain and Sommerfeld, 2003; Yan et al., 2007). For the fluctuating velocity component the model by Lightstone and Hodgson and the simulation using momentum coupling only predict an attenuation of the flow while both the new model and the model by Lain and Sommerfeld predicts augmentation of the turbulence. It can be noticed at the new model performs slightly better than the model by Lain and Sommerfeld. Again it should be noted that it is not possible to predict the exact same clear flow profile as measured by Tsuji et al. This is to a part due to the Boussinesq approximation, fundamental to the k–ε model, which treats the turbulence as being isotropic. Thus the fluctuating velocity u' is calculated as $\sqrt{\frac{2}{3}k}$.

Fig. 7 comprises the results of the numerical simulations and the measurements by Tsuji et al. (1984) for case 2. For all the tested models the mean velocity profiles for this case is almost indistinguishable from the clear flow profile whereas for the measurements the particle-laden profile is somewhat flatter than the clear flow profile and similarly the measurements of the fluctuating velocity component is dampened compared to the clear flow profile. The prediction for the standard approach as well as the prediction with the momentum source term only display the same

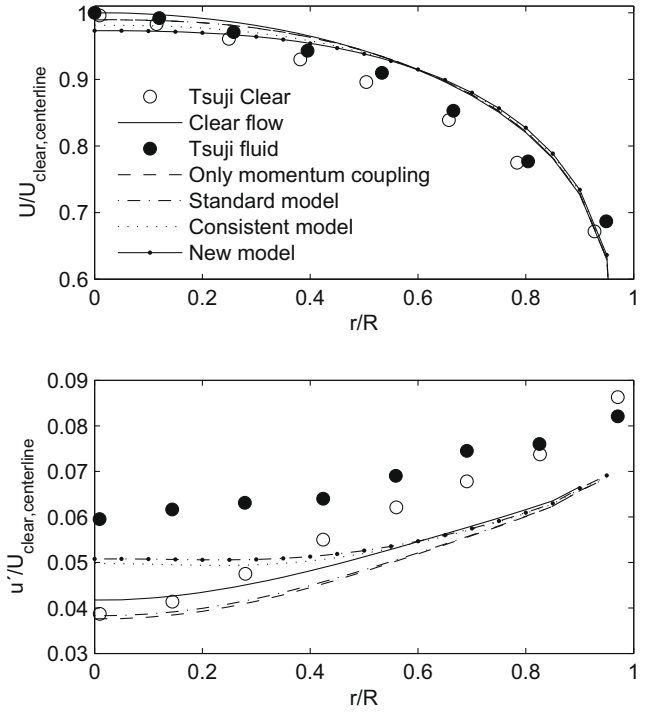

Fig. 6. Non-dimensional radial profiles of the axial mean and fluctuating velocity components for case 1: dp = 1420 μm, z = 0.6, $U_{clear,centerline}$ = 13.4 m/s.

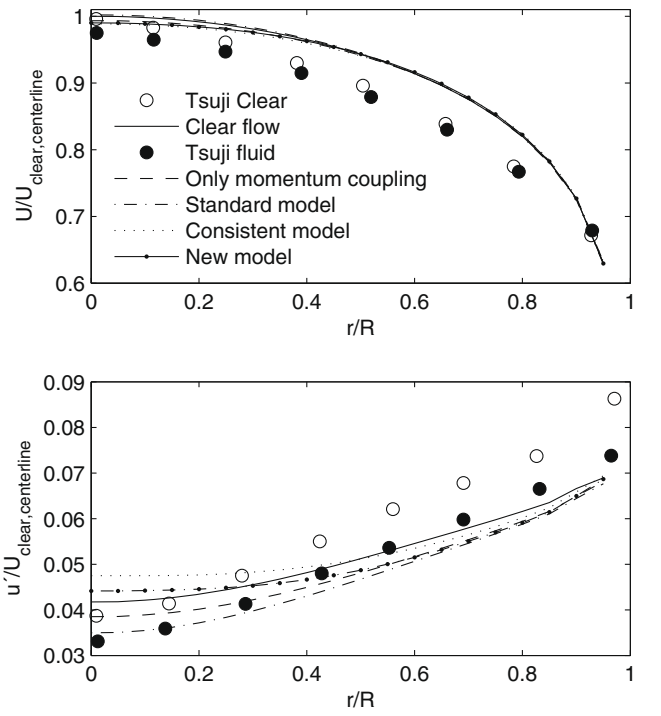

Fig. 7. Non-dimensional radial profiles of the axial mean and fluctuating velocity components for case 2: dp = 243 μm, z = 0.5, $U_{clear,centerline}$ = 13.4 m/s.

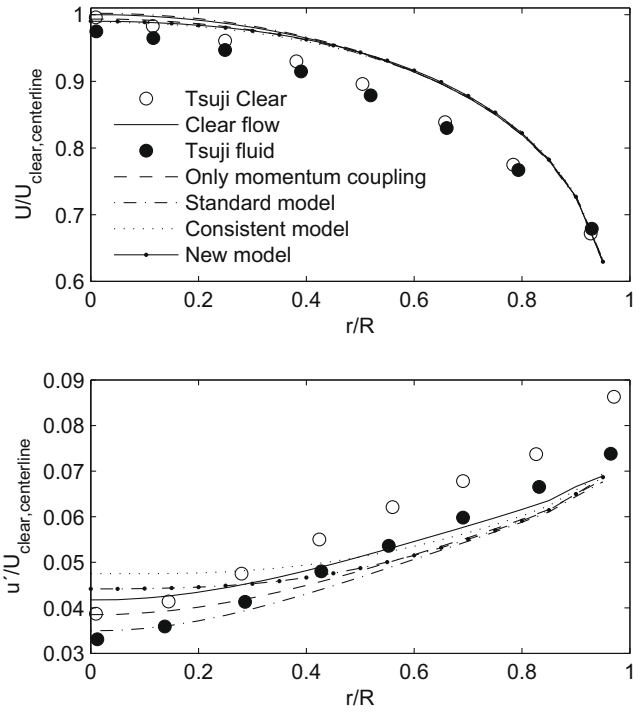

Fig. 8. Non-dimensional radial profiles of the axial mean and fluctuating velocity components for case 3: $dp = 70$ μm, $z = 0.4$, $U_{clear,centerline} = 10.5$ m/s. For the mean velocity profile the experimental results by Kulick et al. (1994) for the clear flow is indistinguishable from the particle-laden flow.

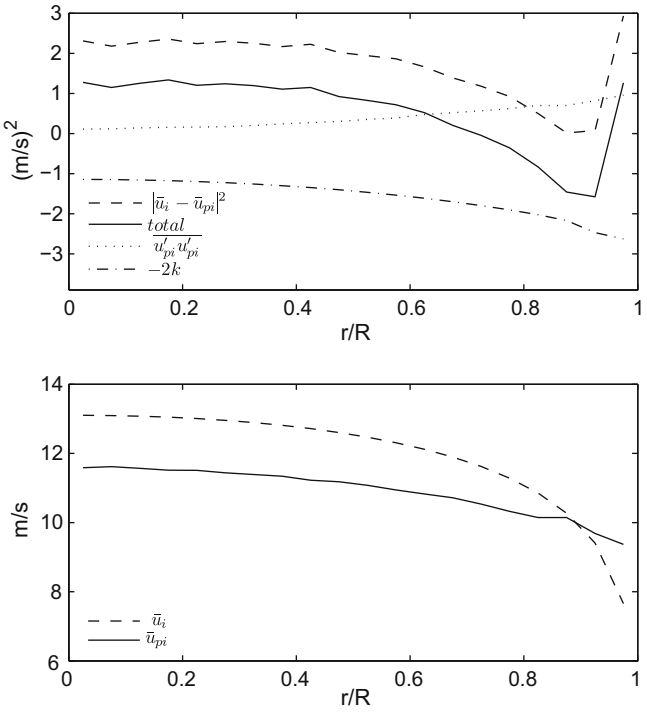

Fig. 9. Evaluation of the different terms in the new model and mean flow velocity profiles for case 2.

trend as the measurements whereas the new model and the consistent approach predicts an augmentation of the carrier phase. For this case the standard approach provides the best approximation to the experimental data at the centerline. It can be noticed that the new model performs better then the consistent approach and the model predicts only a relative small change at the centerline which can be expected on basis of the d_p/l_e ratio.

Fig. 8 comprises the results of the numerical simulation for case 3 which is compared to the experimental results by Kulick et al. (1994). The measurement of the mean velocity profile for the clear flow is indistinguishable from that of the particle-laden flow. For the prediction of the mean velocity profile there is similarly hardly any difference between the clear flow and the prediction by the different models. For the fluctuating flow all models now predicts attenuation of the carrier phase at the centerline. For this case the relative velocity which play an essential role in predicting the augmentation caused by larger particles is relatively small and thus for the consistent model only the effect by the momentum coupling is causing the attenuation. For the new model and the standard model additional terms exists which caused the prediction to become less than that caused by the momentum coupling alone.

Fig. 9 shows an evaluation of the different terms in the new model for case 2. It can be seen that both attenuation and augmentation present at different regions of the flow. The relative velocity approaches zero in a region of the flow since the mean particle velocity is more uniform than the mean fluid velocity. In the region where the relative velocity is small there is significant attenuation of the fluid turbulence. Close to the wall the relative velocity increases rapidly and thus there is significant augmentation in the near wall also for small and heavy particles. At the center of the pipe the square of the relative velocity is larger then the twice the turbulent kinetic energy and the resultant evaluation of the entire source term is thus positive. At the centerline $\overline{u'_{pi}u'_{pi}}$ is an order of magnitude smaller than the other terms and can be neglected. However, this term increases in magnitude closer to the wall due to the particle-wall collisions and always acts as a source. Furthermore, it can be realized the often used assumption where the relative velocity is approximated by the terminal velocity is only valid in the center of the pipe.

5. Discussion and conclusion

In this paper, the performance of a new Lagrangian formulation for the source terms to the turbulence equations has been evaluated and compared with results obtained with the so-called standard and consistent approach as well as with experimental measurements. Previous attempts to model the entire range of turbulence modulation experiments have been only partially successful and suffered from relying on semi-heuristic/empirical formulation which is not consistent with the governing equations of fluid flow. Up to now only the standard and the consistent approach is derived directly from the governing equations for particle-laden flow. The standard approach is only able to predict attenuation whereas the consistent approach only contains mechanisms which enhance the turbulence. The new model relies on a new derivation, consistent with the balance equations, to formulate terms which contains mechanisms for both the suppression and enhancement of turbulence and the new model can be seen as a combination of the standard and the consistent terms. Furthermore, no additional modeling is necessary for the new model since particle and fluid kinetic energy is given explicitly. The performance of the new model surpass that of both the standard and the consistent model for the present range of investigations, however before a stronger conclusion may be stated it is necessary to test this model on other flow situations and for other closure schemes such as the Reynolds Stress Model.

Acknowledgement

This work was supported by Energinet.dk, under Grant PSO 2006 1 6364.

References

Boulet, P., Moissette, S., 2002. Influence of the particle-turbulence modulation modelling in the simulation of a non-isothermal gas–solid flow. International Journal of Heat and Mass Transfer 45 (20), 4201–4216.

Chen, P.E., Wood, C.E., 1985. A turbulence closure model for dilute gas-particle flows. Canadian Journal of Chemical Engineering 63, 349–360.

Crowe, C.T., 2000. On models for turbulence modulation in fluid-particle flows. International Journal of Multiphase Flow 26 (5), 719–727.

Crowe, C.T., Sharma, M.P., Stock, D.E., 1977. Particle-source in cell (Psi-Cell) model for gas-droplet flows. Journal of Fluids Engineering – Transactions of the ASME 99 (2), 325–332.

Elghobashi, S., 1994. On predicting particle-laden turbulent flows. Applied Scientific Research 52 (4), 309–329.

Fluent Inc. 2006, Fluent 6.3 User's Guide.

Gore, R.A., Crowe, C.T., 1989. Effect of particle-size on modulating turbulent intensity. International Journal of Multiphase Flow 15 (2), 279–285.

Gouesbet, G., Berlemont, A., 1999. Eulerian and Lagrangian approaches for predicting the behaviour of discrete particles in turbulent flows. Progress in Energy and Combustion Science 25 (2), 133–159.

Hutchinson, P., Hewitt, G.F., Dukler, A.E., 1971. Deposition of liquid or solid dispersions from turbulent gas stream – stochastic model. Chemical Engineering Science 26 (3), 419.

Kenning, V.M., 1996. Self-induced turbulence in solid-liquid flow, Ph.D. Thesis, Washington State University.

Kenning, V.M., Crowe, C.T., 1997. On the effect of particles on carrier phase turbulence in gas-particle flows. International Journal of Multiphase Flow 23 (2), 403–408.

Kulick, J.D., Fessler, J.R., Eaton, J.K., 1994. Particle response and turbulence modification in fully-developed channel flow. Journal of Fluid Mechanics 277, 109–134.

Lain, S., Sommerfeld, M., 2003. Turbulence modulation in dispersed two-phase flow laden with solids from a Lagrangian perspective. International Journal of Heat and Fluid Flow 24 (4), 616–625.

Lightstone, M.F., Hodgson, S.M., 2004. Turbulence modulation in gas-particle flows: a comparison of selected models. Canadian Journal of Chemical Engineering 82 (2), 209–219.

Sommerfeld, M., van Wachem, B., Oliemans, R. (Eds.), 2007, Best Practice Guidelines – on Computational Multiphase Dynamics for Turbulent Dispersed Multiphase Flows, Version 16-oct-07 edn, ERCOFTAC Special Interest Group on Dispersed Turbulent Multi-Phase Flow.

Squires, K.D., Eaton, J.K. 1992. On the modelling of particle-laden turbulent flows, In: Proceedings of the 6th Workshop on Two-phase Flow Predictions.

Tsuji, Y., Morikawa, Y., Shiomi, H., 1984. LDV measurements of an air solid 2-phase flow in a vertical pipe. Journal of Fluid Mechanics 139 (FEB), 417–434.

Vreman, A.W., 2007. Turbulence characteristics of particle-laden pipe flow. Journal of Fluid Mechanics 584, 235–279.

Yan, F., Lightstone, M.F., Wood, P.E., 2007. Numerical study on turbulence modulation in gas-particle flows. Heat and Mass Transfer 43, 243–253.

Yarin, L.P., Hetsroni, G., 1994. Turbulence intensity in dilute 2-phase flows 3. The particles-turbulence interaction in dilute 2-phase flow. International Journal of Multiphase Flow 20 (1), 27–44.

Yuan, Z., Michaelides, E.E., 1992. Turbulence modulation in particulate flows – a theoretical approach. International Journal of Multiphase Flow 18 (5), 779–785.

6th International Conference on Multiphase Flow,
ICMF 2007, Leipzig, Germany, July 9 – 13, 2007

On the modelling of motion of non-spherical particles in two-phase flow

Matthias Mandø, Chungen Yin, Henrik Sørensen and Lasse Rosendahl

Aalborg University, Institute of Energy Technology
Pontoppidanstræde 101, DK-9220, Aalborg East, Denmark
mma@iet.aau.dk

Keywords: Non-spherical particles, particle-fluid interaction, numerical modelling, turbulence modulation, turbulent dispersion, Lagrangian modelling, Eulerian modelling

Abstract

This review paper is concerned with the current status of the understanding of the motion of non-spherical or irregular particles. Most work up to date dealing with particle-fluid interaction has been limited to rigid spherical particles due to the obvious distinct advantages in both numerical and experimental studies. However, for most industrial applications particles encountered are irregular or non-spherical and often with large aspect ratios. Commonly the use of equivalent diameters and shape factors are used to describe the flight of non-spherical particles. For multi-parameter descriptions, where also the orientation is taken into account, most work is only concerns slow viscous flow where an analytical solution exists. The work done on turbulence modulation by non-spherical particles is scarce and only fundamental aspects are discussed. Finally this work ends with giving suggestions for where further work is needed to advance the knowledge in the field of non-spherical particles.

Introduction

This paper deals with the different approaches to modeling of fluid flow with the presence of a dispersed phase in the form of non-spherical particles. Most commercial Computational Fluid Dynamics (CFD) codes used in the industrial sector for the simulation and prediction of particle behavior in fluid flows rely on methods developed for spherical particles. However, the vast majority of these flows encompass non-spherical particles which often have large aspect ratios. Examples of these flows are many and often specific problems and thereby specific approaches to their solution are associated with each case. Much work on non-spherical particles originates in the paper and pulp industry which deals with the transport of fibers in a liquid solution. This can be generalized as the transport of non-spherical particles with a regular shape and with high aspect ratio. In this category also the flow of disc-shaped blood cells in veins and transport of certain food products can be found. Another case is that of the pneumatic transport of powders, typically grinded or crushed materials with a crystalline origin where the shape of the particles tend to be highly irregular and angular. The major problems in both cases seem to be the prevention of clogs and prediction of pressure loss. Another problem arises from the toner and printing industry where the assessment of quality is directly related to the eccentricity of the toner or ink particles. As the particles are released from the printer head it is observed that the spread of the particles is increased as a function of the deviation from the perfect sphere. This also suggests that non-spherical particles, even with very little eccentricity, are associated with increased dispersion. Complex non-spherical particles which represent the extreme with respect to the surface area to volume ratio such as straw, snow flakes, black liquor particles or agglomerates gives rise to motion which seemingly is almost impossible to predict.

The most common assumption applied in the modeling of particles, regardless of condition, is that of spherical shape. This greatly simplifies the problem and for many cases results in models which are adequate to described experimentally observed phenomenon. Take the simulation of coal combustion in industrial furnaces as it is typically modeled as an example. Coal is ground in a mill prior to combustion to produce particles with a mean diameter[1] of 30 μm and 92 % of particles under 100 μm (Ye et al. 2004). The particles manufactured by the grinding process produce distinctly non-spherical particles due to the crystalline origin of particles. However, coal particles are almost always modeled as zero volume spheres, retaining only the inertial and drag term in the equation of motion and by applying a typical approach for turbulent dispersion, such as the eddy life-time model. Although major assumptions thereby are taken results are deemed to be adequate (considering the knowledge on the field). This approach can be seen as a consequence of insufficient computational resources which in times past have dictated the development of fast codes with limited accuracy. The prediction of the particle paths in industrial furnaces is as such limited by the accuracy of the turbulence and dispersion model used and the effects of the non-spherical shape is included in the

[1] The diameter refers to the mesh diameter and the mean is evaluated on a mass basis.

fitting of parameters in the turbulence model or simply ignored. It is well known that a sphere represents the extreme with respect to the volume-to-surface-area ratio, which impacts the motion of a particle. The particle shape will have a significant effect on the particle-fluid interaction and the dispersion and turbulence modulation characteristics for non-spherical particles may be significantly different than for spherical particles. Considering this, one may think that the current standard for modeling of industrial furnaces may be deemed sufficient only for small, heavy near-spherical particles and only when the need for greater accuracy emerges may we pursue the accurate modeling of non-spherical particles.

However, already in today's world, coal is sought to be exchanged with biomass which poses new modeling challenges. Topics such as CO_2-quotas, renewable energy and independence of foreign resources are dominating the political agenda and the combustion of biomass of straw and wood are gaining a higher priority. However, biomass particles are generally much bigger than coal particles and have much larger aspect ratios. Yes, it is possible to grind the biomass particles down to particle sizes similar to that of pulverized coal but this induces excessive wear and tear on the mills since biomass particles are not crystalline in nature. Hence the combustion of biomass particles in suspension fired boilers uses particles with sizes up to several millimeters (Ye et al. 2004). The motion of such large non-spherical particles cannot be modeled adequately using the current methods.

Characterization of non-spherical particles

The range of non-spherical particles encompasses a large number of mathematically describable shapes (ex. cubes, ellipsoids, tetrahedral), which commonly is referred to as regular shapes. Similarly, shapes that are not possible to describe exactly using mathematical terms are referred to as irregular particles. These thus encompass shapes with a) a well defined geometry such as agricultural related shapes such as grain, straw, wood chips, b.) Shapes with a random like geometry such as pulverized or crushed substances and c.) complex shapes such as agglomerates, rigid black liquor droplets or shell like structures.

Table 1: Commonly used particle shape terminology. [a](Black et al, 1996), [b](Clift, Grace and Weber, 2005), [c](Christensen & Barker, 1965)

Acigular[a]	needle-shaped
Angular[a]	sharp-edged
Crystaline[a]	freely developed geometric shape
Dentritic[a]	a branched crystalline shape
Fibrous[a]	thread-like
Flake-like[a,c]	flat shape
Granular[a]	equidimensional irregular shape
Irregular[a]	lacking any symmetry
Modular[a]	rounded, irregular shape
Spherical[a]	global in shape
Axisymetric[b]	revolution bodies
Orthotropic[b]	plane of symmetry
Spherically isotropic[b]	regular polyhedral
Near-spherical[c]	equidimensional irregular shape
Cylinder-like[c]	one dominating dimension

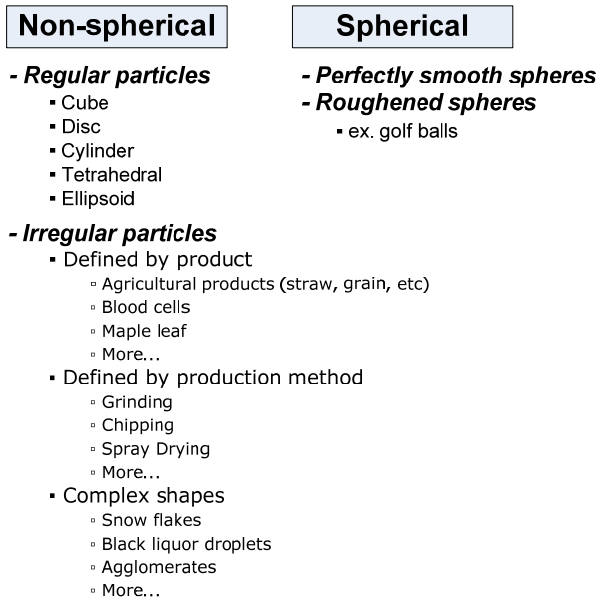

Figure 1: Categorization of non-spherical particles.

Generally a lot of descriptive terms have been used to describe non-spherical particles as can be seen in table 1.

It seems impossible to categories all possible shapes using expressions relating to features of the particle in question simply because the possible variations are limitless. A more feasible way to categorize the different non-spherical particles is to express them either by product or production method as seen in figure 1.

This method focuses on the origin of the particles and does not describe the shape of a single particle but a range of shapes which is found together.

Similarly to the categorization of the shape of particles a number of ways have been defined to quantify the size of particles. Common for most of these definitions is the use of equivalent diameters. The reader is referred to general textbooks such as Allen (1981) for a thorough guide into particle sizing techniques. For this work it is sufficient to state the size definition often associated with CFD modeling of non-spherical particles, namely the volume equivalent diameter, d_{eq}, defined as the diameter of a sphere having the same volume as the particle. Generally the expressions for the different diameter definitions come from specific techniques such as microscopic analysis, sedimentation analysis, laser based methods similar to the origin of the shape descriptions (Black et al, 1996).

Table 2: Commonly used shape factors (Wadell, 1934).

Corey shape factor	Ratio of the smallest principle length axis of the particle to the square root of the intermediate and longest principle length axis
Roundness	Ratio of the average radius of curvature of the corners to the radius of the largest inscribed circle
Sphericity	Ratio between the surface of a sphere with the same volume as the particle and the surface area of the actual particle

The largest problem today comes from the lack of finding an adequate way to describe particles. Smooth spherical particles and regular particles can be described unambiguously in mathematical terms whereas irregular particles defy exact definition. For irregular particles the geometry is to complex to quantify in exact mathematical terms and these shapes are usually dealt with by means of size and shape factors (Kaspers, 1982). To overcome this problem effort has been directed towards finding a single shape factor to describe all possible shapes. Commonly used definitions of shape factors, which can be used on an arbitrary geometry, are listed in Table 2. The most widely used of these is that of the sphericity originally suggested by Wadell (1934). The test for which shape factors are to be evaluated is their correlation of the terminal velocity for various shapes. It is well known that the terminal velocity and the related drag coefficient are strongly influenced by the shape and orientation of a particle as well as it size, density and the fluid properties. It has been proven that the terminal velocity correlates poorly with the sphericity (Clift, Grace and Weber, 2005). In the review of different expressions of the drag coefficient for non-spherical shapes by Chhabra et al (1999), where a large number of experimental data is considered, maximum errors for all correlations exceed 100 % and the best average error is reported to be 16.3 %. It is further commented, as a concluding remark, that improvement in drag predictions only can be accomplished by introducing additional parameters to describe the shape. Generally it suggested to only use such correlations for shapes with a sphericity approaching unity, which would correspond to a near spherical shape (Clift, Grace and Weber 2005), (Curtis & van Wachem, 2004). As it is evident from the investigation by McKay et al (1988) a cylinder and a disc with the same sphericity will have distinctly different terminal velocity, suggesting that an additional parameter for particle shape should contain reflections over the ratio of the different dimensions of the particle. Another problem using the sphericity approach is the difficulties measuring it accurately for irregular particles. Quantification using the sphericity, ψ, requires knowledge of the particles surface area and volume; quantities which is not easily obtained for irregular particles. Often the sphericity is approximated using either information of the volume of the particle and its longest dimension or using information of the linear dimensions of the particle:

$$\psi \approx \sqrt[3]{\frac{V_p}{V_s}} \approx \sqrt[3]{\frac{L \cdot I \cdot S}{L^3}} \qquad (1)$$

The volume of the particle, V_p, can then be found by immersion of the grain in fluid and the volume of the circumscribing sphere, V_s, is found using the longest dimension as diameter. By measuring three dimensions of the particle: the longest, L, the intermediate, I, and the smallest, S, an estimate of the sphericity is made. Calculation of the exact sphericity is only possible by considering regular particles only or by using advanced 3D imaging techniques to reconstruct the shape of irregular particles.

For particles which deviate significantly from the spherical ideal it has been proposed that shapes are classified according to the largest and smallest dimensions (Christensen & Barker, 1965). It is suggested that if the ratio of the maximum length to the minimum length is below 1.7 the particle should be treated as isotropic and correlations of the sphericity could be used. For values above 1.7 the shape is classified either as rod-like, which can be approximated with a cylinder or a prolate spheroid, or flake-like, which can be approximated with that of a disc or an oblate spheroid.

Motion of particles

According to Clift, Grace and Weber (2005) a cylinder under free fall with length/diameter ratio above 1.7 will align it self with the axis parallel to the flow for moderate Reynolds numbers; $0.01<Re<100$ (Re based on the diameter of the cylinder). The upper bound seems to depend on the density and the length/diameter ratio of the particle. In this range of Reynolds numbers it is appropriate to use correlations of the drag coefficient for cylinders in cross flow. This case is probably the most investigated and the experimental data are within ±6% of the best correlations (White, 1991). For values of Re above the order of 100 a cylinder will experience secondary oscillatory motion and depending on the particle density and the fluid properties also rotation around a vertical axis. Drag coefficients are available for this range of Reynolds numbers but are generally associated with a higher uncertainty due to the seemingly chaotic nature of this secondary motion. Similarly the trajectory is also affected by this secondary motion as the cylinder will "side-step" due to the lift forces acting on the particle when its axis is not horizontal.

Referring to the discussion given in Clift, Grace and Weber (2005) and in the paper by Field et al. (1997) a disc in free fall will similarly to a cylinder experience steady motion with its plane normal to the flow for Reynolds numbers between $0.1<Re<100$ (Re based on the diameter of the disc). The drag coefficient will be similar to that of a fixed disc and drag correlations derived from this case can be used. For higher Re the secondary motion has been shown to depend on the dimensionless moment of inertia:

$$I^* = \frac{\pi \rho_p}{64 \rho} \frac{\delta}{d} \qquad (2)$$

where δ/d is the thickness to diameter ratio. Three types of secondary motion can be distinguished: Oscillatory motion, glide-tumble or chaotic motion and tumble motion as seen in figure 2.

As the Reynolds number is increased above the order of 100 the disc will start to oscillate about an axis horizontal to the flow. As the amplitude to the oscillatory motion increases the lift forces acting on the particle will initiate sidewards motion and the particle will move in large curved arcs. This regime is termed glide-tumble[2]. At higher I^* and Re a disc will begin to rotate continuously around its axis and its trajectory will follow an approximately straight line but not

[2] In Field et al. (1997) the glide-tumble regime is referred to as chaotic motion and similarly the oscillatory regime is referred to as periodic motion.

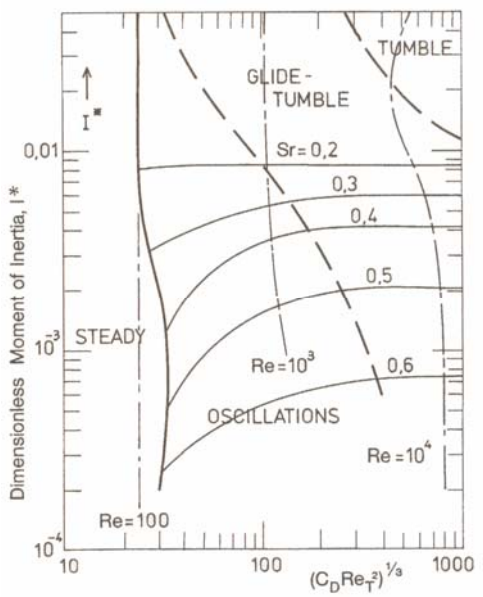

Figure 2: Motion of discs under free fall. Contours of constant Reynolds number Re and Strouhal number Sr are indicated (Clift, Grace and Weber. 2005).

necessary a vertical line. Correlations for the drag coefficient as a function of the Re for different values of *I** have been worked out but similar to the results for the cylinders these are considered less accurate possible due to the floating transition between the different regimes.

Particles of arbitrary shape under free fall in the range 0.1<Re<100 will experience steady motion and tend to orientate themselves so that their maximum cross-section will be normal to the flow. For higher Reynolds numbers the particle will experience secondary motion which strongly depends on the shape. Arbitrary particles under free fall in creeping flow will generally experience a "tumbling" motion where they fall vertical while rotating unless certain symmetry conditions are obeyed. The different regimes of motion may be explained considering an elliptical particle in 2D flow as seen in Figure 3.

A. to D. 0.1<Re<100 In this intermediate range of Reynolds number a steady recirculation zone will form downstream of the particle. Pressure drag becomes increasingly more significant then the friction drag and the distribution of pressure at the surface of the particle will determine its

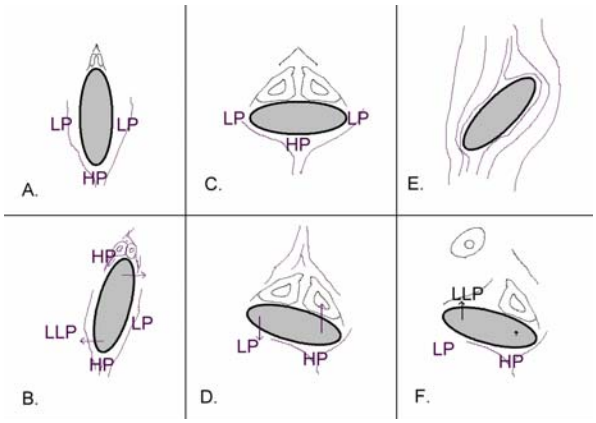

Figure 3: Flow across and orientation of a 2D particle. LP: Low pressure zone, LLP: Lowest low pressure, HP: High pressure.

orientation. A symmetric 2D particle the pressure forces may be in equilibrium for both positions A and C, however only position B is truly stable. Consider a small disturbance which disrupts the equilibrium (B and D); the particle in position A will move away from this quasi-stable equilibrium while a particle in position C will move towards the original equilibrium.

F. 100<Re When the Reynolds number approaches the order of 100 the steady recirculation in the wake of the particle begins to become unstable. First the recirculation zones will oscillate and as the Reynolds number is increased vortex shedding will occur. The pressure distribution on the surface of the particle will still determine the orientation of the particle and the particle will oscillate with the same period as the vortex shedding.

E. Re<0.1 (Stokes flow) For creeping flow no recirculation zone will form and the fluid will stick to the surface of the particle everywhere. The resulting net drag force is not parallel with the flow and the particle will rotate accordingly. An axissymmetric and orthopedic particle tend to have a preferred direction in Stokes flow and will eventually fall with its longest dimension parallel to the flow. This is not necessarily the case for an arbitrary irregular particle. The friction drag will tend to slow down any initial rotation for all shapes, but for very low Reynolds numbers rotation may be retained for a long time.

The motion of a solid particle is governed by conservation equations considering both translation and rotation:

$$m_p \frac{d\mathbf{v}_p}{dt} = \sum_i \mathbf{F}_i \qquad (3)$$

$$I_x \frac{d\omega_x}{dt} = \sum T_{x,i} + \omega_y \omega_z \left(I_y - I_z\right) \qquad (4)$$

$$I_y \frac{d\omega_y}{dt} = \sum T_{y,i} + \omega_z \omega_x \left(I_z - I_x\right) \qquad (5)$$

$$I_z \frac{d\omega_z}{dt} = \sum T_{z,i} + \omega_x \omega_y \left(I_x - I_y\right) \qquad (6)$$

Where T_i is torques, ω_i is angular velocities and I_i is moments of inertia. For a spherical particle only the translation term is retained, and evaluation of the forces acting on the particle yield the well known Basset-Boussinesq-Oseen equation (BBO equation) which is valid for slow viscous flow:

$$\rho_p V_p \frac{d\mathbf{v}}{dt} = \underbrace{6\pi a \mu (\mathbf{u}-\mathbf{v})}_{drag} + \underbrace{V_p (\rho_p - \rho_f)\mathbf{g}}_{gravity} + \underbrace{\rho_f V_p \frac{d\mathbf{u}}{dt}}_{pressure\ gradient} + \underbrace{\tfrac{1}{2}\rho_f V_p \frac{d}{dt}(\mathbf{u}-\mathbf{v})}_{virtual\ mass} \underbrace{-6\pi a^2 \mu \int_0^t \left(\frac{(d/d\tau)(\mathbf{u}-\mathbf{v})}{\left(\pi\mu(t-\tau)/\rho_f\right)^{1/2}} \right) d\tau}_{Basset\ history\ term} \qquad (7)$$

This equation also constitutes the foundation for attempts to describe the motion of spheres at higher Reynolds numbers and attempts to describe the translational motion of non-spherical particles. In the derivation of the equation of motion of small particles in non-uniform flow, Maxey & Riley (1983) showed that additional terms appear due to the non-uniformity; extra terms in the Basset and virtual mass force together with the Faxen force.

The problem arises when it is sought to apply these equation on arbitrary shapes where the lack of an exact mathematical definition necessitates the use of approximations regarding the shape. Even when dealing with regular shapes the formulation of governing equations are associated with difficulties. The terms in the BBO equation are only strictly valid for spheres and it is necessary to apply appropriate modifications to the terms or to introduce new correctional terms in the case of non-spherical shape. Furthermore, when non-spherical particles are attempted to be modeled often large particles are involved. Large particles usually bodes the departure from the Stokes regime meaning that the BBO equation is no longer valid.

The usual order-of-magnitude estimates made for small, heavy spheres in the dilute regime indicate that it is only necessary to retain the inertia, the drag and the gravity term (Lazaro and Lasheras 1989). These estimates also apply for non-spherical particles thereby simplifying the modeling effort for solid particles suspended in a gaseous media. The very small particles, which are subjected to Brownian motion, will not adopt any preferred orientation and it is necessary to correct the equation of motion for molecular slip. Particles subjected to carrier phase turbulence seems to adopt preferred orientation in the intermediate range of Reynolds number ($0.1<Re<100$) depending on ratio of the size of the particle and the turbulence length scale (Klett 1995). The general raisonnement is that particles smaller than the turbulent eddies will be completely entrained, while larger particle only feel the turbulence as an induced oscillatory disturbance. In the heuristic model developed by Klett (1995) a great deal of shapes are considered including cylinders, discs and snow crystals (branched plates). For both cylindrical and disc-like shapes the transition between tumbling motion and oscillating motion is at a particle size in the order of 10 μm and transition to steady falling motion at a particle size in the order of 100 μm depending on the magnitude of the turbulence. Generally the increase in the drag coefficient of non-spherical particles compared to perfect spheres decreases the response time and thereby enables them to better respond to the turbulent fluctuations (Black and Mcquay, 2001), (Yow et al. 2005).

While most particles encountered in multiphase flows will fit into the frame of being either flake-like near-spherical or rod-like some specific shapes defies this categorization. Ex a particle which consists of two cylinders fused together (in a “L” or “T” mode) cannot be expected to behave as similar to a rod-like particle since there not a single dominating dimension. Particles which fall in this category can best be classified as being “complex” and correlations of the drag coefficient or/and modification to the equations of motion will have to be made considering each case separately. According to Chhbra et al (1999) correlations using the sphericity yield particularly poor results for complex shapes. Specific cases of complex particles include black liquor droplets, fractals shapes such as snow particles and wheat straw with nodes. In the work by Kankkunen et al (2005) the shape characteristics of black liquor droplets is investigated. The majority of particles are described as being highly non-spherical and that the traditional methods of describing the size and shape of the particles (i.e. the sphericity and aspects ratio) cannot suffice. In this case it is suggested to use an additional shape factor to take into account the tails on the particles. Snow crystals which can be related to hollow particles, highly porous particles, particle with fractal surfaces and agglomerated particles are quick to capture the interest. However, making shape parameters to describe such shapes and to predict the drag coefficient may be at best a tricky affair.

In the investigation by Tang et al (2004) it is suggested to construct fractal-model-objects to mimic complex shapes and then use the information regarding the volume and surface area given by the model objects in correlations of the sphericity to predict the drag on the actual objects. This way it is possible to account for particles with rough surfaces. However, the deficiency of the sphericity has been discussed previously and it is highly unlikely that such an approach would suffice for highly porous particles. Wheat straw without nodes resemble cylinder and the observations considering the motion this type of particles would be adequate for this case also. Adding a node to the particle would not significantly change the shape of the particle but would dramatically alter its orientation characteristics and its trajectory. The wheat straw with nodes is a prime example of particles with a non-uniform density distribution and do not fit into any of the previously defined categories. Bilanski (1965) showed that straws with a node in one end would orient themselves vertically while straw with a node in the middle or no node tend to orientate themselves horizontally. The difference in orientation yields a resistance coefficient which is approximately 25% higher for straws with no node or node in the middle compared to straws with a node at one end.

Modelling using single parameter description

The simplest approach to dealing with non-spherical particles is by assuming a spherical shape. Hereby the full BBO equation for spherical particles can be utilized with out any further modification. By using the evaluation of the drag coefficient as an estimate for the accuracy we see that this is a poor approximation. This is evident by comparing the estimates of the different drag correlation for non-spherical shapes (reviewed by Chhabra et al (1999)) with the standard drag curve for a sphere. Moreover, the study by Comer and Kleinstreuer (1995) reported specifically that the assumption of spherical shape will result in an underestimation of the drag coefficient of up to 30 % for some spheroids.

The simplest improvement to the spherical assumption is to correct drag coefficient according to experimental findings (Shuen et al, 1985). For a specific shape the drag coefficient can be found as a function of the Reynolds number similar to the expressions which exist for a spherical shape. Another approach for dealing with non-spherical particles is by the size and shape factors to describe an equivalent spherical particle. The raisonnement for this approach is that the vast majority of non-spherical particles are irregular in shape and

that it would be a daunting task to come up with correlations that cover the full range of shapes satisfactory.
Using the assumption of a spherical shape or applying corrections to the drag coefficient to describe the motion of an equivalent spherical particle can be considered as shape "lumping". It is possible to use the full equation of motion, the BBO equation, to describe the path of a particle, since the size is described by an equivalent diameter. For a heavy spherical particle in gaseous medium the only term which is important is the drag and inertia term. This conclusion is transferred to the non-spherical case and it requires no further argumentation to also include body forces. For the intermediate range of Reynolds numbers ($0.1<Re<100$) the resulting drag force is parallel to the flow, but at higher Reynolds numbers the non-spherical shape will promote significantly secondary motion, i.e. the glide-tumble regime of discs.
A complete description of the drag coefficient of a non-spherical particle would be described as:

$$C_d = f\left(\mathrm{Re,shape,orientation}\right)$$

The drag coefficient of the 2D particle in Figure 3 is greater when the particle is orientated vertically than horizontally. The drag coefficient of a prolate spheroid (3D equivalent to the 2D particle) may even be smaller than on an equivalent sphere. So to model the drag coefficient exactly it is necessary to derive an expression which takes all possible inclination angles into account for a specific shape and Reynolds number. Furthermore, not only the translation of the particle, equation (3), needs to be modeled but it is also necessary to keep track of its orientation, equations (4) to (6). From an engineering point of view it is more desirable to settle for a less accurate description which in turn is simpler to handle:

$$C_d = f\left(\mathrm{Re,shape}\right)$$

By ignoring the orientation dependency of the particle on the drag coefficient it is not possible to see the effects of secondary motion if only equation (3) is used and if equation (3) – (6) is used the drag is predicted with less accuracy.
An investigation of co-firing of pulverized coal and biomass has been made by Backreedy et al. (2005). Coal is ground to sizes below 100 μm in diameter and form spherical particles during initial devolatilization. Coal particles are therefore modeled as spheres. The biomass particles, which consist of ground pinewood, are not ground as fine as coal and the larger non-spherical shapes retain their original shape during combustion. The biomass particles are devised into two fractions, some described as flat irregular shapes with sizes of 1-3 mm in length and 0.2 mm in dept and some spherical with diameter of around 1 mm. It is interesting to note that according to Christensen & Barker (1965) the first fraction of particles having a length ratio of the order of 10 is best described as flake-like and should be modeled using appropriate correlation for discs. In the investigation by Backreedy et al. (2005) the sphericity approach has been used. The drag correlation used is the one presented by Haider & Levenspiel (1989) which has been built into the commercial CFD code Fluent (Fluent inc, 2005). As a small side remark it is interesting to note that according to Chhabra et al, (1999) the most accurate of the different drag correlations is not that by Haider & Levenspiel (1989) but the one proposed by Ganser (1993). The investigation of Backreedy et al. (2005) mainly focuses on the burnout properties of biomass where the surface area is important as well as the drag coefficient. Compared to the assumption of spherical shape a non-spherical particle will remain longer time in the combustion zone before it falls down into the ash hopper due to the increased drag. However, in reality the non-spherical particle will also experience increased dispersion due to lift forces imposed by the shape. The non-spherical particle will additionally heat up and combust faster than a spherical particle with same mass due to the larger surface area (Yin et al, 2004).

Multi-parameter description

It is necessary to predict the motion of a particle as accurately as possible since overlaying phenomenon (e.g. combustion) depends on the particle trajectory. To achieve the most correct handling of non-spherical particles it is necessary to account for all significant forces acting on the particle. An enhanced approach to dealing with non-spherical particles is to abandon the idea of equivalent spheres and instead model the orientation of the particles. This involves three main difficulties; first to formulate and account for the transformation between the coordinate system of the flow and that of the particle, secondly to account for and to formulate the significant forces and torques acting on the particle.

Coordinate systems
The equations of motion for an arbitrary particle considering both translation and rotation are given in equation (3) – (6). Commonly the translatory motion is given in the coordinate system of the flow, the inertial frame, and the rotational motion in the coordinate system of the particle, the particle frame.
The transformation between the inertial frame and the particle frame can be found in the classical mechanics book by Goldstein (1980):

$$\mathbf{x}' = \mathbf{A}\cdot\mathbf{x}'' \qquad (8)$$

If $\mathbf{x}$ is the inertial coordinate system, $\mathbf{x}'$ is the particle coordinates with the axis being the principle axes and $\mathbf{x}''$ is the particle frame with the axis parallel to that of the particle. The transformation matrix A can be expressed using the Euler angles $[\theta_1\ \theta_2\ \theta_3]$ or using Euler's four parameters known as quaternions $[\varepsilon_1, \varepsilon_2, \varepsilon_3, \eta]$ (Hughes, 1986). Euler angels are not suited for simulation of particles which undergoes full rotation since the evaluation of their time rate of change displays a singularity. The four Euler parameters represent an expansion of the three Euler angles to eliminate the singularity. For a full description of the transformation matrix the reader is referred to Goldstein (1980) & Hughes (1986) or to any of the many investigations which uses this method directly (Gallily & Cohen, 1979), (Fan & Ahmadi, 1995, 2000), (Schamberger et al, 1990), (Maxey, 1990), (Blaser, 2002) and (Yin et al, 2003, 2004).

Forces and torques

The factors affecting the translation of a non-spherical particle can be seen as the same forces which influences a perfect sphere (accounted for in the BBO equation) together with addition terms accounting for non-sphericity. The factors affecting the non-spherical particles orientation include the velocity gradient and torques which arises due to the vorticity of the flow field and external forces which influences the pressure distribution. Once the center of pressure is not coincident with the center of mass a pitching moment will cause the particle to rotate. Randomizing factors such as Brownian motion, turbulence and particle-particle interactions affects both the translatory motion and the orientation of the non-spherical particle. The properties of the flow, the fluid and the particles determine which factors are relevant to include into the governing equations of motion. The ratio between the density of the fluid and the particle is used in the order of magnitude estimates to exclude specific terms in the BBO equation.

For gas-solid flow only the drag term and body forces together with the inertia term needs to be retained. The Knudsen number is a measure for when the fluid phase cannot be viewed as a continuum and determines if Brownian motion needs to be considered. For air flow with a dispersed phase, particle sizes smaller than 5 μm will be influenced by molecular slip whereas for liquids the size is even smaller (Shin & Maxey, 1997). Flow where the particle-particle interaction is significant is commonly referred to as dense flow and dilute flows denote the regime where the fluid dynamic forces are dominant. One measure for the influence of particle-particle interaction is the volume fraction. Flows with volume fractions smaller than the order of 1/1000 can be considered as dilute (Elghobashi, 1994). Generally these considerations are valid for all fluids; however common assumptions are that the fluid is Newtonian and incompressible. A mixture of non-spherical particles immersed in Newtonian fluid could display non-newtonian properties as a whole (Carlsson, 2007). Besides the above mentioned parameters, the critical factor for the motion of non-spherical particle is obviously their shape. Generally it is not possible to treat irregular particles due to their random nature of the shape and their inability to be described mathematically. Consequently only a very limited number of shapes have been the subject of investigations and modeling attempts, namely ellipsoids and cylinders. Both shapes can be formulated to resemble both rod-like and flake-like particles making them a very useful also when considering irregular particles. A common way to describe both types of shapes is by the aspect ratio and this quantity also constitutes the attempts to relate results between the two shapes

Stokes flow

Stokes flow a characterized by that inertial forces are very low compared to the viscous forces. This criteria is satisfied by either having sufficient low relative motion between the fluid and the particle or by having a sufficient small particle. For a wide range of particulate flows this criteria is satisfied and it makes sense to only consider Stokes flow which simplifies the analysis.

The paper by Jeffery (1922) constitutes the foundation on which most investigations of non-spherical particles are based on. He considered a naturally buoyant ellipsoid which moves steadily through linear shear flow in the Stokes regime. The particle center of mass moves with the flow whereas the particle turns in response to the velocity gradient. He considered the fluiddynamic force and torque which acted on the particle and solved the equations of motion analytically to produce expressions for the rate of change of the angles $[\dot{\theta}_1, \dot{\theta}_2, \dot{\theta}_3]$ of the particle. An ellipsoid will rotate in closed orbits with a specific angular velocity defined by the aspect ratio[3] and the shear rate. Bretherton (1962) and Brenner[4] extended Jeffery's analysis to arbitrary particles in arbitrary flow fields although still in the Stokes regime. Hereby Jeffery's findings are valid also for cylindrical particles provided that an equivalent aspect ratio can be found. The findings by Jeffery (1922) has been experimentally proven first by Taylor (1923) who observed the oscillatory behavior of spheroids and later by Binder (1939) and Trevelyan & Mason (1951) who conducted detailed experiments with cylindrical particles of different aspect ratio on a Couette apparatus. Finally the periodicity of spheroids has been measured in detail by Anczurowski & Mason (1968).

A lot of investigations of different aspects of non-spherical particle in Stokes flow have been made in the past. Reviews of these can be found in the recent publication by Carlsson (2007) and the vintage article by Leal (1980). Instead we will focus on revealing the different contributions to the equation of motion in Stokes flow and on the extension to Brownian and turbulent motion.

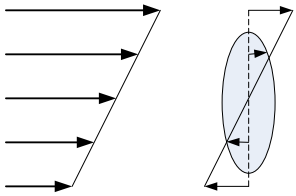

Figure 4: A particle subjected to linear shear.

The translational resistance, as derived by Jeffery (1922) is put into a convenient compact formulation by Gallily & Cohen (1979). The transitional fluid dynamic force is derived as an infinite series of flow velocities and its derivatives which is multiplied with a tensor of translation, **K**. In their analysis the transitional force/resistance the higher order terms are neglected and it reduces to:

$$\mathbf{F}_{F1} = 6\pi a \mu \mathbf{K} \cdot (\mathbf{u} - \mathbf{v}) \qquad (9)$$

which is for a sphere reduces to the familiar expression for Stokes drag. The torques acting on the particle can similarly be seen as an expression of the Stokes drag acting on the surface of the particle. A particle subjected to any form of shear flow, e.g. Poiseuille flow, will begin to rotate. The second term:

$$\mathbf{F}_{F2} = \mu \pi a \mathbf{K} \nabla^2 \mathbf{u} \quad (10)$$

[3] The ellipsoidal aspect ratio defined as r_e=a/b

[4] Brenner's papers: (Brenner, 1964a,b,c,d), (Happel and Brenner, 1965) and (Brenner & Condiff, 1972)

is the second derivative of the flow velocity and reduces to the Faxen force for a sphere accounting for flow curvature. Terms of higher order also contributes to the fluid dynamic force, unlike for a sphere, but can be ignored for small particles since they are proportional to higher order powers of the ellipsoids minor axis, *a* (Fan & Ahmadi, 1995). The analysis by Jeffery (1922) only accounts for the particles resistance to the flow which is sufficient to describe the oscillatory motion.

A sphere in a shear field will experience a lift force known as the Saffmann lift force due to the asymmetrical distribution of surface pressure. The corresponding lift-force for an arbitrary shaped non-spherical particle was derived by Harper & Chang (1968). For an ellipsoid of revolution this yields (Fan & Ahmadi, 2000):

$$\mathbf{F}_L = \frac{\pi^2 \mu a^2}{\nu^{1/2}} \sqrt{\frac{\partial u_x}{\partial y}} \left(\mathbf{K}\cdot\mathbf{L}\cdot\mathbf{K}\right)\left(\mathbf{u}-\mathbf{v}\right) \qquad (11)$$

L is the lift tensor which is not symmetric. The lift force depends on the minor axis of the ellipsoid squared indicating that it is significant only for relatively large particles.

The equation of motion of a sphere also contains non-steady terms which accounts for the particles resistance to acceleration and which become important for density ratios in the order of unity. Lawrence & Weinbaum (1986) investigated a slightly eccentric spheroid in oscillatory motion and derived an expression for the total fluiddymamic force. This consisted of four terms; three of which correspond with the equivalent for a sphere (Stokes drag, virtual mass and Basset force) and a fourth term which is due to the non-spherical shape. For an oblate spheroid with semiaxis: a=b(1+ε) the solution for general motion (inverse Laplace transform) is found as:

$$\begin{aligned}\mathbf{F}_{LW} = &-6\pi\mu a\left(1+\tfrac{1}{5}\varepsilon+\tfrac{37}{175}\varepsilon^2\right)\mathbf{u} \\ &-\frac{2\pi\mu a^3}{3\nu}\left(1+\tfrac{2}{5}\varepsilon+\tfrac{81}{175}\varepsilon^2\right)\frac{d\mathbf{u}}{dt} \\ &-\frac{6\pi^{\frac{1}{2}}\mu a^2}{\nu^{\frac{1}{2}}}\left(1+\tfrac{1}{5}\varepsilon+\tfrac{26}{175}\varepsilon^2\right)\int_0^t \frac{d\mathbf{u}}{d\tau}\frac{d\tau}{(t-\tau)^{\frac{1}{2}}} \\ &-\frac{6\pi^{\frac{1}{2}}\mu a^2}{\nu^{\frac{1}{2}}}\int_0^t \frac{d\mathbf{u}}{d\tau} G(t-\tau)d\tau\end{aligned} \qquad (12)$$

with the kernel function G(t) given as:

$$G(t) = \frac{8\varepsilon^2}{175}\,\mathrm{Im}\{(\pi\alpha)^{\frac{1}{2}} e^{\alpha t} erfc(\alpha t)^{\frac{1}{2}}\} \qquad (13)$$

and

$$\alpha = 3e^{\frac{1}{3}i\pi} = \tfrac{3}{2}(1+\sqrt{3i}) \qquad (14)$$

The fourth term is similar to the Basset force being a memory integral but the behavior for G(t) is different from the Basset terms $t^{1/2}$ dependency. G(t) is not infinite for small t, as $t^{1/2}$, and G(t) is consistently smaller than $t^{1/2}$. According to Lawrence & Weinbaum (1986) since the recent history is not emphasized as it is in the Basset term the contribution from the fourth term will be small. However, this analysis only applies for small eccentricities and for other body shape it is likely that this term is more significant. A further comment is that this solution is not given as orientation dependency which means that it is not likely to predict the actual motion of a particle. However, this expression gives an indication of the influence of non-sphericity on the unsteady terms in the equation of motion for a single particle. In the later work by Lawrence & Weinbaum (1988) it is pointed out that the part in the different terms relating to the eccentricity could be replaced by tensors to be valid for different orientations and arbitrary shapes; however no general solution is effectuated. The terms are also evaluated at different aspect ratios and different frequencies. For bodies which is streamlined with respect to the flow (large aspect ratios) the added mass term is small, whereas the Stokes drag and the Basset term increase due to the increased surface area (length of the body). In the work by Gavze (1990) the tensor notation for the non-spherical BBO equation is elegantly formalized by:

$$\mathbf{F} = -\mathbf{R}u - \mathbf{P}\cdot\dot{u} - \int_0^t \mathbf{T}(t-\tau)\cdot\dot{u}(\tau)d\tau \qquad (15)$$

where

$$\mathbf{F} = \begin{bmatrix} F \\ M \end{bmatrix}, \quad u = \begin{bmatrix} U \\ \omega \end{bmatrix} \qquad (16)$$

and **R**, **P** and **T** are the steady, potential and Basset tensor respectively. However, the actual application of this still depends on finding the basic solutions for different shapes.

As is remarked by Michaelides (1997) in his epic review of the equation of motion the results by Lawrence & Weinbaum (1986,1988) and by Gavze (1990) "challenges the common practice of using the 'equivalent diameter' to account for the shape of irregular solid particles"

Beyond the Stokes regime

As the vast majority of investigations dealing with the modeling of solid particles suspended in fluid flow are concerned with spherical particles so are most investigations dealing with non-spherical particles concerned with Stokes flow at low particle Reynolds numbers. To be exact Jeffery's solution are only strictly valid for zero Reynolds number and even at Re~O(10^{-3}) it has been proved that the inertial effect is sufficient to force non-spherical particle in a different orbit than that predicted by Jeffery (Karnis et al. 1963,1966). For higher Reynolds numbers, Re > 0.1, the effect of flow separation will tend to slow down and stop any rotation caused by a velocity gradient (Ding & Aidun, 2000). Modifications of the drag coefficient for higher Reynolds numbers fully rely on empirical data and are highly depended on the Reynolds number as well as the orientation of the particle. This significantly complicates the equations of motion and is probably the raison why the sphericity approach is so widely used. General higher particle Reynolds numbers is associated with large particle sizes and typically also with turbulent flows which complicates the analysis further.

Recent advances into the modeling of non-spherical particles at Reynolds numbers above unity has sprung from

the work of Ding & Aidun (2000), Qi & Luo (2003) and Qi (1997, 1999, 2000, 2001, 2005, 2006) who all used the lattice Boltzmann formulation of the Navier-Stokes for different particle shapes. Ding & Aidun (2000) reported for an ellipsoid in Coutte flow with fixed minor axis in the flow vorticity direction a critical Reynolds number of 81 for when rotation seized due to streamline separation. For the same case but with the particle allowed to rotate freely no critical Reynolds was recorded and the type of rotation depended on Reynolds number describing three distinct states up to a Reynolds number of 467 (Qi & Luo, 2003). The recent publication by Qi (2006) comprises the simulation of flexible fibers with variable stiffness and showed that the rotational period decrease as the fiber flexibility increases. The lattice Boltzmann method has been proven to be ably to reproduce experimental findings for Reynolds numbers above unity and is as such a valuable research tool. However, for application with an arbitrary geometry and multiple particles this method becomes far too computational expensive for any practical use.

A more practical method for high Reynolds number flow is the one presented in Yin et al. (2003, 2004) for a large cylindrical particle with density ratio in the order of unity. For translational motion the starting point is the BBO equation for a spherical particle. The pressure gradient and virtual mass term are retained as is and the orientation dependency of the particle is not modeled. Also the inertia and buoyancy term are retained while the Basset term is neglected. The orientation dependency is only modeled in the drag term and a new lift term where the area normal to the direction to the force is used. Both forces utilize correlations of the drag coefficient which is found on basis of the sphericity factor. This means that the drag coefficient is independent of the orientation but dependent on the particle Reynolds number. The lift force is found on basis of the major axis direction considering the restraints on the lift force[5] and the lift coefficient is found on basis of the drag force as (Hoerner, 1965):

$$\frac{|\mathbf{F}_L|}{|\mathbf{F}_D|} = \left|\sin^2(\alpha_i)\cos(\alpha_i)\right| \qquad (17)$$

The torques acting on the particle are found considering both the resistance on a rotating body and the fluiddynamic forces (drag, lift, pressure gradient and virtual mass) acting in the center of pressure instead of the center of mass. The center of pressure is suggested to be located as

$$x_{cp} = 0.25b(1-e^{3(1-\beta)})\left|\cos^3\alpha_i\right| \qquad (18)$$

where b is the semi major axis length and β the aspect ratio. The forces multiplied with this length yielding the torque are the same as for the translational velocity. As it has been exemplified with equation (17) and (18) this model is to a large extent based on purely empirical mechanisms and has as such been validated against a cylinder settling in a stagnant fluid. However, further validation in other flows is necessary for the expressions suggested to become fully accepted. Furthermore, since this is suggested to be used for turbulent flow additional terms accounting for the particle-turbulence interaction is needed.

Brownian and turbulent motion

Besides the fluid dynamic forces the motion and orientation of a particle is affected by Brownian and turbulent motion as well as particle-particle interaction which can be seen as randomizing factors (Zhang et al, 2006). Both Brownian and turbulent motion are associated rotational and translational dispersion. For the orientation of non-spherical particles the relative influence of the fluid dynamic forces and the randomizing factors is described by the characteristic rotational Peclet number (Bernstein & Shapiro, 1994):

$$Pe = W_0 / D_0 \qquad (19)$$

where W_0 is a characteristic velocity gradient and D_0 is the particle's rotational diffusion coefficient. D_0 comprises effects from both the Brownian and the turbulent diffusion and is simply calculated as $D_0=D_B+D_t$. Guidelines for calculation of the diffusion coefficients are given in (Bernstein & Shapiro, 1994). The rotational Peclet number can be seen as a measure for when randomizing factors should be taken into consideration. For high Peclet numbers the fluid dynamic forces tend to give the particles a preferred direction in a statistical sense[6] whereas for low Peclet numbers the turbulence or Brownian motion acts to give the particle an random orientation.

The turbulence influence on the translatory motion of the particle may be judged by evaluating the ratio between the particles relaxation time and a characteristic time scale of the turbulence. This ratio is known as the turbulence Stokes number:

$$St = \frac{\tau_p}{T_L} \qquad (20)$$

which provides an indication of the expected response to local fluctuations. For $St \ll 1$ particles will follow all fluctuations while for $St \gg 1$ particles will not follow the fluctuations.

There are two overall approaches which is used to deal with the effect of turbulence and Brownian motion; the Lagrangian and the Eulerian. The Lagrangian approach tracks particles as they move through the flow field under influence of fluid dynamic forces. The trajectory of a large number of particles is calculated by solving the particles equation of motion through a known flow field. The statistical result of the trajectories can be used to estimate the probability density function (PDF) at a given location. The effect of turbulence on the particles can be accounted for by resolving the turbulent flow field or by resolving the mean flow and accounting for the fluctuations using a stochastic model. Brownian motion is modeled in the Lagrangian frame using slip factors to modify the equations of motion or/and applying a similar stochastic model. In the Eulerian approach PDF's of the non-spherical particles orientation and concentration are calculated for the entire

[5] Invariant under a 180° rotation and vanish if $\alpha_i = 0,\pi$

[6] Although the motion is described by Jeffery's orbits, the particles spend most of their time with their long axis nearly aligned with the flow direction (Carlsson, 2007)

flow field considering the flux of particles and orientations. Turbulent and Brownian motion are accounted for directly using dispersion coefficients. There are advantages and disadvantages using both approaches. The Lagrangian frame is the most intuitive for particles in a dilute suspension since these are discrete in nature and not a continuous phase as they are seen in the Eulerian approach. However, the Lagrangian approach requires a large number of particle tracks to be statistically independent which makes it computationally expensive. The Eulerian approach is considered to be more efficient and it is easy to account for turbulent and Brownian motion together with particle collisions for a single size of particles.

The first work describing the motion of non-spherical particles in a Lagrangian frame is that of Galilly & Cohen (1979). Although the studied ellipsoidal particles with sizes down to a,b =(0.5,5)μm they justified their neglect of stochastic behavior, due to Brownian motion, by comparing the Brownian fluctuational velocity with that of the mean velocity. Often the influence of turbulence is simulated using flow fields which resemble turbulent motion. The flight of non-spherical particles in isotropic turbulence is studied using a Gaussian random field where the instantaneous velocity field is given as series of Fourier nodes with zero mean and specified standard deviation (Fan & Ahmadi, 1995),(Olson,2001). The same idea has also been used to create vortex like structures which can be considered as a more qualitative description of turbulence. As such the turbulence boundary layer has been modeled using periodic vortical flow structures within various distances from the wall by Fan & Ahmadi (2000) and flow field consisting of four counter rotating 2D vortices by Shin & Maxey (1997).

The major limitation for investigations incorporating turbulence effects is that the flow around the particles is modeled as Stokes flow, using the fluid dynamics of Jeffery (1922), where the major axis length is smaller than the Kolmogorov length scale and the particle Reynolds number smaller than 0.1. For turbulent flow this typically results in rather small particles where also Brownian motion becomes important. The study by Fan & Ahmadi (2000) introduces an additional Brownian force and Brownian torques in the equations of motion to supplement the fluid dynamic forces. At the same time the fluid dynamic forces are modified by introducing approximations of the translational and rotational slip factors. Keeping in line with the notion of the random nature of Brownian motion, this is again modeled as an independent Gaussian process. Ideally models addressing non-spherical particles in turbulence should be put into the same context as the popular two-equation turbulence models to be applied on an arbitrary flow field and still be within the reach of present computational resources. This has still only been done using the sphericity approach (Sun et al, 2004), (Backreedy et al, 2005).

The classical work for the Eulerian reference frame is often referred to that of Hinze (1975). The basic idea is the is to use the Eulerian convection-dispersion equation to express the probability distribution, $\psi(\mathbf{r},\mathbf{p},t)$ of orientation, $\mathbf{p}$, position, $\mathbf{r}$. Using the notation of Olson et al. (2004) this can be expressed compactly as:

$$\frac{\partial \Psi}{\partial t} = D_p \nabla_r^2 \Psi - \nabla_r \cdot (\omega \Psi) + D_t \nabla^2 \Psi - \nabla \cdot (\mathbf{V} \Psi) \quad (21)$$

where D_t and D_p are the rotational and translational dispersion coefficients respectively, ω and V are the angular and mean translational velocities. Including turbulent or Brownian motion is a matter of adjusting the dispersions coefficients accordingly. In the context of 2 equation turbulence models the turbulent dispersion can be expressed simple by:

$$D_p \approx 0.7 \left(\frac{4\varepsilon}{15\nu} \right)^{1/2} \quad (22)$$

where ε is the dissipation rate which is directly available from for example the k-ε model. Other estimates are given in the recent puplications of Olson et al. (2004), Paschkewitz et al. (2004), Zhang et al. (2005) and Zhang et al. (2006). Usually the expressions given are complex relations of the orientation and interaction with the turbulence. Due to the nature of the Eulerian frame one would expect that the coefficients given needs to be fine tuned in order to reproduce experimental results and can as such not be considered as universal models. The model by Zhang et al. (2005) has been compared with the experimental data by Bernstein & Shapiro (1994). The numerical result is able to reproduce the same tendencies as the experiments with respect to the orientation distribution but at some points the model may be off by as much as 100 %.

Turbulent dispersion and turbulence modulation

Concerning particles in turbulent flows two features have been the focus of much research in recent years. That is the effect of turbulence on particle known as turbulent dispersion and the effect of particles on the carrier phase turbulence known as turbulence modulation. For the turbulent dispersion of spherical particle a number of models exist of which some are known to yield reasonable results for a range of flows (Shirolkar, 1996). For non-spherical particle the quantitative observation suggest that the increase in the drag coefficient also increases the dispersion coefficient compared to that of spherical particles (Losenno, 2004). However, the opposite effect is recorded in the theoretical work by Olson & Kerekes (1998) where the dispersion coefficients decreased for larger values of the body length to Lagrangian integral length scale of turbulence ratio. Turbulence modulation is even for spherical particles far from being well understood and no model exist which can reproduce all flow scenarios (Lain & Sommerfeld, 2003). The general trend for spherical particles seems to be that larger ratios of particle diameter to turbulence length scale augment the turbulence intensity while small values cause attenuation (Gore & Crowe, 1989). For non-spherical particles the quantitative observation is again that the increased drag coefficient has a greater effect on the turbulence compared to an equivalent spherical particle (Sun et al, 2004). This applies both for the augmentation by large particles and attenuation from small particles. Paschkewitz et al. (2004) showed in their numerical model that long slender particles would modify

the turbulence by aligning in the intervortex regions and causing increased stresses which act to dissipate the vortices. Due to the weakening of the near wall vortex structure, fibers strongly affect the friction characteristics at the wall and drag reduction of up to 26 % have been measured. By varying the aspect ratio of the fibers it is ascertained that this effect is most significant for large aspect ratios. A decrease in the aspect ratio increases the effective viscosity and thereby reduces the drag reduction efficiency. Generally the non-spherical attribute would be expected to generate anisotropic stresses contrary to spheres. Compared to spheres non-spherical particles have an additional freedom of movement; that is rotation, which resembles the turbulent eddy-like motion. In that light, the inertia of rotating particles can be seen to act to sustain the turbulence. On the other hand considering a non-spherical particle transported by vortex structures would in addition to attenuation caused by the translational motion also be put into rotational motion. Compared to spherical particles this extra freedom of movement could dramatically increase the dissipation characteristics. Finally, we have also seen that a non-spherical particle subjected to shear flow will begin to rotate due to fluid dynamic forces. Considering this rotation as a promoter of turbulence it constitutes an additional route to extract energy from the main flow and give rise to additional turbulent motion. This is an area which need more work for one to be apple to draw decisive conclusions.

Discussion

The motion of non-spherical particles is characterized by oscillatory motion which for specific shapes in specific flow regime causes severe secondary motion and significantly distinguishes it from the flight of a sphere. However, the most widely used method to model non-spherical particles it by using equivalent diameters and shape factors for which we with little effort can use methods and governing equation developed for spheres. These methods should only be used for shapes which with none or limited secondary motion. Using the criterion by Christensen & Baker (1965) only particles with an aspect ratio below 1.7 should be modeled using single parameter methods. An alternative to the sphericity approach is to actual measure the drag coefficient for the considered shape. For more complex geometries the sphericity approach is highly inaccurate and it is advantageous to use custom correlations.

Orientation depended forces, originally developed by Jeffery (1922), valid in the Stokes regime are almost without exception the back bone in all simulations to date. However, in the situation of large particles in high Reynolds number flow (e.g. combustion of biomass particles) these seize to be valid. Progress in this range of Reynolds numbers has been achieved by relying on experimental investigations to produce empirical correlations of the drag coefficient. The major problem with this approach is that the variation of shapes is limitless and it would become something of a Sisyphean challenge to account for all. Again in the context of Chritensen & Baker (1965) the shapes considered could be limited to flake-like (disc/oblate spheroid) and rod-like (cylinder/prolate spheroid) particles.

Lagrangian models constitutes the natural frame for particles but tend to be computational expensive compared to Eulerian models. When also considering the orientation of particles the demand on the computational resources is further increased which is a limiting factor for the potential use in industrial applications. Keeping in the same line of thought Lagrangian models also need to be formulated in the context of widely used turbulence models such as the k-ε model.

Eulerian models are less computational expensive and the dispersive effect are easy to incorporate. However, in most practical flow there will be both a size and shape distribution present which is not possible to incorporate into Eulerian models unless additional transport equations are solved for each size and shape. Furthermore, usually the combustion of particles is not modeled in the Eulerian frame further limiting its usefulness. When not considering this, the part where Eulerian models for non-spherical particulate flow need most attention is in the validation against experimental results.

As a closing remark whether we are taking about single parameter descriptions, Lagrangian or Eulerian multi parameter models or models to predict the interaction with turbulence the most obvious area which need further work is the comparison of these models with experimental results.

Acknowledgements

This work was supported by Energinet.dk, under grant PSO 6364.

References

Allen, T. Particle size measurement. Chapman & Hall (1981)

Anczurowski, E. & Mason, S.G. The kinetics of flowing dispersions. III. Equilibrium orientations of rods and discs (experimental). Journal of colloid interface science. Vol. 23, 533-546 (1968)

Backreedy, R.I., Fletcher, L.M., Jones, J.M., Ma, L., Pourkashanian, M. & Williams, A. Co-firing pulverized coal and biomass: a modeling approach. Proceedings of the Combustion Institute, Vol. 30, 2955-2964 (2005)

Black, D.L., Mcquay, M.Q. & Bonin, M.P. Laser-based tech niques for particle size measurement: a review of sizing methods and their industrial application. Progress in Energy and Combustion Science. Vol. 22, 267-306 (1996)

Bernstein, O. & Shapiro, M. Direct determination of the orientation distribution of cylindrical particles immersed in laminar and turbulent shear flows. Journal of aerosol science. Vol. 25 (1), 113-136 (1994)

Bilanski, W.K. & Lal, R. Behavior of threshed materials in a vertical wind tunnel. Transactions of the ASAE Vol. 8, 411-416 (1965)

Binder, R.C. The motion of cylindrical particles in viscous flow. Journal of Applied Physics. Vol. 10, 711-713 (1939)

Black, D.L. & McQuay, M.Q. Laser-based particle measurements of spherical and Nonspherical particles. International Journal of Multiphase flow, Vol. 27, 1333-1362 (2001)

Blaser, S. Forces on the surface of small ellipsoidal particles immersed in a linear flow field. Chemical engineering Science. Vol. 57, 515-526 (2002)

Brenner, H. The Stokes resistance of a slightly deformed sphere. Chemical Engineering Science. Vol. 19, 519-539 (1964a)

Brenner, H. The Stokes resistance of an arbitrary particle-II. an extension. Chemical Engineering Science. Vol. 19, 599-629 (1964b)

Brenner, H. The Stokes resistance of an arbitrary particle-III. shear fields. Chemical Engineering Science. Vol. 19, 631-651 (1964c)

Brenner, H. The Stokes resistance of an arbitrary particle-IV. arbitrary fields of flow. Chemical Engineering Science. Vol. 19, 703-727(1964d)

Brenner, H. & Condiff, D. Transport mechanics in systems of orientable particles. III arbitrary particles. Journal of Colloid and Interface Science. Vol. 42 (2), 228-274 (1972)

Bretherton, F.P. the motion of rigid particles in a shear flow at low Reynolds number. Journal of Fliud Mechanics. Vol 14, 284-304 (1962)

Carlsson, A. Orientation of fibres in suspensions flowing over a solid surface, licentiate thesis, Royal Institute of Technology, Stockholm, Sweeden, (2007)

Chhabra, R.P., Agarwal, L. & Sinha, N.K. Drag on non-spherical particles: an evaluation of available methods. Powder Technology, Vol. 101, 288-295 (1999)

Christiansen, E.B. & Barker, D.H. Effect of shape and density on free settling of particles at high Reynolds number. AICHE journal. Vol. 11 (1), 145 (1965)

Clift, R., Grace, J.R & Weber, M.E. Bubbles, Drops, and particles. Dover publications. (2005)

Comer, J.K. & Kleinstreuer, C. A numerical investigation af laminar flow past nonspherical solids and droplets. Transactions of the ASME. Vol. 117, 170-175 (1995)

Curtis, J.S. & van Wachem B. Modeling particle-laden flows: A research outlook. AIChE journal. Vol. 50 (11), 2638-2645 (2004)

Ding, E-J. & Aidun, C.K. The dynamics and scaling law for particles suspended in shear flow with inertia. Journal of fluid mechanics. Vol. 423, 317 (2000)

Elghobashi, S. On predicting particle-laden turbulent flows. Applied Scientific Research. Vol. 52 (4), 309-329 (1994)

Fan, F-G. & Ahmadi, G. Dispersion of ellipsoidal particles in a isotropic pseudo-turbulent flow field, Transactions of the ASME, Vol. 177, 154-161 (1995)

Fan, F-G. & Ahmadi, G. Wall deposition of small ellipsoids from turbulent air lows – A Brownian dynamics simulation, Vol. 177, 1205-1229 (2000)

Field, S.B., Klaus, M., Moore, M.G. & Nori, F. Chaotic dynamics of falling discs. Nature. Vol. 388, 252-254 (1997)

FLUENT inc, FLUENT 6.2 User's Guide, Fluent inc (2005)

Gallily, I. & Cohen, A-H. On the orderly nature of the motion of non-spherical aerosol particles. II. Inertial collision between a spherical large droplet and an axial symmetrical elongated particle. Journal of Colloid and Interphase Science. Vol. 68 (2), 338-356 (1979)

Ganser, G.H. A rational approach to drag prediction of spherical and non-spherical particles. Powder Technology. Vol. 77, 143-152 (1993)

Gavze, E. The accelerated motion of rigid bodies in non-steady Stokes flow. International Journal of Multiphase flow. Vol. 16, 153-166 (1990)

Goldstein, H. Classical Mechanics. Addison-Wesley (1980)

Gore, R.A. & Crowe C.T. Effect of particle size on modulating turbulent intensity. International journal of multiphase flow. Vol. 15 (2), 279-285 (1989)

Haider, A. & Levenspiel, O. Drag coefficient and terminal velocity of spherical and non-spherical particles. Powder Technology. Vol. 58, 63-70 (1989)

Happel, J. & Brenner, H. Low Reynolds number hydrodynamics. Prentice Hall (1965)

Harper, E.Y. & Chang, I.D. Maximum dissipation resulting from lift in a slow viscous shear flow. Journal of fluid mechanics. Vol. 33, 209 (1968)

Hinze, J.O. Turbulence, second ed. McGraw-Hill (1975)

Hoerner, J.F. Fluid-dynamics drag. Hoerner Fluid Dynamics. (Published by the author) (1965)

Hughes, P.C. Spacecraft attitude Dynamics. Wiley. (1986)

Jeffery, B.G. The motion of ellipsoidal particles immersed in a vicious fluid. Proceedings of the Royal Society. Vol. 102A, 161-179 (1922)

Kankkunen, A., Miikkulainen, P., Järvinen, M. & Fogelholm, C.-J. Shape characteristics of non-spherical black liquor droplets, Pulp & Paper Canada Vol. 106:12, 71-74 (2005)

Karnis, A., Goldsmith, H. L. & Mason, S. G. Axial migration of particles in Poiseuille flow. Nature. Vol. 200, 159–160 (1963)

Karnis, A., Goldsmith, H. L. & Mason, S. G. The flow of suspensions through tubes. V. Inertial effects. Canadian Journal of Chemical Engineering. Vol. 44, 181–193 (1966)

Kaspers, G. Aerosol science and technology. Vol. 1, 187 (1982)

Klett, J.D. Orientation Model for Particles in Turbulence. Journal of the Atmospheric Sciences, Vol. 52, 2276-2285 (1995)

Lain, S. Sommerfeld, M. Turbulence modulation in dispersed two-phase flow laden with solids from a Lagrangian perspective. International Journal of Heat and Fluid Flow. Vol. 24, 616- 625 (2003)

Lawrence, C.J. & Weinbaum S. The force on a axisymmetric body in linearized, time-dependent motion: a new memory term. Journal of Fluid Mechanics, Vol. 171, 209-218 (1986)

Lawrence, C.J. & Weinbaum S. The unsteady force on a body at low Reynolds number; the axisymmetric motion of a spheroid. Journal of Fluid Mechanics, Vol. 180, 463-489 (1988)

Lazaro, B.J. & Lasheras, J.C. Particle dispersion in a turbulent plane, free shear layer. Physics of Fluids A, Vol. 1, 1135-1044 (1989)

Leal. L.G. Particle motion in a viscous fluid. Annual revision of fluid mechanics. Vol. 12, 435-476 (1980)

Losenno, C.G.R. An investigation of irregular particles in free-fall, PhD thesis, University of Edinburgh (2004)

Maxey, M.R. & Riley, J.J. Equation of motion for a small rigid sphere in nonuniform flow. Physics of Fluids. Vol. 26, 883-889 (1983)

Maxey, M.R. On the advection of Spherical and Non-spherical Particles in Non-uniform flow. Philosofical Transaction of the Royal Society of London, Series A. Vol. 333, 289-307 (1990)

McKay, G., Murphy, W.R. & Hillis, M. Settling characteristics of discs and cylinders. Chemical Engineering Research and Design. Vol. 66, 107-112 (1988)

Michaelides, E.E. Review – The transient equation of motion for particles, bubbles, and droplets. Journal of Fluids Engineering, Vol. 119, 233-247 (1997)

Olsen, J.A. & Kerekes, R.J. The motion of fibres in turbulent flow. Journal of Fluid Mechanics. Vol. 377, 47-64 (1998)

Olsen, J.A. The motion of fibres in turbulent flow, stochastic simulation of isotropic homogeneous turbulence. International Journal of Multiphase Flow. Vol. 27, 2083-2103 (2001)

Olsen, J.A. Frigaard, I. Chan, C. & Hamalainen, J.P. Modeling a turbulent fibre suspension flowing in a planar contraction: The one-dimensional headbox. International Journal of Multiphase Flow. Vol. 30, 51-66 (2004)

Paschkewitz, J.S., Dubief, Y., Dimitropoulos, C.D., Shaqfeh, E.S.G. & Moin, P. Numerical simulation of turbulent drag reduction using rigid fibres. Journal of Fluid Mechanics. Vol. 518, 281-317 (2004)

Qi, D.W. Non-spheric colloidal suspensions in three-dimensional space. International journal of modern physics. Vol. 8, 985 (1997)

Qi, D.W. Lattice Boltzmann simulations of particles in no-zero-Reynolds-number flows. Journal of Fluid Mechanics. Vol. 385, 41 (1999)

Qi, D.W. Lattice Boltzmann simulations of fluidization of rectangular particles, International Journal of Multiphase Flow. Vol. 26, 421 (2000)

Qi, D.W. Simulations of fluidization of cylindrical particles in a 3-D space. International Journal of Multiphase Flow. Vol. 27, 107 (2001)

Qi, D.W. & Luo, L-S. Rotational and orientational behaviour of three-dimensional spheroidal particles in Couette flows. Journal of Fluid Mechanics. Vol. 477, 201-213 (2003)

Qi, D.W. Many-particle interactions in Coutte flows. Progress in computational fluids dynamics. Vol. 5, 104-109 (2005)

Qi, D.W. Direct simulations of flexible cylindrical fiber suspensions in finite Reynolds number flows. Journal of Chemical Physics. Vol. 125, 114901 (2006)

Schamberger, M.R., Peters, J.E. & Leong, K.H. Collection of Prolate Spheroidal Aerosol Particles by Charged Spherical Collectors. Journal of Aerosol Science. Vol. 21, 539-554 (1990)

Shin, H. & Maxey, M.R. Chaotic motion of non-spherical particles settling in a cellular flow field. Physical Review E. Vol. 56 (5), 5431-5444 (1997)

Shuen J-S., Solomon, A.S.P., Zhang, Q-F. & Faeth, G.M. Structure of particle-Laden Jets: Measurements and predictions. AIAA journal. Vol. 23 (3), 396-404 (1985)

Shirolkar, J.S., Coimbra, C.F.M. & McQuay, M.Q. Fundamental aspect of modeling turbulent particle dispersion in dilute flows. Progress in energy and combustion. Vol. 22, 363-399 (1996)

Sun, L., Lin, J-Z., Wu, F-L. & Chen, Y-M. Effect of non-spherical particles on the fluid turbulence in a particulate pipe flow. Journal of Hydrodynamics. Ser.B. Vol. 16 (6), 721-729 (2004)

Tang, P., Chan, H.-K. & Raper, J.A. Prediction of aerodynamic diameter of particles with rough surfaces, Powder Technology, Vol. 147, 64-78 (2004)

Taylor, G.I. Axial and traverse Stokes flow past slender axissymmetric bodies. Proceedings of the Royal Society of London. Series A. Vol. 103, 58-61 (1923)

Trevelyan, J. & Mason, S.G. Particle motion in sheared suspensions I. Rotation. Journal of Colloid Science. Vol. 6, 354-367 (1951)

Wadell, H. J Franklin Institute. Vol. 217, 459 (1934)

White, F.M. Viscous Fluid Flow. McGraw-Hill (1991)

Ye, T.H., Azevedo, J., Costa, M. & Semiao, V. Co-combustion of pulverized coal, pine-shells and textile wastes in a propane-fired furnace: Measurement and predictions. Combustion science and technology. Vol. 176, 2071-2104 (2004)

Yin, C., Rosendahl, L., Kær, S.K. & Sørensen, H. Modeling of cylindrical particles in nonuniform flow. Chemical Engineering Science Vol. 58, 3489-3498 (2003)

Yin, C., Rosendahl, L., Kær, S.K. & Condra, T.J. Use of numerical modeling in the design for co-firing biomass in wall-fired burners. Chemical Engineering Science Vol. 59, 3281-3292 (2004)

Yow, H.N. Pitt, M.J. & Salman, A.D. Drag correlation for particles of regular shape. Advanced powder technology. Vol. 16 (4), 363-372 (2005)

Zhang, L-X., Lin, J-Z. & Chan, T.L. Orientation distribution of cylindrical particles suspended in a turbulent pipe flow. Physics of Fluids. Vol. 17, 093105 (2005)

Zhang, L-X., Lin, J-Z. & Zhang, W. Theoretical model of particle orientation distribution function in a cylindrical particle suspension subject to turbulent shear flow. Progress in Natural Science. Vol. 16 (1), 16-20 (2006)